AN ABSTRACT OF THE DISSERTATION OF

Lyndsey E. Shorey for the degree of Doctor of Philosophy in Toxicology presented on May 24, 2012.
Title: Chemopreventative and Chemotherapeutic Properties of Whole Cruciferous Vegetables and Phytochemical Components in Acute T-cell Lymphoblastic Leukemia/lymphoma.

Abstract approved:

David E. Williams

Acute lymphoblastic leukemia (ALL) encompasses a spectrum of lymphoid progenitors that have undergone malignant transformation and clonal proliferation at various stages of differentiation. Some cases of ALL have been documented to have prenatal origins and in particular neonatal exposure to various environmental pollutants is associated with increased disease risk, including childhood lymphoma and leukemia. Dibenzo[*def,p*]chrysene (DBC) is a polycyclic aromatic hydrocarbon (PAH) and in our laboratory has been established as a transplacental carcinogen in mice, producing aggressive T-cell lymphoblastic lymphomas, lung, liver, uterine, ovarian, and testicular lesions, depending on timing and dose of exposure.

Investigation of the transplacental and translactational transfer of DBC was warranted following a cross-foster experiment demonstrating the greatest tumorigenic response occurred in offspring both gestating in and nursed by an exposed female. [^{14}C]-DBC (GD17) dosing was utilized to examine time-dependent alterations of [^{14}C] in maternal and fetal tissues, excreta, and residual levels at weaning. Fetal tissue levels of [^{14}C]-DBC equivalents were 10-fold lower than maternal tissue, and after weaning the residual body burden was roughly equivalent in offspring exposed only *in utero* or only via lactation.

Certain bioactive food components, including indole-3-carbinol (I3C), 3,3'-diindolylmethane (DIM), and sulforaphane (SFN) from cruciferous vegetables have been shown to target cellular pathways regulating carcinogenesis. In the above mentioned DBC initiated model of carcinogenesis, I3C is an effective transplacental chemopreventive agent. We sought to extend our chemoprevention studies in mice to a human neoplasm in cell culture, analogous to the observed murine T-cell lymphomas. Treatment of the human T-ALL cell line CCRF-CEM (CEM) with I3C reduced cell proliferation and viability only at supraphysiologic concentrations whereas DIM, the primary acid condensation product of I3C, had a marked effect at low micromolar concentrations *in vitro* and reduced growth of CEM xenografts *in vivo*. Additional T-ALL lines, selected to represent the heterogeneity of the disease, (CCRF-HSB2, Jurkat, and SUP-T1) responded similarly *in vitro*, demonstrating a potential therapeutic value of DIM in T-ALL.

Given that epigenetic reprograming is especially active during fetal development and that DNA hypermethylation contributes to the etiology of T-ALL we examined genome-wide DNA methylation in CEM. Differential methylation analysis revealed that DIM and I3C alter CpG methylation in unique, yet overlapping, gene targets. DIM treated cells exhibited a dose-dependent decrease in hypermethylation, an observation consistent with an epigenetic mechanism of cancer suppression. Pyroseqencing and RTPCR technologies were utilized to validate changes in DNA methylation and to compare these patterns with a transcriptional response in both novel targets and candidate genes selected from the literature.

Collectively, these studies merited returning to the murine transplacental model for further investigation of genetic and epigenetic changes upon maternal dietary intervention with I3C. More importantly we incorporated whole cruciferous vegetable diets (10% broccoli sprouts or 10% Brussels sprouts), SFN diet, or the combination of SFN and I3C, in order to examine matrix and mixture effects. Preliminary analysis suggests a worse prognosis for those animals exposed *in utero* to SFN or the whole foods, especially males. As this is the first study to administer SFN

or whole cruciferous vegetables in a transplacental model of carcinogenesis, our results warrant further study on the concentration dependent influence of these potent phytochemicals during the perinatal window.

Chemopreventative and Chemotherapeutic Properties of Whole Cruciferous Vegetables and Phytochemical Components in Acute T-cell Lymphoblastic Leukemia/lymphoma

by

Lyndsey E. Shorey

A DISSERTATION

Submitted to

Oregon State University

in partial fulfillment of
the requirements for the
degree of
Doctor of Philosophy

Presented May 24, 2012

Commencement June 2012

Doctor of Philosophy dissertation of Lyndsey E. Shorey presented on May 24, 2012.

APPROVED:

Major Professor, representing Toxicology

Head of the Department of Environmental and Molecular Toxicology

Dean of the Graduate School

I understand that my dissertation will become part of the permanent collection of Oregon State University libraries. My signature below authorizes release of my dissertation to any reader upon request.

Lyndsey E. Shorey, Author

ACKNOWLEDGEMENTS

I would like to express my sincere appreciation first to my mentor, Dr. David Williams, for the opportunity and privilege of conducting my PhD research and training under his advisement. His generosity, patience, and expertise have provided an ideal environment for me to develop as a scientist. During this time I have learned critical life and career skills that I know will prove indispensable in the near future.

I also would like to thank a number of faculty members who have served as mentors including my committee members Drs. Andrew Buermeyer, Valerian Dolja, Michael Freitag, and Emily Ho; my training grant rotation advisors Drs. Kim Anderson and Robert Tanguay; and additionally Dr. Roderick Dashwood, for their scientific contributions and support during this chapter in my life. Additionally, I am deeply grateful to Dr. Abby Benninghoff who, as a postdoctoral trainee in our laboratory, was and continues to be a source of motivation, knowledge, and friendship.

To my OSU colleagues throughout the years and all of the Cancer Chemo-Prevention and Program Project Grant group members, I thank you for your kind attention, advice, and criticism. Marilyn Henderson, Beth Siddens, Dr. Sharon Kreuger, Mohaiza Dashwood and Dr. Carmen Wong generously provided indispensable technical training and advice. This past animal study would not have been possible without the assistance of David Strickland, Rachel Azevedo, Elyssa Ridinger, and David Sampson.

Lastly, I would like to thank my family for their everlasting support and understanding while I have pursued my dreams so far from home. They are a constant source of love and a reminder of all that I have worked for. Special recognition also goes to my Oregon “family” and friends, who have been by my side during some of the toughest and most joyous moments of my life. Without my friends and family I cannot imagine that this dream would turn into reality.

CONTRIBUTION OF AUTHORS

Chapter 2: David Williams (DW), William Baird, and Richard Corley provided assistance in experimental design, data interpretation and manuscript preparation. Lyndsey Shorey (LS) and David Castro contributed equally to the conduct of the study and preparation of the manuscript. Lisbeth Siddens provided technical assistance and manuscript proofreading. Melissa Matzke and Katrina Waters performed statistical modeling and analysis. Christiane Löhr (CL) was responsible for the histological analysis.

Chapter 3: Abby Benninghoff and DW provided assistance in experimental design, data interpretation and manuscript preparation. LS conducted the *in vitro* work with CEM cells, the xenograft experiment at OSU, and prepared the manuscript. Amanda Hagman conducted work with addition cell lines at USU. Emily Ho (EH) and Roderick Dashwood (RD) provided technical expertise and manuscript critiques.

Chapter 4: DW provided assistance in experimental design, data interpretation, and manuscript preparation. LS carried out the study and prepared the manuscript. Erin Madeen assisted with animal husbandry and sample collection. Lauren Atwell conducted LC-MS/MS analysis of whole food powders and neonatal plasma, and assisted with relevant manuscript sections. Clifford Perera performed statistical analysis and CL was responsible for the histological analysis. EH and RD provided assistance with experimental design.

Appendix A1: DW provided assistance in experimental design, data interpretation, and manuscript preparation. LS and Pushpinder Kaur carried out the study and prepared the manuscript. Andrés Houseman provided statistical expertise and assistance with DMR analysis. EH and RD provided assistance with experimental design and technical expertise.

TABLE OF CONTENTS

TABLE OF CONTENTS (Continued)

LIST OF FIGURES

LIST OF TABLES

LIST OF APPENDICES

LIST OF APPENDIX FIGURES

LIST OF APPENDIX TABLES

Chapter 1 General introduction

1.1 Transplacental carcinogenesis

Women are unavoidably exposed to environmental pollutants during pregnancy and the developing fetus and neonate are especially sensitive to chemical insults due to increased rates of cell division, decreased metabolic capacity, epigenetic plasticity, and immature DNA repair mechanisms [1,2]. Cumulatively, these factors result in greater relative DNA damage and a more rapid frequency of mutations than in adult tissues [3]. Efforts to correlate exposure to ambient pollution during pregnancy with adverse outcomes have largely consisted of population based studies, polymorphism studies, and quantitative biomarker analysis such as carcinogen-DNA adducts and chromosome specific aberrations [4-7]. For example, activating polymorphisms in *CYP1A1* or *CYP2E1*, or null mutations in *GSTM1* have been consistently associated with an increased risk of childhood cancer including acute lymphoblastic leukemia/lymphoma (ALL) [reviewed in 8, Table 1]. Empirical evidence for transplacental carcinogenesis in humans exists only for diethylstilbesterol and transabdominal irradiation, yet these examples support the potential for causation of childhood cancers by environmental *in utero* exposures [9,10]. Cumulatively, the circumstantial evidence indicates that environmental exposures during gestation could initiate childhood neoplasms.

From studies in animal models, there is further direct evidence that transplacental exposure to xenobiotics and environmental pollutants including arsenic, cigarette smoke, cisplatin, N-nitroso-N-methylurea, polycyclic aromatic hydrocarbons (PAHs), and benzene can induce carcinogenesis in offspring [11-15]. PAHs are produced from the incomplete combustion of carbon based materials, such as fossil fuels, and are environmental pollutants of concern based on their ubiquity and mutagenicity [16]. It is estimated that over 95% of exposure to higher molecular weight and more carcinogenic PAHs occurs through the diet, with significant contributions from cooked meats and plant-based cooking oils [17]. Pharmacokinetic studies in animal models have demonstrated that PAHs directly cross the placenta to

target fetal tissues [18,19]. Based on these studies, the relative fetal tissue concentration of PAHs following transplacental exposure is expected to be approximately 1% of maternal burden, yet Whyatt et al., demonstrated that levels of PAH-DNA adducts were higher in white blood cells from newborns than paired maternal samples [3].

Since 1970, 7-12-dimethylbenz[*a*]anthracene (DMBA) has been the most commonly studied PAH in murine transplacental models. Depending on the dose, delivery, and strain sensitivity, transplacental DMBA exposure in mice results in neoplasms of the breast, ovary, colon, skin, liver, lung, and lymphocytes [20-27]. Other PAHs that have been utilized in rodent transplacental models of carcinogenesis include benzo[*a*]pyrene (BaP), dibenzo[*def,p*]chrysene (DBC) and 3-methylcolanthrene (3-MC) [27-29]. Again, the dose and timing of exposure to these PAHs are critical determinants of the level and spectrum of carcinogenesis, as are maternal and fetal phenotype [19,28,30,31].

Our laboratory has previously established that a single oral dose of DBC (15 mg/kg) to pregnant B6129SF1/J mice results in significant offspring morbidity starting at 3 months of age (equivalent to ~8 years in humans), due to aggressive thymic lymphomas [28,30-34]. Flow cytometric analysis of a small sample of these thoracic masses determined a consistent T-cell origin ($CD3^+$) and a predominantly single positive ($CD4^-/CD8^+$) immunophenotype. Those animals that survive through this sensitive period develop lung tumors (100% incidence) and liver tumors (preferentially males), identified upon termination of the study at 10 months [28]. Perinatal chemical exposure scenarios in animal models commonly result in adult type neoplasms either due to long latency periods or the requirement of additional promotional exposure events. For example, inorganic arsenic administered to pregnant mice from gestation day 8 – 18 dose-dependently increased hepatic carcinoma in males and ovarian tumors in females [12], neoplasms which are rarely diagnosed in juveniles [35]. Therefore, our model is unique as it allows us to examine the impact of perinatal exposure on the risk of both childhood and adulthood

malignancies and has been further utilized to examine transplacental chemoprevention, discussed in detail below.

1.2 T-cell acute lymphoblastic leukemia/lymphoma (T-ALL) and polycyclic aromatic hydrocarbons (PAHs)

Although the etiology of childhood cancer is unknown, in the United States it is the number one cause of disease-related death in children less than 14 years of age [35]. Acute lymphoblastic leukemia/lymphoma, a heterogeneous disease of malignant lymphoid progenitors, is most common with > 5,000 U.S. cases diagnosed annually in this age group [36]. Approximately 1 in 6 of these cases will consist of T-cell progenitors, arrested at various stages in differentiation and historically these patients have been less responsive to combination chemotherapy and are more likely to relapse than patients with B-cell ALL [37]. Therefore, identifying preventative and therapeutic agents which target neoplastic T-lymphoblasts could significantly reduce cancer related mortality in children.

As T-cell differentiation occurs in discrete stages, malignant transformation often involves aberrations in the molecular pathways which regulate this progressive process [38]. The mechanism by which our adaptive immune system achieves diversity, somatic recombination, makes the DNA of lymphocytes highly vulnerable to chromosomal aberrations [39]. Examples of oncogenic conversions may involve T-cell receptor signaling (i.e.*TCR*β), hematopoietic transcription factors (i.e., *TAL1*/*SCL:* T cell acute leukemia 1/stem cell hematopoietic transcription factor*; HOXA10:* homeobox gene A10), or transmembrane cell signaling receptors (i.e., *NOTCH1)* [40]. These deviations from normal T-cell biology are highly represented among T-ALL patients, suggesting they may be suitable therapeutic targets.

The vulnerability of proliferating lymphocytes to environmental PAHs has been well demonstrated in both chronic and acute exposure scenarios. Occupational exposure to elevated PAH levels in coke oven and asphalt workers, emission inspectors, and incineration operators is correlated with decreased T-lymphocyte

proliferation in response to stimulus and with direct DNA damage as measured by the Comet assay [41,42]. Organs involved in T-cell production and maturation (i.e. spleen and thymus) constitutively express *CYP1B1* during both fetal development and adulthood [43], as does bone marrow. In mice the aryl hydrocarbon receptor (*Ahr*) and more specifically *Cyp1b1* have been demonstrated to regulate the metabolic activation and immunotoxicity of specific PAHs [44,45]. In both adult and transplacental mouse models of PAH-induced leukemia/lymphoma, expression of *Cyp1b1* was required for metabolic activation and susceptibility [31,46]. Direct effects of PAHs on the immune system include (but are not limited to) splenic and thymic atrophy, decreased T-cell viability and proliferation, and decreased response to antigen stimulus. Therefore, PAH exposure may result in defective immune-surveillance, thus increasing overall cancer risk, and/or direct initiation within lymphoid organs [47]. In particular, acute childhood leukemia (and other cancers) has been associated with decreased aryl hydrocarbon hydroxylase activity, suggesting a role for xenobiotic exposure and metabolic activation in risk [48,49].

The epidemiology of prenatal exposure to cigarette smoke, a source of PAHs, has been widely studied with inconsistent results. Polymorphisms in xenobiotic metabolizing enzymes are thought to influence the risk of childhood leukemia associated with maternal or paternal cigarette smoking [50-52]. One case-control study determined that maternal smoking during pregnancy increased the risk of ALL nearly 2-fold and that paternal smoking had a lesser but significant effect [53]. A large prospective study in Sweden found no increased risk of ALL associated with maternal smoking but did find evidence for other leukemia subtypes [54]. Others have found no correlation between maternal smoking and childhood leukemia but a positive relationship with paternal smoking [55].

A collection of work by Perera et al., uses a molecular epidemiology approach, adding biomarkers of PAH exposure and damage, environmental monitoring data, and genotype information to the risk equation. They have demonstrated that neonatal exposure to PAHs and environmental tobacco smoke is associated with reduced birth

weight and head circumference, risk factors for a number of adult diseases [2,56]. In multiple settings with increased ambient PAHs (i.e. proximal to the World Trade Center on 9/11/2001), they have observed a positive correlation between environmental PAH levels, fetal PAH-adduct levels, and reduced fetal growth [3,57-59]. Furthermore, increased chromosome aberrations in fetal cord blood correlate with PAH exposure, as measured by environmental monitoring, suggesting a potentially greater risk of carcinogenesis later in life [7,60].

1.3 Lifestyle modification and cancer risk

In 1997 a panel of scientists from the World Cancer Research Fund and the American Institute for Cancer Research estimated that 30-40% of all cancers could be prevented by modification of lifestyle factors such as diet and exercise, with specific emphasis on whole grains, fruits, and vegetables [61]. Ten years later, the second edition of this work reported evidence for a protective effect of fruits and vegetables on cancer risk ranging from “insubstantial” to “probable” depending on the food and cancer site [62]. Thus, while vegetables are generally known to be healthful as they are high in fiber, vitamins and minerals, and low in fat and cholesterol, it has been difficult to demonstrate a direct association between overall vegetable consumption and cancer prevention in humans, likely due the heterogeneity of exposures, genetics, and ultimately the diseases collectively referred to as cancer [63,64]. However, certain types of vegetables produce phytochemicals that by definition are not essential nutrients but may have beneficial health properties [65].

Phytochemicals derived from soy, tea, allium vegetables, cruciferous vegetables, and turmeric have been the focus of many *in vitro*, *in vivo*, and clinical studies based on their ability to modulate cancer-related pathways and conversely, cancer risk [66]. For example, caffeine in green and black tea has been demonstrated to induce *Cyp1A1/ 1A2* and reduce lung tumorigenesis in F344 rats initiated by the nicotine-derived, tobacco-specific-carcinogen, 4-(methylnitrosamino)-l-(3-pyridyl)-l-butanone (NNK) [67]. Caffeine additionally induced CYP1B1 activity in maternal

liver and reduced the incidence of thymic lymphoma and lung tumors in offspring in a murine transplacental model of carcinogenesis [33]. Soy or soy isoflavones have been reported to alter serum hormone levels and modulate risk of estrogen or androgen sensitive cancers (i.e. breast and prostate) and to reduce inflammation through the NFκB pathway [68]. Curcumin, derived from the turmeric root, impacts a wide range of biological targets in cancer such as de-phosphorylation / inactivation of constitutively active PI3K signaling in acute leukemia cells [69].

1.4 Cruciferous vegetables

Cruciferous vegetables have potential to reduce the risk of certain cancers. Epidemiological studies have suggested an inverse relationship between cruciferous vegetable consumption and gastric cancer, colo-rectal cancer, lung cancer, prostate cancer, breast cancer, bladder cancer, and endometrial cancer [70,71]. One explanation as to why these studies have been more suggestive than definitive may be genetic differences in how individuals metabolize these compounds; possibly some individuals would need to consume more cruciferous vegetables than others in order to receive the same level of protection [63,64]. Broccoli, Brussels sprouts, mustard, kale, cabbage, horseradish and arugula are in the Brassicaceae (cruciferae) plant family and are a rich source of glucosinolates at approximately 20 μmol/g of plant material [72]. Glucosinolates are sulfur-containing compounds which contribute to the sometimes bitter or pungent aroma and flavor of these vegetables.

Two classes of chemicals generated from the hydrolysis of glucosinolates, known as “indoles” and “isothiocyanates”, have been widely studied for their bioactive properties. The enzyme myrosinase, released from the “myrosin” cells within the plant tissue when damaged (i.e. chopped or chewed) [72], breaks the β-thioglucoside bond of a glucosinolate yielding water, glucose, and an unstable aglucon intermediate [73]. Over 120 different glucosinolates have been identified and when acted upon by myrosinase, yield unique products, although only a portion of these are found in common dietary sources [74]. Some glucosinolates are found similarly in all

cruciferous vegetables yet others are extremely abundant in particular vegetable varieties as depicted in Table 1.1.

Table 1.1 Cancer-protective indoles, ITCs and precursors in cruciferous vegetables.

Common source(s)	Glucosinolate name	ITC/indole common name	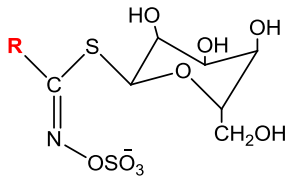 Structure of R group
broccoli / broccoli sprouts	Glucoraphanin	Sulforaphane	
	Glucoerucin	Erucin	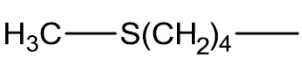
Brussels sprouts, cauliflower, flat-leafed kale	Glucobrassicin	Indole-3-carbinol	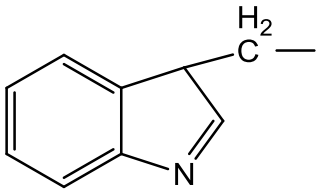
mustard greens/seeds	Singrin	Allyl - ITC	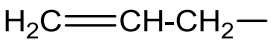
horseradish, watercress	Gluconasturtiin	Phenethyl-ITC	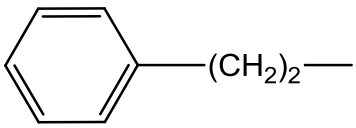
garden cress	Glucotropaeolin	Benzyl - ITC	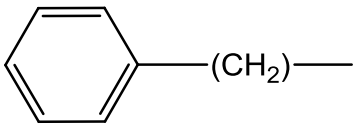

Compiled from the following sources: [75-77]

1.4.1 Indole-3-carbinol and 3,3'-diindolylmethane

Source and chemistry. Indole-3-carbinol (I3C) is derived from the glucosinolate, glucobrassicin, which is abundant in Brussels sprouts, kale, and

cabbage varietals. Indole glucosinolates, such as glucobrassicin, are derived from the amino acid tryptophan and undergo enzymatic and spontaneous breakdown to yield not only I3C, but also ascorbigen in the presence of ascorbate (vitamin C) or indole-3-acetonitrile in the presence of epithospecifier protein (ESP) [78,79]. I3C is highly unstable in an acidic environment, such as the stomach, undergoing condensation reactions with additional I3C molecules to form what are collectively referred to as acid condensation products (ACPs) [80]. In neutral cell culture media, greater than 50% conversion to a dimer known as 3,3'-diindolylmethane (DIM) occurs within 24 hours [81]. I3C in media without cells is also oxidized to indole-3-carboxaldehyde and indole-3-carboxylic acid as shown in Figure 1.1 [78]. Moreover, DIM, but not I3C, accumulates in the nucleus of cultured human breast cancer cells almost immediately after treatment with DIM and after a longer period when cells are treated with I3C [82,83].

Additional ACPs likely contribute to the anti-cancer effects associated with I3C treatment, based on their biological activities *in vitro* and *in vivo*. For example, the linear trimer (LTR-1) and ICZ oligomers bind to the AHR and activate expression of genes containing dioxin-response-elements (DREs). This was demonstrated in MCF-7 (ER dependent) breast cells by induction of ethoxyresorufin-O-deethylase (EROD) activity, a biomarker of CYP1A1 induction [84]. Microinjection of an acid produced reaction mixture (RXM) in trout embryos, in combination with aflatoxin B_1 (AFB_1), reduced AFB_1-DNA adducts by 65% compared with controls given AFB_1 alone. I3C failed to inhibit carcinogen-DNA binding yet DIM or cyclic trimer (CT) alone reduced adducts by 37% and 51%, respectfully [80]. Furthermore, oral administration of either I3C or RXM, or intraperitoneal (i.p.) administration of RXM, to male Sprague-Dawley rats dramatically induced hepatic and intestinal EROD activity while i.p. administration of I3C was largely ineffective [85].

Bioavailability, safety, and physiological relevance. In mice administered oral I3C at 250 mg/kg body weight, I3C was demonstrated to be rapidly absorbed, distributed to multiple tissues ranging from the liver to brain (in that order of

magnitude), and to fall below the limit of detection within one hour after dosing. While I3C plasma concentrations peaked within the first 15 minutes, DIM and the linear trimer (LTr) peaked at 2 hours and 6 hours, respectively, and reached concentrations equivalent to one-sixth and one-tenth of the parent compound. At 24 hours post-dose, DIM was still measurable in brain [86].

Conversely, the absolute bioavailability of I3C in humans is unknown, although a number of studies have demonstrated a biochemical or therapeutic response to I3C supplementation, suggesting that absorption of either I3C or its breakdown products does occur [reviewed in 87]. As expected, based on the results in rodents, supplementation with I3C (up to 1200 mg) to healthy human volunteers did not produce any measureable I3C in plasma in the earliest sample collected at one hour, however plasma DIM concentrations peaked by two hours (Cmax~2.5 μM) and continued to be detectable out to 24 hours [88]. This is an equivalent dose of I3C by allometric scaling to the 250 mg/kg dose in mice and peak plasma concentrations of DIM were similar in concentration (~2.5 vs ~3 μM) and timing (~2 hours) between the two species, suggesting that pharmacokinetics are similar in humans and rodents [86].

Enhanced absorption DIM, or BioResponse DIM (BR-DIM), is a commercially available supplement, formulated to improve bioavailability of DIM, and contains about 30% (wt/wt) crystalline DIM. Oral administration of crystalline versus the formulated BR-DIM confirmed a 50% improvement in bioavailability in mice [89]. In humans, a single dose of BR-DIM of 300 mg (roughly equivalent to 90 g DIM) resulted in maximum plasma concentrations of 0.4 μM in one study [90] whereas higher plasma concentrations (mean 0.96 μM) were reported for the same dose administered to four non-metastatic prostate cancer patients [91].

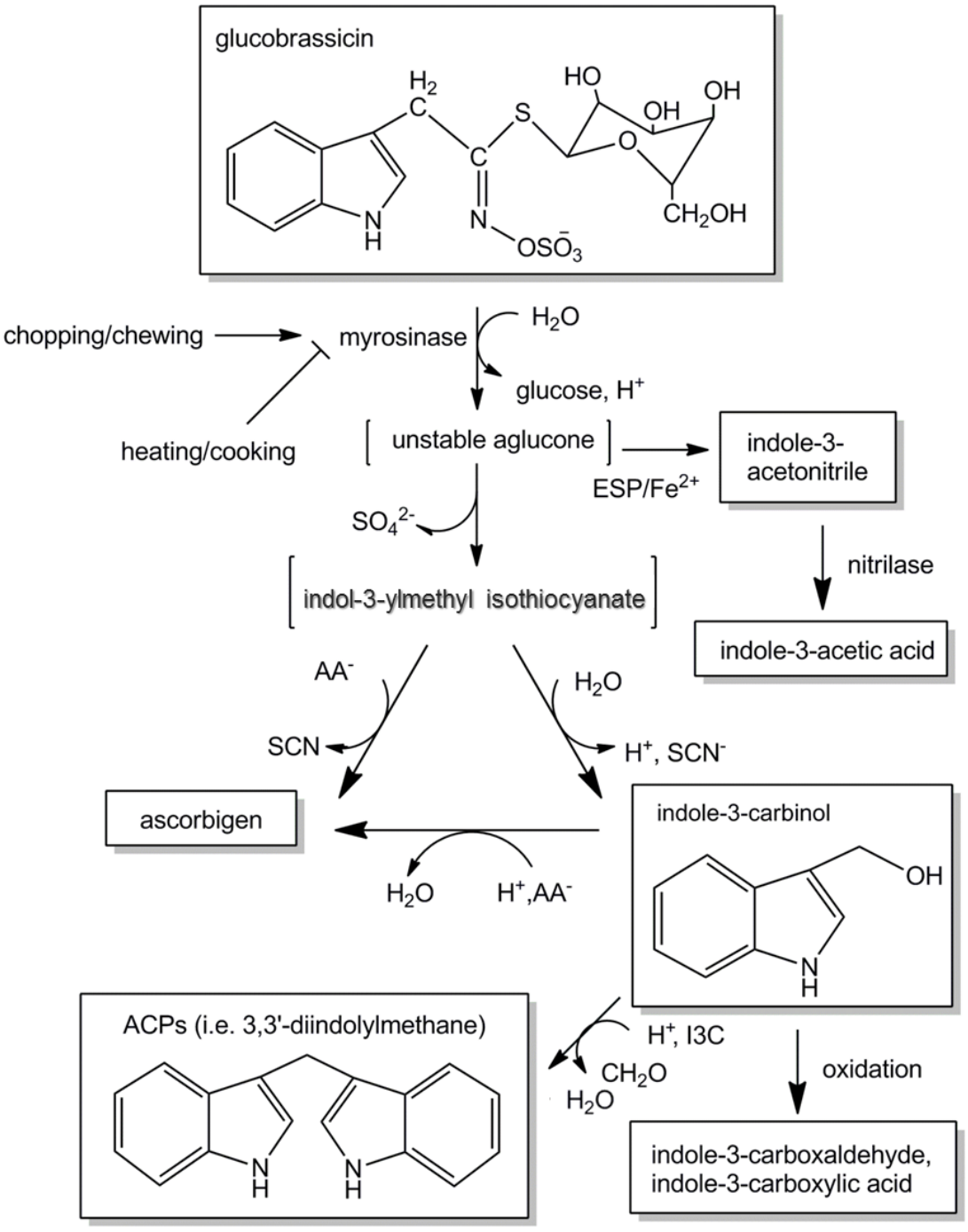

Figure 1.1 Conversion of glucobrassicin to indole-3-carbinol and related products.

In the above studies few adverse effects were reported and included mild symptoms of gastrointestinal distress and vomiting. Long term supplementation with lower levels of DIM (2 mg/kg/day) or I3C (6 mg/kg/day) were well tolerated [92,93], although the possibility for supplement users to consume more than the recommended dose is of concern as high doses of isothiocyanates or glucosinolates may be genotoxic [94,95]. Chronic dietary exposure to I3C or BR-DIM in Sprague-Dawley rats, at levels based on human supplement doses for DIM, resulted in hepatic and colonic CYP1A1 induction to a much greater extent with I3C treatment versus DIM, and to higher total hepatic CYP levels in males versus females in either treatment group [96]. As these enzymes are involved in the activation of environmental chemicals and pharmaceuticals, adverse drug interactions or cancer promotion are of potential concern. This suggests that whole food sources and concentrations of these phytochemicals may be a safer alternative to supplements for chemoprevention, while the purified phytochemicals may be good candidates for chemotherapy.

1.4.2 Sulforaphane

Source and chemistry. Interest in ITCs as antineoplastic agents has been growing since the 1960s and more recently sulforaphane (SFN), derived from glucoraphanin (GFN), has become one of the most studied ITCs. SFN was first identified as a potential chemopreventative agent in 1992, although it was previously known for its antimicrobial properties [97]. A major dietary source of GFN is broccoli with the highest concentration in the plant seed. Although it is not recommended to eat the seeds due to the presence of toxins, fresh sprouts are a rich source of GFN and SFN and, as the plant matures and grows, the GFN content is distributed throughout, having the effect of dilution [74]. ITCs, such as SFN, are the primary product following the hydrolysis of aliphatic or aromatic glucosinolates when the reaction occurs at a neutral pH [72]. Factors affecting the hydrolysis of glucosinolates will be discussed in further detail below. SFN and isothiocyanates, in general, are further metabolized via the mercapturic acid pathway beginning with the conjugation of free SFN to glutathione spontaneously or by glutathione-S-transferases (GST) to yield

SFN-GSH, followed by sequential modification of the conjugated glutathione to yield cysteinyl-glycine (SFN-CysGly), cysteine (SFN-Cys), and finally *N*-acetyl-cysteine conjugates (SFN-NAC) [98].

Bioavailability, safety, and physiological relevance. *In vitro* studies from Zhang and Callaway have demonstrated that SFN is rapidly accumulated in the cell, reaching concentrations 100 to 200-fold that of the media, converted to SFN-GSH, and exported with an intracellular half-life of approximately one hour [99]. The rapid uptake is attributed to the cellular content of glutathione that complexes with SFN, resulting in glutathione depletion and variable levels of extractable intracellular SFN conjugates at test concentrations of 50-500 μM [100]. A dose-dependent pharmacokinetic profile for SFN has also been described in rats with absolute bioavailability ranging from 20 – 80 % over a ten-fold dose range, selected to represent human levels of consumption from fresh broccoli, with the highest bioavailability at the lowest concentration. Furthermore, intracellular SFN/SFN conjugates were rapidly eliminated from the cell through a mechanism involving active membrane drug transporters [99]. In mice SFN metabolites have been reported to reach micromolar concentrations in blood, to accumulate in tissues in a dose dependent fashion, and to be cleared below detection limits within 24 hours [101]. Collectively these findings suggest that continuous exposure of SFN may be necessary in order to optimize therapeutic activity.

Safety testing of purified SFN and its precursor, glucoraphanin (GFN), has been limited to animal models for GFN and only *in vitro* for SFN. A recent review of the genotoxic/mutagenic potential of SFN and related isothiocyanates (ITCs) highlights that concentrations at or above 10 μM *in vitro* can induce DNA damage which may be related to the electrophilicity of ITCs, generation of reactive oxygen species, and the depletion of cellular glutathione pools [94]. Nuclear factor erythroid 2-like 2 (Nrf2) is generally sequestered in the cytoplasm in a complex with Kelch-like ECH-associated protein 1 (Keap1). Upon activation, for example following SFN interaction, this complex dissociates, releasing Nrf2 to translocate to the nucleus

where it binds to the antioxidant response element (ARE) in the 5' flanking region of target genes.

Thus, longer duration exposures to ITCs at lower concentrations are expected to upregulate glutathione biosynthesis through Keap1-Nrf2-ARE mediated gene expression [100]. *In vitro* and *in vivo* GFN has also been shown to induce oxidative stress and Phase I enzyme systems, suggested to increase rather than protect against cancer risk [95,102]. Therefore, it is important to consider the factors which mediate conversion of glucosinolates to isothiocyanates and the relative levels of exposure expected when consuming a supplement versus a whole food (discussed below).

1.4.3 Chemopreventative mechanisms of cruciferous vegetable phytochemicals

Multiple mechanisms exist for the anti-carcinogenic actions of indoles and isothiocyanates (ITCs). These mechanisms are broadly classified as either "blocking" or "suppressive", based on the respective phases of cancer development during which these mechanisms are effective, known as "initiation" and "progression", respectively. Before these phytochemicals were widely investigated for their anti-cancer properties, they were shown to modulate metabolism and detoxification of foreign substances in the body [103]. Efficient detoxification is thought to rely on the proper balance of Phase I and Phase II enzymes [104]. An example of Phase I mediated metabolism is the hydroxylation of nonpolar PAHs by cytochrome P450 enzymes (CYPs) to reactive PAH-epoxides, PAH-diols, and PAH-diol-epoxides, products which are further conjugated by Phase II enzymes, for excretion.

The induction of Phase I enzymes following I3C treatment *in vitro*, oral consumption of I3C, or i.p. injection of ACPs *in vivo*, is a well-documented phenomenon. For example, both *CYP1A1* and *CYP1B1* expression in MCF-7 cells is increased at sub-micromolar concentrations of I3C (0.1 μM), however DIM alone is less potent, inducing *CYP1A1* at concentrations > 50 μM [105,106]. Similarly in a feeding study with I3C (50 mg/kg) or DIM (20 mg/kg), CYP1A1 was induced by the

treatments 82- and 16-fold, respectively, in liver versus and 10- and 8-fold in the colons of male Sprague-Dawley rats [96].

Early study of SFN as a putative chemopreventative agent focused on its ability to modulate xenobiotic metabolism, predominantly by Nrf2-ARE mediated induction of Phase II enzymes such as GSTs, NAD(P)H-quinone oxidoreductase (NQO1), superoxide dismutase (SOD), and UDP-gluconosyltransfersases (UGTs) [74]. DIM is a weaker inducer of Nrf2 gene targets than SFN but a stronger inducer than I3C, based on ARE driven luciferase activity, although the relative expression of downstream genes is variable and tissue specific [107-109]. For example, *NQO1* (mRNA) was induced in human keratinocytes by SFN but not by I3C, yet SOD1 (protein), *NQO1*, *UGT1A1*, and *GSTm2* were elevated in human hepatoma cells upon treatment with I3C. PAHs and other carcinogens are detoxified following bioactivation by CYP enzymes, in part through the action of UGT and NQO1 [110]. Therefore indoles and ITCs are considered blocking agents as they are capable of altering the rate and extent to which a person, tissue, or cell can eliminate certain absorbed carcinogens.

It is generally thought that SFN is an ideal chemopreventative agent as it exhibits monofunctional enzyme induction properties, blocking Phase I activity and therefore decreasing carcinogen bioactivation, while simultaneously inducing Phase II elimination enzymes [97]. Conversely, GFN at high doses (120-240 mg/kg) induces both Phase I and Phase II enzymes (bifunctional) in the liver [102]. However, bifunctional enzyme inducers, such as I3C and GFN, are not inherently cancer promoting agents and careful consideration of dose, timing of exposure, and target organ will likely determine their effects *in vivo*. For example, I3C protected against NNK-induced lung tumorigenesis with increased hepatic NNK metabolism and significantly less NNK reaching the target organ [111]. It is also important to note that, while GFN has not been shown directly to increase cancer risk, there is a need for further study of this compound as commercially available broccoli supplements are rich sources of GFN, and often lack myrosinase to sufficiently produce SFN *in vivo*.

I3C, DIM, and SFN can also be effective in reducing the progression of initiated cancer cells by targeting a number of cancer survival pathways. Chronic inflammation in cancer is negatively modulated by SFN and DIM, in part through Nrf2-ARE signaling, as mentioned above. Collectively, these phytochemicals are known to inhibit cell-cycle progression through modulation of regulatory check-point proteins (i.e. p21, cyclins, and cyclin-dependent kinase inhibitors) that is often accompanied with apoptosis [112-116]. I3C and DIM have anti-estrogenic properties with weak affinity for the estrogen receptor and the ability to modulate estrogen metabolism through induction of CYP enzymes [117]. Both SFN-Cys and SFN-NAC inhibit global histone deacetylase (HDAC) activity [118]; interestingly, these were the predominant metabolites in mouse prostate, which may be relevant to the mechanism of chemoprotection in this and other tissues [101]. DIM has also been demonstrated to reduce class I HDAC enzyme expression through a proteasome mediated pathway in human colon cancer cells [119]. Furthermore, these phytochemicals have been shown to modulate NF-κB, Akt, MAPK, and additional signaling networks relevant to carcinogenesis, likely through complex mechanisms involving receptor cross-talk [74,120-122].

1.4.4 Factors affecting glucosinolate metabolism

It is impossible to accurately predict the level of I3C or SFN in a particular serving of broccoli, though certain factors have been identified which influence its formation *in vivo*. Cooking to high temperatures can inactivate myrosinase and lead to incomplete conversion of glucosinolates [123]. The presence of ferrous ions and the pH during hydrolysis effects the relative formation of isothiocyanate compared to nitriles, thiocyanates, and epithionitriles [72]. Certain plants, such as broccoli, also contain epithiospecifier protein (ESP) that converts the aglucon intermediate to sulforaphane nitrile (SFN-nitrile) in the case of glucoraphanin or indole-3-acetonitrile from glucobrassicin [73,78] (Figure 1.1). Mild heating of broccoli can inactivate ESP, leaving myrosinase intact, increasing SFN formation 2-7 fold [124]. This is significant considering that concentrations an order of magnitude higher of SFN-nitrile

versus SFN were required to induce the same level of phase II enzymes in mouse hepatoma cells [73]. Cultivation and storage processes or preparation techniques such as chopping, pickling, freezing, stir-frying, or microwave cooking also variably influence the amount of glucosinolates in the edible portion of these vegetables [123]. Lastly, glucosinolates that are not hydrolyzed by endogenous plant myrosinase can be processed by gut microflora with β-thioglucosidase activity [125].

1.4.5 Bioavailability, safety, and physiological relevance of I3C/SFN from whole cruciferous vegetables

The bioavailability of I3C, or its acid condensation products from whole food sources, has received little attention. A sensitive and validated method (LC-MS/MS) for the quantification of low levels of I3C, ACPs, and I3C metabolites in plasma and urine has been published. However, I3C was not detected likely due to the delay in sample collection from the time of broccoli consumption, as I3C in human plasma peaks around two hours after dosing [88,126]. Thus, further consideration of whole cruciferous vegetables as a source of I3C is needed and the above mentioned LC-MS/MS method should be validated in an animal model in order to assess target tissue concentrations following oral consumption of whole cruciferous vegetables versus supplements.

The bioavailability of SFN from whole food preparations has conversely been the subject of numerous studies, most of which focus on broccoli as a source. The most concentrated source of SFN from broccoli is from the seed itself which is further diluted as the plant matures and increases in volume [74]. Broccoli sprouts are a rich source of SFN and other isothiocyanates and, as expected, the bioavailability of SFN from broccoli sprouts is dependent on the preparation. Approximately 50% of the dose is excreted as urinary mercapturic acid metabolites following human consumption of intact fresh sprouts, compared with ~15% from boiled sprout homogenate, ~80% for fresh chewed sprouts, and ~93% from sprout homogenate with exogenous myrosinase [127]. Higher bioavailability was reported for human volunteers consuming raw mature broccoli (37%) versus microwaved mature broccoli

(3.4%) due to inactivation of plant myrosinase [128]. Significantly less SFN was excreted after 6 hours in volunteers consuming dried versus fresh broccoli sprouts containing 70 μmol SFN, although cumulative excretion was equivalent after 24 hours, suggesting intact GFN reaching the gut was hydrolyzed by resident microflora [129,130].

A similar study comparing fresh sprout intake with a commercially available broccoli supplement lacking myrosinase (BroccoMax), confirmed that bioavailability of SFN was greatly reduced in the absence of plant myrosinase, although the relative plasma and urine profiles of SFN metabolites were unchanged between the treatment groups 12 hours post dose [98]. Repeated consumption of fresh broccoli sprouts, mature broccoli slurry, or broccoli supplements at 24 hour intervals did not increase cumulative excretion profiles of SFN and metabolites in humans despite a long terminal excretion profile [131]. These findings are consistent with those *in vitro,* described above, demonstrating rapid cellular uptake and elimination of SFN such that repeated dosing may be necessary at very short time intervals in order to maintain therapeutic cellular concentrations.

Fewer investigations of safety have been conducted for pure SFN, compared to I3C or DIM, and none have been conducted in humans. Conversely, tolerance and safety has been based on broccoli derived extracts since these have been the delivery mechanism of SFN in human trials. No significant toxicity markers or adverse events were reported in a formal phase I study at such doses [132]. However, investigations of the safety or efficacy of either ITC-rich or glucosinolate-(GLS) rich broccoli sprout extracts in humans have focused only on doses achievable through reasonable consumption of the whole food (generally less than one-half cup) [98,132]. Thus, further safety testing could be performed in animal models in light of the availability of broccoli based supplements that differ from whole food with respect to concentration of GLS, ITCs, and myrosinase content.

For those who are looking for an alternative to consuming cruciferous vegetables directly, a supplement may be an attractive vehicle for sulforaphane and

I3C. Importantly, commercially available broccoli supplements that lack myrosinase do not deliver the expected dose of isothiocyanates based on glucosinolates content, a fact that consumers are likely unaware of [133]. However, a recent paper demonstrated that consumption of fresh broccoli sprouts, in combination with such a supplement, increases the plasma concentration dramatically over the consumption of either source alone [130]. Therefore, consumers desiring an alternative to raw vegetable consumption may benefit from supplementation in combination with an exogenous source of myrosinase.

1.4.6 Preclinical rodent studies with whole cruciferous vegetables

Only a small number of studies demonstrate a direct effect of whole cruciferous vegetables on carcinogenesis. For example, Sprague-Dawley rats fed Brussels sprouts during the initiation period, or administered broccoli sprout extract 2 hours prior to DMBA gavage, had significantly reduced mammary tumor incidence [134,135]. Broccoli sprout extract has further been examined with positive results in models of bladder carcinogenesis and skin tumorigenesis [136,137]. Multiple reports highlight the bioactivity of whole cruciferous vegetables relevant to carcinogenesis; most commonly noted is the alteration of Phase I and Phase II enzyme expression and activity in organs pertinent to carcinogen metabolism (i.e. liver, kidney, and colon) and/or in target sites of carcinogenesis (i.e lung, bladder, skin, and prostate) [135,138-142]. The evidence for modulation of these biomarkers varies with the amount and timing of supplementation but also the cultivation and preparation of the whole food for dietary intervention as described above. Thus, additional animal studies directly examining the effects of whole cruciferous vegetables, versus SFN or I3C, on site- and carcinogen-specific carcinogenesis are necessary in order to better interpret these biomarkers and ultimately use them to predict human relevance.

1.5 Fetal origins and epigenetic regulation

The concept that the fetal and early postnatal environment may program the developing individual to have altered susceptibility to disease in adulthood is an

exciting and growing field of research termed “fetal origins of adult disease”. It has been demonstrated that both carcinogens, such as DMBA, and nutrients (i.e. folate) can alter cancer risk in subsequent generations that are not exposed directly to the bioactive agents [20]. Loktionov et al., and others [143-145] have hypothesized that the transgenerational transmission of carcinogenesis is likely due to mutations in the germline that increase the susceptibility of progeny to later environmental insults.

Epigenetics is generally defined as the collective mechanisms which regulate cellular gene expression or phenotype in the absence of modification to the DNA sequence [146]. The most well studied epigenetic mechanisms include methylation of cytosine residues at cytosine-guanine dinucleotide sequences (CpG sites), the post-translational modification of histone proteins (i.e. methylation, acetylation, phosphorylation), and the post-transcriptional regulation of mRNA by micro-RNA (miRNA), small non-coding RNA strands [147]. Interestingly, these patterns may be heritable from one generation to the next or through cell divisions and are potentially reversible. There is convincing evidence that epigenetic mechanisms play a role in the fetal origins of adult disease, exemplified by a well-known case study on the implications of prenatal malnutrition, the “Dutch Hunger Winter”. Within this cohort of individuals exposed to famine *in utero*, reduced glucose tolerance, altered lipid profiles, a greater risk of cardiovascular disease, and increased incidence of obstructive respiratory diseases has been observed [reviewed in 148].

Specific to the risk of childhood cancer, such factors as maternal obesity/fetal over-nutrition or micronutrient deficiency during gestation have been investigated as risk factors [149,150]. Interestingly, methylation at the imprinted gene, *IGF2* (insulin-like growth factor II), was persistently reduced among this cohort compared with their same-sex siblings not exposed to famine *in utero* [151]. Conversely, general fetal over-nutrition, indicated by high birth-weight, has been identified a as risk factor in childhood hematopoietic malignancies, possibly through an *IGF*-dependent mechanism [152].

Perinatal dietary folate has been extensively studied prior and since the mandatory fortification of grain-foods to prevent neural tube defects with controversial results. For example, supplementation of weanling Apc/min mice at 4-10 times the basal requirement of folate protected against intestinal polyps (adenomas) [153]. Feeding 20x the basal requirement of folate in a chemically induced model of colorectal cancer in Sprague-Dawley rats showed no improvement over 4x concentrations and actually lessened the protective effect of folate [154].

In addition to genetic abnormalities (chromosomal translocations, inversions, duplications), aberrant DNA methylation is a well-established phenomenon in T-ALL and other hematopoietic malignancies. Patients with a "hypermethylator phenotype" have a worse prognosis and increased methylation at relapse [155,156]. For example, in 95 patients with ALL, cases with hypermethylation (compared with normal PBMCs) at multiple genes (such as *RARB*, *FHIT*, *p15*, and *DAPK*) were more likely to be of T-cell than B-cell origin [157]. In another study looking at cases of high hyperdiploid ALL, *RARB* and *FHIT* were again identified as hypermethylated although only *RARB* expression was lost [158]. Following genome-wide methylation analysis of 23 ALL cell lines, 15 genes were validated in 61 primary patient samples as being hypermethylated and re-expressed upon treatment with the DNA de-methylating and histone acetylating therapeutics, 5-AZA and trichostatin A (TSA), respectfully. Many of the hypermethylated genes identified but not validated by Kuang et al., included *TERT*, *WNT2B*, *CYP1B1*, and multiple HOX genes (*HLX1*, *DLX4*, etc.) [159]. Commonly identified pathways, including *WNT* signaling, kinase activation (*MAPK* and *EPHRIN*), transcription factors (*HOX*), and tumor suppressors (*p15*, *p21*), represent potential therapeutic targets [155,160].

As therapeutics with global and potent effects on epigenetic regulatory factors may disrupt the delicate balance of epigenetic regulation, a safer alternative may be modification of our food intake for chemoprevention. Experiments in animal models have demonstrated that exposure to certain environmental factors, such as bisphenol A, can alter DNA methylation patterns and moreover that supplementation with

methyl donor-enriched diets can counteract these changes [161]. However, as mentioned above, supplementation at supra-physiological doses for some bioactives may actually promote tumorigenesis. Therefore much more research is needed to understand the mechanism of such environment-diet interactions, the optimal timing of consumption, food matrix-effects, mixture-effects, and portions of foods that may afford protection against disease.

1.6 Transplacental chemoprevention

A limited number of transplacental studies have been conducted to examine maternal dietary modulation of cancer risk, with three among that list conducted in our laboratory (reviewed in Table 1.2). An early study by Rao et al., investigated the transplacental modulation of DMBA-induced mammary carcinogenesis by the food preservative and antioxidant butylated hydroxyanisole (BHA) in Swiss albino mice [162]. In the same laboratory model, translactational or transplacental exposure to Garam masala, an Indian spice mixture and traditional medicine, dose-dependently reduced multiple-site tumor incidence [23]. In a similar experiment, 65% of progeny developed tumors at multiple sites following transplacental DMBA exposure; administration of mustard seed oil, containing allyl-isothiocyanate, from GD 13-19 reduced this incidence to 29% at 0.05 ml/day and 16% at 0.1 ml/day. Comparable incidences of tumors were identified in translactationally exposed offspring (70% with DMBA, 32% and 18% in low and high mustard seed oil groups) yet the same dose levels of corn oil provided no protection during either period. This lack of tissue specificity and additional study of xenobiotic metabolizing enzymes lead the authors to conclude that these agents work at least in part through detoxication/blocking mechanisms [22].

As mentioned in section 1.1, our laboratory has previously established that a single oral dose of DBC (15 mg/kg) to pregnant B6129SF1 females, mated with 129S1/ScImJ males, results in aggressive thymic lymphoma in roughly 50% of offspring and lung tumors in 100% of survivors.

Table 1.2 Transplacental and translactational chemoprotection by dietary agents in preclinical rodent models.

Dietary agent	Treatment Protocol	Carcinogen	Treatment Protocol	Species/strain	Target tissue	Observations	Ref
Chlorophyllin/ chlorophyll/ spinach	2000 ppm CHL or 10% spinach; GD 9 to wean or co-gavage	DBC	15 mg/kg; GD 17 p.o.	B6129SF1 x 129S1/SvImJ mice	lymphoid and lung	Co-gavage of CHL and DBC reduced lymphoma related mortality and lung tumor multiplicity	[34]
Green tea/ EGCG/ caffeine	0.5% 1st trimester,1.0% 2nd, 1.5% 3rd in drinking water					Caffeine and caffeinated green tea reduced lymphoma related mortality; all treatments reduced lung tumor	[33]
Indole-3-carbinol	2000 ppm in diet; GD 9 to wean					Perinatal I3C reduced lymphoma related mortality and reduced lung tumor multiplicity	[32]
Mustard seed oil	0.05 or 0.10 ml/day; GD 13-19	DMBA	3 mg/day; GD 15--17	Swiss albino mice	multiple tumor sites		[22]
Garam masala	0.05 or 0.10 ml/day; PND 1-15		3 mg/day; PND 3,6,9,12, and 15			Dramatic and dose-dependent reduction in tumor incidence and number of tumors per TBA	[23]
	10 or 30 mg/day; GD 13-19		5 mg/day; GD 15--17				
	10 or 30 mg/day; PND 1-15		3 mg/day; PND 3,6,9,12, and 15				
Fiber: whole-wheat vs flax flour sources	6% in diet; GD7 to birth		5 mg/rat; PND 50 p.o.	Sprague Dawley rat	mammary gland	Fiber from whole wheat flour reduced; fiber from flax increased mammary tumor incidence and multiplicity	[169]
Flax seed	5 or 10%; GD7 to birth					5% and 10% flaxseed shortened mammary tumor latency, and 10% flaxseed increased tumor multiplicity	[168]
Choline	8, 36, or 0 mmol/kg; GD 11-17		25 mg/kg; PND 65 p.o.			Choline supplementation (36 mmol/kg) reduced tumor growth rate and prolonged survival to euthanasia	[167]
Olive oil vs corn oil	7 or 15%; 5 wks prenatal to wean		2 mg/rat on PND 35 and PND 42			Olive oil decreased incidence of mammary tumors relative to corn oil and increased markers of apoptosis	[166]
n-3 fish oil	p.o. in utero, perinatal, puberty, or adult		10 mg/rat; PND 55 p.o.			Perinatal exposure to fish oil increased tumor latency, decreased incidence	[165]
Canola oil (n-3 PUFA)	2 wks prenatal to wean	n/a	n/a	C3(1) Tag		Replacing corn oil with canola oil increased tumor latency, decreased tumor incidence and multiplicity	[164]
Vitamin E	0.1% VE; 4 wks prenatal to GD13 or 19	n/a		transgenic p53	multiple tissues	Low *In utero* VE reduced DNA oxidation and spontaneous tumor incidence in p53-deficient offspring	[163]
	10% VE; 4 wks prenatal to GD13 or 19					High *In utero* VE increased DNA oxidation in fetal tissues and spontaneous tumors in p53-deficient offspring	[173]
Soy protein isolate vs genestein	SPI 200 g/kg vs GEN 2.5 g/kg; GD 4 - 21	NMU	50 mg/kg i.v.; PND 51	Sprague Dawley rat	mammary gland	SPI but not GEN reduced tumor grade and multiplicity, increased latency	[171]
Soy isoflavones		AOM	15 mg/kg s.c.; PND 47 and PND 55		colon	*In utero* SPI but not GEN increased the percentage of animals bearing multiple colon tumors	[170]
	40 or 1000 mg/kg; prenatal through study		15 mg/kg s.c.; PND 45 and PND 52			40 mg/kg soy isoflavone slightly reduced tumor size; both diets induced Erβ	[172]

Abbreviations: GD – gestation day; PND – post natal day; VE – Vitamin E; DBC – dibenzo[def,p]chrysene; DMBA – dimethylbenzanthracene; ENU - ethylnitrosourea; SPI - soy protein isolate; GEN - genistein; TBA - tumor bearing animal; AOM - azoxymethane; s.c. - subcutaneous; i.v. - intra veinous; p.o. - per oral (gavage)

Maternal supplementation during the initiation period with I3C afforded significant protection at either site while chlorophyllin (CHL), a water-soluble derivative of chlorophyll (Chl), Chl, or spinach supplementation had no effect unless CHL was co-administered with DBC by gavage [32,34]. Interestingly, caffeine, but not the green tea derived polyphenol epigallocatechin-3-gallate (EGCG), or green tea itself, protected against lymphoma-related mortality in this model while all tea-derived treatments reduced lung tumor multiplicity [33]. Collectively these studies demonstrate that timing and matrix of treatment alters the chemoprotective effects of dietary phytochemicals and that protection may be tissue-specific.

It is accepted that the anticancer effects of dietary supplementation, prior or concurrently with carcinogen exposure, may work in part through a blocking mechanism, often by increasing metabolic clearance of the initiating agent. However when maternal dietary supplementation *in utero* precedes the initiation event, for example during puberty in a DMBA induced model of mammary tumorigenesis, it is possible that epigenetic factors play a role. Indeed, replacement of corn oil in the maternal diet with either olive oil, fish oil, or canola oil was protective in DMBA or SV40 T antigen-induced mammary carcinogenesis, collectively highlighting the importance of omega-3 polyunsaturated fats (n-3 PUFA) over n-6 PUFA [164-166]. In fact the long chain n-3 PUFA, docosahexanoic acid (DHA), found in fish oil, ameliorates intrauterine growth restriction when supplemented to the maternal diet while modifying chromatin modifying enzymes and histone methylation in the lung of post-natal pups [174].

1.7 Dissertation specific aims and hypotheses

Cancer is the number one disease-related cause of death in children, with hematopoetic neoplasms, such as leukemia and lymphoma, being most common [35]. Epidemiological evidence in humans supports data from animal models, demonstrating an increased cancer risk with *in utero* exposure to certain environmental chemicals, including polycyclic aromatic hydrocarbons (PAHs) [8,17].

In our laboratory, pregnant B6129SF1/J mice exposed to the potent carcinogen dibenzo[*def,p*]chrysene bear offspring with a significant risk of mortality due to aggressive T-cell lymphoblastic lymphomas [28]. As it has been estimated that 30-40 percent of cancers can be prevented through dietary and lifestyle modifications [65,175], this model of transplacental carcinogenesis has been adapted to examine the effect of maternal diet on the risk of cancer to offspring. The chemoprotective activities of phytochemicals derived from cruciferous vegetables, namely I3C, DIM and SFN, include altered metabolism of carcinogens and endogenous hormones, reduction of inflammation, induction of apoptosis or cell cycle arrest, and altered expression and activity of histone deacetylases [176-178].

Maternal consumption of I3C in our murine transplacental model greatly reduces the incidence of thymic lymphoma in offspring, though the mechanism for this protection has not been fully established [28]. Furthermore, it is not previously known whether the observed chemopreventative effect against transplacental T-ALL in mice will translate to chemoprotection in the human disease. This gap in knowledge limits our ability to potentially reduce the risk of childhood T-ALL by maternal consumption of cruciferous vegetables or to therapeutically exploit the active phytochemicals present in these vegetables. The long-term goal for this work is to understand the molecular mechanisms which drive transplacental DBC carcinogenesis that are ameliorated by supplementation of the maternal diet with cruciferous vegetables, or active components, and to identify conserved molecular targets in the human disease. My central hypothesis is that activation of conserved T-ALL signaling pathways between humans and mice are preventable or reversible upon exposure to I3C, DIM, SFN, and/or their combination in whole cruciferous vegetables.

Specific Aim 1: To determine the distribution of DBC and/or metabolites to fetal tissues following transplacental or lactation exposure, relative to maternal tissue distribution (Chapter 2).

My working hypothesis is that DBC is rapidly absorbed following maternal dosing and a small percentage of this dose is distributed to fetal tissues via the placenta, and

to a lesser extent through breast milk. I predict that thymus, lung, and liver may receive a greater relative exposure, contributing to the previously observed carcinogenesis at these sites.

Specific Aim 2: To determine the effects of I3C or its primary acid condensation product, DIM, on a spectrum of human T-ALL cell lines *in vitro* and in a preclinical xenograft model using dietary supplementation (Chapter 3).

My working hypothesis is that I3C/DIM will modulate cell-cycle progression and apoptosis in human T-ALL cells, as demonstrated in other cancer cell types, through known regulatory targets (i.e. D-type cyclins, cyclin-dependent-kinases, and BCL-2 family members). Further, I predict that dietary exposure to these phytochemicals will reduce the growth of human T-ALL cells implanted in an immunodeficient mouse.

Specific Aim 3: To evaluate relative effects of maternal dietary supplementation with varying concentrations of I3C, SFN, or whole food sources in a transplacental model of carcinogenesis (Chapter 4).

My working hypothesis is that SFN, broccoli sprouts, and Brussels sprouts will decrease lymphoma-related mortality and lung tumorigenesis initiated by DBC, based on their chemoprotective effects in other PAH-initiated models. I predict that I3C will also be protective, based on previous results, and in a dose-dependent fashion.

Specific Aim 4: To examine global DNA methylation changes by cruciferous vegetable components in T-ALL using the Nimblegen 3 x 720K CpG Island Plus RefSeq Promoter Arrays (Appendix 1).

My working hypothesis is that the human T-ALL cell line, CCRF-CEM, exhibits local patterns of DNA hypermethylation, consistent with carcinogenesis, and that treatment with I3C, DIM, or a formulated DIM will reverse this pattern at specific gene promoters. I predict that DIM will have a stronger effect than I3C, based on their relative anti-proliferative potency *in vitro*.

Chapter 2 Transplacental carcinogenesis with dibenzo[*def,p*]chrysene (DBC): timing of maternal exposures determines target tissue response in offspring

[#]Lyndsey E. Shorey[1,2], [#]David J. Castro[1,3], William Baird[1,4,5], Lisbeth Siddens[1,4,5], Christiane Löhr[4,5,6], Melissa M. Matzke[7], Katrina Waters[5,7], Richard A. Corley[5,7] and David E. Williams[1,3,4,5]

[1]Department of Environmental and Molecular Toxicology, [2]The Linus Pauling Institute, [4]Environmental Health Sciences Center, [5]The Superfund Research Center, [6]The College of Veterinary Medicine, Oregon State University, Corvallis, OR 97331, and [7]Pacific Northwest National Laboratory, Richland WA 99352 USA

[#]Contributed equally to the conduct of the study and preparation of the manuscript
[3]Present address: Sanford-Burnham Medical Research Institute, La Jolla, CA 92037

Cancer Letters
Volume 317, Issue 1, Pages 49-55
November 13, 2011

2.1 Abstract

Dibenzo[*def,p*]chrysene (DBC) is a transplacental carcinogen in mice (15 mg/kg;gestation day (GD) 17). To mimic residual exposure throughout pregnancy, dams received 4 smaller doses of DBC (3.75mg/kg) on GD 5, 9, 13 and 17. This regimen alleviated the previously established carcinogenic responses in the thymus, lung, and liver. However, there was a marked increase in ovarian tumors (females) and hyperplastic testes (males). [^{14}C]-DBC (GD17) dosing revealed transplacental distribution to fetal tissues at 10-fold lower concentrations than in paired maternal tissue and residual [^{14}C] 3 weeks post dose. This study highlights the importance of developmental stage in susceptibility to environmental carcinogens.

Key words: transplacental cancer, PAHs, T-cell lymphoma

2.2 Introduction

The "Fetal Basis of Adult Disease" or Barker Hypothesis is relevant to a number of chronic diseases in humans including diabetes, asthma, cardiovascular disease, and cancer as well as neurological and behavior toxicities [1,179-181]. With respect to cancer, a number of epidemiology studies have documented that exposure of pregnant women to environmental carcinogens such as cigarette smoke enhances the risk for the offspring of developing a number of cancers [53,182,183]. Animal models have documented that a number of chemicals are transplacental carcinogens including the tobacco specific nitrosamine NNK, the cooked meat mutagen PhIP (2-amino-1-methyl-6-phenylimidazo[4,5-*b*]pyridine), benzene, arsenic, phenytoin, drugs targeting HIV and polycyclic aromatic hydrocarbons (PAHs) [8,12,28,184-188]. PAHs have been documented to be bioavailable to the fetus and to generate DNA damage [2,59,189,190]. Dibenzo[*def,p*]chrysene (DBC) is an extremely potent environmental PAH in animal models of carcinogenesis and has recently been reclassified by the International Agency for Research on Cancer (IARC) from possibly carcinogenic (2B)

to probably carcinogenic in humans (2A) [191]. Our laboratory has demonstrated that exposure of pregnant mice (C57B6129F1 dams bred to 129 males) to a single dose of DBC (15 mg/kg by gavage) during late pregnancy was carcinogenic to the offspring [28]. Over half the offspring had to be euthanized due to an aggressive T-cell lymphoblastic lymphoma that invaded almost every organ. The surviving mice at 10 months had a 100% incidence of pulmonary tumors (multiplicity of about 15) and approximately 70% of the males (and almost no females) had liver lesions (primarily precancerous lesions and adenomas) [28]. Subsequent studies with *Cyp1b1* knockout mice demonstrated that fetal *Cyp1b1* was required for development of the T-cell lymphoma [31]. Cross-fostering studies further demonstrated that the 2-3 day *in utero* exposure to DBC resulted in much higher lymphoma-associated mortality than exposure to residual DBC in the breast milk over the 3 weeks of nursing [30].

Developmental expression of CYPs in the 1 family is important in the transplacental toxicities of PAHs [192]. Studies with expressed mouse and human CYPs have found that CYP1A1 and CYP1B1 are effective in the bioactivation of PAHs to mutagenic and carcinogenic metabolites, primarily diol-epoxides. For example, benzo[*a*]pyrene-7,8-*trans*-dihydrodiol-9,10-*syn*-epoxide (BPDE) is one of the more potent mutagenic products of CYP metabolism of benzo[*a*]pyrene and forms DNA adducts, primarily at 2'-deoxyguanosine and 2'-deoxyadenosine [193]. Expressed CYP1A2 exhibits lower activity toward PAHs than other members of the CYP1 family [194] and is not expressed at appreciable levels in the mouse until after birth [195]. Surprisingly, CYP1A1 (not expressed constitutively in liver but inducible by aryl hydrocarbon receptor (AHR) ligands, including PAHs) activity appears to provide protection against PAH toxicity as the *Cyp1a1* null mice exhibited enhanced sensitivity to PAHs [44]. *Cyp1b1*, like *Cyp1a1*, is not expressed constitutively in liver but is inducible via the AHR (although not to the same degree as *Cyp1a1*); rather it is found constitutively in a number of extrahepatic tissues including testis, ovary, thymus, breast and prostate [196] and is expressed at high levels in the third trimester of pregnancy [195].

As the major enzymes involved in PAH bioactivation are expressed in a tissue- and developmental-specific manner during embryogenesis, and to better model human exposures, we examined DBC transplacental carcinogenesis when maternal exposure occurred during all trimesters. For comparison with a single 15 mg/kg dose on GD17, the dose was divided into 4 smaller doses administered (3.75 mg/Kg by gavage) on GDs 5, 9, 13 and 17. These periods cover all three trimesters including the first which is often the most sensitive to teratogenic effects. We report here that this multiple-dosing regimen of DBC to the pregnant mouse produced a marked alteration in the carcinogenic response in the offspring. Studies with [^{14}C]-DBC were also performed to determine the time-dependent levels of radioisotope distribution in maternal and fetal target tissues, as well as in urine and feces, following a single oral dose (15mg/kg GD17).

2.3 Materials and methods

Chemicals. DBC (CAS No.: 191-30-0; formerly referred to as dibenzo[*a*,*l*]pyrene) was obtained from the National Cancer Institute (NCI) Chemical Reference Standard Repository at Midwest Research Institute (Kansas City, MO)and was greater than 98% purity as determined by HPLC with UV detection [28]. Uniformly labeled [^{14}C]-DBC was obtained from the NCI Radiochemical Carcinogen Reference Standard Repository previously operated by Chemsyn Science Laboratories (Lenexa, KS) with a specific activity of 51.4 mCi/mmol. This material was purified by Tjaden Biosciences, LLC (Burlington, IA) to >99% radiochemical purity. Other reagents utilized in this study were as described previously [28,30,31].

Animals and Diets. Breeding pairs of mice (B6129SF1/J females and 129S1/SvImJ males, eight weeks of age) were purchased from Jackson Laboratories (Bar Harbor, ME) and housed under pathogen-free conditions (micro-isolator cages from Life Products, Inc., Seaford, DE with Care FRESH bedding) at 20° ± 1°C and 50% ± 10% humidity with a light/dark cycle of 12 hrs. Following arrival, mice were acclimated for 1 week prior to the initiation of breeding. Offspring were housed

separately by sex and litter and fed AIN93G until three months of age and then AIN93M (both from Research Diets, New Brunswick, NJ) diet until the study was terminated at 10 months. Mice were observed daily for any signs of pain or discomfort and if any were observed the mice were euthanized by CO_2 asphyxiation followed by necropsy. All procedures used for the handling and treatment of mice in this study were approved by the Oregon State University Institutional Animal Care and Use Committee.

Study Design. Females were paired with males and monitored daily for the appearance of a vaginal plug (denoted GD0). The dams were dosed either with a single gavage of 15 mg/kg DBC in corn oil (5 ml/kg) on GD17 or with four total gavages (3.75 mg/kg DBC each) given to the dam on GD 5, 9, 13 and 17. Offspring were housed and monitored as described above until 10 months of age. To determine the distribution of total [^{14}C]-DBC equivalents to the fetus, a subset of dams were randomly chosen and administered 300 μCi [^{14}C]-DBC/kg, diluted to a specific activity of 20 μCi/mg DBC (to yield a dose of 15 mg/kg on GD17), again by gavage in corn oil. The first experiment consisted of a time course with four dams dosed on GD17 and four respective litters collected at each time point (2, 4, 6 or 8 hrs after dosing). Dams and fetuses were euthanized appropriately (CO_2 asphyxiation and cervical dislocation for dams and decapitation for fetuses), blood was collected into heparinized vials and spun at 15,000 g for 15 min to separate plasma. Tissues and plasma (as well as maternal urine and feces) were stored at -80°C until analysis. A second cross foster experiment was conducted to assess transplacental versus translactational exposure as previously described [30]. Briefly, dams were gavaged with [^{14}C]-DBC (n=3) or corn oil (n=3) on GD17 and monitored for the delivery of offspring. After birth, neonates from DBC-treated mothers were randomly assigned to a foster corn oil-treated mother and vice versa so as to receive exposure only *in utero* or through lactation. At post-natal day 21 (PND21), when these mice are normally weaned, tissues and plasma from a total of 40 pups (6 litters) and the 3 dams

administered [^{14}C]-DBC were euthanized and tissues collected as described above, again pooling within a litter as the dam represents the experimental unit.

Histopathology. At 10 months of age surviving mice were euthanized by CO_2 asphyxiation and a number of tissues (thymus, lung, liver, spleen, heart, kidney, testis, ovary, uterus, colon, skin, and any (abnormal) lymph nodes) examined first by gross necropsy and then fixed in 10% formalin. Fixed tissues were routinely processed to paraffin blocks, and hematoxylin and eosin-stained sections were analyzed by a board-certified histopathologist as previously described [28].

Sample preparation for liquid scintillation [^{14}C]-DBC analysis. Fetal tissues including lung, liver, GI tract (stomach through colon with contents) were pooled by tissue type within a litter and solubilized directly as described previously [32]. Maternal plasma, spleen and lung or homogenized portions of liver, GI tract (with contents), placenta, and kidney, were solubilized accordingly. Feces required extended solubilization time and bleach to remove color. Samples were then clarified with 1:5 H_2O_2: 2-propanol, treated with glacial acetic acid to remove chemiluminescence and stored overnight in the dark before measuring radioactivity by liquid scintillation.

Statistical Analysis. Litter size and sex ratio were assessed with Fisher's exact test comparison of vehicle control and DBC treatment groups and found to not be significantly different at $p < 0.05$. Comparisons of tumor multiplicity between four low doses of DBC and a single dose of DBC evaluated the number of tumors per mouse for those with tumors. A mixed-effects linear model was used to determine if there was statistically significant evidence between dose groups in body weight and multiplicity. The random effects of gender and litter were included in the model. There was statistically significant evidence of differences in body weight between the control and DBC groups ($p < 0.001$), as well as differences in multiplicity between the four low doses and single high dose groups ($p < 0.001$). In addition, there was evidence of considerable variance across the random effects gender and litter in the measurement of body weight. Statistical analyses were performed using Matlab R2011a (Version

7.12.0.635). Maternal and pooled-litter (fetal) [^{14}C]-DBC concentrations in both the time-dependent tissue distribution and cross-foster studies were roughly log normal and hence log transformed for analysis. Each tissue (or ratio of tissues) of interest was analyzed separately. [^{14}C]-DBC concentrations were compared between the four time points by overall ANOVA (n=4 dams/litters sacrificed per time point) followed by trend and/or other contrasts. For the cross-fostered study there were n=3 pairs, so that the data are shown for each cross-foster litter pair and the by-tissue paired t-tests; comparing the exposure routes, had low power (2 denominator degrees of freedom and considerable residual variation).

2.4 Results and discussion

Maternal and Fetal Toxicity: Previous studies, utilizing this same cross of mouse strains and dosing with DBC on GD 17, did not result in any maternal or fetal toxicities as evidenced by the lack of an impact on the sex ratio (1.20 and 1.09, respectively), litter size (7.8 and 7.1) or birth weight [28]. In the present study there was no treatment-related effect on litter size or offspring gender (Table 2.1). Treatment of dams with multiple doses of DBC did not result in smaller pups at birth but there was a significant difference with respect to body weight of the pups upon weaning (11.8 g versus 9.6 g, $p < 0.0001$).

Table 2.1 Gender, birth weights, and litter size.

Group (#litters)	Males,Females (M/F)	Pups/Litter	B.W. (at weaning)
Controls (5)	17,16 (1.06)	6.6 ± 1.0	11.8 ± 0.9
DBC (5)	18,13 (1.38)	6.2 ± 2.1	9.6 ± 1.6*

*$p < 0.0001$

DBC Transplacental Carcinogenesis: The greatest difference in tumor response in the offspring from *in utero* exposure following treatment of dams with DBC at 4 doses of 3.75 mg/kg (maternal body weight) at GDs 5, 9, 13 and 17, compared to a single dose of 15 mg/kg at GD 17, was a total lack of mortality due to an aggressive T-cell lymphoblastic lymphoma. This lymphoma appears from ages 3-6

months much like what is observed in *Tp53* $^{(-/-)}$ mice on the same genetic background [197]. Following termination of the study, when offspring were 10 months of age, a marked difference in target organ response was observed between treatment regimes. The incidence of lung tumors in all our previous studies employing the single high dose was 100% and the average lung tumor multiplicity was 13-15 (tumors/tumor-bearing mouse) [28,30,31,33,34]. When a smaller DBC dose is administered over all trimesters, the lung tumor incidence was reduced to 80% (data not shown) and the multiplicity significantly reduced to 2.6 ± 0.4 ($p < 0.0001$) (Figure 2.1, right panel).

Gestational age at exposure to ethylnitrosourea (ENU) markedly influences the multiplicity, size and morphology of lung tumors [198,199]. The greatest period of susceptibility to transplacental ENU lung tumorigenesis appears to be around GD16, possibly due to variable rates of clonal expansion in the developing tissue [199], with lung morphogenesis beginning on GD10 [200]. In addition to changes in cellular proliferation and differentiation throughout gestation, age-specific susceptibility to mutagenic transplacental carcinogens such as ENU or PAHs may be due to differences in expression of metabolic enzymes or in repair pathway activation. As treatments were administered in this study on GD 5, 9, 13, and 17, it is possible that this window of susceptibility and the lower individual doses were both factors in the reduced lung tumor multiplicity observed. The reduction in liver lesions was also striking. Previously, the single high dose resulted in a lesion (precancerous lesions and adenomas) incidence of 70% (almost exclusively in males) while the multiple low doses yielded only a 6.3% incidence (data not shown).

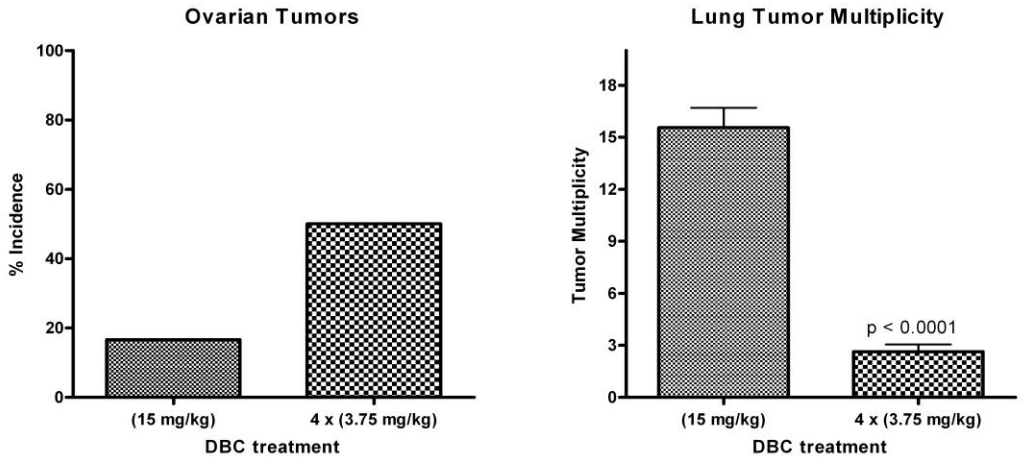

Figure 2.1 Ovarian and lung tumor incidence and multiplicity.
Offspring born to a mother treated with multiple doses of DBC (3.75 mg/kg GDs 5, 9, 13, 17) versus a single dose at 15 mg/kg GD17 have increased ovarian tumor incidence (left panel) and decreased lung tumor multiplicity (right panel).

In contrast to the reduced response in lymphoma, lung and liver tumors, a marked increase in the incidence of ovarian tumors was observed (Figure 2.1, left panel and Figure 2.2A). Histologically, the ovarian tumors presented as sex-cord stromal tumors and included granulosa cell tumors, granulosa cell-theca cell tumor, and luteoma. Some of the tumors had extensive necrosis and hemorrhage. It is possible that exposure to DBC earlier in gestation (during organogenesis and gonad differentiation) is responsible for this pathology. Exposure of C57BL/6 mice to the PAHs benzo[*a*]pyrene (BaP) and 7,12-dimethylbenz[*a*]anthracene (DMBA) *in utero* during early development (maternal treatment with 6 mg/kg total just prior to conception) reduced the number of primordial follicles by over two thirds [201]. Interestingly, the ovarian toxicity also occurred following lactational exposure but the greatest impact was if the mothers of female offspring were exposed both pre-pregnancy and during lactation. The toxicity was shown by Jurisicova et al., to be aryl hydrocarbon receptor (AHR)-dependent with the use of AHR antagonists [201]. We did not determine the impact of $Ahr^{b\text{-}1/d}$ (responsive) versus $Ahr^{d/d}$ (non-responsive) genotype on the degree of ovarian toxicity nor did we examine lactational exposure as

a separate factor (pups were exposed to residual DBC from distribution to maternal breast during gestation). The uteri of ovarian tumor-bearing mice were examined and all showed cystic endometrial hyperplasia, a fairly common finding in older mice but previously not seen to any great degree in 10 month-old offspring from the B6129F1 x 129 cross.

In male offspring, abnormally small testes were seen, a pathology not previously observed with the late gestation single DBC dose (Figure 2.2B). Histologically, these testes showed diffuse atrophy of seminiferous tubules, marked Leydig cell hyperplasia, and scattered granulomas. Ohsako et al., [202] found that exposure of mice on GD14 to the high potency AHR ligand TCDD resulted in an AHR-dependent negative impact on prostate development. TCCD has been known to be a reproductive toxicant in mice and other rodents, reducing ano-genital distance and sperm viability later in life [203,204]. Leydig cell hyperplasia has been documented in male mice following transplacental exposure to estradiol and diethylstilbestrol [205,206]. Evidence also exists in humans for maternal smoking similarly producing a negative impact on testicular development, possibly due in part to PAH exposure [207,208].

Our results suggest differential tissue susceptibility to DBC, depending on age of development at exposure. These findings are similar to studies with an environmental mixture of PAHs, cigarette smoke, that differentially affects cancer incidence and target organ depending on the developmental window of exposure in mice [209]. An alternative explanation, provided by Buters *et al.*, is that lower individual doses of DBC exert less acute toxicity to immune cells thereby prolonging survival time and allowing alternative tissue malignancies to develop [210].

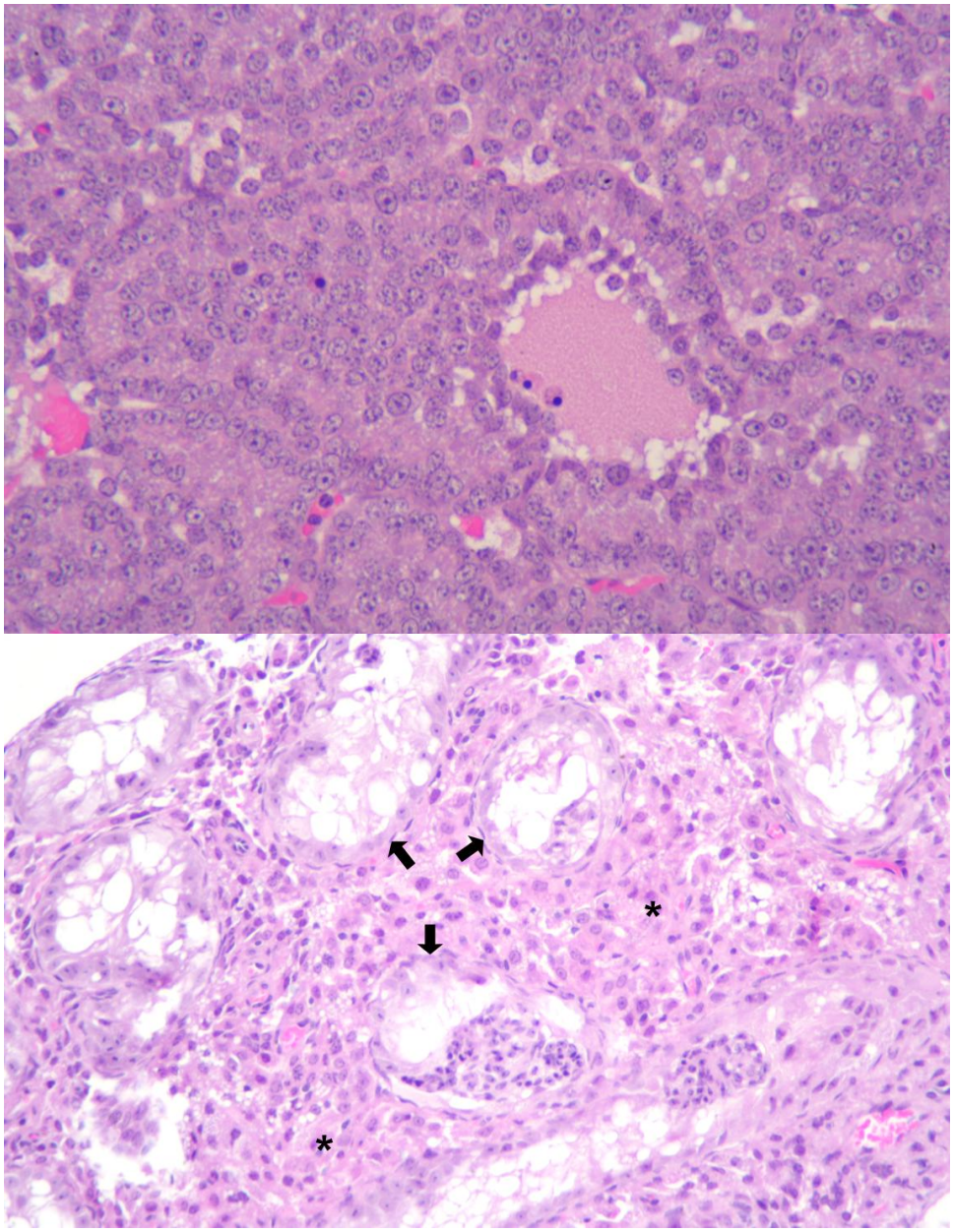

Figure 2.2 H&E stained sections of reproductive tissues.

(Top) Photomicrograph of a granulosa cell tumor in the ovary of a 10-month-old offspring born to a mother treated with DBC (3.75 mg/kg GDs 5, 9, 13, 17). (Bottom) This unusually small testis collected at necropsy from a 10-month-old offspring born to a mother treated with DBC (3.75 mg/kg GDs 5, 9, 13, 17) shows atrophic seminiferous tubules (arrows). Note the increased number of interstitial (Leydig) cells (asterisks).

[^{14}C]-DBC Distribution. Tissue levels of [^{14}C]-DBC equivalents (DBC plus metabolites) were measured in maternal and fetal tissues, as well as in urine, plasma, and feces in separate animals euthanized at 2, 4, 6 and 8 hrs following a single (15 mg/kg, ~10 μCi) dose by gavage on GD17. The geometric mean of maternal plasma from mice sacrificed at 2, 4, or 6 hrs was fairly constant at about 1.5 μg/ml DBC equivalents (Figure 2.3B) whereas the animals euthanized at 8 hrs had about 1.8-fold lower levels (C_{max} of approximately 3 μM). Maternal GI tract with contents exhibited a significant increase between animals euthanized at 2 hrs and animals euthanized at 4 hrs and the majority of radioisotope (~75%) remained there throughout the 8 hr period (Figure 2.3A). Interestingly, the placenta was the only maternal tissue measured to increase in concentration between 6 and 8 hrs. The placental tissue in mice administered [^{14}C]-benzo[a]pyrene (BaP) has similarly been shown to retain radioactivity much longer than other maternal organs [18]. When expressed as a ratio relative to plasma concentration, the following maternal tissues exhibited an approximately constant percent increase per hr (kidney, 23.6%; liver, 19.6%; lung, 9.9%, and placenta, 26.4%).

Compared to maternal plasma, the fetal tissues exhibited 4- to 13-fold lower levels of [^{14}C]-DBC over the 2 to 8 hrs after gavage (Figure 2.3B). Levels of [^{14}C] were still increasing at 8 hrs in the fetal GI tract and thymus but appeared to have reached a plateau in lung and liver. The concentrations at 8 hrs were 773, 748 and 1274 ng [^{14}C]-DBC equivalents/g tissue (wet wt.) in fetal thymus, lung and liver, respectively (Figure 2.3C). For animals euthanized at 8 hrs, maternal lung and liver levels were 8- and 16-fold higher, than the respective fetal tissue (Figure 2.3A,C). The fetal tissue:plasma ratios did not increase over the first 6 hrs nor did they differ between tissues, however at 8 hrs this ratio increased dramatically as plasma levels dropped, with fetal GI tract:plasma significantly higher than other tissues.

The elimination of [^{14}C]-DBC in maternal urine and feces was also followed over the 2-8 hr time-course demonstrating that the great majority of [^{14}C]-DBC equivalents were eliminated in the feces as expected for an oral exposure (Figure

2.3D). However, this study was not designed to characterize the pharmacokinetics of DBC or its metabolites directly nor was it of sufficient duration to fully define the clearance of [^{14}C]-DBC as shown in Figure 2.4. Such a study is currently in progress where the pharmacokinetics of DBC and its diol and tetrol metabolites are being evaluated more extensively in cohorts of 36 non-pregnant and 36 pregnant (GD17) mice (B6129SF1/J) administered DBC at the same dose level (15 mg/kg) used in the current studies. Preliminary results indicate that the half-lives for the clearance of DBC from blood determined in subgroups of 3-4 mice sacrificed at various times over 48 hr increased from approximately 7.2 hr in non-pregnant mice to 14 hr in pregnant mice. This longer half-life corresponded to increased peak concentrations and areas under the curve for DBC in blood in pregnant mice (13.7 +/- 10.4 µM and 2911 µmol*min/L, respectively) vs. non-pregnant mice (3.5 +/- 0.3 and 1136 µmol*min/L, respectively). Work is in progress to more completely evaluate the impact of pregnancy on the pharmacokinetics of DBC and its metabolites in blood, feces, urine, tissues, and fetuses (where applicable) from these mice. Such data will facilitate the continued development and refinement of a physiologically based pharmacokinetic model for DBC that will ultimately be used to relate dose levels used in these mouse carcinogenicity studies to relevant human exposure scenarios[211].

In our previous studies on the transplacental carcinogenesis properties of DBC, we performed a study with a cross-foster design [30]. We were somewhat surprised to see that the majority of the T-cell lymphoblastic lymphoma mortality was due to the short 2-3 day *in utero* exposure; pups exposed only through breast milk had little mortality. Lung tumor multiplicity at 10 months of age was also significantly higher in offspring only exposed *in utero*. We speculated that the difference may be that DBC, like other PAHs, had a relatively short half-life in the dam and by parturition, little DBC remained to partition into breast milk.

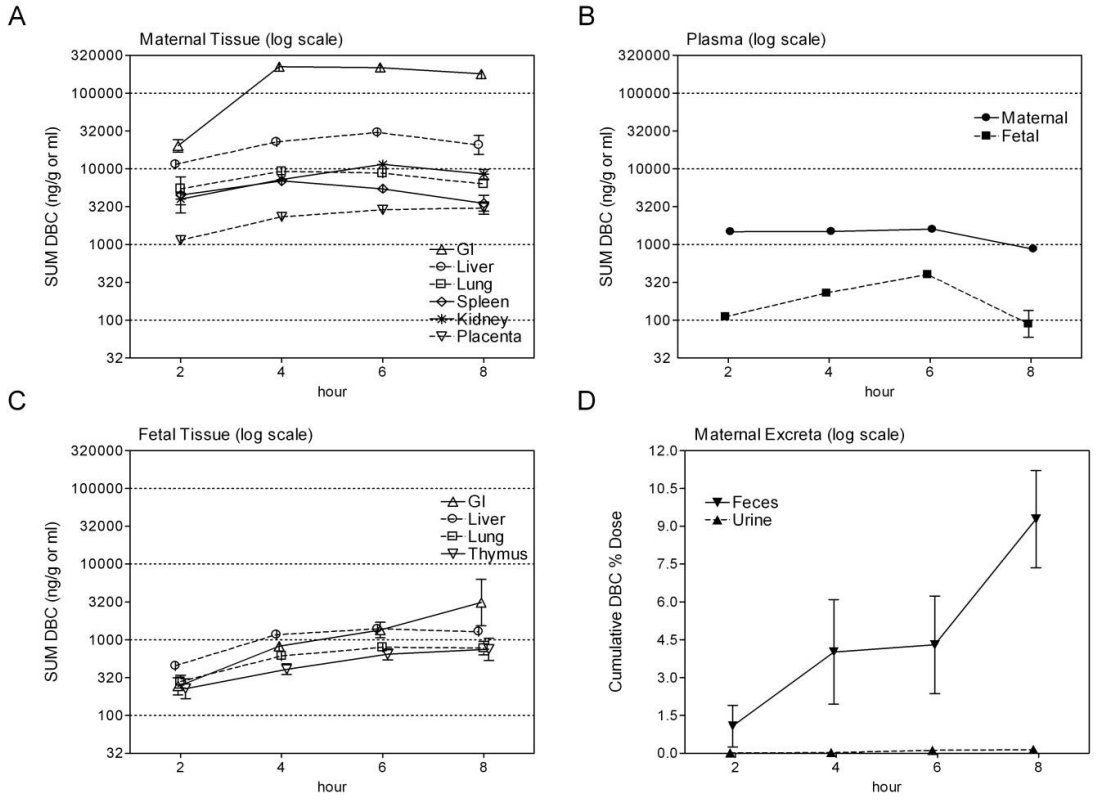

Figure 2.3 Maternal and fetal [^{14}C] distribution and excretion.
Pregnant mice received a single oral dose of 15 mg [^{14}C]-DBC/kg body weight on GD17. Transplacental transfer to fetus and maternal distribution of [^{14}C]-DBC, or metabolite equivalents (SUM DBC), was evaluated at 2, 4, 6, and 8 hrs post-dose. Bars represent the mean and standard error, n=4 litters or 4 dams per time-point. Total [^{14}C]-DBC for maternal and fetal tissues over time is depicted in panels A and C, respectively, whereas the maternal and fetal plasma levels are shown in panel B. Time-dependent cumulative excretion of [^{14}C]-DBC equivalents in feces and urine is shown in panel D.

It was outside the scope of this study to examine the residual DBC at the onset of lactational exposure or to measure partitioning of DBC into breast milk. When cross-fostered litters were matched according to exposed dam, we were unable to detect any significant difference in the concentration of [^{14}C]-DBC equivalents in offspring exposed only *in utero* versus through continuous lactational exposure at the end of 3 weeks (Figure 2.4). This demonstrates that DBC reaches the previously characterized target organs (thymus, lung, and liver) following exposure to a single

dose of DBC (15mg/kg on GD17) both transplacentally and translactationally. However, our results represent total [^{14}C] with no further identification of the chemical identity. Thus, a more thorough study of the pharmacokinetics of DBC in this transplacental model requires that we characterize DBC metabolites and DBC-covalent adducts in the various maternal and fetal tissues throughout gestation and lactation, and is now ongoing as described above.

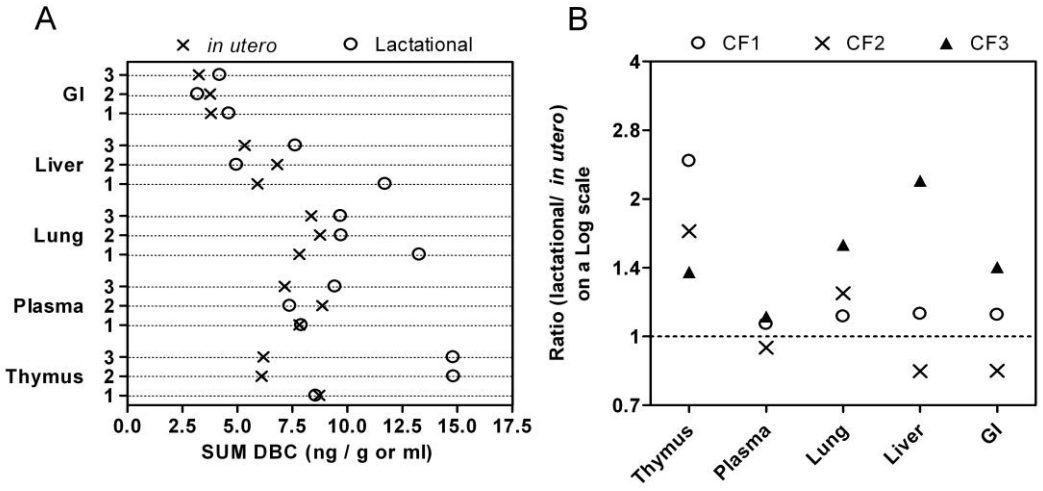

Figure 2.4 Neonatal tissue and plasma concentrations at weaning (PND21) are similar following *in utero* or lactational exposure to [^{14}C]-DBC.

Three litters were exposed *in utero* following oral gavage of the mother with [^{14}C]-DBC and at birth exchanged with a litter from a vehicle-treated dam (cross-fostered) such that the paired litter received DBC exposure via lactation. Raw data for three pairs of cross-fostered litters demonstrate variable tissue profiles according to the cross-fostered group (panel A). The log 2 ratio of SUM DBC (DBC or metabolite equivalents) from paired lactational/ *in utero* exposure litters (panel B) is generally greater than 1 (represented by the dotted horizontal line).

DBC-DNA adducts in fetal lung, reported in one of our previous studies [34], was similar to maternal lung. The major DNA adducts of DBC are derived from CYP1-dependent epoxygenation, followed by hydrolysis to the trans-dihydrodiol (DBCD) which is epoxygenated a second time to 11,12-*trans*-dihydrodiol-13,14-epoxide (DBCDE, 4 possible enantiomers). These fjord region PAH diol-epoxides, in most animal models [212-214], are more carcinogenic than the bay region BPDEs.

Human and mouse CYP1B1 are very efficient at carrying out both epoxygenations, followed by CYP1A1 with a smaller contribution from CYP1A2 [193,194].

The absolute requirement for *Cyp1b1* expression in fetal thymus [31] for induction of T-cell lymphoma suggests that one or more of the key steps in the bioactivation of DBC occurs in the fetal compartment. Given the very high chemical reactivity of the most potent of the diol-epoxide metabolites, DBCDE, it is unlikely that it crosses the placenta and distributes to fetal thymus tissues without hydrolysis or reaction with nucleophiles.

In conclusion, we have demonstrated in this manuscript that the target tissue response for PAH-dependent transplacental carcinogenesis in this mouse model is dependent, to a large degree, on the stage of development during exposure. The high sensitivity to developing T-cell lymphoma when the dam is dosed on GD17 is consistent with the developmental expression of Cyp1b1 (thymus expresses the highest level of Cyp1b1 mRNA during late gestation in both mouse and human) [43,197]. Current studies are underway to determine if the ontogeny of expression of various members of the Cyp1 family are critical for prediction of target organs for transplacental carcinogenesis (or other developmental toxicities) and if these genes could be promising targets for chemoprevention [215,216] of transplacental cancer. Finally, studies of the potency of actual PAH environmental mixtures as transplacental carcinogens are underway to better assess potential human health risk.

Acknowledgements**:** The authors would like to thank Marilyn Henderson, Tammie McQuistan, and Abby Benninghoff for their technical expertise and Mandy Louderback for animal handling assistance. Support from this study was provided by the following PHS grants from NIH, P42 ES016465, P01 CA90890, T32ES07060 and P30 ES03850 along with assistance from The Linus Pauling Institute at Oregon State University.

Chapter 3 3,3'-Diindolylmethane induces G_1 arrest and apoptosis in human acute T-cell lymphoblastic leukemia cells

Lyndsey E. Shorey[1,2], Amanda M. Hagman[3], David E. Williams[1,2], Emily Ho [2,4], Roderick H. Dashwood[1,2] and Abby D. Benninghoff [3,5,6]

[1]Department of Environmental and Molecular Toxicology, [2]Linus Pauling Institute, [4]Department of Nutrition and Exercise Sciences, Oregon State University, Corvallis, OR 97330, USA., [3]Department of Animal, Dairy and Veterinary Sciences, [5]School of Veterinary Medicine, [6]USTAR Applied Nutrition Research, Utah State University, Logan, Utah 84322-9815, USA.

PLoS ONE
Volume 7, Issue 4
April 13, 2012

3.1 Abstract

Certain bioactive food components, including indole-3-carbinol (I3C) and 3,3'-diindolylmethane (DIM) from cruciferous vegetables, have been shown to target cellular pathways regulating carcinogenesis. Previously, our laboratory showed that dietary I3C is an effective transplacental chemopreventive agent in a dibenzo[*def,p*]chrysene (DBC)-dependent model of murine T-cell lymphoblastic lymphoma. The primary objective of the present study was to extend our chemoprevention studies in mice to an analogous human neoplasm in cell culture. Therefore, we tested the hypothesis that I3C or DIM may be chemotherapeutic in human T-cell acute lymphoblastic leukemia (T-ALL) cells. Treatment of the T-ALL cell lines CCRF-CEM, CCRF-HSB2, SUP-T1 and Jurkat with DIM *in vitro* significantly reduced cell proliferation and viability at concentrations 8- to 25-fold lower than the parent compound I3C. DIM (7.5 μM) arrested CEM and HSB2 cells at the G1 phase of the cell cycle and 15 μM DIM significantly increased the percentage of apoptotic cells in all T-ALL lines. In CEM cells, DIM reduced protein expression of cyclin dependent kinases 4 and 6 (CDK4, CDK6) and D-type cyclin 3 (CCND3); DIM also significantly altered expression of eight transcripts related to human apoptosis *(BCL2L10, CD40LG, HRK, TNF, TNFRSF1A, TNFRSF25, TNFSF8, TRAF4*). Similar anticancer effects of DIM were observed *in vivo*. Dietary exposure to 100 ppm DIM significantly decreased the rate of growth of human CEM xenografts in immunodeficient SCID mice, reduced final tumor size by 44% and increased the apoptotic index compared to control-fed mice. Taken together, our results demonstrate a potential for therapeutic application of DIM in T-ALL.

Key words: Diindolylmethane, indole-3-carbinol, lymphoblastic leukemia, T-ALL, antiproliferative, cell-cycle regulation, apoptosis, cancer prevention

3.2 Introduction

Acute lymphoblastic leukemia (ALL), the most frequently diagnosed cancer in children ages 0 to 19 years [35], comprises a diverse population of malignant lymphoid progenitors undergoing clonal proliferation at various stages of differentiation [217]. The American Cancer Society estimates that 6,050 people in the United States will be diagnosed with ALL in 2012 [36], and incidence rates of ALL have increased significantly over the past thirty years [35]. Cases of T-cell origin (T-ALL) comprise 15% of ALL patients. Prognosis for these patients is poor, because they are less responsive to combination chemotherapy and are more likely to relapse than their B-cell counterparts [37].

New strategies in cancer therapy utilize drugs that specifically target aberrant signaling pathways in order to reduce toxic side effects, yet such specific therapies are only effective in a small percentage of this highly heterogeneous disease population. For example, more than half of T-ALL cases are characterized by a gain-of-function mutation in the Notch1 receptor, which leads to constitutive activation of Notch-mediated cell proliferation and survival [218-220]. Therapeutic gamma secretase inhibitors (GSIs) prevent cleavage of the intracellular Notch (ICN) domain and subsequent transcriptional activation of Notch target genes [221-223]. Subpopulations of T-ALL patients and cell lines (including CEM, SUP-T1, and Jurkat cells) are insensitive to GSI therapy, presumably due to mutations that result in constitutive ICN expression or additional mutations in genes downstream [221] such as phosphatase and tensin homolog (*PTEN*), a tumor suppressor and negative regulator of the PI3K/AKT/mTOR signaling pathway [224]. Due to the complexity and diversity of T-ALL signaling pathways, therapeutic efficacy and safety may be improved through the use of natural products that target multiple cancer signaling pathways, either alone or adjuvant to systemic or directed chemotherapy [66,225].

Evidence from epidemiological and animal studies shows that modification of the diet to increase consumption of cruciferous vegetables is sufficient to reduce cancer risk [reviewed in 65,72]. Furthermore, maternal consumption of vegetables

was shown to be inversely associated with ALL in a population-based study [226]. The bioactive food component indole-3-carbinol (I3C) is produced from the hydrolysis of glucobrassicin, present at high concentrations in cruciferous vegetables such as Brussels sprouts, broccoli, cabbage and cauliflower [70]. The anticancer effects of I3C have been well-documented in various tumor cell types including colon, breast, and prostate [reviewed in 178,227]. However, I3C is unstable in acidic environments such as the stomach and rapidly undergoes self-dimerization and oligomerization to yield over 15 acid-condensation products (ACPs) [228]. A major product of this reaction *in vitro* [229] and *in vivo* [90] is 3,3'-diindolylmethane (DIM). Because DIM has greater stability than the parent compound [86,228,230], it is expected that DIM contributes significantly to the anticancer effects of dietary I3C and is more effective at an equivalent molar dose.

Herein, we report for the first time that DIM markedly reduces the proliferation and survival of four different human T-ALL cell lines, which were selected to represent the heterogeneity of the disease. The anticancer effects of DIM were exerted by modification of critical regulators in the cell cycle pathway leading to induction of G1 arrest and apoptosis. Subtle differences in sensitivity within this group of cell lines were observed, although DIM was more potent than its parent compound I3C in all cases. Of particular importance was the observation that DIM reduced growth of human CEM cells in a xenograft model when supplemented through the diet. Collectively, the data presented below suggest that DIM could be an effective anticancer agent in T-ALL cases originating from T cells at different stages of differentiation and at concentrations that can be reasonably achieved *in vivo* in humans and in animal models**.**

3.3 Materials and methods

Materials

The following chemicals and reagents were purchased from the indicated suppliers: I3C from Sigma-Aldrich Co. (St. Louis, MO), Matrigel Matrix from BD

Biosciences (Franklin Lakes, NJ) and ViaCount Flex Reagent from Millipore (Billerica, MA). DNase I and the NuPAGE system for SDS-PAGE, including 10% and 4-12% Bis-Tris gels and appropriate electrophoresis and transfer buffers, were purchased from Invitrogen (Carlsbad, CA). Antibodies for immunoblotting were obtained from Cell Signaling Technology (Danvers, MA), including β-actin and α-tubulin primary antibodies and the Cell-Cycle Regulation Antibody Sampler Kit (contains primary antibodies for CCND3, CDK4, and CDK6 as well as HRP-linked anti-mouse and anti-rabbit IgG secondary antibodies). DIM was kindly provided in a bioavailable formula (BioResponse-DIM, herein referred to as DIM) by BioResponse, LCC (Boulder, CO), which was certified to contain 30% DIM (wt/wt) by Eurofins-Alpha Laboratories (Petaluma, CA). This bioavailable form of DIM, rather than the pure crystalline DIM, has been utilized for many of the preclinical and clinical studies in the published literature and is the common form provided in commercial dietary supplements. For these reasons, we selected the BioResponse formula for the experiments outlined below. Experimental concentrations reported in this study were adjusted accordingly (e.g. treatment with 12.3 μg/ml BioResponse DIM is equivalent to 3.7 μg/ml DIM, or 15 μM DIM).

In vitro experiments with human T-ALL cells

Cell line and culture conditions. T-ALL is a heterogeneous disease resulting from the developmental arrest and abnormal proliferation of T-cells at different stages of maturation [231]. Four human T-ALL lines representing this heterogeneity were selected for this study, including human CCRF-CEM (CEM) cells, CCRF-HSB2 (HSB2) cells, SUP-T1 cells and Jurkat cells (see Table 3.1). Cell lines were characterized by their respective vendors at time of accessioning, and cells were passaged fewer than 15 times and no longer than 3 months after acquisition. All cell lines were maintained in phenol red-free RPMI-1640 medium (Sigma-Aldrich) containing 10% (v/v) charcoal-stripped, heat-inactivated fetal bovine serum (FBS; Atlas Biologicals, Fort Collins, CO or Caisson Laboratories, Logan, UT) in a humidified incubator at 37°C with 5% CO_2. The CEM line was selected for further

characterization and study in a xenograft model based on its classification as an immature lymphoblastic T-cell population with an immunophenotype similar to that observed in our murine model of transplacental carcinogenesis [28] and its demonstrated ability to form solid tumors in subcutaneous xenograft models [232]. DIM and I3C were prepared as concentrated stock solutions in DMSO, which were stored at -80°C protected from light. For *in vitro* experiments, cells were seeded 24 hr prior to treatment at appropriate concentrations for each specific endpoint. On the day of treatment, dilutions of DIM and I3C were prepared so that all experimental treatments contained 0.1% DMSO (v/v), including a vehicle control.

Cell proliferation, viability, and apoptosis. T-ALL cells were treated with 0 up to 60 μM DIM or 0 up to 500 μM I3C for up to 48 hr. The concentration of viable cells was determined at each indicated time point by the ViaCount Assay (Millipore, Billerica, MA) as recommended by the manufacturer using either the GUAVA Personal Cell Analyzer (Guava Technologies Inc, Hayward, CA) or the C6 flow cytometer (BD Accuri Cytometers Inc, Ann Arbor, MI); assay performance was comparable on both instruments. Raw data were compared to the time-zero control for cell proliferation and the time-matched control for viability. Concentration values for 50% inhibition (IC_{50}) of T-ALL cell proliferation and viability by I3C and DIM were calculated by non-linear regression using a sigmoidal dose-response with variable slope (Prism 5, GraphPad Software, LaJolla, CA).

Cell-cycle analysis. T-ALL cells were treated with 0 to 15 μM DIM for up to 48 hr, rinsed in cold PBS, fixed in ice cold 70% EtOH, and stored at least overnight at -20°C. On the day of analysis, cells were washed with PBS and incubated for 30 min in the dark in staining solution (25 μg/ml propidium iodide, 0.1 % (v/v) Trition X-100 and 0.2 mg/ml RNase in PBS). Flow cytometry was used to determine cellular DNA distribution using the GUAVA PCA or Accuri C6 instruments and the numbers of cells in each cycle were analyzed using MultiCycle software (Phoenix Flow System, San Diego, CA) or FlowJo Cytometry Analysis Software (Ashland, OR).

Immunoblotting. Cells were treated with 0 to 15 μM DIM for 12 or 24 hr or with 0 to 500 μM I3C for 24 hr, then lysed in IP lysis buffer (20 mM Tris, 150 mM NaCl, 1 mM EDTA, 1 mM EGTA, 1% (v/v) Triton X-100, 2.5 mM $Na_4P_2O_7 \bullet 10H_2O$, 1 mM $C_3H_9O_6P$, 1 mM Na_3VO_4, 1 μg/ml leupeptin and 0.5% protease inhibitor cocktail III (EMD Chemicals, Gibbstown, NJ)). Protein concentration was determined using the Coomasie Plus Assay (Thermo Scientific, Rockford, IL) and an equal amount of protein for each sample was separated by SDS-page electrophoresis and transferred to nitrocellulose membranes. Membranes were blocked for 1 hr in 5% non-fat milk or BSA prior to overnight incubation at 4°C with primary antibodies for CCND3, CDK4, or CDK6 (all 1:1000 dilution). Membranes were subsequently incubated with the appropriate HRP-conjugated secondary antibody for 1 hr. Immunoreactive proteins were visualized using an Alpha Innotech Imaging Station (Cell Biosciences, Santa Clara, CA) and the Western Lightning ECL reagent (Perkin Elmer, Waltham, MA). Protein bands of interest were measured by densitometry using FluorChem 8800 software (Cell Biosciences, Santa Clara, CA). Membranes were stripped using Restore Western Blot Stripping Buffer (Thermo Scientific) and tested for removal of antibodies before re-probing with β-actin or α-tubulin. Changes in protein expression, normalized to β-actin or α-tubulin, were calculated as the mean difference in percentage compared to time-matched vehicle controls (0.1% DMSO), which were assigned a value of 100%.

TUNEL analysis *in vitro*. The terminal deoxynucleotidyl transferase dUTP nick end labeling method (TUNEL) was applied to CEM treated with 0-15 μM DIM for 48 hr. The In Situ Cell Death Detection kit with Fluorocein (Roche) was used to label DNA strand breaks and the Guava Express Plus program was used to sort and quantify the amount of TdT incorporation. Detailed methods, including sample preparation and fluorescent microscopy, are provided in Supplemental Materials. The apoptotic index (AI) was calculated from the flow cytometry results as follows: AI = (number of TUNEL-positive cells/total number of cells) x 100.

Table 3.1 Human T-ALL cell lines used in this study.

Cell line (abbreviation)	CCRF-HSB2 (HSB2)	CCRF-CEM (CEM)	SUP-T1	Jurkat (JM)	Ref.
Source (Cat #)*	NIH-AIDS (497)	ATCC (CCL-119)	NIH-AIDS (100)	NIH-AIDS (4668)	
Age in years/gender	11/m	3/f	3/m	14/m	[231]
Immunophenotypic classification [a]	Pre-T	Pre-T	Cortical T	Mature T	[231]
CD3 (cytoplasmic)	−	+	+	+	[231]
CD3 (surface)	−	−	−	+	[231]
CD4	−	+	+	+	[231]
CD8	−	−	+	−	[231]
CD1a	−	−	+	−	[231]
Somatic mutations in T-ALL tumor suppressors [a]					
CDKN2A(p16)	+	+	+	+	[233]
RB1	−	−	−	−	[233]
TP53	−	+	+	+	[233]
PTEN	−	+	−	+	[233]
Oncogene profile (frequency in T-ALL)					
NOTCH1 activating mutation (50-60%) [a]	+	+	+	+	[233,234]
TAL1 expression (25%)[b]	+++	++	−	++	[234]
STIL-TAL1 fusion[a]	+	+	−	−	[234]
LYH1 expression[b]	+	++	−	−	[234]

* ATCC, American Type Tissue Collection; NIH AIDS Research and Reference Reagent Program.

[a] Indicates presence (+) or absence (-).

[b] Indicates relative expression (-, +,++, or +++).

Quantitative PCR for apoptosis pathway. Total RNA was extracted using TRIZOL reagent (Sigma-Aldrich) as recommended by the manufacturer from triplicate samples of CEM cells treated with 7.5 μM DIM for 4 or 24 hr. cDNA synthesis was performed using 2 μg RNA per sample with the RT2 First Strand synthesis Kit (SABiosciences, Frederick, MD); quantitative PCR analysis for 84 genes related to human apoptosis was performed using the RT2 Profiler PCR Array System (SABiosciences) with the iCYCLER iQ5 Real-Time PCR System (Bio-Rad, Hercules, CA). Relative gene expression was calculated using the ΔΔCt method [235] with the housekeeping genes B2M and GAPDH selected for normalization. Transcripts were considered absent if Ct >35 and were removed from analysis.

In vivo xenograft study with human CEM cells

Animal care and diet preparation. All protocols for the handling and treatment of mice were reviewed and approved by the Oregon State University Institutional Animal Care and Use Committee (Animal Care and Use Protocol #3837). Male NOD.CB17-Prkdcscid/SzJ (SCID) mice were purchased from Jackson Laboratories (Bar Harbor, ME) at 7 weeks of age and housed at the Laboratory Animal Resource Center at Oregon State University under controlled conditions of 20 ± 1°C and 50 ± 10% humidity with a 12:12 hr light/dark cycle in micro-isolator cages (Super Mouse750TM Micro-Isolator TM, Life Products, Seaford, DE) with CareFRESH bedding. Mice were acclimated for one-week prior to any experimental procedures. Experimental diets were prepared by incorporating 500 or 2000 mg I3C, or 350 mg BioResponse-DIM (contains 100 mg DIM) per kg of powdered AIN93G diet (Research Diets, New Brunswick, NJ). All prepared diets were γ-irradiated (2.5 mRads) and stored at -20°C, protected from light throughout the course of the study.

CEM cell xenograft study. Detailed methods for the xenograft study are provided in the Supplemental Materials. Briefly, CEM cells were freshly collected, prepared in a 1:1 (v/v) solution of medium/Matrigel, and engrafted subcutaneously (10^7 cells/site) into SCID mice. Mice were fed diets containing 500 ppm I3C, 2000

ppm I3C, or 100 ppm DIM (350 ppm BioResponse-DIM) ad libitum for one-week prior to engraftment and throughout the course of the study. Xenograft measurements were conducted every third day with digital calipers, and tumor volume was estimated using the equation for an ellipsoid ($L \times W^2 \times \pi/6$).

TUNEL analysis of human CEM cell xenografts. Detailed methods for staining and analysis of xenograft tissues by TUNEL for detection of apoptosis are provided in Supplemental Materials. Briefly, serial sections of xenografts were stained using the In Situ Cell Death Detection kit, POD (Roche) with few modifications from the manufacturer's protocol. The apoptotic-index (AI) was calculated as follows: AI = (manual count TUNEL positive/auto count negative) × 100.

Statistical analyses

GraphPad Prism 5 software (LaJolla, CA) was used for all statistical analyses. One or two-way ANOVA were performed as appropriate for the number of experimental factors being examined. Statistical significance was inferred when $p < 0.05$ and was denoted in each figure as follows: *, $p < 0.05$; **, $p < 0.01$, and ***, $p < 0.001$. Non-linear regression analyses were performed using the equation for exponential growth to determine the impact of experimental diet on the doubling time (DT) of CEM xenografts. DT was calculated as follows: $DT = [(T_o-T_i)\ln_2]/\ln(V_o/V_i)$ where T_i and T_o represent the initial and final time points and V_i and V_o represent initial and final tumor volumes. A significant effect of DIM on gene expression was inferred when the relative fold change was greater than 1.5-fold ($\log_2 R < -0.58$ or > 0.58) with a *p-value* < 0.05 (Student's t-test) compared to time-matched controls.

3.4 Results

Impact of DIM treatment CEM cells in vitro

DIM and I3C inhibit CEM cell proliferation. To determine the impact of DIM and I3C on growth of a representative human T-ALL cell line, a time-course study was performed over a range of concentrations using CEM cells. DIM and I3C blocked the proliferation of CEM cells in a time- and concentration-dependent manner (Figure 3.1A-B). Treatment with the highest concentrations of DIM or I3C significantly reduced CEM cell viability by up to 58 or 82%, respectively (Figure 3.1C-D). Significant inhibition of proliferation and a decrease in viability was observed after 24 hr treatment with DIM or I3C, with the greatest response observed by 48 hr. However, I3C was substantially less effective and much greater concentrations (> 62.5 μM) were required to significantly reduce CEM cell growth or decrease viability compared to DIM (> 7.5 μM).

Comparison of efficacy of DIM and I3C in multiple T-ALL cell lines. Concentration-response experiments were performed in four different T-ALL cell lines to determine whether DIM and I3C are similarly effective in reducing growth of T-ALL cells derived from T-cells at different stages of differentiation. In all cell types, *in vitro* treatment with DIM for 48 hr markedly reduced cell proliferation (IC_{50} values of 8 to 15 μM) and cell viability (IC_{50} values of 7 to 27 μM), whereas I3C was much less effective (proliferation IC_{50} values of 86 to 262 μM; viability IC_{50} values of 83 to 284 μM) (Figure 3.2; Table 3.2). HSB2 cells were the most sensitive to inhibition of cell growth by DIM and I3C.

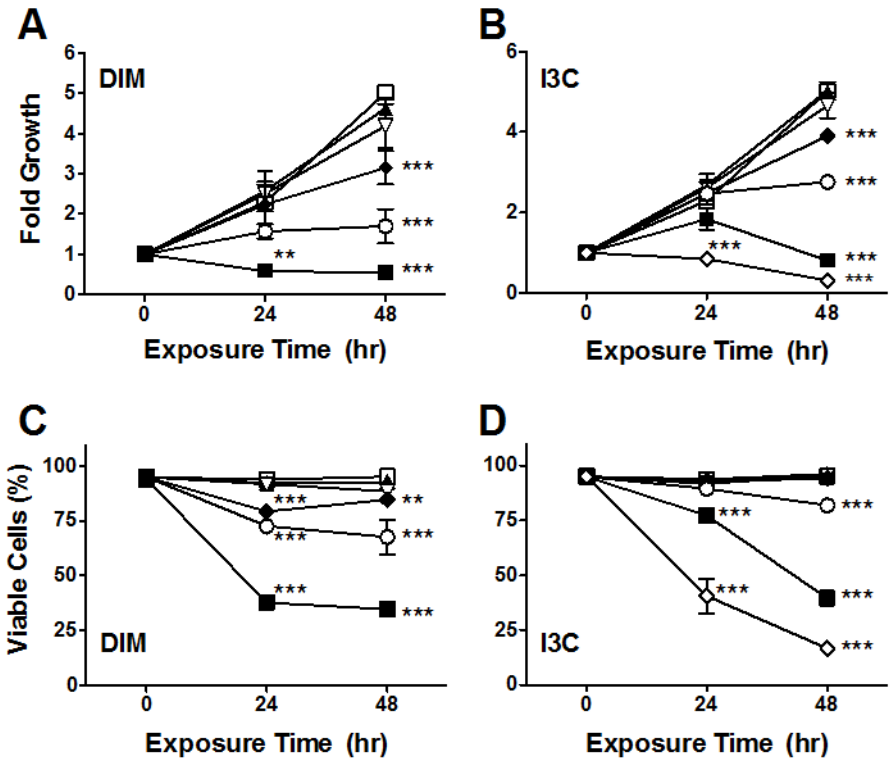

Figure 3.1 I3C and DIM reduce proliferation and viability of CEM cells.
Cells were treated with 0 (□), 1.9 (▲), 3.8 (▽), 7.5 (◆), 15 (○), or 30 (■) μM DIM (panels A,C) or 0 (□), 15.6 (▲), 31.3 (▽), 62.5 (◆), 125 (○), 250 (■), or 500 (◇) μM I3C (panels B,D) for 24 or 48 hr, then stained with ViaCount reagent for analysis of viable cell concentration and percent viability. Values are the mean fold change in cell proliferation (panels A, B) or percent viability (panels C, D) ± SEM (n = 3 independent experiments) normalized to control cells at 0 hr. **, $p < 0.01$ and ***, $p < 0.001$, as determined by two-way ANOVA with Bonferroni post-hoc test comparisons for significant effects of DIM treatments at each time point compared to time-matched vehicle control (0.1% DMSO).

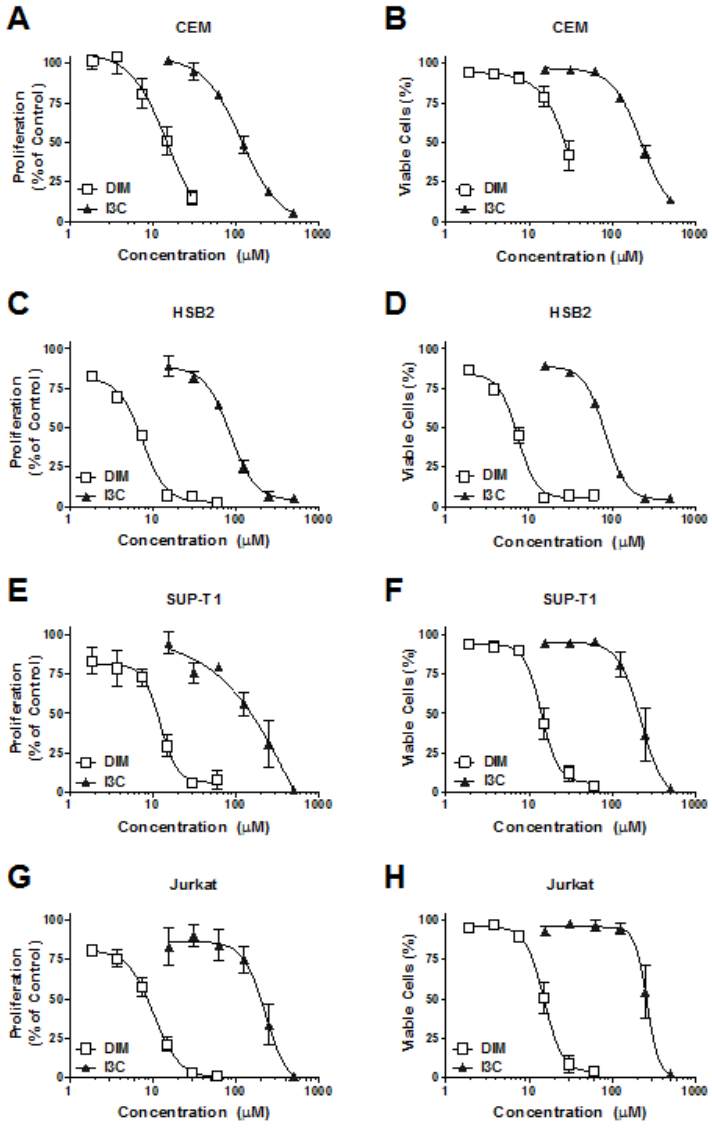

Figure 3.2 Comparison of I3C and DIM in multiple human T-ALL cell lines.

Human CEM, HSB2, SUP-T1 and Jurkat cells were treated for 48 hr with I3C (15.6 up to 500 μM) or DIM (1.9 up to 60 μM), then stained with ViaCount reagent for analysis of cell concentration and percent viability. Values are the mean level of cell proliferation (panels A-D) or the mean percent viable cells (panels E-F) ± SEM (n = 3 independent experiments), normalized to the time-matched vehicle control (0.1% DMSO). Non-linear regression analysis (four parameter, variable slope) was performed (GraphPad Prism) to generate the concentration-response curve for each chemical in each cell line, from which IC_{50} values were obtained (see Table 3.2).

Table 3.2 Inhibition of T-ALL cell growth by DIM and I3C.

	IC_{50} (μM) for DIM		IC_{50} (μM) for I3C	
Cell line	Proliferation	Viability	Proliferation	Viability
CEM	15	27	122	223
HSB2	8	7	86	83
SUP-T1	13	14	262	284
Jurkat	9	15	228	222

Note: Non-linear regression analyses (four parameters, variable slope) were performed using data generated from each DIM and I3C concentration-response curve generated for each of the four cell lines tested (GraphPad Prism v5.0, San Diego, CA). IC_{50} values are the concentrations of DIM or I3C required to inhibit cell proliferation or viability by 50% compared to the vehicle control (0.1% DMSO).

DIM induces cell cycle arrest in CEM and HSB2 cells. The marked suppression of proliferation by DIM prompted us to evaluate cellular DNA content by flow cytometry in each of the four T-ALL cell lines. Treatment of CEM or HSB2 cells with 7.5 or 15 μM DIM for 48 hr resulted in a significant G1 cell cycle arrest, with substantially fewer cells progressing to the G2/M phase (Figure 3.3). Shorter duration DIM treatment (6 and 12 hr) in CEM cells also caused a significant G1 arrest (data not shown). On the other hand, DIM treatment did not significantly alter cell cycle progression in either SUP-T1 or Jurkat cells (Figure 3.3). Additionally, at the higher concentrations of DIM tested, a sub-G1 peak was observed in the raw histogram data (for example in CEM cells approximately 10% at 7.5 μM, and about 14% at 15 μM; data not shown) indicating an increasing population of apoptotic cells.

Next, we measured the expression of key regulatory proteins of cell cycle progression by immunoassay in CEM cells. DIM suppressed expression of key cell cycle regulatory proteins *in vitro*, a finding that is consistent with DIM-induced G1 growth arrest (Figure 3.4). Treatment with DIM for 12 or 24 hr decreased expression of CCND3 and CDK4 proteins in a concentration-dependent manner (i.e., 38% and 56% decrease after treatment with 15 μM DIM for 24 hr, respectively), whereas a trend for decreasing CDK6 expression was evident (up to 48% decrease after 15 μM

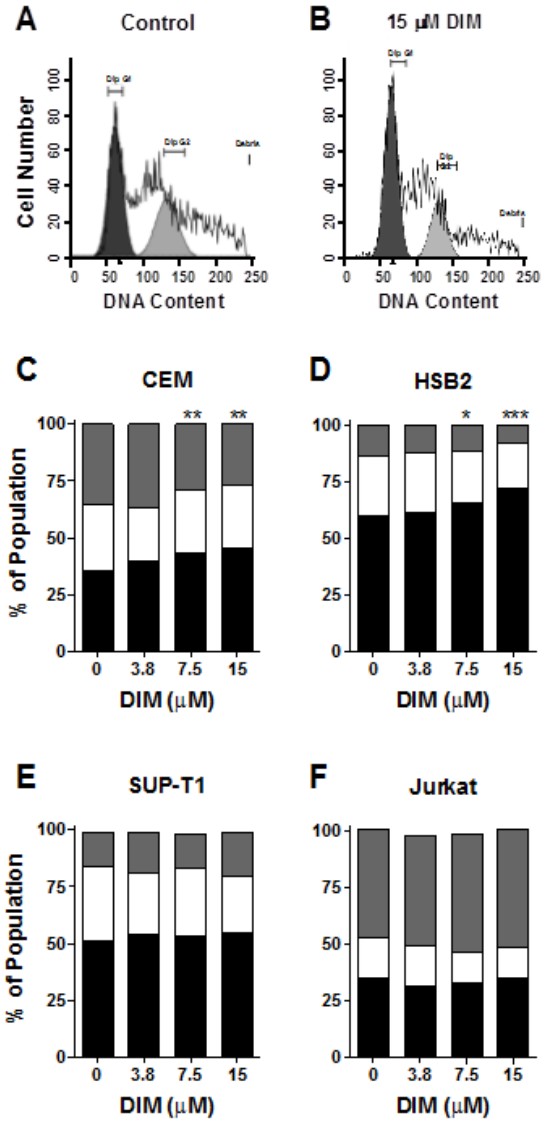

Figure 3.3 DIM induces cell-cycle arrest in CEM and HSB2 cells.

Cells were treated with 0, 3.8, 7.5, or 15 μM DIM for 48 hr, then fixed in ice-cold 70% EtOH and stained with propidium iodide. DNA content distribution was analyzed by GUAVA PCA or Accuri C6 flow cytometry. (A-B) Representative histograms are shown for control and 15 μM DIM treatments at 48 hr in human CEM cells. (C-D) Distributions of CEM, HSB2, SUP-T1 or Jurkat cells in G1 (black), S (white), and G2 (grey) phases of cell-cycle progression at 48 hr (n = 3 to 5 independent experiments). *, $p < 0.05$; **, $p < 0.01$ or *** $p < 0.001$ for G1 arrest compared to the vehicle control (0.1% DMSO) as determined by one-way RM ANOVA (matching by experiment day) with Dunnett's multiple comparisons post-hoc test.

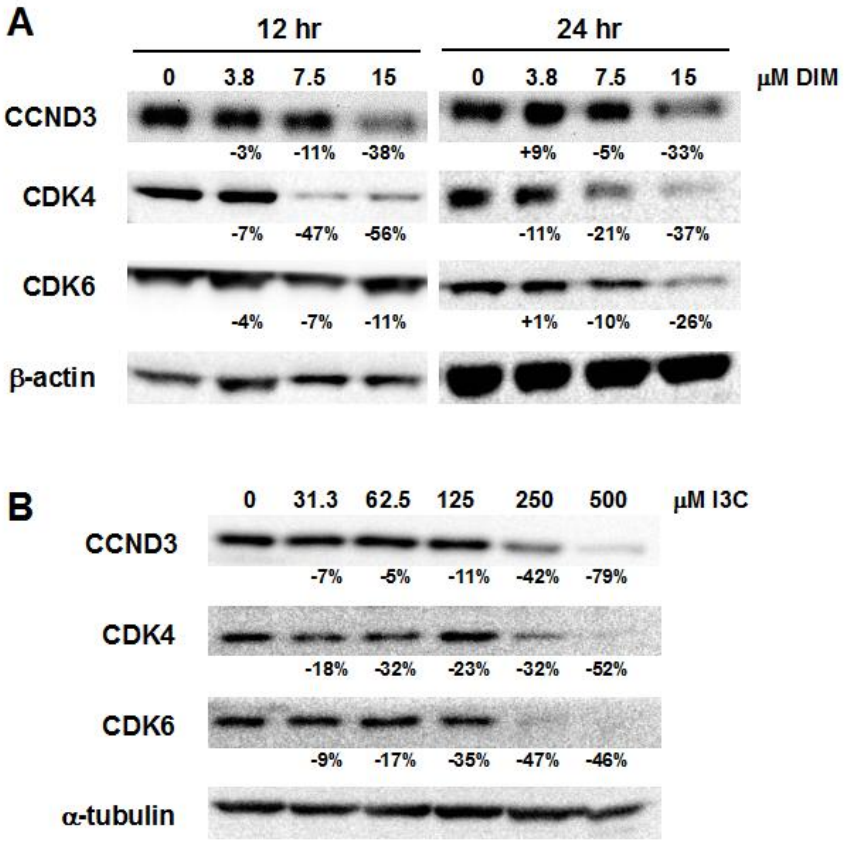

Figure 3.4 DIM reduces expression of cell-cycle regulatory proteins.

Following either 12 hr (gray bars) or 24 hr (black bars) treatment with increasing concentrations of DIM, CEM cells were harvested and protein immunoassays were performed for detection of CCND3, CDK4 and CDK6 proteins (three replicate experiments performed). (A) A representative immunoblot is shown for each protein assay. (B) Values shown are average protein expression ± SEM normalized to β-actin, expressed as a percentage difference from time-matched vehicle controls (0.1% DMSO), which were assigned a value of 100%. *, $p < 0.05$ or **, $p < 0.01$ compared to 0 μM DIM (vehicle control) as determined by one-way ANOVA with Dunnett's post-hoc test for multiple comparisons; overall ANOVA p-values within each time group are indicated in each panel. In some cases where the p-value for the ANOVA was not < 0.05, a significant linear trend was evident, as indicated by trend p-values in the figure. Finally, a Student's t-test (***, $p < 0.001$) was performed to compare 15 μM DIM to vehicle control for CCND3 expression at 24 hr because high variability observed at the 3.8 μM concentration confounded the ANOVA post-hoc results (overall effect of DIM was significant).

DIM for 24 hr). I3C also decreased expression of CCND3, CDK6 and CDK4 at 24 hr (data not shown), albeit at supra-physiological concentrations (>100 μM) that have been shown to be cytotoxic in healthy peripheral blood mononuclear cells [236].

DIM induces apoptosis in T-ALL cells. Two methods for assessing the impact of DIM on apoptosis were used in this study. First, the portion of apoptotic cells following treatment with DIM for 48 hr was determined by the ViaCount assay. In all four T-ALL cell types, treatment with 15 μM DIM caused a significant increase in the percentage of apoptotic cells (Figure 3.5), although the sensitivity to DIM varied with cell type. For example, HSB2 cells were the most sensitive to DIM-induced apoptosis (significant increase in apoptosis at DIM concentrations > 7.5 μM up to 52%), whereas apoptosis was only modestly increased in Jurkat cells (10% apoptosis at 15 μM DIM).

Next, the extent of DNA strand breaks *in vitro* was analyzed using the TUNEL method and a commercially available kit (In Situ Cell Death Detection Kit, Roche) in the CEM cell line only. Marked incorporation of fluorescein-dUTP was evident by fluorescence microscopy (Figure 3.6A). Fixed and stained samples were applied to a benchtop flow cytometer (Guava, Millipore) for quantitative analysis of results. This approach identified populations of both low and high TdT incorporation by fluorescence intensity, reflective of low and high cellular levels of apoptosis (Figure 3.6B). For all concentrations of DIM tested, the low intensity apoptotic index increased in a concentration-dependent manner relative to controls, with the percentage of CEM cells undergoing low levels of apoptosis ranging from 2 to 13%. At higher concentrations (≥ 7.5 μM) of DIM, an increase in the number of cells with a high level of apoptotic response was also observed. Apoptosis was detected in 22% of the cell population at the highest concentration of DIM tested.

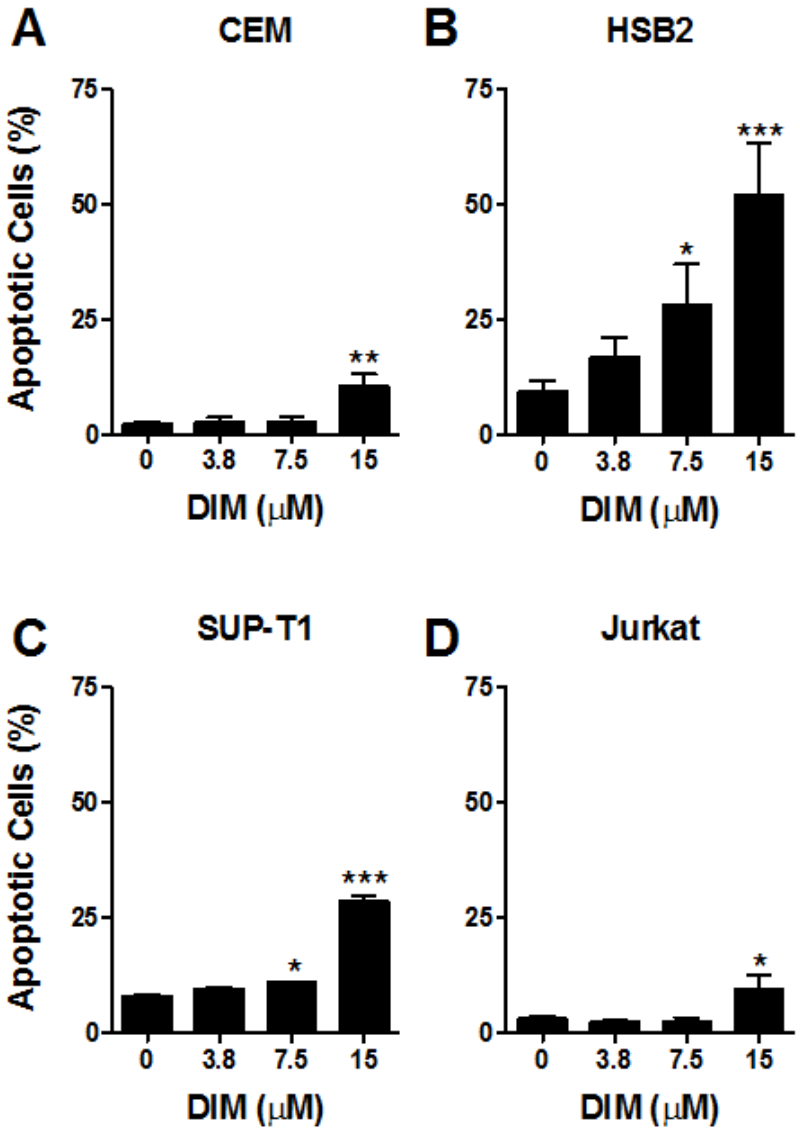

Figure 3.5 DIM induces apoptosis in human T-ALL cells.

CEM, HSB2, SUP-T1 and Jurkat cells were treated with 3.8 to 15 μM DIM for 48 hr. Values are the proportion of apoptotic cells as determined using the ViaCount assay + SEM (n = 3 to 4 independent experiments). *, $p < 0.05$; **, $p < 0.01$ or *** $p < 0.001$ for compared to the vehicle control (0 μM DIM, 0.1% DMSO) as determined by one-way RM ANOVA (matching by experiment day) with Dunnett's multiple comparisons post-hoc test.

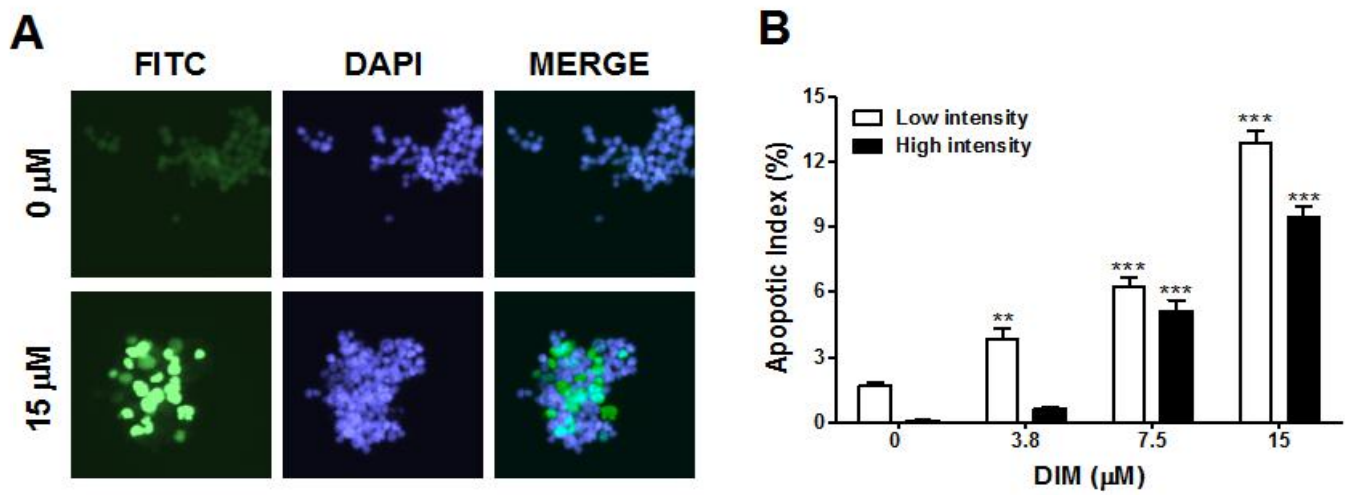

Figure 3.6 DIM induces apoptosis in CEM cells as detected by TUNEL**.**

The In situ cell death detection kit (TUNEL) was applied to fixed CEM cells treated with 0 to 15 µM DIM for 48 hr. (A) Fluorescence images of control (0 µM) and DIM-treated (15 µM) cells were taken at 20x magnification following TUNEL labeling in mounting medium with DAPI. (B) Flow cytometry was used to identify and quantify cells with no, low (open bar) or high (solid bar) intensity staining. **, $p < 0.01$ or ***, $p < 0.001$ as determined by one-way ANOVA with Dunnett's post-hoc test comparisons for significant effects of DIM treatments within each intensity category as compared to vehicle control (0 µM DIM, 0.1% DMSO).

DIM alters expression of genes regulating the apoptosis pathway. We determined the effects of DIM on expression of gene targets relevant for regulation of apoptosis in human cells. Fold-change values and results of the statistical analyses for all gene targets on the apoptosis PCR pathway array are provided in Suppl. Table 3.1. *In vitro* exposure to 7.5 μM DIM for 4 hr significantly altered the expression level of eight genes more than 1.5-fold ($p < 0.05$) with respect to the time-matched controls (Table 3.3). This set of genes accounted for 9.5% of transcripts queried by the quantitative PCR apoptosis pathway array. Among those transcripts, BCL2L10, CD40LG, HRK, TNFRSR1A and TNFSF8 were significantly induced, while only TNF was repressed. Following 24 hr of DIM exposure, expression levels of CD40LG and HRK remained elevated, while TNFRSF25 and TRAF4 were significantly repressed (<-1.5-fold, $p < 0.05$) (Table 3.3).

Table 3.3 DIM-induced changes in expression of select apoptosis-related genes *

			Log_2 R (*P*-value) †	
Unigene	**Symbol**	**Description**	**4 hrs**	**24 hrs**
Hs.283672	*BCL2L10*	BCL2-like 10 (apoptosis facilitator)	**1.05** (0.459)	**0.63** (0.023)
Hs.592244	*CD40LG*	CD40 ligand	**0.75** (0.019)	**0.62** (0.043)
Hs.87247	*HRK*	Harakiri, BCL2 interacting protein (contains only BH3 domain)	**0.88** (0.014)	**1.35** (0.004)
Hs.241570	*TNF*	Tumor necrosis factor (TNF superfamily, member 2)	**-0.63** (0.016)	-0.39 (0.026)
Hs.279594	*TNFRSF1A*	Tumor necrosis factor receptor superfamily, member 1A	**1.22** (0.002)	-0.46 (0.331)
Hs.462529	*TNFRSF25*	Tumor necrosis factor receptor superfamily, member 25	nd ‡	**-1.15** (0.015)
Hs.654445	*TNFSF8*	Tumor necrosis factor (ligand) superfamily, member 8	**0.90** (0.026)	0.34 (0.009)
Hs.8375	*TRAF4*	TNF receptor-associated factor 4	nd	**-0.59** (0.017)

* A complete table of DIM-induced changes in gene expression, including all genes on the RT2 Profiler Apoptosis array, is provided in the supplementary materials. † Log2 fold-change (R) values are highlighted in bold if level of change is >1.5-fold (Log2 R<-0.58 or >0.58) compared to vehicle (0.1% DMSO) control. P-values were determined by a Student's t-test assuming equal variances. ‡ nd, not detected by RT2 PCR profiler array at this time point (Ct > 35).

Impact of DIM and I3C treatment on growth of CEM xenografts

DIM and I3C inhibit growth of CEM xenografts *in vivo*. Another key objective of this study was to determine whether dietary DIM or I3C reduced the growth of human CEM cells *in vivo* using a SCID mouse xenograft model. The rate of body weight gain or average final body weight was not significantly affected by any of the dietary treatments (Suppl. Figure 3.1). On average, animals in the DIM group consumed about 0.4 mg DIM/day, based on per cage diet consumption data (Suppl. Figure 3.1B). The rate of successful CEM engraftment in this study was high (57/59 animals), with solid nodules palpable within one week (approximately 250 mm^3). In this study, short-term (1 week pre-engraftment + 28 days post-engraftment; 35 days total) dietary treatment with 100 ppm DIM, 500 ppm I3C or 2000 ppm I3C did not significantly affect average body weight or rate of body weight gain (Suppl. Figure 3.1A). Animals fed 500 ppm I3C apparently consumed less food on a daily basis compared to the other diet groups (Suppl. Figure 3.1B.), and one animal was removed from this group due to an unrelated health problem. Tumor volume in control-fed animals increased by about 600%, with an average doubling time (DT) of 6.4 days (Figure 3.7; Table 3.4).

Dietary DIM significantly reduced growth of CEM xenografts ($p = 0.041$, two-way RM ANOVA), and a significant effect of dietary DIM on CEM nodule size was detected by day 25 ($p < 0.05$, Bonferroni's post-hoc tests compared to control) (Figure 3.7A). At the conclusion of the study, the final average tumor size in DIM-treated animals was substantially and significantly reduced (44% decrease in volume) compared to control animals. Moreover, the rate of growth of CEM cell xenografts in animals fed 100 ppm DIM was significantly slower with a DT of 10.2 days (Table 3.4) compared to 6.4 days for control fed animals ($p <0.001$ by one-way ANOVA). I3C was less effective at reducing xenograft growth; 500 and 2000 ppm diet concentrations decreased tumor volume by 25% or 27% by day 28, respectively, although these levels of effect were not statistically significant (500 ppm I3C, $p = 0.356$; 2000 ppm I3C, $p = 0.271$, by two-way RM ANOVA) (Figure 3.7B). However, tumor growth rate was

significantly reduced by 2000 ppm I3C, with a calculated doubling time of 8.5 days (p = 0.006) (Table 3.4).

Dietary DIM induces apoptosis in CEM cells *in vivo*. Because high rates of apoptosis were detected in CEM cells exposed to DIM *in vitro*, apoptosis was also assessed in CEM xenografts following dietary exposure to 100 ppm DIM, 500 ppm I3C, and 2000 ppm I3C (Figure 3.8A). Dietary DIM resulted in a significant (p < 0.001), two-fold increase in the number of TUNEL-positive cells in mice fed DIM (3.4 ± 0.5%) compared to control mice (1.7 ± 0.2%). Alternatively, AI values for xenograft sections from mice exposed to 500 or 2000 ppm I3C were not significantly different from control (Figure 3.8B).

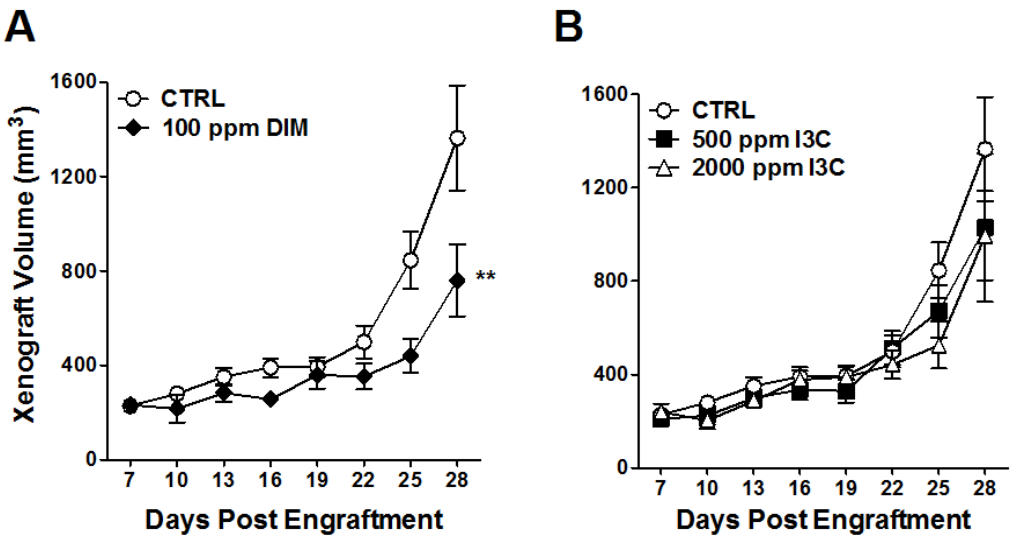

Figure 3.7 DIM and I3C suppress CEM cell xenograft growth.
Male NOD.CB17-Prkdcscid/SzJ mice were engrafted with CEM cells as described in Materials and Methods and fed control diet (CTRL), 100 ppm DIM (panel A) or 500 or 2000 ppm I3C (panel B) for 28 days. Growth of xenografts was assessed every third day and compared to nodule volumes in control-fed animals. *, p < 0.05 or **, p < 0.01 as determined by two-way repeated measures ANOVA with Bonferroni post-hoc tests to evaluate the effects of diet on tumor growth at each time point compared to the time-matched control. P-values for overall effect of each treatment on tumor growth compared to control are: 100 ppm DIM, p = 0.041; 500 ppm I3C, p = 0.356; and 2000 ppm I3C, p = 0.271.

Table 3.4 Growth of human CEM cell xenografts in SCID mice fed DIM or I3C.

Treatment	Final tumor volume mm^3 ± SEM	Tumor doubling time † Days (95% CI)
Control	1360 ± 222	6.43 (5.22 – 8.35)
100 ppm DIM (350 ppm BR-DIM)	761 ± 153 **	10.2 (7.51 – 15.9) ###
500 ppm I3C	1030 ± 318	7.57 (5.43 – 12.5)
2000 ppm I3C	994 ± 191	8.45 (6.47 – 12.2) ##

Note: **, $p < 0.01$ as determined by two-way ANOVA with Dunnett's post-hoc test comparisons for significant effect of experimental diet compared to the time-matched control (day 28 values for tumor volumne are shown). ##, $p < 0.01$ or ###, $p < 0.001$ as determined by one-way ANOVA with Dunnett's post-hoc test comparisons for significant effects of experimental diets compared to control.

† Tumor growth rates were modeled by non-linear regression analyses using the exponential growth equation with least-squares fit (Prism 5). Average doubling time (DT) values are shown and were calculated as follows: $DT = [(T_o-T_i)\times\ln 2]/\ln(V_o/V_i)$ where T_i and T_o represent the initial and final time points and V_i and V_o represent initial and final tumor volumes. P-values (extra sum of squares F test) are reported for comparison of calculated growth curves for indicated treatments compared to control diet.

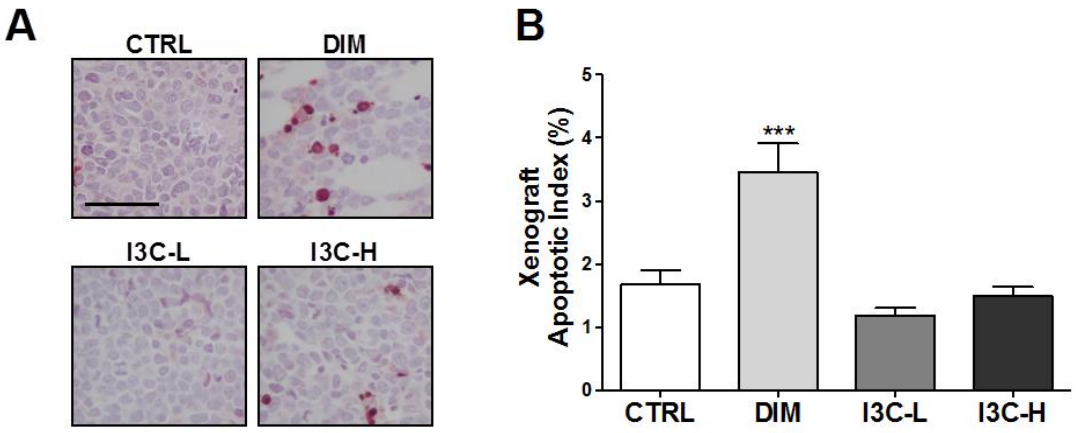

Figure 3.8 DIM induces apoptosis *in vivo.*

(A) The In situ cell death detection kit (TUNEL) was applied to xenograft sections following exposure to control diet (CTRL), 100 ppm DIM, 500 ppm I3C (I3C-L), or 2000 ppm I3C (I3C-H). Dark staining indicates apoptotic cells, and the scale bar represents 50 μm. (B) Manual and software-assisted counting was performed for xenograft sections as described in Supplemental Materials to calculate the percentage of positive cells. ***, $p < 0.001$ as determined by one-way ANOVA with Dunnett's multiple comparisons post-hoc test.

3.5 Discussion

We provide evidence for the first time that DIM significantly impairs the growth of human T-ALL cells *in vitro* and *in vivo*. Moreover, we show that DIM blocks growth of T-ALL cell types that represent the spectrum of T-cell differentiation arrest occurring within this disease, ranging from least differentiated to nearly mature (HSB2 > CEM > SUP-T1 > Jurkat). All four T-ALL cell types studied responded to DIM treatment in a dose-dependent manner, as shown by inhibition of cell proliferation and viability and increased levels of apoptosis; in addition, a G1 cell cycle arrest was observed in HSB2 and CEM cells, lines that represent early (pre-T) differentiated cells. In this study, we also show that the I3C derivative, DIM, was far more potent than its precursor and exhibited therapeutic effects on a variety of highly aggressive juvenile T-ALL cell lines, including Jurkat and CEM, at physiological concentrations. Others have reported that I3C suppressed NFκB stimulation by TNF and downstream gene products, including CCND1, BCL-2 and TRAF1, in myeloid and leukemia (Jurkat) cells [237], but I3C was not capable of blocking the growth of T-cell lines that were not infected with human T-cell leukemia virus type-1 (MOLT-4, Jurkat and CCRF-CEM) [236].

The SCID mouse model supports the solid growth of subcutaneously injected human acute leukemia blast cells in a manner that is easily measurable and exhibits a dissemination pattern analogous to the human disease [238,239]. We supplemented this pre-clinical model with dietary indoles to determine the extent of xenograft growth suppression following absorption, metabolism and disposition to the grafted cells. This study is the first to employ continuous exposure of I3C or DIM through the diet, as opposed to bolus administration via gavage or injection, with a human cell xenograft model in SCID mice. In the present study, growth of human CEM cell xenografts in mice consuming DIM (approximately 0.4 mg/day) was only about half that of the control animals, an observation that is comparable to other studies with breast cancer cell xenografts that employed even greater amounts of DIM or more direct routes of exposure. For example, oral gavage of about 1 mg DIM/day (3.5 mg

BioResponse-DIM/day) decreased growth of MDA-MB-231 xenografted cells by approximately 30% after 3 weeks of exposure [240] whereas daily 5 mg/kg s.c. injections of DIM at the site of MCF-7 xenografts reduced tumor volume by about 45% [241].

We selected a dietary concentration of 2000 ppm I3C level based on the apparent anticancer effects at this level observed in our previous studies [32,242]. The likely proportion of this I3C diet to be converted to DIM following *in vivo* condensation corresponds to a diet concentration of 350 ppm DIM, based on a 2:1 molar ratio and assuming a 20% conversion rate [86,228]. The BioResponse-DIM formulation is a commercially available dietary supplement, sold for human consumption, that is also used in animal studies and clinical trials; thus, 350 ppm BioResponse-DIM (100 ppm DIM) was selected in anticipation of comparable bioactivity to the 2000 ppm I3C treatment [86]. Pharmacokinetic studies in mice comparing this formulated DIM to crystalline DIM demonstrate a 50% improvement in adsorption [86]. This difference in bioavailability, along with the rapid elimination of I3C and formation of additional bioactive I3C derivatives, may account for the reduced efficacy of 2000 ppm I3C *in vivo* compared to 100 ppm DIM.

DIM was also significantly more potent than I3C *in vitro* based on the relative IC_{50} values for inhibition of cell proliferation and viability across all cell lines tested. Moreover, the anti-proliferative effect of I3C was delayed compared to DIM, suggesting that conversion of I3C to DIM and other ACPs in the culture media may contribute to the physiological effects of I3C. A recent report by Bradlow and Zeligs [81] showed that addition of 100 μM I3C to culture media at a neutral pH results in concentrations of DIM of about 25 μM within 24 hrs. However, because the degree of difference in potency of DIM and I3C varied across the four T-ALL cell lines tested and by the endpoint examined (viability, proliferation), the apparent lower potency of I3C compared to DIM cannot be fully explained by conversion of I3C to DIM in the culture media.

Other plausible explanations exist for the distinctive responses to DIM observed in the four T-ALL cell lines studied, which are characterized by different lineages of T-cell differentiation (pre-T, cortical-T and mature-T), as well as different ages and genders of the source patients (Table 3.1). Gene deletions and mutations as well as epigenetic mechanisms of gene dysregulation are commonly implicated in the oncogenesis of T-cells and in therapeutic outcome [38,40,243]. Common leukemic signature genes include those involved in normal T-cell receptor signaling and T-cell differentiation such as *NOTCH1*, *NOTCH3*, *HOX11*, *TAL1*, *LYL1* and *LMO1* [218,243]. A selection of these therapeutically relevant targets and their status in HSB2, CEM, SUP-T1 and Jurkat cells are listed in Table 3.1.

Although beyond the scope of this study, the different combinations of these aberrations across the cell lines tested are likely to play a role in the therapeutic effect of DIM. The variable responses to both targeted and conventional chemotherapeutic drugs that have been previously observed in T-ALL cells are likely a consequence of the respective mutations harbored by the cell lines [e.g., 224,244]. Thus, the observation that DIM had variable potency for blocking growth of T-ALL cells (though effective in all four cell lines tested) is not necessarily unexpected given the apparent variability in response of T-ALL cells to drug therapies.

Treatment of CEM and HSB cells with DIM caused a blockade of cell-cycle progression at the G1 phase checkpoint, although this effect was not observed in more differentiated T-ALL cell lines (SUP-T1 or Jurkat); DIM (and I3C) also suppressed expression of CCND3, CDK4 and CDK6 cell cycle regulatory proteins in CEM cells. Early progression of the eukaryotic cell cycle is positively regulated by the coupling of D-type cyclins with the highly homologous CDK4 or CDK6 proteins and negatively regulated by cyclin dependent kinase inhibitors and phosphatases [245]. I3C and DIM inhibit proliferation and cell cycle progression of various tumor cells, including breast [113], prostate [246], and colon [247], via down-regulation of cyclins and cyclin dependent kinases and/or up-regulation of cyclin dependent kinase inhibitors, such as p21 or p27 [112,113,246]. The *INK4A* gene locus, which encodes the cyclin

dependent kinase inhibitors *p16* and *p19*, is inactivated in up to 80% of T-ALL cases and in all T-ALL cell lines tested [233,248]. CDK6 is the initial CDK induced during T-lymphocyte activation/proliferation and is highly expressed in T-cell lymphoblastic leukemias/lymphomas [249]; similarly, over-expression of cyclin D3 is oncogenic in an array of mouse and human T-ALL cell lines [250]. Aberrant expression of cyclin D3 and cyclin dependent kinases during leukemic transformation underscores their relevance as therapeutic targets for I3C/DIM.

DIM treatment effectively induced apoptosis in human T-ALL cells *in vitro* and *in vivo*, although the apoptotic response to *in vitro* treatment with DIM varied greatly among the cell lines tested. HSB2 cells, which represent T-ALL originating from T-cells at a very early stage of differentiation, were highly sensitive to DIM-induced apoptosis compared to other T-ALL cell types that were only modestly affected. This observation reinforces a general conclusion of this report that HSB2 cells are more sensitive to the anticancer effects of DIM *in vitro*. DIM treatment of CEM cells *in vitro* also altered expression of mRNA transcripts belonging to the BCL-2 superfamily or involved in TNF signaling, suggesting the involvement of both intrinsic and extrinsic apoptotic pathways. Others have shown that *in vitro* treatment with I3C or DIM inhibits NFκB activity in human breast and prostate cancer cells undergoing apoptosis [178,251] and reduces *BCL-2* mRNA and protein expression in breast cancer cells [252]. Moreover, expression of *HRK* (a BH3 domain-only BCL2 family member) is induced in hematopoietic progenitor cells upon growth factor removal or chemotherapeutic administration [253]. In this study, treatment of CEM cells with 7.5 μM DIM rapidly and continuously elevated *HRK* expression *in vitro*, which represents a putative and novel therapeutic target of these dietary indoles.

Bioactive dietary components may be utilized as part of a healthy lifestyle aimed at disease prevention or therapy. The ability of I3C/DIM to target multiple pro-survival pathways in cancer cells, while causing few adverse effects on normal cells, has been explored in a number of cancer models with substantial success. Collectively, our work points to the potential benefit of exposure to these agents at

early life stages for chemoprotection, from gestation through adolescence, when leukemia is most prevalent [32, this study]. Based on available human and animal data [89,90], the concentrations of DIM used in this study *in vitro* are likely achievable *in vivo*. In conclusion, our observations suggest that DIM may be a beneficial chemotherapeutic agent or adjunct therapy for T-ALL patients.

Acknowledgements: The authors would like to thank the staff of the Laboratory Animal Resource Center and the Cancer Chemoprevention Core at Oregon State University, as well as the Agricultural Experiment Station at Utah State University. We greatly appreciate the technical assistance provided by Mohaiza Dashwood, Dr. Carmen Wong, Dr. Praveen Rajendran, Marilyn Henderson and Lisbeth Siddens

Chapter 4 Differential modulation of dibenzo[*def,p*]chrysene transplacental carcinogenesis: maternal diets rich in indole-3-carbinol versus sulforaphane

Lyndsey E. Shorey[1,2] , Erin P. Madeen[1,2] , Lauren L. Atwell[1,2,3], Emily Ho[1,2,3] , Christiane V. Löhr[4,5], Clifford B. Pereira[5,6], Roderick H. Dashwood[1,2] and David E. Williams[1,2,6]

[1]Department of Environmental and Molecular Toxicology, [2]Linus Pauling Institute, [3]Department of Nutrition and Exercise Sciences, [4]College of Veterinary Medicine, [5]Environmental Health Sciences Center and [6]Department of Statistics, Oregon State University, Corvallis, OR 97330, USA.

Formatted for submission to *Carcinogenesis*

4.1 Abstract

Cruciferous vegetable components have been documented to exhibit anticancer properties ranging from altered carcinogen metabolism to restoration of epigenetic machinery, deregulated in cancer progression. Epidemiological data supports a plausible inverse relationship between consumption of whole cruciferous vegetables and cancer risk although confounding variables in human data make it difficult to gain mechanistic insight. Therefore, preclinical animal models are critical to our understanding of the genome/epigenome-diet/environment interactions at play in the well-established role for nutrition in cancer. In particular, the developing fetus is highly susceptible to changes in nutritional status and to environmental toxicants. Thus, we have exploited an animal model of transplacental carcinogenesis in order to assess the impact of maternal dietary supplementation on cancer risk in offspring. In this study transplacental and lactational exposure to dibenzo[*def,p*]chrysene (DBC) resulted in significant mortality of offspring related to an aggressive T-cell lymphoblastic lymphoma. Indole-3-carbinol (I3C) reduced offspring mortality as expected based on a previous study employing a greater concentration, yet not significantly. Brussels sprout and broccoli sprout powders selected for their relative abundance of glucosinolate precursors to I3C and sulforaphane (SFN), respectively, surprisingly enhanced DBC-induced tumorigenesis when incorporated into the maternal diet at 10% wt/wt. SFN alone also appeared to decrease the latency of DBC-dependent mortality however I3C abrogated the effect of SFN when administered in combination. Survivors at the termination of the study (10 months) exhibited 100% lung tumor incidence with similarly altered patterns of multiplicity as with survival. To the best of our knowledge this is the first investigation of transplacental exposure to SFN. We were able to measure SFN metabolites in the plasma of neonates exposed via the maternal diet, and provide justification for the further study of the safety and bioactivity of cruciferous vegetable phytochemicals at supplemental concentrations in the developing fetus.

4.2 Introduction

Polycyclic aromatic hydrocarbons (PAHs) are produced from the combustion of fossil fuels and within that chemical class DBC is a potent carcinogen in animal models [212,214,254] and a probable human carcinogen [191]. The relative tissue concentration in neonates exposed transplacentally to PAHs is expected to be approximately 1% of maternal burden [19], yet Whyatt et al., demonstrated that levels of PAH-DNA adducts were higher in newborn white blood cells than in paired maternal samples, demonstrating the increased sensitivity of the neonate to environmental carcinogens [3]. Various PAHs have been evaluated in preclinical rodent models as transplacental carcinogens including 3-methylcholanthrene (3-MC), 7,12-dimethylbenzanthrene (DMBA), and benzo[*a*]pyrene (BaP) [27,255,256]. Our laboratory previously established that transplacental and/or lactational exposure to dibenzo[*def,p*]chrysene (DBC) produces T-cell lymphoblastic lymphomas during early adulthood, in addition to lung tumors and liver tumors (preferentially in males) later in life [28,30-34]

Although the etiology for acute lymphoblastic leukemia/lymphoma is not precisely known, it remains the most prevalent childhood cancer [35]. Furthermore, polymorphisms in *CYP1A1* and *GSTM1*, two enzymes involved in the bioactivation and elimination of PAHs have been associated with increased risk of childhood leukemia [257,258]. Multiple lymphatic tissues including bone marrow, spleen, and thymus constitutively express *CYP1B1* during both fetal development and adulthood, the CYP isoform responsible for immunotoxic and carcinogenic effects of specific PAHs [43-45]. For example, the preleukemic effects of DMBA are almost completely ablated in Cyp1b1 null animals while DBC-induced lymphomas in our transplacental model depend on Cyp1b1 gene dosage [31,46].

The diet is a primary source of exposure to PAHs among non-smokers, especially PAHs of large molecular weight (5-6 rings) having mutagenic properties [17]. Conversely, evidence from epidemiological and animal studies suggests that modification of the diet to increase consumption of cruciferous vegetables is sufficient

to reduce the occurrence of some common cancers [259-262]. Broccoli, Brussels sprouts, mustard, kale, cabbage, horseradish and arugula are vegetables in the Brassicaceae (cruciferae) plant family and are a rich source of glucosinolates, substituted β-thiglucoside N-hydroxysulfates [72]. Breakdown products known as "indoles" and "isothiocyanates" are widely accepted as contributing to the beneficial properties of crucifers.

For example, I3C is derived from the glucosinolate glucobrassicin, abundant in Brussels sprouts, kale, and cabbage varietals, and has been widely studied for its anticancer properties [reviewed in 122,227,263]. Interest in isothiocyanates as antineoplastic agents has been growing since the 1960s and more recently sulforaphane (SFN), derived from glucoraphanin and abundant in broccoli and broccoli sprouts, has become the most studied isothiocyanate due to its potency for induction of Phase II enzymes. Both I3C and SFN modulate a wide-range of biological targets and consequently may influence risk at all stages of cancer from initiation through metastasis. For example I3C and SFN alter the expression and activity of Phase I cytochrome P450 enzymes and Phase II detoxifying enzymes, cell signaling kinases (i.e. *MAPK, NF-κB*), and histone deacetylase (HDAC) expression and activity [109,120,264,265].

Moreover, I3C supplemented to the maternal diet at 2000 ppm in our transplacental model of carcinogenesis reduces T-cell lymphoblastic lymphoma mortality and decreases lung tumor multiplicity in surviving offspring [28]. SFN has been demonstrated to inhibit CYP1A1 and CYP1A2 activity induced by the prototypic PAH, BaP, in MCF-7 cells at low micromolar concentrations that are achievable *in vivo* [266,267]. *In vivo* SFN also decreased BaP mediated AHR activation and CYP450 content while inducing phase II enzyme systems [268]. These changes were associated with restored mitochondrial glutathione levels in the lungs of animals exposed to BaP, reduced lipid peroxidation, and lessened alveolar hyperplasia [269,270]. Based on these findings and others, we hypothesize that I3C at lower concentrations than previously tested, SFN, and their whole food sources will protect

against DBC-induced transplacental carcinogenesis. To this end, we conducted a large preclinical animal study with multiple dietary regimens in order to compare the efficacy of these purified phytochemical components to Brussels sprouts, broccoli sprouts, or to one another.

4.3 Materials and methods

Chemicals and Diet

DBC was obtained from the NCI carcinogen repository at the Midwest Research Institute (Kansas City, MO) and was confirmed as > 98% pure by HPLC. Custom diets and semi-purified control diets, AIN93G and AIN93M, were purchased from Research Diets (New Brunswick, NJ). Dietary additives were purchased from the following suppliers: I3C, Cat # 17256, Sigma Aldrich (St. Louis, MO); SFN, Cat # S699115, Toronto Research Chemicals (North York, Ontario); Brussels sprout powder, Cat # N54 and broccoli sprout powder, Cat # N216, Future Ceuticals (Momence, IL). Custom diets were prepared with AIN93G diet base, adjusted for macronutrient content between diets by Research Diets (Table 4.1). Diets were stored protected from light at -20°C throughout the feeding phase of the trial. Whole food powders were analyzed by American Analytical Chemistry Laboratories Corporation for I3C content and by Van Drunen Farms/ Future Ceuticals for glucoraphanin content, and subsequently in-house as described below.

Table 4.1 Designed composition of custom maternal diets based on AIN93G.

	CTRL	100 ppm I3C	500 ppm I3C	1000 ppm I3C	10% Brussels sprouts	10% broccoli sprouts	400 ppm SFN	500 ppm I3C + 600 ppm SFN "Combo"
Dietary composition (gram %)								
Protein	20	20	20	20	17	16	20	20
Carbohydrate	64	64	64	64	61	61	64	64
Fat	7	7	7	7	7	6	7	7
Base diet ingredient (gram/kg)								
Casein	200	200	200	200	168	164	200	200
L-Cysteine	3	3	3	3	3	3	3	3
Corn Starch	397	397	397	397	375	388	397	397
Maltodextrin	132	132	132	132	132	132	132	132
Sucrose	100	100	100	100	93	98	100	100
Cellulose	50	50	50	50	22	34	50	50
Soybean Oil	70	70	70	70	67	66.5	70	70
t-Butylhydroquinone	0.014	0.014	0.014	0.014	0.014	0.014	0.014	0.014
Mineral Mix S10022G	35	35	35	35	35	35	35	35
Vitamin Mix V10037	10	10	10	10	10	10	10	10
Choline Bitartrate	2.5	2.5	2.5	2.5	2.5	2.5	2.5	2.5
Active diet ingredient (gram/kg)								
Indole-3-carbinol	0	**0.1**	**0.5**	**1.0**	0	0	0	**0.5**
N54 Brussels sprout powder	0	0	0	0	**100**	0	0	0
N216 broccoli sprout powder	0	0	0	0	0	**100**	0	0
Sulforaphane	0	0	0	0	0	0	**0.4**	**0.6**

Glucoraphanin extraction and analysis from freeze-dried powders

Approximately 30 mg of powder (broccoli or Brussels sprout), in triplicate for each powder, was weighed into 2 ml vials and the weights recorded. Glucotropaeolin (GTP) (Applichem cat # A5300,0020) was used as an internal standard, and 100% MeOH (375 µl) was added to each powder sample and sonicated for 10 min before centrifuging (Spectrafuge 24D at 16,300 x g for 5 min) and transferring supernatant to a conical tube. Three additional MeOH extractions were collected similarly and the four extracts pooled. Supernatants were centrifuged through 0.22-µm nylon Spin-X® filter columns (VWR cat# 29442-760), diluted with 0.1% (v/v) formic acid in H_2O, and stored at -80°C until analysis by HPLC-MS/MS. Ten µl was injected in duplicate and HPLC conditions were as follows: Phenomenex Synergi Hydro-RP column (80 Å, 150 x 2 mm, 4 µm pore size), mobile phases of 0.1% (v/v) formic acid in acetonitrile and 0.1% (v/v) formic acid in H_2O, 0.25 ml/min flow rate at 25°C. An Applied Biosystems MDX Sciex 3200™ triple quadrupole mass spectrometer was used in negative ion mode to detect GFN (436 > 97) and GTP (408 > 97). Quantification was performed based on a 6-point calibration curve that spanned the extract concentrations and showed excellent linearity ($r^2 = 0.999$).

Sulforaphane extraction and analysis from freeze-dried powders

Six samples of approximately 30 mg were weighed into 2 ml vials and the weights recorded for each powder (broccoli or Brussels sprout). Three samples per powder type were supplemented with 0.64 units of exogenous Sinapis alba (white mustard) myrosinase (Sigma-Aldrich cat#T4528) before incubation in 1 mL dH_2O at 60°C, in the dark, for 2 hr. Hydrolyzed samples were centrifuged at 16,300 x g for 5 min to pellet powder, and supernatants were filtered through 0.22-µm nylon Spin-X® filter columns (VWR cat# 29442-760), diluted with 0.1% (v/v) formic acid in H_2O, and stored at -80°C until analysis by HPLC-MS/MS. Deuterated SFN-NAC was used as an internal standard. Ten µl of extract was injected in duplicate and HPLC conditions were as follows: Phenomenex® Kinetex PFP column (100 Å, 100 x 2.1

mm, 2.6 μm pore size), mobile phases of 0.1% (v/v) formic acid in acetonitrile and 0.1% (v/v) formic acid in H_2O, 0.25 ml/min flow rate at 40°C. An Applied Biosystems MDX Sciex 3200™ triple quadrupole mass spectrometer was used in positive ion mode to detect SFN (178 > 114) and deuterated SFN-NAC (344.1 > 114). Quantification was performed based on a 7-point calibration curve that spanned the extract concentrations and showed excellent linearity ($r^2 = 0.999$).

Indole-3-carbinol extraction and analysis from freeze-dried powders

Broccoli sprout/Brussels sprout powders were analyzed for I3C content with slight modification of a previously published method [139]. In brief, powders were hydrolyzed in triplicate in H_2O (10 mg/mL) for 4 hr at room temperature away from light, with periodic vortexing. Solutions were centrifuged at 3,600 x g for 5 min to pellet sprout powder and supernatant was extracted twice with 5 ml of dichloromethane. Extracts were pooled and evaporated under a stream of nitrogen gas before resuspending in 200 μl of acetonitrile. Acetonitrile extracts were further centrifuged at 16,000 x g to remove any precipitates and 50 μl of supernatant injected onto a Polarity C_{18} 5μm (4.6 x 250 mm) column for detection of I3C. A Waters 2695 separations module with Waters 2996 photodiode array detector was utilized with mobile phase conditions as described previously [242]. Spiked extracts were analyzed to calculate recovery and to select an appropriate time period of hydrolysis. Quantification was performed based on a 13-point calibration curve that spanned the extract concentrations with excellent linearity ($r^2 = 0.997$).

Animals and treatment protocols

All protocols for the handling and treatment of mice were approved by the Oregon State University Institutional Animal Care and Use Committee. Seven to eight week old B6129SF1 female and 129S1/ScImJ male mice (Jackson Laboratories, Bar Harbor, ME) were maintained in a pathogen-free environment in micro-isolator cages (Life Products, Inc., Seaford, DE) with CareFRESH bedding at 20 ± 1°C and 50 ± 10% humidity with a light dark cycle of 12 hrs.

Experimental design

After acclimation for one-week, mice were provided AIN93G diet *ad libitum* and paired for breeding. Day 0 of gestation was based on appearance of the vaginal plug at which time males were removed to a separate cage and female weights recorded. Pregnant dams were administered an oral gavage of 15 mg/kg (5 ml/kg body weight) DBC in corn oil or vehicle control on gestation day 17 (GD17) between 8:00 and 10:00 AM. On GD9 the maternal AIN93G diet was replaced with experimental or control pellets according to treatment group (Table 4.1) and maternal dietary supplementation continued until weaning (post-natal day 21 (PND21)). Doses and duration of dietary intervention with purified I3C were based on a previous study in this laboratory demonstrating transplacental chemoprevention [32]. Three litters from each treatment group having 7 or more pups were designated for future molecular work and SFN analysis, and the newborn pups (post-natal day 0 (PND0)) were immediately removed following delivery, decapitated and rapidly dissected. Thymus, lung, and liver were preserved in RNAlater solution according to the manufacturer's recommendations (Life Technologies, Grand Island, NY). Blood was pooled within a litter and processed for SFN metabolite analysis as described below. Remaining litters were kept with the mother until weaning at which time male and female siblings were separated into new micro-isolator cages and given access to AIN93G control diet. Animals were monitored twice daily for signs of morbidity, pain, or distress, at which time animals were euthanized with an overdose of CO_2 followed by cervical dislocation. A full necropsy was conducted and thymus, heart, lung, liver, kidneys, spleen, digestive organs, and reproductive organs inspected for gross abnormalities before fixing tissues in 10% neutral buffered formalin. Surviving animals at 10 months of age were euthanized and necropsied as above with the following exceptions: consistently located portions of lung and liver were preserved in RNAlater for future analysis and lungs were closely assessed for lesion multiplicity and size. A portion of ear from each animal was collected and frozen for DNA extraction and genotyping.

Neonatal plasma SFN metabolite analysis

Whole blood was obtained from pups at various times after birth, spun at 16,000 x g for 1 minute, and plasma was acidified immediately with 10% (v/v) trifluoroacetic acid to stabilize SFN compounds and facilitate protein precipitation before storage at -80°C. To prepare samples for LC-MS/MS, plasma was thawed and centrifuged at 4°C for 5 min at 16,000 x g. Supernatants were centrifuged twice through 0.22-µm nylon Spin-X® filter columns (VWR cat# 29442-760). Filtrates were frozen at -80°C until analysis by HPLC-MS/MS. Ten µl of filtrate was analyzed in duplicate as described previously with the exception of mass spectrometer model, (Applied Biosystems MDX Sciex 4000™ triple quadrupole) used in positive ion mode to detect SFN (178 > 114), SFN-Cys (299 > 114), SFN-CG (356 > 114), SFN-GSH (485 > 179), and SFN-NAC (341.1 > 114) [101]. Quantification was determined using calibration curves (≥ 6-points) for each metabolite and showed excellent linearity (average r^2=0.994, SD_{r2}=0.005).

Histopathology

Tissues collected upon necropsy (heart, thymus, lung, spleen, liver, kidney, stomach, abnormal lymph nodes, testes or ovaries and colon) were fixed in 10% formalin. Early mortality samples (< 10 weeks of age) and a balanced sub-set of samples collected at the termination of the study were stained with hematoxylin and eosin and examined by a clinical pathologist as described previously in order to confirm gross observations [28,30-34].

Genotyping for Ahr^{b-1} "responsive" and Ahr^{d} "non-responsive" alleles

DNA was isolated from a small portion of ear by digesting in DirectPCR lysis reagent (Viagen Biotech, Inc. Los Angelos, CA) containing proteinase K at 55ºC until homogenous. Lysates were then heated to 85ºC to inactivate proteinase K, centrifuged to pellet unlysed material and 0.4 µl of supernatant used directly in a PCR reaction containing allele specific primers to permit single-tube genotyping of *Ahr* alleles as described previously [28].

Statistical analyses

The experimental unit in transplacental studies is the mother. Pup level responses are therefore clustered within each litter/mother so that statistical methods require random litters be nested within treatments in order to match the experimental design. Pup level responses were compared between treatments, genders and genotypes (including interactions). Pup survival times were analyzed using Cox proportional hazards regression (SAS Phreg procedure) with random litters (frailty model). Treatment comparison results shown here are for a model with additive cohort effects. It was found that randomization resulted in litter sizes that differed somewhat between treatments. A more complex model with an adjustment for litter size indicated a somewhat increased hazard of dying with increased litter size but did not change any of the comparisons of interest, so that the results for the simpler model without the covariate are shown here. Pup tumor multiplicity in survivors was analyzed with a linear mixed model (SAS mixed procedure) including random litter effects.

4.4 Results

Broccoli sprout and Brussels sprout powder characterization

We obtained freeze-dried sprout powders for maternal supplementation in this study as this process maintains myrosinase activity and consequently bioactivity, for example induction of colonic and hepatic quinone reductase [139,141]. Our study design was based on manufacturer estimated concentrations of I3C and SFN in the purchased products. However, as these values were provided in some cases as a range of previously observed values, we thought it prudent to analyze in-house the concentration of SFN and I3C in the powders after we received them. As expected, SFN levels were significantly higher in the broccoli sprout powder, relative to the Brussels sprout powder, based on HPLC-MS/MS analysis following hydrolysis with exogenous myrosinase (Table 4.2). However, these levels are markedly different than

those advertised by the manufacturer as "SFN potential – 5000 ppm", an estimate based on glucoraphanin levels and a predicted hydrolysis conversion of 50%.

Table 4.2 Whole food powder analysis of active ingredients.

	SFN ppm ± s.d. [a]	GFN ppm ± s.d. [b]	I3C ppm ± s.d. [c]
Broccoli Sprout Powder	1775 ± 66.3	12905 ± 223.8	n.d.
Brussels Sprout Powder	85.2 ± 1.5	n.d. - 1661.8 [c]	151 ± 10.7

[a] SFN measured by HPLC-MS/MS following hydrolysis for 2 hr with exogenous myrosinase source (0.64 units/ml).
[b] Glucoraphanin measured by HPLC-MS/MS as described in Materials and Methods.
[c] Analysis by HPLC coupled to detection by UV-VIS (280 nm) and standard curve quantification.

As I3C is not routinely measured by the powder supplier, a preliminary analysis was conducted by American Analytical Chemistry Laboratories prior to our receiving the powder. Again, the method used for I3C quantification in the powder was found to grossly overestimate the actual concentration. We subsequently learned that UV-VIS absorbance at 280 nm was the routine assay used for this analysis. Conversely we coupled UV-VIS detection at 280 nm to high performance liquid chromatography in order to separate I3C from other analytes present in the extract, which also absorb at this wavelength. We achieved outstanding linearity over a 13-point standard curve ($r^2 = 0.997$) ranging from 0.75 to 75 nmol in 50 µl of extract (~25-2500 ppm adjusted powder concentration). Our extraction efficiency was 60.3 ± 3.4% based on spike-recovery experiments and this was accounted for in our quantification. In the Brussels sprout powder we detected 151 ± 10.7 ppm I3C compared to 2100 ppm indicated by the UV-VIS method without HPLC separation. We detected no I3C in the broccoli sprout powder although drum dried sprouts from the same supplier and variety (*Brassica oleraca italica*) were reported to contain 5.88 ppm [139], which is below our method's limit of quantitation.

Maternal consumption of I3C, SFN, or whole food sources variably modulates mortality in offspring from transplacental DBC-induced lymphoma

As previously demonstrated, transplacental and lactational exposure to the potent PAH carcinogen, DBC, resulted in significant offspring morbidity/mortality between 12 and 35 weeks of age [28,30-34]. This morbidity is the result of highly aggressive thymic lymphomas, previously confirmed to be of T-cell origin [28]. All animals from dams receiving control diet and vehicle in place of carcinogen survived until termination of the study at 10 months and displayed no signs of illness throughout the study or at necropsy. Litter size and gender ratios varied between treatment groups as outlined in Table 4.3. There were strong litter effects on survival $p = 0.04$, with some evidence to suggest that animals from larger litters were at increased risk of morbidity.

Table 4.3 Demographics of offspring according to treatment group.

	pups	litters	genotype	gender
Treatment group	N	mean size ± SEM (n)	*Ahr*$^{b\text{-}1/d}$ / *Ahr*$^{d/d}$ (sample size)[a]	female / male
Corn Oil Ctrl	21	5.3 ± 1.4 (5)	1.10 (21)	1.63
DBC Ctrl	26	5.2 ± 0.7 (6)	1.78 (25)	0.63
100 ppm I3C	30	5.0 ± 0.9 (6)	1.64 (29)	1.14
500 ppm I3C	46	7.7 ± 1.0 (8)	1.14 (45)	0.84
1000 ppm I3C	33	4.1 ± 0.9 (6)	0.83 (33)	2.00
10% Brussels sprouts	41	6.8 ± 0.7 (7)	1.28 (37)	1.28
10% Broccoli sprouts	49	7.0 ± 0.3 (6)	1.15 (43)	0.69
400 ppm SFN	48	8.0 ± 0.5 (6)	0.95 (41)	1.40
500 ppm I3C + 600 ppm SFN ("Combo")	42	7.0 ± 1.3 (4)	0.56 (42)	1.33

[a] Samples were not collected from a subset of animals due to mortality between health checks

Offspring were assessed twice daily throughout the course of the study and upon symptoms of distress or discomfort, the animals were euthanized. Figure 4.1 (top) depicts the survival of offspring born to mothers receiving dietary

supplementation with varying concentrations of I3C. Incorporation of I3C into the maternal diet appeared to reduce the lymphoma related mortality of offspring (hazard ratio of 0.476 at 500 ppm), to a lesser extent than in a previous study with diet supplementation at 2000 ppm, as expected [32]. Interestingly, survival protection by I3C in this study did not correlate with its concentration of incorporation to the diet (p = 0.34). The 500 ppm dietary concentration exhibited the most protection, although the reduction in mortality did not reach statistical significance (unadjusted p = 0.24) (Figure 4.1).

Surprisingly, in the SFN and whole food treatment groups, early and often asymptomatic mortality was observed in a subset of pups before 10 weeks of age, when the onset of lymphoma symptoms generally occurs. Of the pups born to mothers receiving Brussels sprouts, 7% died before 10 weeks of age as did 10.2% and 17.7% of animals from the broccoli sprout and SFN treatment groups, respectively (Figure 4.1). Histological examination of tissues collected from these early morbidities did not reveal any consistent etiology and only one instance of lymphoma prior to 10 weeks of age was confirmed (Supplemental Table S-4.1). Conversely, no early mortalities were observed in the vehicle control, DBC control, I3C, or I3C + SFN groups. Survival curves for offspring from broccoli and SFN fed dams were strikingly similar ($p > 0.5$), suggesting that high levels of SFN in the broccoli may contribute to increased mortality (Figure 4.1 – bottom). This is further supported by measurements of SFN and relative concentration in the broccoli powder compared to Brussels sprout powder (Table 4.2). Interestingly, when I3C was incorporated into the maternal diet in combination with an equivalent molar amount of SFN, no early mortalities occurred as in the SFN and whole food diet groups, and overall survival trends were more similar to treatment groups with I3C alone (Figure 4.1).

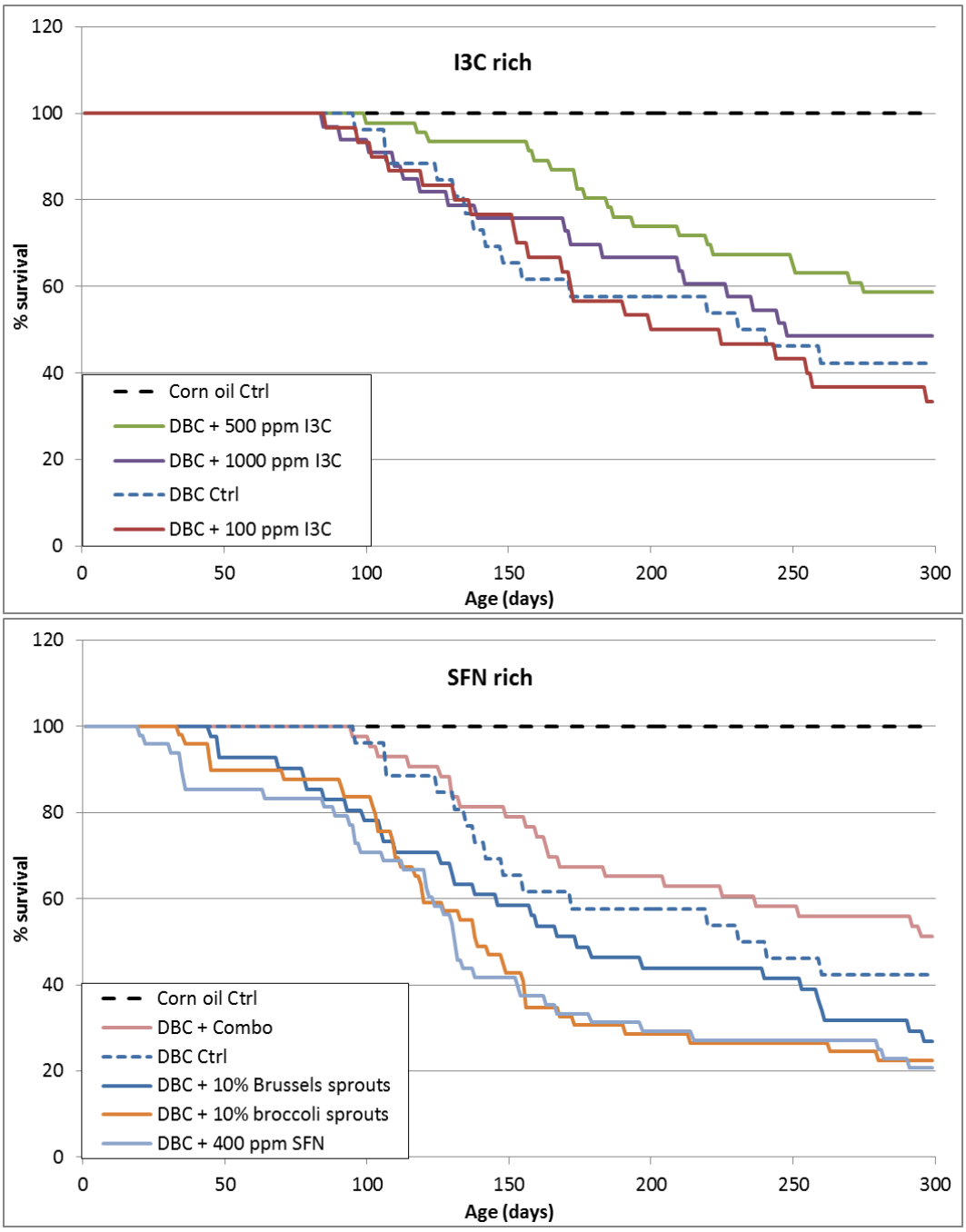

Figure 4.1 Survival of offspring born to mothers given vehicle, DBC, or DBC with dietary supplementation.

DBC was administered at 15 mg/kg by oral gavage on GD 17 in corn oil. During gestation and lactation (GD9 – PND 21) dams also received dietary supplementation as described in Materials and Methods ("Combo" signifies 500 ppm I3C + 600 ppm SFN). Treatment legends are arranged in descending order of survival at termination of the study.

After adjusting for effects of varying litter size, the increased risk of mortality for offspring born to mothers receiving SFN versus SFN + I3C was 2.88 fold (p = 0.004); unadjusted the effect was even more dramatic (hazard ratio of 3.00). Comparing all dietary treatments versus DBC alone increases the chance of so-called false positives (Type 1 error), and the Dunnett method of p-value adjustment takes this into consideration. None of the treatment groups were statistically different from DBC alone after p-value adjustment due in part to the high number of treatment groups and unstructured testing method, the small number of animals in the DBC group, and the fact that DBC results fell toward the middle of all treatments. However without adjustment broccoli treatment increased risk by 2.07 (p = 0.135) and SFN treatment by 2.50 (p = 0.030).

Previously we have identified *Ahr* status of mothers and offspring to influence survival with pups born to mothers having a responsive phenotype ($Ahr^{b\text{-}1/d}$) receiving protection over the non-responsive allele ($Ahr^{d/d}$) [28]. We found no evidence in this study of genotype or cohort being the primary effects on survival ($p > 0.5$ and $p = 0.4$ respectively), however there was some evidence to suggest an interaction between gender and treatment related outcome (p = 0.09). After partitioning the data to evaluate gender, it is obvious that the majority of treatment effects are attributed to males as evidenced by the larger spread in survival curves among this group (male treatment effect: p = 0.0002 versus female effect: p = 0.07). The survival curves for males (with the exception of SFN and whole food treatments) dropped between 91 and 168 days (13 – 24 weeks) after which time the slope of the curves appear to plateau, while female survival curves steadily decline over the entire study period (Figure 4.2). Interestingly, in female offspring alone the I3C treatment survival curves appear to follow a dose-dependent pattern, although this effect was not statistically significant due to the small sample size after partitioning by gender.

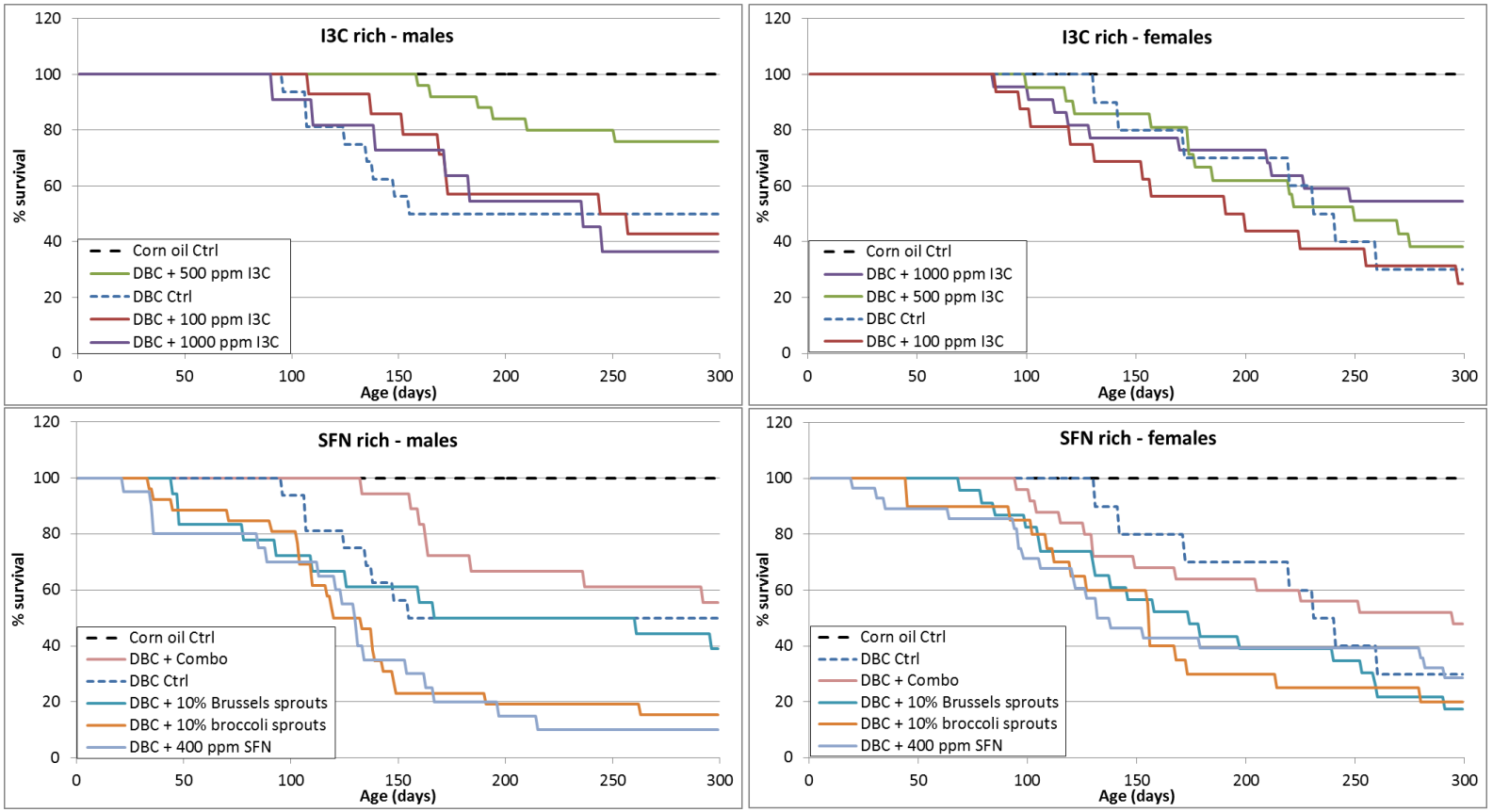

Figure 4.2 Gender specific survival of offspring exposed *in utero* and lactationally to DBC and dietary intervention.

Maternal consumption of I3C but not SFN or whole food sources reduces DBC-dependent transplacental lung cancer in surviving offspring at 10 months

In this established model of transplacental carcinogenesis, mice surviving until termination of the study (10 months of age) exhibit 100% incidence of lung tumors with varying degrees of progression (hyperplasia, adenoma, adenoma with progression, and carcinoma) [28]. Animals euthanized due to lymphoma-dependent morbidity prior to 10 months in this study often exhibited lung lesions and a previous report by our laboratory has documented increasing multiplicity as a function of age [33]. We closely examined the lung of all animals surviving to study termination for tumor multiplicity and tumor diameter before preserving the tissues for histology.

Table 4.4 Lung tumor incidence and multiplicity in 10 month old survivors.

	Incidence		Multiplicity			
Treatment group	n	%	range	simple mean	un-adjusted p-value	adjusted p-value[a]
Corn Oil Ctrl	21	0	0	0.0	n/a	n/a
DBC Ctrl	11	100	5 - 25	16.2	n/a	n/a
100 ppm I3C	10	100	4 - 30	17.6	0.488	0.961
500 ppm I3C	27	100	5 - 21	12.4	0.159	0.518
1000 ppm I3C[b]	16	100	5 - 28	11.3	0.111	0.398
10% Brussels sprouts	11	100	7 - 25	15.4	0.663	0.997
10% Broccoli sprouts	11	100	5 - 25	17.3	0.897	1.000
400 ppm SFN	10	100	4 - 35	14.9	0.649	0.996
500 ppm I3C + 600 ppm SFN	22	100	2 - 19	10.4	**0.046**	0.187

[a] Adjusted (Dunnett method) for multiple pairwise comparisons of model estimated treatment means versus DBC Ctrl

[b] For the model estimated means for the 4 doses of I3C (0, 100, 500, 1000) there is evidence of a linear trend component ($p = 0.019$)

A similar pattern of treatment related effect (compared with survival) was revealed following analysis of lung tumor multiplicity, with the exception of I3C treatments (Table 4.4). An inverse trend for tumor multiplicity was observed with increasing concentrations of I3C (p = 0.019). Neither the SFN or whole food treatment groups (broccoli sprouts or Brussels sprouts) reduced the number of lung lesions per animal yet the SFN + I3C group (COMBO) markedly reduced lung tumor multiplicity in surviving animals (simple mean = 16.2 DBC versus 10.4 in COMBO, unadjusted p = 0.046), suggesting a protective effect of I3C.

Detection of SFN metabolites in plasma of neonates exposed transplacentally to SFN

Previously it has been demonstrated in adult ICR mice administered 20 μmol SFN by oral gavage, roughly equivalent to the daily intake of dams given 600 ppm SFN diet in this study, that SFN and metabolites plasma levels peaked on average around 15 μM [101]. Thus we sought to determine whether SFN or its metabolites cross the placental for detection in neonatal plasma. As SFN is rapidly metabolized via the mercapturic acid pathway with a half-life of approximately 2 hrs [271], blood was collected immediately after delivery when possible and pooled within a litter before separating and acidifying plasma as described in Materials and Methods. We observed that SFN indeed crossed the placenta during maternal dietary supplementation between GD9 and birth (GD19). Three out of four metabolites analyzed (SFN-GSH, SFN-Cys, and SFN-NAC) were quantifiable with sum concentrations of metabolites reaching roughly 2 μM in the 600 ppm SFN + 500 ppm I3C treatment group. The variability between litters likely reflects the differences in the length of time from birth to sample collection (as some dams gave birth late at night) and also the variable time since the dam last fed. However, a dose-dependent relationship between maternal level of SFN intervention and neonatal plasma concentration of SFN metabolites was observed (Figure 4.3).

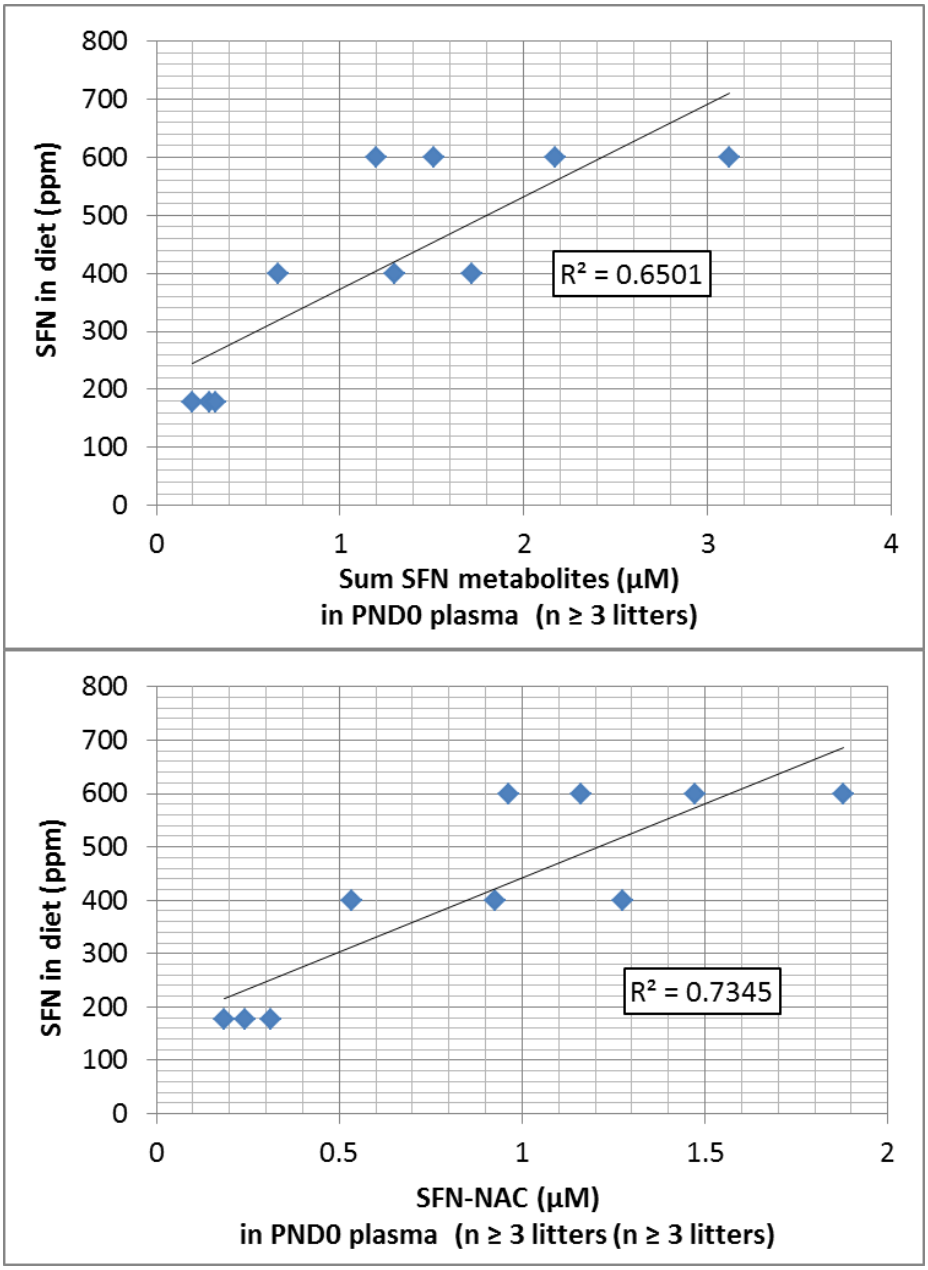

Figure 4.3 Correlation of neonatal plasma SFN concentrations with maternal supplement levels.

Neonatal (PND0) plasma concentrations of SFN metabolites (SFN-GSH, SFN-CG, SFN-Cys, and SFN-NAC) were analyzed by LC-MS/MS. SFN-NAC was the dominant metabolite; SFN-CG and parent SFN were below detection. SFN in diet (ppm) is based on designed diets of 600 ppm and 400 ppm SFN and on measured SFN amount in broccoli sprout diet (Table 4.2). SFN metabolites were largely undetected in the Brussels sprout treatment group or below limits of quantitation.

4.5 Discussion

There are currently over 40 clinical trials listed on www.clinicaltrials.gov utilizing cruciferous vegetable extracts or derived phytochemicals (I3C, SFN, or 3,3'-diindolylmethane), highlighting the potential for food-based disease prevention and therapy. Although a greater number of preclinical studies have been conducted to examine effectiveness, safety, pharmacokinetics, and mechanisms of action for these compounds, there are still many challenging questions to be asked. One particular gap in the knowledge base pertains to the critical neonatal window where developmental programming is modifiable by environmental and nutritional factors, and may determine disease risk later in life [272]. This "fetal origins of disease, or Barker's hypothesis" prompted us to investigate the effects of maternal dietary supplementation with phytochemicals derived from cruciferous vegetables either in purified form or as part of the whole-food matrix.

Our results show that I3C, abundant in Brussels sprouts and cabbage, modestly protects against DBC-induced T-cell lymphoma and more dramatically, lung tumor multiplicity. We have previously demonstrated a greater effect of maternal dietary I3C supplementation at a higher concentration, as expected [32]. The dose-dependent protective effect of I3C on lung tumorigenesis is consistent with results in A/J mice initiated with a mixture of carcinogens found in tobacco smoke (NNK and BaP) [273]. Surprisingly, we observed increased morbidity and no reduction in lung tumorigenesis in offspring born to mothers receiving SFN or its primary source, broccoli sprouts, converse to many reports of chemoprotection in adult animal models [262,268,274].

A well-supported mechanism of chemoprevention by SFN in adult animal models is its potent induction of Phase II enzymes, involved in detoxification to favor carcinogen deactivation [97]. SFN has also been shown to inhibit the activity of CYP enzymes and to reduce CYP1A1 and 1A2 activity induced by the prototypical PAH, BaP [266,268]. Conversely, I3C is termed a bi-functional inducer in that both Phase I and Phase II enzyme systems are induced upon oral exposure [275]. For example, oral pretreatment of Sprague-Dawley rats with I3C dramatically induced EROD activity in

the small intestine, thereby decreasing systemic exposure to BaP and DNA adduct levels in the lung, while intraperitoneal injection of I3C did not [276]. Small intestine CYP activity was further demonstrated to be critical in order to decrease systemic exposure to BaP through tissue-specific knock out of either *Cyp1a1* or its electron donor, NADPH CYP oxidoreductase [277,278]. The small intestine will be a major site of exposure to SFN either ingested intact or formed *in vivo* from glucoraphanin (in the case of broccoli sprouts), demonstrated to have the highest concentration of SFN metabolites after oral exposure in adult ICR mice [101]. Thus, inhibition of CYP activity by SFN in the small intestine could potentially increase systemic circulation of DBC in the pregnant female, and increase exposure to the developing fetus.

We have previously shown using radiolabeled DBC that approximately 1% of the 15 mg/kg dose given orally to pregnant B6129 female mice reaches the fetus as DBC or DBC metabolites [19]. However, PAH-DNA adducts are higher in newborns compared with paired maternal samples, likely due to decreased metabolic and repair capacity [3]. Carcinogenic potential of DBC depends primarily upon metabolic activation by CYP1B1 and epoxide hydrolase first to the *trans*-11,12-dihydrodiol and subsequently to the ultimate carcinogen and DNA binding species, the 11,12-*trans*-dihydrodiol-13,14-epoxide (DB[*def,p*]CDE) [31,279,280]. In a neonatal carcinogenesis assay acute toxicity was observed in 100% of animals at a cumulative dose of 400 nmol of the *trans*-11,12-dihydrodiol species (~12 mg/kg assuming a 10 g pup) and in ~50% of animals administered only 0.4 nmol of the *anti*-DB[*def,p*]CDE diastereomer [254]. The authors also noted chronic toxicity with parent DBC exposure or its metabolites, potentially through an immunosuppressive mechanism. Oral BaP treatment to *Cyp1a1* knockout mice produces lethality following dramatic immunosuppression evidenced by wasting and atrophy of hematopoietic tissues (thymus, bone marrow, liver, and spleen) [44,281]. Indeed, we did observe one incidence of bacterial sepsis in the early mortality cases from the SFN treatment group (Supplemental Table S-4.1). Thus one possible explanation for the increased mortality

in offspring born to dams supplemented with SFN or whole foods rich in SFN is immunotoxicity as a function of increased DBC exposure.

Isothyiocyanates at high concentrations (≥10 μM) are genotoxic, possibly due to their electrophilic reactivity or induction of oxidative stress [reviewed in 94]. As SFN and related compounds are metabolized via the mercapturic acid pathway they deplete the cellular pool of glutathione, although this is rapidly restored through a feedback mechanism involving Nrf2-ARE [282]. Glutathione is also important for the conjugation and detoxification of PAH-oxide and diol-epoxide metabolites [110] and depletion of GSH resulted in increased testicular toxicity, following transplacental exposure to BaP [283]. Thus, altered maternal metabolism to decrease pre-systemic DBC clearance is only one possible explanation for the adverse effects observed in SFN exposed offspring.

However, we show in this study, for the first time, that SFN is transplacentally available to the fetus in a concentration dependent manner, with the highest SFN metabolite concentration (≤ 2 μM) observed in the offspring from mothers receiving 600 ppm SFN in combination with 500 ppm I3C. No early mortalities were observed in these offspring and survivors were similarly protected compared to those exposed only to I3C, suggesting that fetal plasma concentration of SFN alone does not equate with toxicity. The adverse impact of SFN on offspring survival and null impact on lung tumorigenesis was similarly negated in the group whose mothers received I3C in combination with SFN. This combination did not appear to increase protection relative to I3C alone; interestingly I3C and SFN have been reported to be antagonistic or synergistic in activating Nrf2-ARE activity *in vitro*, depending on the concentration tested [109].

Testing the safety of SFN and broccoli sprout supplements during pregnancy is warranted given the commercial availability of such supplements and the observations in this study. However, it is important to note that the doses used here far exceed what would be achieved with moderate consumption of fresh vegetables. Further work is

necessary to elucidate the molecular pathways altered by DBC alone and in combination with these dietary supplements, and is ongoing. Thus, transplacental animal models of carcinogenesis provide an opportunity to investigate cancer risk in the context of neonatal nutrition and furthermore to test the safety of nutritional supplements in this sensitive population.

Acknowledgements: The authors would like to thank the staff of the Laboratory Animal Resource Center and the Cancer Chemoprevention Core Labs at Oregon State University. We greatly appreciate the experimental guidance provided by Lisbeth Siddens and the assistance of David Strickland, Rachel Azevedo, Elyssa Ridinger, and David Sampson with animal husbandry and sampling. This study was primarily funded by the National Cancer Institute, grant number P01 CA90890 and was made possible, in part, by contributions from the Mass Spectrometry Facilities and Services Core of the Environmental Health Sciences Center, grant number P30 ES00210 from the National Institute of Environmental Health Sciences along with grant number T32 ES07060, and lastly the Linus Pauling Institute at Oregon State University.

Chapter 5 General discussion

Acute lymphoblastic leukemia (ALL) encompasses neoplasms of both B- and T-cell origin, and is the most common type of childhood malignancy in the US [35]. Although the etiology of this and other childhood neoplasms is unknown, maternal exposure to environmental pollutants such as PAHs and cigarette smoke is associated with DNA damage in the developing fetus [3,284] and moreover increased risk of childhood cancers (i.e. leukemia, lymphoma, neuroblastoma, retinoblastoma, Wilm's tumor, etc.) [53,182,183]. Furthermore, the developing fetus is dramatically more susceptible than the mother based on measurements of differential exposure and DNA-adduct levels [3,58,59], likely due to reduced elimination and repair capacities.

Indole-3-carbinol (I3C), derived from cruciferous vegetables was previously determined to protect against transplacentally initiated carcinogenesis when supplemented to the maternal diet [32]. The initial objective behind this collection of work was to assess the translational relevance of this preclinical transplacental model of carcinogenesis, in assessing the effect of cruciferous vegetable components in maternal diet on childhood T-ALL risk. To this end I first evaluated the murine maternal and fetal tissue distribution of the carcinogenic PAH, dibenzo[*def,p*]chrysene (DBC), to further characterize our transplacental model and possibly provide mechanistic insight (Specific Aim 1). As expected for an oral exposure, the high molecular weight of DBC, and previously observed elimination pathways of PAHs, the majority of DBC administered to pregnant mice on gestation day (GD) GD17 was excreted via the feces within the first 8 hrs following exposure.

The rapid maternal clearance of DBC observed in this study aids to improve our understanding of the following scenarios: 1) transplacental versus *in utero* exposure, and 2) multiple fractional doses administered on GDs 5, 9, 13, and 17 (chronic throughout gestation) versus the same cumulative dose administered on GD17 (acute). The first exposure scenario was previously examined in our laboratory

and it was determined that the carcinogenic response (i.e. lymphoma related mortality and lung tumor multiplicity) was significantly less if exposure to DBC was only via lactation [30]. Given that the majority of the DBC dose would be eliminated by the mothers prior to lactational transfer (after birth, 2 days post dose), based on my distribution studies, it cannot be determined whether the fetus exposed *in utero* was in fact more susceptible than the neonate exposed via lactation for this study. This would require maternal dosing to occur in a window relative to lactation onset, yet this is difficult from an experimental viewpoint, as disruption of the mother close to birth can lead to pup cannibalism. However, based on the relatively low residual amount of DBC expected in maternal circulation at this lactation onset, the observed synergistic relationship between *in utero* and lactational DBC exposure with regard to lymphoma dependent mortality was surprising. Indeed I show in this dissertation that the residual neonatal tissue burden of DBC after 3 weeks of cross-foster is not significantly different in pups exposed only *in utero* or only *via* lactation, in support of reduced elimination capacity in neonates.

The second exposure scenario of multiple fractional doses (chronic) versus a larger single cumulative dose (acute) highlights the importance of exposure timing, relative to organ development and proliferation (Specific Aim 1). A complete lack of lymphoma-related mortality was observed when DBC was administered to pregnant mice on GDs 5, 9, 13, and 17 (3.75 mg/kg) compared with historic survival rates of roughly 50% when administered at 15 mg/kg on GD17 [28,30-34]. Furthermore, lung tumor incidence was dramatically reduced in the exposure scenario with multiple dosing. One explanation for the reduced carcinogenic response is that the cumulative dose to the fetal lung was less with multiple lower doses, because the maternal clearance would be nearly complete within the 96 hr window separating exposures. However, given the reduced fetal elimination capacity, the DBC reaching the target tissues with each exposure is likely to accumulate. Thus a more likely explanation for the reduced lung tumor multiplicity is that lung morphogenesis begins late in gestation

(GD10 in mice) [200], and the lung tissue is rapidly dividing thereafter [199], making this a critical window of susceptibility.

Lastly, by examining the relative fetal tissue concentrations of DBC (or DBC-metabolites), I determined that the magnitude of tissue exposure did not correlate with target tissue response (i.e. thymus DBC concentrations were lowest but is the major target organ in this model). These findings suggest that tissue specific metabolic capacity may be more important in defining target organ response. In fact the fetal lung and thymus both express *CYP1B1* mRNA, the known enzyme responsible for bioactivation of DBC, which is absolutely required for transplacental T-ALL development in this model [31,195]. The actual protein expression and activity of CYP enzymes throughout gestation in mice and humans is unknown and is the subject of ongoing studies in our laboratory.

Extrapolating either of these exposure scenarios to humans is a difficult task, due to species differences in anatomy, physiology, and biochemistry which coordinately regulate fetal development. However several factors intrinsic to genotoxic/carcinogenic mechanisms can be examined in preclinical animal models and may be useful in predicting human cancer risk [reviewed in 8]. Furthermore, the relative timing of carcinogenic and chemopreventative agents *in vivo* can dramatically alter cancer risk, as demonstrated with I3C in an aflatoxin-initiated trout model of hepatocarcinoma [285]. Future studies in our laboratory will examine whether dietary supplementation with I3C post-weaning can suppress the growth of transplacentally initiated T-cell lymphoma. Towards this end, I selected a human cell line representative of the T-cell lymphoblastic leukemia/lymphoma observed in our transplacental model, based on cell differentiation markers ($CD3^+$, $CD4^+$), in order to assess chemoprevention by I3C/DIM through suppressive mechanisms (Specific Aim 2).

I3C and DIM have previously been reported to inhibit the proliferation and survival of a range of tumor cell types, including breast [113], prostate [246], and colon [247], in part via down-regulation of cyclins and cyclin dependent kinases

and/or up-regulation of cyclin dependent kinase inhibitors, such as *p21* or *p27* [112,113,246]. I aimed to confirm these molecular targets in a T-ALL cell population for the first time. Herein I report that DIM treatment was significantly more potent than I3C in all four human T-ALL cell lines tested. Importantly, the concentrations of I3C required to elicit significant apoptosis and cell cycle arrest have been demonstrated to be cytotoxic in healthy peripheral blood mononuclear cells [236].

I3C is rapidly turned over *in vivo* as described in section 1.5, while DIM accumulates in the nucleus of treated cells and is detectable in plasma following oral consumption for up to 24 hrs [82,83,86]. Therefore it is unlikely that such high cytotoxic concentrations of I3C would be achievable *in vivo*, especially when consumed through the diet. It has been suggested based on the relative instability of I3C that DIM is responsible for the bioactivity of its precursor, however this likely only applies to specific molecular targets and exposure scenarios. For example, I3C but not DIM has been demonstrated to be protective in a chemically-induced model of carcinogenesis [286] while feeding either phytochemical inhibited prostate carcinogenesis in TRAMP mice [287,288]. Therefore additional acid condensation products and I3C metabolites may contribute the observed differential effects from DIM treatment alone.

As the diet is a natural source for these phytochemicals, I next asked whether I3C (or breakdown products) or DIM *in vivo* (administered through the diet) could reach therapeutic concentrations at the site of engrafted T-ALL cells and reduce CEM cell proliferation as observed *in vitro*. I supplemented the diets of immunodeficient mice with either I3C (2000 or 500 ppm) or DIM (100 ppm in a bioavailable formula), beginning one week prior to engraftment with human CEM cells, and continuing for four weeks thereafter. Similar to our results *in vitro*, DIM significantly reduced xenograft volume and doubling time, suggesting that the therapeutic DIM concentrations used *in vitro* were within a physiologically achievable range. Increased TUNEL-positive cells in DIM treated xenografts and *in vitro* cultures suggest a chemotherapeutic mechanism involving apoptosis. In fact a recent publication has

corroborated the effectiveness of DIM in inducing apoptosis in human leukemia cells, through a caspase-dependent mechanism that was prevented by enforced activation of Akt [289]. I3C in this study was less effective than DIM both *in vivo* and *in vitro*, suggesting that DIM may greatly contribute to suppressive mechanisms of dietary chemoprevention by I3C in this model.

Cruciferous vegetables contain a number of bioactive components in addition to I3C/DIM that may interact with the activity of these phytochemicals including vitamins (A, C, and Bs), polyphenols, fiber, selenium, zinc, iron, and folate. As reviewed in Chapter 1, additional isothiocyanates in cruciferous vegetables including allyl-ITC, benzyl-ITC, phenethyl-ITC (PEITC) and most notably sulforaphane (SFN) in broccoli sprouts have also demonstrated chemoprotective properties. Most anti-cancer studies have generally focused on only one of these active ingredients at a time and often at concentrations far exceeding what is consumed through the diet. However, some evidence *in vitro* suggests the interactions within binary combinations of I3C, SFN, DIM, and PEITC vary depending on the concentration and combination of compounds. For example, 25 μM DIM + 1 μM SFN synergistically induced ARE activity, as did 6.25 μM I3C + 1 μM SFN, while 25 μM I3C + 1 μM SFN was antagonistic in human hepatoma cells [109]. At the low total concentration of 2.5 μM, all combinations of DIM with SFN (ratios 1:4 - 4:1) were antagonistic in blocking proliferation of human colon carcinoma cells and synergistic interaction only occurred at higher combined concentrations (25 – 40 μM) [290].

SFN has never been examined in a transplacentally initiated model of carcinogenesis, however *in vitro* we observed significant G2/M cell cycle arrest at low micromolar concentrations of SFN in CEM cells. These levels may be achievable for chemoprevention *in vivo*, based on peak plasma concentration of SFN metabolites (>2μM) in humans following consumption of broccoli sprouts [133]. Moreover, in hypertensive stroke-prone rats (SHRsp), maternal supplementation with broccoli sprouts reduced NFκB activation and tissue inflammation of offspring [291]. Therefore, I returned to our transplacental model of carcinogenesis in order to assess

the relative chemoprotective effects of these purified phytochemicals versus each other and compared with their whole food sources (Specific Aim 3). Previously our laboratory demonstrated that 2000 ppm I3C in the maternal diet was significantly protective against DBC-dependent transplacental carcinogenesis [32]. The current study examined 100 ppm, 500 ppm, or 1000 ppm I3C and determined no significant effect of any concentration with respect to survival; nor did I observe a concentration-response. The lack of statistical significance is likely due to an insufficient number of test animals in the control population and interaction of gender and litter size with treatment effects in our statistical model.

Within this mouse model, development of T-ALL symptoms generally begins at about twelve weeks of age in offspring. Previously we have observed a small number of spontaneous mortalities prior to lymphoma development, usually associated with anemia, although not related to any particular treatments. In the current study we noted asymptomatic moralities as early as 2.7 weeks of age and in total twenty animals (9%) died before reaching 12 weeks of age. All animals with early mortalities were exposed *in utero* to SFN, broccoli sprouts, or Brussels sprouts. In common among these treatments was the presence of SFN, albeit at different levels, with minimal amounts of I3C measured only in the Brussels sprout diet. Similar to treatment effects on lymphoma, diets containing SFN were not protective against lung tumor multiplicity with the exception of the equimolar combination with I3C. An inverse trend between multiplicity and I3C dose was observed while the combination diet had the most dramatic effect of all treatments on the number of lung lesions per animal. Lastly, I report that the toxicity of SFN was not correlated with the calculated amount of SFN in the diets or in neonatal plasma concentrations as evidenced by LC-MS/MS analysis.

Polycyclic aromatic hydrocarbons (PAHs) are ubiquitous environmental pollutants produced as combustion byproducts with common sources including cigarette smoke, fossil fuel exhaust, and charcoal cooking. It is accepted that the mutagenic and carcinogenic potential of these chemicals relies on their bioactivation,

carried out in part by cytochrome P450 (CYP450) enzyme isoforms 1A1 and 1B1, to reactive DNA and protein binding species. Elimination of the prototypical PAH, benzo[*a*]pyrene, following oral exposure is greatly reduced when *Cyp1a1* or its electron donor, P450 reductase, is genetically knocked out in the small intestine of C57BL/6 wild-type mice [277,278]. Global *Cyp1a1* knockout (k.o.) alone or in conjuction with *1b1* k.o. leads to higher blood levels of BaP (wt), increased BaP-adduct levels (highest in liver, spleen and bone marrow) versus wild type, and severe immunotoxicity in *Cyp1a1* single knockout animals [44,281]. I3C or β-napthoflavone similarly reduce systemic BaP circulation when supplemented orally, suggesting that pre-systemic clearance of DBC through CYP1A1 induction in our model by I3C may be crucial to its chemopreventative mechanism [276]. Indeed, feeding 2000 ppm I3C to pregnant Sprague-Dawley rats induced both maternal and fetal *Cyp1a1* in the liver [292].

Sulforaphane conversely has been shown to inhibit Phase I enzyme activity induced by BaP both *in vitro* and *in vivo* [266,268]. In adult animals this has been demonstrated to have a favorable outcome on cancer risk, as SFN simultaneously induces Phase II enzyme activities and therefore may ultimately favor carcinogen deactivation. However, in a transplacental model SFN may increase maternal systemic circulation of carcinogen, resulting in greater fetal exposure and the toxicity and lack of chemoprotection in this study. Previous work by our laboratory demonstrated that the maternal Ahr status modifies the risk to offspring in this model with mice born to Ahr "responsive" mothers receiving protection, presumably through increased maternal metabolism and excretion of DBC [28]. Although the concentrations of SFN used in this study are outside what would be achieved with reasonable consumption of broccoli sprouts (1-5 servings), lower and more relevant consumption in male Wistar rats was shown to decrease hepatic CYP activity [293]. Therefore further study is necessary to evaluate this hypothesis, to determine whether maternal consumption of broccoli sprouts alters the metabolism and transplacental

transfer of xenobiotics, and to investigate the overall effects of SFN on the developing fetus.

During both development and carcinogenesis epigenetic machinery coordinately alter patterns of gene expression in order to control cellular differentiation, proliferation, and other signaling events required by these highly regulated processed. For example, the primordial germ cells (PGCs) within the fetus (roughly between gestation days 7 and 12 in a mouse model) undergo active demethylation before differentiating into oocytes or sperm [294] and to date DNA methylation has been the only epigenetic mark shown to be directly transmissible through cellular divisions [295]. Genomic imprinting, regulated by DNA methylation and chromatin structure, allows for monoallelic gene expression of either maternal or paternal origin non-imprinted alleles in the absence of changes to genomic sequence [296-298]. This process can be altered by fetal growth restricting conditions, nutrition, and by maternal exposure to toxicants, such as cigarette smoke [299-301]. Furthermore carcinogenesis is marked by global DNA hypomethylation and gene-specific hypermethylation, associated with silencing of tumor suppressor genes and chromosome instability.

Therefore we proposed that DNA methylation in either of our models of T-ALL (mouse transplacentally initiated or human CEM cells) would be susceptible to change with phytochemical treatment. To this end I have collected tissues from both young (PND1) and old (10 months) animals exposed transplacentally to DBC with and without maternal dietary supplementation for future analysis of epigenetic marks. As proof of principle and validation of methodology I report that CEM cells exhibit a number of hypermethylated genes, some of which are modified with DIM or I3C treatment *in vitro* (Appendix A1). Interestingly the pathways identified by functional analysis of differentially methylated genes (DMRs) are largely related to development/morphogenesis, apoptosis, and cancer-related signaling. Furthermore, a number of these pathways and genes have been previously identified to be hypermethylated in hematological malignancies and in some examples relevant to

clinical prognosis or therapeutic outcome. Although different levels and formulas of DIM treatment resulted in variable magnitudes of altered DNA methylation, the lists of genes identified by 3 different DIM treatments were remarkable similar. I3C treatment variably altered DNA methylation patterns compared with DIM although candidate gene validation revealed poor correlation between differential methylation analysis results and re-expression. Further validation of DNA methylation by pyrosequencing is necessary to confirm results from the Nimblegen platform, and in order to deduce actual relationships between methylation and expression in our data, and is ongoing.

Collectively the results described herein suggest that dietary phytochemicals derived from cruciferous vegetables exhibit bioactivity versus T-cell lymphoblastic lymphoma\leukemia (T-ALL) during both initiation and progression phases of carcinogenesis. It is likely that a range of mechanisms are responsible for the observed chemoprotective effects, and that these mechanisms vary among the studied phytochemicals and between the two models. However the long-term goal and future direction of this work is to identify overlapping and critical molecular targets. These phytochemicals are rapidly absorbed and eliminated *in vivo* and thus the timing of exposure is critical to their therapeutic effect. These bioactives hold promise for chemoprevention and chemotherapy, yet a better understanding of their interactions within a food matrix and their effects at supplemental levels is necessary before establishing intake recommendations. Similar to most nutritional supplements, pregnant and lactating women are not recommended to consume such commercially available products as I3C or broccoli sprout extract. As the developing fetus and the very young are especially sensitive to altered nutritional status and environmental exposures, preclinical animal models serve as a useful tool for directly examining the influence of maternal diet on offspring health.

BIBLIOGRAPHY

1. Burdge GC, Lillycrop KA (2010) Nutrition, epigenetics, and developmental plasticity: implications for understanding human disease. Annu Rev Nutr 30: 315-339.

2. Perera FP, Jedrychowski W, Rauh V, Whyatt RM (1999) Molecular epidemiologic research on the effects of environmental pollutants on the fetus. Environ Health Perspect 107 Suppl 3: 451-460.

3. Whyatt RM, Jedrychowski W, Hemminki K, Santella RM, Tsai WY, et al. (2001) Biomarkers of polycyclic aromatic hydrocarbon-DNA damage and cigarette smoke exposures in paired maternal and newborn blood samples as a measure of differential susceptibility. Cancer Epidemiol Biomarkers Prev 10: 581-588.

4. Topinka J, Milcova A, Libalova H, Novakova Z, Rossner P, Jr., et al. (2009) Biomarkers of exposure to tobacco smoke and environmental pollutants in mothers and their transplacental transfer to the foetus. Part I: bulky DNA adducts. Mutat Res 669: 13-19.

5. Georgiadis P, Topinka J, Vlachodimitropoulos D, Stoikidou M, Gioka M, et al. (2005) Interactions between CYP1A1 polymorphisms and exposure to environmental tobacco smoke in the modulation of lymphocyte bulky DNA adducts and chromosomal aberrations. Carcinogenesis 26: 93-101.

6. Whyatt RM, Bell DA, Jedrychowski W, Santella RM, Garte SJ, et al. (1998) Polycyclic aromatic hydrocarbon-DNA adducts in human placenta and modulation by CYP1A1 induction and genotype. Carcinogenesis 19: 1389-1392.

7. Orjuela MA, Liu X, Warburton D, Siebert AL, Cujar C, et al. (2010) Prenatal PAH exposure is associated with chromosome-specific aberrations in cord blood. Mutat Res 703: 108-114.

8. Anderson LM (2004) Predictive values of traditional animal bioassay studies for human perinatal carcinogenesis risk determination. Toxicol Appl Pharmacol 199: 162-174.

9. Anderson LM, Diwan BA, Fear NT, Roman E (2000) Critical windows of exposure for children's health: cancer in human epidemiological studies and neoplasms in experimental animal models. Environ Health Perspect 108 Suppl 3: 573-594.

10. Lightfoot TJ, Roman E (2004) Causes of childhood leukaemia and lymphoma. Toxicol Appl Pharmacol 199: 104-117.

11. Badham HJ, LeBrun DP, Rutter A, Winn LM (2010) Transplacental benzene exposure increases tumor incidence in mouse offspring: possible role of fetal benzene metabolism. Carcinogenesis 31: 1142-1148.

12. Waalkes MP, Liu J, Diwan BA (2007) Transplacental arsenic carcinogenesis in mice. Toxicol Appl Pharmacol 222: 271-280.

13. Nicolov IG, Chernozemsky IN (1979) Tumors and hyperplastic lesions in Syrian hamsters following transplacental and neonatal treatment with cigarette smoke condensate. J Cancer Res Clin Oncol 94: 249-256.

14. Diwan BA, Anderson LM, Rehm S, Rice JM (1993) Transplacental carcinogenicity of cisplatin: initiation of skin tumors and induction of other preneoplastic and neoplastic lesions in SENCAR mice. Cancer Res 53: 3874-3876.

15. Brucher JM, Ermel AE (1974) Central neuroblastoma induced by transplacental administration of methylnitrosourea in Wistar-R rats. An electron microscopic study. J Neurol 208: 1-16.

16. Bostrom CE, Gerde P, Hanberg A, Jernstrom B, Johansson C, et al. (2002) Cancer risk assessment, indicators, and guidelines for polycyclic aromatic hydrocarbons in the ambient air. Environ Health Perspect 110 Suppl 3: 451-488.

17. Ramesh A, Walker SA, Hood DB, Guillen MD, Schneider K, et al. (2004) Bioavailability and risk assessment of orally ingested polycyclic aromatic hydrocarbons. Int J Toxicol 23: 301-333.

18. Neubert D, Tapken S (1988) Transfer of benzo(a)pyrene into mouse embryos and fetuses. Arch Toxicol 62: 236-239.

19. Shorey LE, Castro DJ, Baird WM, Siddens LK, Lohr CV, et al. (2012) Transplacental carcinogenesis with dibenzo[def,p]chrysene (DBC): timing of maternal exposures determines target tissue response in offspring. Cancer Lett 317: 49-55.

20. Loktionov A, Hollstein M, Martel N, Galendo D, Cabral JR, et al. (1990) Tissue-specific activating mutations of Ha- and Ki-ras oncogenes in skin, lung, and liver tumors induced in mice following transplacental exposure to DMBA. Mol Carcinog 3: 134-140.

21. Munoz EF, Diwan BA, Calvert RJ, Weghorst CM, Anderson J, et al. (1996) Transplacental mutagenicity of cisplatin: H-ras codon 12 and 13 mutations in skin tumors of SENCAR mice. Carcinogenesis 17: 2741-2745.

22. Hashim S, Banerjee S, Madhubala R, Rao AR (1998) Chemoprevention of DMBA-induced transplacental and translactational carcinogenesis in mice by oil from mustard seeds (Brassica spp.). Cancer Lett 134: 217-226.

23. Rao AR, Hashim S (1995) Chemopreventive action of oriental food-seasoning spices mixture Garam masala on DMBA-induced transplacental and translactational carcinogenesis in mice. Nutr Cancer 23: 91-101.

24. Kossoy G, Yarden G, Benhur H, Sandler B, Zusman, II, et al. (2000) Transplacental effects of a 15% olive-oil diet on chemically-induced tumorigenesis in offspring. Oncol Rep 7: 1145-1148.

25. Mohr U, Emura M, Aufderheide M, Riebe M, Ernst H (1989) Possible role of genetic predisposition in multigeneration carcinogenesis. IARC Sci Publ: 93-103.

26. Boylan ES, Calhoon RE (1983) Transplacental action of diethylstilbestrol on mammary carcinogenesis in female rats given one or two doses of 7,12-dimethylbenz(a)anthracene. Cancer Res 43: 4879-4884.

27. Anderson LM, Ruskie S, Carter J, Pittinger S, Kovatch RM, et al. (1995) Fetal mouse susceptibility to transplacental carcinogenesis: differential influence of Ah receptor phenotype on effects of 3-methylcholanthrene, 12-dimethylbenz[a]anthracene, and benzo[a]pyrene. Pharmacogenetics 5: 364-372.

28. Yu Z, Loehr CV, Fischer KA, Louderback MA, Krueger SK, et al. (2006) In utero exposure of mice to dibenzo[a,l]pyrene produces lymphoma in the offspring: role of the aryl hydrocarbon receptor. Cancer Res 66: 755-762.

29. Donovan PJ, Smith GT, Nardone R (2004) The mutagenic effects of 7,12-dimethylbenz[a]anthacene, 3-methylcholanthrene and benzo[a]pyrene to the developing Syrian hamster fetus measured by an in vivo/in vitro mutation assay. Mutat Res 554: 111-120.

30. Castro DJ, Löhr CV, Fischer KA, Pereira CB, Williams DE (2008) Lymphoma and lung cancer in offspring born to pregnant mice dosed with dibenzo[a,l]pyrene: the importance of in utero vs. lactational exposure. Toxicol Appl Pharmacol 233: 454-458.

31. Castro DJ, Baird WM, Pereira CB, Giovanini J, Löhr CV, et al. (2008) Fetal mouse Cyp1b1 and transplacental carcinogenesis from maternal exposure to dibenzo(a,l)pyrene. Cancer Prev Res 1: 128-134.

32. Yu Z, Mahadevan B, Löhr CV, Fischer KA, Louderback MA, et al. (2006) Indole-3-carbinol in the maternal diet provides chemoprotection for the fetus against transplacental carcinogenesis by the polycyclic aromatic hydrocarbon dibenzo[a,l]pyrene. Carcinogenesis 27: 2116-2123.

33. Castro DJ, Yu Z, Löhr CV, Pereira CB, Giovanini JN, et al. (2008) Chemoprevention of dibenzo[a,l]pyrene transplacental carcinogenesis in mice born to mothers administered green tea: primary role of caffeine. Carcinogenesis 29: 1581-1586.

34. Castro DJ, Lohr CV, Fischer KA, Waters KM, Webb-Robertson BJ, et al. (2009) Identifying efficacious approaches to chemoprevention with chlorophyllin, purified chlorophylls and freeze-dried spinach in a mouse model of transplacental carcinogenesis. Carcinogenesis 30: 315-320.

35. Howlader N, Noone A, Krapcho M, Neyman N, Aminou R, et al. (2011) SEER Cancer Statistics Review, 1975–2008. Bethesda, MD: National Cancer Institute.

36. Society AC (2012) Cancer Facts & Figures 2012. Atlanta, GA.

37. Goldberg JM, Silverman LB, Levy DE, Dalton VK, Gelber RD, et al. (2003) Childhood T-cell acute lymphoblastic leukemia: the Dana-Farber Cancer Institute acute lymphoblastic leukemia consortium experience. J Clin Oncol 21: 3616-3622.

38. Aifantis I, Raetz E, Buonamici S (2008) Molecular pathogenesis of T-cell leukaemia and lymphoma. Nat Rev Immunol 8: 380-390.

39. Burkhardt B (2010) Paediatric lymphoblastic T-cell leukaemia and lymphoma: one or two diseases? Br J Haematol 149: 653-668.

40. Teitell MA, Pandolfi PP (2009) Molecular genetics of acute lymphoblastic leukemia. Annu Rev Pathol 4: 175-198.

41. Karakaya A, Ates I, Yucesoy B (2004) Effects of occupational polycyclic aromatic hydrocarbon exposure on T-lymphocyte functions and natural killer cell activity in asphalt and coke oven workers. Hum Exp Toxicol 23: 317-322.

42. Sul D, Oh E, Im H, Yang M, Kim CW, et al. (2003) DNA damage in T- and B-lymphocytes and granulocytes in emission inspection and incineration workers exposed to polycyclic aromatic hydrocarbons. Mutat Res 538: 109-119.

43. Choudhary D, Jansson I, Stoilov I, Sarfarazi M, Schenkman JB (2005) Expression patterns of mouse and human CYP orthologs (families 1-4) during development and in different adult tissues. Arch Biochem Biophys 436: 50-61.

44. Uno S, Dalton TP, Dragin N, Curran CP, Derkenne S, et al. (2006) Oral benzo[a]pyrene in Cyp1 knockout mouse lines: CYP1A1 important in detoxication, CYP1B1 metabolism required for immune damage independent of total-body burden and clearance rate. Mol Pharmacol 69: 1103-1114.

45. Miyata M, Furukawa M, Takahashi K, Gonzalez FJ, Yamazoe Y (2001) Mechanism of 7,12-dimethylbenz[a]anthracene-induced immunotoxicity: role of metabolic activation at the target organ. Jpn J Pharmacol 86: 302-309.

46. Heidel SM, MacWilliams PS, Baird WM, Dashwood WM, Buters JT, et al. (2000) Cytochrome P4501B1 mediates induction of bone marrow cytotoxicity and preleukemia cells in mice treated with 7,12-dimethylbenz[a]anthracene. Cancer Res 60: 3454-3460.

47. Wojdani A, Alfred LJ (1984) Alterations in cell-mediated immune functions induced in mouse splenic lymphocytes by polycyclic aromatic hydrocarbons. Cancer Res 44: 942-945.

48. Blumer JL, Dunn R, Esterhay MD, Yamashita TS, Gross S (1981) Lymphocyte aromatic hydrocarbon responsiveness in acute leukemia of childhood. Blood 58: 1081-1088.

49. Yamashita TS, Frank D, Dunn R, Gross SJ, Blumer JL (1989) Pedigree analysis of aryl hydrocarbon hydroxylase inducibility in acute leukemia of childhood. Leuk Res 13: 771-779.

50. Infante-Rivard C, Krajinovic M, Labuda D, Sinnett D (2000) Parental smoking, CYP1A1 genetic polymorphisms and childhood leukemia (Quebec, Canada). Cancer Causes Control 11: 547-553.

51. Clavel J, Bellec S, Rebouissou S, Menegaux F, Feunteun J, et al. (2005) Childhood leukaemia, polymorphisms of metabolism enzyme genes, and interactions with maternal tobacco, coffee and alcohol consumption during pregnancy. Eur J Cancer Prev 14: 531-540.

52. Lee KM, Ward MH, Han S, Ahn HS, Kang HJ, et al. (2009) Paternal smoking, genetic polymorphisms in CYP1A1 and childhood leukemia risk. Leuk Res 33: 250-258.

53. John EM, Savitz DA, Sandler DP (1991) Prenatal exposure to parents' smoking and childhood cancer. Am J Epidemiol 133: 123-132.

54. Mucci LA, Granath F, Cnattingius S (2004) Maternal smoking and childhood leukemia and lymphoma risk among 1,440,542 Swedish children. Cancer Epidemiol Biomarkers Prev 13: 1528-1533.

55. Milne E, Greenop KR, Scott RJ, Bailey HD, Attia J, et al. (2012) Parental prenatal smoking and risk of childhood acute lymphoblastic leukemia. Am J Epidemiol 175: 43-53.

56. Lederman SA, Rauh V, Weiss L, Stein JL, Hoepner LA, et al. (2004) The effects of the World Trade Center event on birth outcomes among term deliveries at three lower Manhattan hospitals. Environ Health Perspect 112: 1772-1778.

57. Perera FP, Tang D, Tu YH, Cruz LA, Borjas M, et al. (2004) Biomarkers in maternal and newborn blood indicate heightened fetal susceptibility to procarcinogenic DNA damage. Environ Health Perspect 112: 1133-1136.

58. Perera F, Tang D, Whyatt R, Lederman SA, Jedrychowski W (2005) DNA damage from polycyclic aromatic hydrocarbons measured by benzo[a]pyrene-DNA adducts in mothers and newborns from Northern Manhattan, the World Trade Center Area, Poland, and China. Cancer Epidemiol Biomarkers Prev 14: 709-714.

59. Perera FP, Tang D, Rauh V, Lester K, Tsai WY, et al. (2005) Relationships among polycyclic aromatic hydrocarbon-DNA adducts, proximity to the World Trade Center, and effects on fetal growth. Environ Health Perspect 113: 1062-1067.

60. Bocskay KA, Tang D, Orjuela MA, Liu X, Warburton DP, et al. (2005) Chromosomal aberrations in cord blood are associated with prenatal exposure to carcinogenic polycyclic aromatic hydrocarbons. Cancer Epidemiol Biomarkers Prev 14: 506-511.

61. WCRF/AICR (1997) Food, Nutrition, Physical Activity, and the Prevention of Cancer: a Global Perspective, Washington, DC.

62. WCRF/AICR (2007) Food, Nutrition, Physical Activity, and the Prevention of Cancer: a Global Perspective, Washington, DC.

63. Lampe JW (2009) Interindividual differences in response to plant-based diets: implications for cancer risk. Am J Clin Nutr 89: 1553S-1557S.

64. Ambrosone CB, Tang L (2009) Cruciferous vegetable intake and cancer prevention: role of nutrigenetics. Cancer Prev Res 2: 298-300.

65. Donaldson MS (2004) Nutrition and cancer: a review of the evidence for an anti-cancer diet. Nutr J 3: e19.

66. Sarkar FH, Li Y (2004) Cell signaling pathways altered by natural chemopreventive agents. Mutat Res 555: 53-64.

67. Chung FL, Wang M, Rivenson A, Iatropoulos MJ, Reinhardt JC, et al. (1998) Inhibition of lung carcinogenesis by black tea in Fischer rats treated with a tobacco-specific carcinogen: caffeine as an important constituent. Cancer Res 58: 4096-4101.

68. Hsu A, Bray TM, Ho E (2010) Anti-inflammatory activity of soy and tea in prostate cancer prevention. Exp Biol Med 235: 659-667.

69. Hussain AR, Al-Rasheed M, Manogaran PS, Al-Hussein KA, Platanias LC, et al. (2006) Curcumin induces apoptosis via inhibition of PI3'-kinase/AKT pathway in acute T cell leukemias. Apoptosis 11: 245-254.

70. Higdon JV, Delage B, Williams DE, Dashwood RH (2007) Cruciferous vegetables and human cancer risk: epidemiologic evidence and mechanistic basis. Pharmacol Res 55: 224-236.

71. Herr I, Buchler MW (2010) Dietary constituents of broccoli and other cruciferous vegetables: implications for prevention and therapy of cancer. Cancer Treat Rev 36: 377-383.

72. Hayes JD, Kelleher MO, Eggleston IM (2008) The cancer chemopreventive actions of phytochemicals derived from glucosinolates. Eur J Nutr 47 Suppl 2: 73-88.

73. Matusheski NV, Jeffery EH (2001) Comparison of the bioactivity of two glucoraphanin hydrolysis products found in broccoli, sulforaphane and sulforaphane nitrile. J Agric Food Chem 49: 5743-5749.

74. Juge N, Mithen RF, Traka M (2007) Molecular basis for chemoprevention by sulforaphane: a comprehensive review. Cell Mol Life Sci 64: 1105-1127.

75. Carlson D, Kwolek, W. and Williams, P (1987) Glucosinolates in crucifer vegetables: broccoli, Brussels sprouts, cauliflower, collards, kale, mustard greens, and kohlrabi. J Amer Soc Hort Sci 112: 173-178.

76. Kushad MM, Brown AF, Kurilich AC, Juvik JA, Klein BP, et al. (1999) Variation of glucosinolates in vegetable crops of Brassica oleracea. J Agric Food Chem 47: 1541-1548.

77. Verkerk R, van der Gaag MS, Dekker M, Jongen WM (1997) Effects of processing conditions on glucosinolates in cruciferous vegetables. Cancer Lett 114: 193-194.

78. Agerbirk N, De vos M, Kim JH, Jander G (2009) Indole glucosinolate breakdown and its biological effects. Phytochem Rev 8: 101-120.

79. Burow M, Zhang Z-Y, Ober JA, Lambrix VM, Wittstock U, et al. (2008) ESP and ESM1 mediate indol-3-acetonitrile production from indol-3-ylmethyl glucosinolate in Arabidopsis. Phytochemistry 69: 663–671.

80. Dashwood RH, Fong AT, Arbogast DN, Bjeldanes LF, Hendricks JD, et al. (1994) Anticarcinogenic activity of indole-3-carbinol acid products: ultrasensitive bioassay by trout embryo microinjection. Cancer Res 54: 3617-3619.

81. Bradlow HL, Zeligs MA (2010) Diindolylmethane (DIM) spontaneously forms from indole-3-carbinol (I3C) during cell culture experiments. In Vivo 24: 387-391.

82. Staub RE, Onisko B, Bjeldanes LF (2006) Fate of 3,3'-diindolylmethane in cultured MCF-7 human breast cancer cells. Chem Res Toxicol 19: 436-442.

83. Staub RE, Feng C, Onisko B, Bailey GS, Firestone GL, et al. (2002) Fate of indole-3-carbinol in cultured human breast tumor cells. Chem Res Toxicol 15: 101-109.

84. Chang YC, Riby J, Chang GH, Peng BC, Firestone G, et al. (1999) Cytostatic and antiestrogenic effects of 2-(indol-3-ylmethyl)-3,3'-diindolylmethane, a major in vivo product of dietary indole-3-carbinol. Biochem Pharmacol 58: 825-834.

85. Bradfield CA, Bjeldanes LF (1987) Structure-activity relationships of dietary indoles: a proposed mechanism of action as modifiers of xenobiotic metabolism. J Toxicol Environ Health 21: 311-323.

86. Anderton MJ, Manson MM, Verschoyle RD, Gescher A, Lamb JH, et al. (2004) Pharmacokinetics and tissue disposition of indole-3-carbinol and its acid

condensation products after oral administration to mice. Clin Cancer Res 10: 5233-5241.

87. Howells LM, Moiseeva EP, Neal CP, Foreman BE, Andreadi CK, et al. (2007) Predicting the physiological relevance of in vitro cancer preventive activities of phytochemicals. Acta Pharmacol Sin 28: 1274-1304.

88. Reed GA, Arneson DW, Putnam WC, Smith HJ, Gray JC, et al. (2006) Single-dose and multiple-dose administration of indole-3-carbinol to women: pharmacokinetics based on 3,3'-diindolylmethane. Cancer Epidemiol Biomarkers Prev 15: 2477-2481.

89. Anderton MJ, Manson MM, Verschoyle R, Gescher A, Steward WP, et al. (2004) Physiological modeling of formulated and crystalline 3,3'-diindolylmethane pharmacokinetics following oral administration in mice. Drug Metab Dispos 32: 632-638.

90. Reed GA, Sunega JM, Sullivan DK, Gray JC, Mayo MS, et al. (2008) Single-dose pharmacokinetics and tolerability of absorption-enhanced 3,3'-diindolylmethane in healthy subjects. Cancer Epidemiol Biomarkers Prev 17: 2619-2624.

91. Heath EI, Heilbrun LK, Li J, Vaishampayan U, Harper F, et al. (2010) A phase I dose-escalation study of oral BR-DIM (BioResponse 3,3'- Diindolylmethane) in castrate-resistant, non-metastatic prostate cancer. Am J Transl Res 2: 402-411.

92. Del Priore G, Gudipudi DK, Montemarano N, Restivo AM, Malanowska-Stega J, et al. (2010) Oral diindolylmethane (DIM): pilot evaluation of a nonsurgical treatment for cervical dysplasia. Gynecol Oncol 116: 464-467.

93. Bradlow HL, Michnovicz JJ, Halper M, Miller DG, Wong GY, et al. (1994) Long-term responses of women to indole-3-carbinol or a high fiber diet. Cancer Epidemiol Biomarkers Prev 3: 591-595.

94. Fimognari C, Turrini E, Ferruzzi L, Lenzi M, Hrelia P (2011) Natural isothiocyanates: Genotoxic potential versus chemoprevention. Mutat Res 750: 107-131.

95. Paolini M, Perocco P, Canistro D, Valgimigli L, Pedulli GF, et al. (2004) Induction of cytochrome P450, generation of oxidative stress and in vitro cell-transforming and DNA-damaging activities by glucoraphanin, the bioprecursor of the chemopreventive agent sulforaphane found in broccoli. Carcinogenesis 25: 61-67.

96. Leibelt DA, Hedstrom OR, Fischer KA, Pereira CB, Williams DE (2003) Evaluation of chronic dietary exposure to indole-3-carbinol and absorption-enhanced 3,3'-diindolylmethane in sprague-dawley rats. Toxicol Sci 74: 10-21.

97. Zhang Y, Talalay P, Cho CG, Posner GH (1992) A major inducer of anticarcinogenic protective enzymes from broccoli: isolation and elucidation of structure. Proc Natl Acad Sci (USA) 89: 2399-2403.

98. Clarke JD, Hsu A, Riedl K, Bella D, Schwartz SJ, et al. (2011) Bioavailability and inter-conversion of sulforaphane and erucin in human subjects consuming broccoli sprouts or broccoli supplement in a cross-over study design. Pharmacol Res 64: 456-463.

99. Zhang Y, Callaway EC (2002) High cellular accumulation of sulphoraphane, a dietary anticarcinogen, is followed by rapid transporter-mediated export as a glutathione conjugate. Biochem J 364: 301-307.

100. Zhang Y (2000) Role of glutathione in the accumulation of anticarcinogenic isothiocyanates and their glutathione conjugates by murine hepatoma cells. Carcinogenesis 21: 1175-1182.

101. Clarke JD, Hsu A, Williams DE, Dashwood RH, Stevens JF, et al. (2011) Metabolism and tissue distribution of sulforaphane in Nrf2 knockout and wild-type mice. Pharm Res 28: 3171-3179.

102. Perocco P, Bronzetti G, Canistro D, Valgimigli L, Sapone A, et al. (2006) Glucoraphanin, the bioprecursor of the widely extolled chemopreventive agent sulforaphane found in broccoli, induces phase-I xenobiotic metabolizing enzymes and increases free radical generation in rat liver. Mutat Res 595: 125-136.

103. Loub WD, Wattenberg LW, Davis DW (1975) Aryl hydrocarbon hydroxylase induction in rat tissues by naturally occurring indoles of cruciferous plants. J Natl Cancer Inst 54: 985-988.

104. Nebert DW, Dalton TP (2006) The role of cytochrome P450 enzymes in endogenous signalling pathways and environmental carcinogenesis. Nat Rev Cancer 6: 947-960.

105. Chen I, McDougal A, Wang F, Safe S (1998) Aryl hydrocarbon receptor-mediated antiestrogenic and antitumorigenic activity of diindolylmethane. Carcinogenesis 19: 1631-1639.

106. Ociepa-Zawal M, Rubis B, Lacinski M, Trzeciak WH (2007) The effect of indole-3-carbinol on the expression of CYP1A1, CYP1B1 and AhR genes and proliferation of MCF-7 cells. Acta Biochim Pol 54: 113-117.

107. Wagner AE, Ernst I, Iori R, Desel C, Rimbach G (2010) Sulforaphane but not ascorbigen, indole-3-carbinole and ascorbic acid activates the transcription factor Nrf2 and induces phase-2 and antioxidant enzymes in human keratinocytes in culture. Exp Dermatol 19: 137-144.

108. Ernst IM, Schuemann C, Wagner AE, Rimbach G (2011) 3,3'-Diindolylmethane but not indole-3-carbinol activates Nrf2 and induces Nrf2 target gene expression in cultured murine fibroblasts. Free Radic Res 45: 941-949.

109. Saw CL, Cintron M, Wu TY, Guo Y, Huang Y, et al. (2011) Pharmacodynamics of dietary phytochemical indoles I3C and DIM: Induction of Nrf2-mediated phase II drug metabolizing and antioxidant genes and synergism with isothiocyanates. Biopharm Drug Dispos 32: 289-300.

110. Shimada T (2006) Xenobiotic-metabolizing enzymes involved in activation and detoxification of carcinogenic polycyclic aromatic hydrocarbons. Drug Metab Pharmacokinet 21: 257-276.

111. Morse MA, LaGreca SD, Amin SG, Chung FL (1990) Effects of indole-3-carbinol on lung tumorigenesis and DNA methylation induced by 4-(methylnitrosamino)-1-(3-pyridyl)-1-butanone (NNK) and on the metabolism and disposition of NNK in A/J mice. Cancer Res 50: 2613-2617.

112. Choi HJ, Lim do Y, Park JH (2009) Induction of G1 and G2/M cell cycle arrests by the dietary compound 3,3'-diindolylmethane in HT-29 human colon cancer cells. BMC Gastroenterol 9: e39.

113. Firestone GL, Bjeldanes LF (2003) Indole-3-carbinol and 3-3'-diindolylmethane antiproliferative signaling pathways control cell-cycle gene transcription in human breast cancer cells by regulating promoter-Sp1 transcription factor interactions. J Nutr 133: 2448S-2455S.

114. Hong C, Kim HA, Firestone GL, Bjeldanes LF (2002) 3,3'-Diindolylmethane (DIM) induces a G(1) cell cycle arrest in human breast cancer cells that is accompanied by Sp1-mediated activation of p21(WAF1/CIP1) expression. Carcinogenesis 23: 1297-1305.

115. Fimognari C, Nusse M, Berti F, Iori R, Cantelli-Forti G, et al. (2003) Sulforaphane modulates cell cycle and apoptosis in transformed and non-transformed human T lymphocytes. Ann N Y Acad Sci 1010: 393-398.

116. Kim JH, Han Kwon K, Jung JY, Han HS, Hyun Shim J, et al. (2010) Sulforaphane increases cyclin-dependent kinase inhibitor, p21 protein in human oral carcinoma cells and nude mouse animal model to induce G(2)/M cell cycle arrest. J Clin Biochem Nutr 46: 60-67.

117. Matthews J, Gustafsson JA (2006) Estrogen receptor and aryl hydrocarbon receptor signaling pathways. Nucl Recept Signal 4: e016.

118. Myzak MC, Karplus PA, Chung FL, Dashwood RH (2004) A novel mechanism of chemoprotection by sulforaphane: inhibition of histone deacetylase. Cancer Res 64: 5767-5774.

119. Li Y, Li X, Guo B (2010) Chemopreventive agent 3,3'-diindolylmethane selectively induces proteasomal degradation of class I histone deacetylases. Cancer Res 70: 646-654.

120. Clarke JD, Dashwood RH, Ho E (2008) Multi-targeted prevention of cancer by sulforaphane. Cancer Lett 269: 291-304.

121. Banerjee S, Kong D, Wang Z, Bao B, Hillman GG, et al. (2011) Attenuation of multi-targeted proliferation-linked signaling by 3,3'-diindolylmethane (DIM): from bench to clinic. Mutat Res 728: 47-66.

122. Sarkar FH, Li Y, Wang Z, Kong D (2009) Cellular signaling perturbation by natural products. Cell Signal 21: 1541-1547.

123. Verkerk R, Schreiner M, Krumbein A, Ciska E, Holst B, et al. (2009) Glucosinolates in Brassica vegetables: the influence of the food supply chain on intake, bioavailability and human health. Mol Nutr Food Res 53 Suppl 2: S219 –S265.

124. Matusheski NV, Juvik JA, Jeffery EH (2004) Heating decreases epithiospecifier protein activity and increases sulforaphane formation in broccoli. Phytochemistry 65: 1273-1281.

125. Lai RH, Miller MJ, Jeffery E (2010) Glucoraphanin hydrolysis by microbiota in the rat cecum results in sulforaphane absorption. Food Funct 1: 161-166.

126. Hauder J, Winkler S, Bub A, Rufer CE, Pignitter M, et al. (2011) LC-MS/MS quantification of sulforaphane and indole-3-carbinol metabolites in human plasma and urine after dietary intake of selenium-fortified broccoli. J Agric Food Chem 59: 8047-8057.

127. Shapiro TA, Fahey JW, Wade KL, Stephenson KK, Talalay P (2001) Chemoprotective glucosinolates and isothiocyanates of broccoli sprouts: metabolism and excretion in humans. Cancer Epidemiol Biomarkers Prev 10: 501-508.

128. Vermeulen M, Klopping-Ketelaars IW, van den Berg R, Vaes WH (2008) Bioavailability and kinetics of sulforaphane in humans after consumption of cooked versus raw broccoli. J Agric Food Chem 56: 10505-10509.

129. Cramer JM, Jeffery EH (2011) Sulforaphane absorption and excretion following ingestion of a semi-purified broccoli powder rich in glucoraphanin and broccoli sprouts in healthy men. Nutr Cancer 63: 196-201.

130. Cramer JM, Teran-Garcia M, Jeffery EH (2011) Enhancing sulforaphane absorption and excretion in healthy men through the combined consumption of fresh broccoli sprouts and a glucoraphanin-rich powder. Br J Nutr [Epub ahead of print]: 1-6.

131. Hanlon N, Coldham N, Gielbert A, Sauer MJ, Ioannides C (2009) Repeated intake of broccoli does not lead to higher plasma levels of sulforaphane in human volunteers. Cancer Lett 284: 15-20.

132. Shapiro TA, Fahey JW, Dinkova-Kostova AT, Holtzclaw WD, Stephenson KK, et al. (2006) Safety, tolerance, and metabolism of broccoli sprout glucosinolates and isothiocyanates: a clinical phase I study. Nutr Cancer 55: 53-62.

133. Clarke JD, Riedl K, Bella D, Schwartz SJ, Stevens JF, et al. (2011) Comparison of isothiocyanate metabolite levels and histone deacetylase activity in human subjects consuming broccoli sprouts or broccoli supplement. J Agric Food Chem 59: 10955-10963.

134. Stoewsand GS, Anderson JL, Munson L (1988) Protective effect of dietary brussels sprouts against mammary carcinogenesis in Sprague-Dawley rats. Cancer Lett 39: 199-207.

135. Fahey JW, Zhang Y, Talalay P (1997) Broccoli sprouts: an exceptionally rich source of inducers of enzymes that protect against chemical carcinogens. Proc Natl Acad Sci (USA) 94: 10367-10372.

136. Munday R, Mhawech-Fauceglia P, Munday CM, Paonessa JD, Tang L, et al. (2008) Inhibition of urinary bladder carcinogenesis by broccoli sprouts. Cancer Res 68: 1593-1600.

137. Dinkova-Kostova AT, Jenkins SN, Fahey JW, Ye L, Wehage SL, et al. (2006) Protection against UV-light-induced skin carcinogenesis in SKH-1 high-risk mice by sulforaphane-containing broccoli sprout extracts. Cancer Lett 240: 243-252.

138. Wang GC, Farnham MW, Jeffery EH (2012) Impact of thermal processing on sulforaphane yield from broccoli (Brassica oleracea L. var italica). J Agric Food Chem [Epub ahead of print].

139. Liu AG, Volker SE, Jeffery EH, Erdman JW, Jr. (2009) Feeding tomato and broccoli powders enriched with bioactives improves bioactivity markers in rats. J Agric Food Chem 57: 7304-7310.

140. Keck AS, Qiao Q, Jeffery EH (2003) Food matrix effects on bioactivity of broccoli-derived sulforaphane in liver and colon of F344 rats. J Agric Food Chem 51: 3320-3327.

141. Hwang ES, Jeffery EH (2004) Effects of different processing methods on induction of quinone reductase by dietary broccoli in rats. J Med Food 7: 95-99.

142. Dinkova-Kostova AT, Fahey JW, Wade KL, Jenkins SN, Shapiro TA, et al. (2007) Induction of the phase 2 response in mouse and human skin by

sulforaphane-containing broccoli sprout extracts. Cancer Epidemiol Biomarkers Prev 16: 847-851.

143. Nomura T (2003) Transgenerational carcinogenesis: induction and transmission of genetic alterations and mechanisms of carcinogenesis. Mutat Res 544: 425-432.

144. Yamasaki H, Loktionov A, Tomatis L (1992) Perinatal and multigenerational effect of carcinogens: possible contribution to determination of cancer susceptibility. Environ Health Perspect 98: 39-43.

145. Mohr U, Dasenbrock C, Tillmann T, Kohler M, Kamino K, et al. (1999) Possible carcinogenic effects of X-rays in a transgenerational study with CBA mice. Carcinogenesis 20: 325-332.

146. Holliday R (2006) Epigenetics: a historical overview. Epigenetics 1: 76-80.

147. LeBaron MJ, Rasoulpour RJ, Klapacz J, Ellis-Hutchings RG, Hollnagel HM, et al. (2010) Epigenetics and chemical safety assessment. Mutat Res 705: 83-95.

148. Roseboom TJ, van der Meulen JH, Ravelli AC, Osmond C, Barker DJ, et al. (2001) Effects of prenatal exposure to the Dutch famine on adult disease in later life: an overview. Mol Cell Endocrinol 185: 93-98.

149. Alfaradhi MZ, Ozanne SE (2011) Developmental programming in response to maternal overnutrition. Front Genet 2: e27.

150. Newhook LA, Sloka S, Grant M, Randell E, Kovacs CS, et al. (2009) Vitamin D insufficiency common in newborns, children and pregnant women living in Newfoundland and Labrador, Canada. Matern Child Nutr 5: 186-191.

151. Heijmans BT, Tobi EW, Stein AD, Putter H, Blauw GJ, et al. (2008) Persistent epigenetic differences associated with prenatal exposure to famine in humans. Proc Natl Acad Sci (USA) 105: 17046-17049.

152. Callan AC, Milne E (2009) Involvement of the IGF system in fetal growth and childhood cancer: an overview of potential mechanisms. Cancer Causes Control 20: 1783-1798.

153. Song J, Medline A, Mason JB, Gallinger S, Kim YI (2000) Effects of dietary folate on intestinal tumorigenesis in the ApcMin mouse. Cancer Res 60: 5434-5440.

154. Kim YI, Salomon RN, Graeme-Cook F, Choi SW, Smith DE, et al. (1996) Dietary folate protects against the development of macroscopic colonic neoplasia in a dose responsive manner in rats. Gut 39: 732-740.

155. Garcia-Manero G, Yang H, Kuang SQ, O'Brien S, Thomas D, et al. (2009) Epigenetics of acute lymphocytic leukemia. Semin Hematol 46: 24-32.

156. Hogan LE, Meyer JA, Yang J, Wang J, Wong N, et al. (2011) Integrated genomic analysis of relapsed childhood acute lymphoblastic leukemia reveals therapeutic strategies. Blood 118: 5218-5226.

157. Takeuchi S, Matsushita M, Zimmermann M, Ikezoe T, Komatsu N, et al. (2011) Clinical significance of aberrant DNA methylation in childhood acute lymphoblastic leukemia. Leuk Res 35: 1345-1349.

158. Paulsson K, An Q, Moorman AV, Parker H, Molloy G, et al. (2009) Methylation of tumour suppressor gene promoters in the presence and absence of transcriptional silencing in high hyperdiploid acute lymphoblastic leukaemia. Br J Haematol 144: 838-847.

159. Kuang SQ, Tong WG, Yang H, Lin W, Lee MK, et al. (2008) Genome-wide identification of aberrantly methylated promoter associated CpG islands in acute lymphocytic leukemia. Leukemia 22: 1529-1538.

160. Dunwell TL, Hesson LB, Pavlova T, Zabarovska V, Kashuba V, et al. (2009) Epigenetic analysis of childhood acute lymphoblastic leukemia. Epigenetics 4: 185-193.

161. Dolinoy DC, Huang D, Jirtle RL (2007) Maternal nutrient supplementation counteracts bisphenol A-induced DNA hypomethylation in early development. Proc Natl Acad Sci (USA) 104: 13056-13061.

162. Rao AR, Hussain SP, Jannu L (1989) Modulation of 7,12-dimethylbenz[a]anthracene-induced transmammary carcinogenesis by disulfiram and butylated hydroxyanisole in mice. Jpn J Cancer Res 80: 1171-1175.

163. Chen CS, Squire JA, Wells PG (2009) Reduced tumorigenesis in p53 knockout mice exposed in utero to low-dose vitamin E. Cancer 115: 1563-1575.

164. Ion G, Akinsete JA, Hardman WE (2010) Maternal consumption of canola oil suppressed mammary gland tumorigenesis in C3(1) TAg mice offspring. BMC Cancer 10: e81.

165. Su HM, Hsieh PH, Chen HF (2010) A maternal high n-6 fat diet with fish oil supplementation during pregnancy and lactation in rats decreases breast cancer risk in the female offspring. J Nutr Biochem 21: 1033-1037.

166. Stark AH, Kossoy G, Zusman I, Yarden G, Madar Z (2003) Olive oil consumption during pregnancy and lactation in rats influences mammary cancer development in female offspring. Nutr Cancer 46: 59-65.

167. Kovacheva VP, Davison JM, Mellott TJ, Rogers AE, Yang S, et al. (2009) Raising gestational choline intake alters gene expression in DMBA-evoked mammary tumors and prolongs survival. Faseb J 23: 1054-1063.

168. Khan G, Penttinen P, Cabanes A, Foxworth A, Chezek A, et al. (2007) Maternal flaxseed diet during pregnancy or lactation increases female rat offspring's

susceptibility to carcinogen-induced mammary tumorigenesis. Reprod Toxicol 23: 397-406.

169. Yu B, Khan G, Foxworth A, Huang K, Hilakivi-Clarke L (2006) Maternal dietary exposure to fiber during pregnancy and mammary tumorigenesis among rat offspring. Int J Cancer 119: 2279-2286.

170. Raju J, Bielecki A, Caldwell D, Lok E, Taylor M, et al. (2009) Soy isoflavones modulate azoxymethane-induced rat colon carcinogenesis exposed pre- and postnatally and inhibit growth of DLD-1 human colon adenocarcinoma cells by increasing the expression of estrogen receptor-beta. J Nutr 139: 474-481.

171. Su Y, Eason RR, Geng Y, Till SR, Badger TM, et al. (2007) In utero exposure to maternal diets containing soy protein isolate, but not genistein alone, protects young adult rat offspring from NMU-induced mammary tumorigenesis. Carcinogenesis 28: 1046-1051.

172. Xiao R, Hennings LJ, Badger TM, Simmen FA (2007) Fetal programming of colon cancer in adult rats: correlations with altered neonatal growth trajectory, circulating IGF-I and IGF binding proteins, and testosterone. J Endocrinol 195: 79-87.

173. Chen CS, Wells PG (2006) Enhanced tumorigenesis in p53 knockout mice exposed in utero to high-dose vitamin E. Carcinogenesis 27: 1358-1368.

174. Joss-Moore LA, Wang Y, Baack ML, Yao J, Norris AW, et al. (2010) IUGR decreases PPARgamma and SETD8 expression in neonatal rat lung and these effects are ameliorated by maternal DHA supplementation. Early Hum Dev 86: 785-791.

175. Doll R, Peto R (1981) The causes of cancer: quantitative estimates of avoidable risks of cancer in the United States today. J Natl Cancer Inst 66: 1191-1308.

176. Cheung KL, Kong AN (2010) Molecular targets of dietary phenethyl isothiocyanate and sulforaphane for cancer chemoprevention. AAPS J 12: 87-97.

177. Dashwood RH, Ho E (2008) Dietary agents as histone deacetylase inhibitors: sulforaphane and structurally related isothiocyanates. Nutr Rev 66 Suppl 1: S36-38.

178. Aggarwal BB, Ichikawa H (2005) Molecular targets and anticancer potential of indole-3-carbinol and its derivatives. Cell Cycle 4: 1201-1215.

179. Morley R (2006) Fetal origins of adult disease. Semin Fetal Neonatal Med 11: 73-78.

180. Barker DJ (2007) The origins of the developmental origins theory. J Intern Med 261: 412-417.

181. Dolinoy DC, Das R, Weidman JR, Jirtle RL (2007) Metastable epialleles, imprinting, and the fetal origins of adult diseases. Pediatr Res 61: 30R-37R.

182. Sasco AJ, Vainio H (1999) From in utero and childhood exposure to parental smoking to childhood cancer: a possible link and the need for action. Hum Exp Toxicol 18: 192-201.

183. Sandler DP, Everson RB, Wilcox AJ, Browder JP (1985) Cancer risk in adulthood from early life exposure to parents' smoking. Am J Public Health 75: 487-492.

184. Anderson LM, Hecht SS, Dixon DE, Dove LF, Kovatch RM, et al. (1989) Evaluation of the transplacental tumorigenicity of the tobacco-specific carcinogen 4-(methylnitrosamino)-1-(3-pyridyl)-1-butanone in mice. Cancer Res 49: 3770-3775.

185. Fujii K, Nomoto K, Nakamura K (1987) Tumor induction in mice administered neonatally with 3-amino-1,4-dimethyl-5H-pyrido[4,3-b]indole or 3-amino-1-methyl-5H-pyrido[4,3-b]indole. Carcinogenesis 8: 1721-1723.

186. Poirier MC, Olivero OA, Walker DM, Walker VE (2004) Perinatal genotoxicity and carcinogenicity of anti-retroviral nucleoside analog drugs. Toxicol Appl Pharmacol 199: 151-161.

187. Murray JC, Hill RM, Hegemier S, Hurwitz RL (1996) Lymphoblastic lymphoma following prenatal exposure to phenytoin. J Pediatr Hematol Oncol 18: 241-243.

188. Miller MS, Jones AB, Park SS, Anderson LM (1990) The formation of 3-methylcholanthrene-initiated lung tumors correlates with induction of cytochrome P450IA1 by the carcinogen in fetal but not adult mice. Toxicol Appl Pharmacol 104: 235-245.

189. Perera FP, Rauh V, Whyatt RM, Tsai WY, Bernert JT, et al. (2004) Molecular evidence of an interaction between prenatal environmental exposures and birth outcomes in a multiethnic population. Environ Health Perspect 112: 626-630.

190. Jedrychowski W, Galas A, Pac A, Flak E, Camman D, et al. (2005) Prenatal ambient air exposure to polycyclic aromatic hydrocarbons and the occurrence of respiratory symptoms over the first year of life. Eur J Epidemiol 20: 775-782.

191. IARC (2010) Some non-heterocyclic polycyclic aromatic hydrocarbons and some related exposures. IARC Monogr Eval Carcinog Risks Hum 92: 1-853.

192. Xu M, Nelson GB, Moore JE, McCoy TP, Dai J, et al. (2005) Induction of Cyp1a1 and Cyp1b1 and formation of DNA adducts in C57BL/6, Balb/c, and F1 mice following in utero exposure to 3-methylcholanthrene. Toxicol Appl Pharmacol 209: 28-38.

193. Shimada T, Oda Y, Gillam EM, Guengerich FP, Inoue K (2001) Metabolic activation of polycyclic aromatic hydrocarbons and other procarcinogens by cytochromes P450 1A1 and P450 1B1 allelic variants and other human cytochromes P450 in Salmonella typhimurium NM2009. Drug Metab Dispos 29: 1176-1182.

194. Shimada T, Fujii-Kuriyama Y (2004) Metabolic activation of polycyclic aromatic hydrocarbons to carcinogens by cytochromes P450 1A1 and 1B1. Cancer Sci 95: 1-6.

195. Choudhary D, Jansson I, Schenkman JB, Sarfarazi M, Stoilov I (2003) Comparative expression profiling of 40 mouse cytochrome P450 genes in embryonic and adult tissues. Arch Biochem Biophys 414: 91-100.

196. Murray GI, Melvin WT, Greenlee WF, Burke MD (2001) Regulation, function, and tissue-specific expression of cytochrome P450 CYP1B1. Annu Rev Pharmacol Toxicol 41: 297-316.

197. Donehower LA, Harvey M, Slagle BL, McArthur MJ, Montgomery CA, Jr., et al. (1992) Mice deficient for p53 are developmentally normal but susceptible to spontaneous tumours. Nature 356: 215-221.

198. Rehm S, Devor DE, Henneman JR, Ward JM (1991) Origin of spontaneous and transplacentally induced mouse lung tumors from alveolar type II cells. Exp Lung Res 17: 181-195.

199. Branstetter DG, Stoner GD, Budd C, Conran PB, Goldblatt PJ (1988) Effect of gestational development of lung tumor size and morphology in the mouse. Cancer Res 48: 379-386.

200. Warburton D, Gauldie J, Bellusci S, Shi W (2006) Lung development and susceptibility to chronic obstructive pulmonary disease. Proc Am Thorac Soc 3: 668-672.

201. Jurisicova A, Taniuchi A, Li H, Shang Y, Antenos M, et al. (2007) Maternal exposure to polycyclic aromatic hydrocarbons diminishes murine ovarian reserve via induction of Harakiri. J Clin Invest 117: 3971-3978.

202. Ohsako S, Fukuzawa N, Ishimura R, Kawakami T, Wu Q, et al. (2010) Comparative contribution of the aryl hydrocarbon receptor gene to perinatal stage development and dioxin-induced toxicity between the urogenital complex and testis in the mouse. Biol Reprod 82: 636-643.

203. Mably TA, Moore RW, Peterson RE (1992) In utero and lactational exposure of male rats to 2,3,7,8-tetrachlorodibenzo-p-dioxin. 1. Effects on androgenic status. Toxicol Appl Pharmacol 114: 97-107.

204. Gray LE, Jr., Kelce WR, Monosson E, Ostby JS, Birnbaum LS (1995) Exposure to TCDD during development permanently alters reproductive function in male Long Evans rats and hamsters: reduced ejaculated and epididymal sperm

numbers and sex accessory gland weights in offspring with normal androgenic status. Toxicol Appl Pharmacol 131: 108-118.

205. Yasuda Y, Konishi H, Tanimura T (1986) Leydig cell hyperplasia in fetal mice treated transplacentally with ethinyl estradiol. Teratology 33: 281-288.

206. Perez-Martinez C, Garcia-Iglesias MJ, Ferreras-Estrada MC, Bravo-Moral AM, Espinosa-Alvarez J, et al. (1996) Effects of in-utero exposure to zeranol or diethylstilboestrol on morphological development of the fetal testis in mice. J Comp Pathol 114: 407-418.

207. Coutts SM, Fulton N, Anderson RA (2007) Environmental toxicant-induced germ cell apoptosis in the human fetal testis. Hum Reprod 22: 2912-2918.

208. Fowler PA, Cassie S, Rhind SM, Brewer MJ, Collinson JM, et al. (2008) Maternal smoking during pregnancy specifically reduces human fetal desert hedgehog gene expression during testis development. J Clin Endocrinol Metab 93: 619-626.

209. Balansky R, Ganchev G, Iltcheva M, Nikolov M, Steele VE, et al. (2012) Differential carcinogenicity of cigarette smoke in mice exposed either transplacentally, early in life or in adulthood. Int J Cancer 130: 1001-1010.

210. Buters J, Quintanilla-Martinez L, Schober W, Soballa VJ, Hintermair J, et al. (2003) CYP1B1 determines susceptibility to low doses of 7,12-dimethylbenz[a]anthracene-induced ovarian cancers in mice: correlation of CYP1B1-mediated DNA adducts with carcinogenicity. Carcinogenesis 24: 327-334.

211. Crowell SR, Amin SG, Anderson KA, Krishnegowda G, Sharma AK, et al. (2011) Preliminary physiologically based pharmacokinetic models for benzo[a]pyrene and dibenzo[def,p]chrysene in rodents. Toxicol Appl Pharmacol 257: 365-376.

212. Cavalieri EL, Higginbotham S, RamaKrishna NV, Devanesan PD, Todorovic R, et al. (1991) Comparative dose-response tumorigenicity studies of dibenzo[a,l]pyrene versus 7,12-dimethylbenz[a]anthracene, benzo[a]pyrene and two dibenzo[a,l]pyrene dihydrodiols in mouse skin and rat mammary gland. Carcinogenesis 12: 1939-1944.

213. Higginbotham S, RamaKrishna NV, Johansson SL, Rogan EG, Cavalieri EL (1993) Tumor-initiating activity and carcinogenicity of dibenzo[a,l]pyrene versus 7,12-dimethylbenz[a]anthracene and benzo[a]pyrene at low doses in mouse skin. Carcinogenesis 14: 875-878.

214. Prahalad AK, Ross JA, Nelson GB, Roop BC, King LC, et al. (1997) Dibenzo[a,l]pyrene-induced DNA adduction, tumorigenicity, and Ki-ras oncogene mutations in strain A/J mouse lung. Carcinogenesis 18: 1955-1963.

215. Peter Guengerich F, Chun YJ, Kim D, Gillam EM, Shimada T (2003) Cytochrome P450 1B1: a target for inhibition in anticarcinogenesis strategies. Mutat Res 523-524: 173-182.

216. Chun YJ, Kim S (2003) Discovery of cytochrome P450 1B1 inhibitors as new promising anti-cancer agents. Med Res Rev 23: 657-668.

217. Cardoso BA, Girio A, Henriques C, Martins LR, Santos C, et al. (2008) Aberrant signaling in T-cell acute lymphoblastic leukemia: biological and therapeutic implications. Braz J Med Biol Res 41: 344-350.

218. Ferrando AA (2009) The role of NOTCH1 signaling in T-ALL. Hematology Am Soc Hematol Educ Program 2009: 353-361.

219. Grabher C, von Boehmer H, Look AT (2006) Notch 1 activation in the molecular pathogenesis of T-cell acute lymphoblastic leukaemia. Nat Rev Cancer 6: 347-359.

220. Weng AP, Ferrando AA, Lee W, Morris JPt, Silverman LB, et al. (2004) Activating mutations of NOTCH1 in human T cell acute lymphoblastic leukemia. Science 306: 269-271.

221. Palomero T, Dominguez M, Ferrando AA (2008) The role of the PTEN/AKT Pathway in NOTCH1-induced leukemia. Cell Cycle 7: 965-970.

222. Tammam J, Ware C, Efferson C, O'Neil J, Rao S, et al. (2009) Down-regulation of the Notch pathway mediated by a gamma-secretase inhibitor induces anti-tumour effects in mouse models of T-cell leukaemia. Br J Pharmacol 158: 1183-1195.

223. Rao SS, O'Neil J, Liberator CD, Hardwick JS, Dai X, et al. (2009) Inhibition of NOTCH signaling by gamma secretase inhibitor engages the RB pathway and elicits cell cycle exit in T-cell acute lymphoblastic leukemia cells. Cancer Res 69: 3060-3068.

224. Guo D, Teng Q, Ji C (2011) NOTCH and phosphatidylinositide 3-kinase/phosphatase and tensin homolog deleted on chromosome ten/AKT/mammalian target of rapamycin (mTOR) signaling in T-cell development and T-cell acute lymphoblastic leukemia. Leuk Lymphoma 52: 1200-1210.

225. Zhao WL (2010) Targeted therapy in T-cell malignancies: dysregulation of the cellular signaling pathways. Leukemia 24: 13-21.

226. Jensen CD, Block G, Buffler P, Ma X, Selvin S, et al. (2004) Maternal dietary risk factors in childhood acute lymphoblastic leukemia (United States). Cancer Causes Control 15: 559-570.

227. Bradlow HL (2008) Review. Indole-3-carbinol as a chemoprotective agent in breast and prostate cancer. In Vivo 22: 441-445.

228. Anderton MJ, Jukes R, Lamb JH, Manson MM, Gescher A, et al. (2003) Liquid chromatographic assay for the simultaneous determination of indole-3-carbinol and its acid condensation products in plasma. J Chromatogr B Analyt Technol Biomed Life Sci 787: 281-291.

229. Grose KR, Bjeldanes LF (1992) Oligomerization of indole-3-carbinol in aqueous acid. Chem Res Toxicol 5: 188-193.

230. Sepkovic DW, Bradlow HL, Bell M (2001) Quantitative determination of 3,3'-diindolylmethane in urine of individuals receiving indole-3-carbinol. Nutr Cancer 41: 57-63.

231. Burger R, Hansen-Hagge TE, Drexler HG, Gramatzki M (1999) Heterogeneity of T-acute lymphoblastic leukemia (T-ALL) cell lines: suggestion for classification by immunophenotype and T-cell receptor studies. Leuk Res 23: 19-27.

232. Houghton PJ, Mirro J, Jr., Goorha RM, Raimondi SC, Fridland A, et al. (1989) Growth and differentiation of a human T-cell leukemia cell line, CCRF-CEM, grafted in mice. Cancer Res 49: 7124-7131.

233. Bamford S, Dawson E, Forbes S, Clements J, Pettett R, et al. (2004) The COSMIC (Catalogue of Somatic Mutations in Cancer) database and website. Br J Cancer 91: 355-358.

234. Nagel S, Venturini L, Meyer C, Kaufmann M, Scherr M, et al. (2010) Multiple mechanisms induce ectopic expression of LYL1 in subsets of T-ALL cell lines. Leuk Res 34: 521-528.

235. Pfaffl MW (2001) A new mathematical model for relative quantification in real-time RT-PCR. Nucleic Acids Res 29: e45.

236. Machijima Y, Ishikawa C, Sawada S, Okudaira T, Uchihara JN, et al. (2009) Anti-adult T-cell leukemia/lymphoma effects of indole-3-carbinol. Retrovirology 6: e7.

237. Takada Y, Andreeff M, Aggarwal BB (2005) Indole-3-carbinol suppresses NF-kappaB and IkappaBalpha kinase activation, causing inhibition of expression of NF-kappaB-regulated antiapoptotic and metastatic gene products and enhancement of apoptosis in myeloid and leukemia cells. Blood 106: 641-649.

238. Yan Y, Wieman EA, Guan X, Jakubowski AA, Steinherz PG, et al. (2009) Autonomous growth potential of leukemia blast cells is associated with poor prognosis in human acute leukemias. J Hematol Oncol 2: e51.

239. Yan Y, Salomon O, McGuirk J, Dennig D, Fernandez J, et al. (1996) Growth pattern and clinical correlation of subcutaneously inoculated human primary acute leukemias in severe combined immunodeficiency mice. Blood 88: 3137-3146.

240. Rahman KM, Ali S, Aboukameel A, Sarkar SH, Wang Z, et al. (2007) Inactivation of NF-kappaB by 3,3'-diindolylmethane contributes to increased apoptosis induced by chemotherapeutic agent in breast cancer cells. Mol Cancer Ther 6: 2757-2765.

241. Chang X, Tou JC, Hong C, Kim HA, Riby JE, et al. (2005) 3,3'-Diindolylmethane inhibits angiogenesis and the growth of transplantable human breast carcinoma in athymic mice. Carcinogenesis 26: 771-778.

242. Stresser DM, Williams DE, Griffin DA, Bailey GS (1995) Mechanisms of tumor modulation by indole-3-carbinol. Disposition and excretion in male Fischer 344 rats. Drug Metab Dispos 23: 965-975.

243. Screpanti I, Bellavia D, Campese AF, Frati L, Gulino A (2003) Notch, a unifying target in T-cell acute lymphoblastic leukemia? Trends Mol Med 9: 30-35.

244. Liu S, Breit S, Danckwardt S, Muckenthaler MU, Kulozik AE (2009) Downregulation of Notch signaling by gamma-secretase inhibition can abrogate chemotherapy-induced apoptosis in T-ALL cell lines. Ann Hematol 88: 613-621.

245. Shapiro GI, Edwards CD, Rollins BJ (2000) The physiology of p16(INK4A)-mediated G1 proliferative arrest. Cell Biochem Biophys 33: 189-197.

246. Garikapaty VP, Ashok BT, Tadi K, Mittelman A, Tiwari RK (2006) 3,3'-Diindolylmethane downregulates pro-survival pathway in hormone independent prostate cancer. Biochem Biophys Res Commun 340: 718-725.

247. Neave AS, Sarup SM, Seidelin M, Duus F, Vang O (2005) Characterization of the N-methoxyindole-3-carbinol (NI3C)--induced cell cycle arrest in human colon cancer cell lines. Toxicol Sci 83: 126-135.

248. Ausserlechner MJ, Obexer P, Wiegers GJ, Hartmann BL, Geley S, et al. (2001) The cell cycle inhibitor p16(INK4A) sensitizes lymphoblastic leukemia cells to apoptosis by physiologic glucocorticoid levels. J Biol Chem 276: 10984-10989.

249. Chilosi M, Doglioni C, Yan Z, Lestani M, Menestrina F, et al. (1998) Differential expression of cyclin-dependent kinase 6 in cortical thymocytes and T-cell lymphoblastic lymphoma/leukemia. Am J Pathol 152: 209-217.

250. Sicinska E, Aifantis I, Le Cam L, Swat W, Borowski C, et al. (2003) Requirement for cyclin D3 in lymphocyte development and T cell leukemias. Cancer Cell 4: 451-461.

251. Rahman KW, Sarkar FH (2005) Inhibition of nuclear translocation of nuclear factor-{kappa}B contributes to 3,3'-diindolylmethane-induced apoptosis in breast cancer cells. Cancer Res 65: 364-371.

252. Hong C, Firestone GL, Bjeldanes LF (2002) Bcl-2 family-mediated apoptotic effects of 3,3'-diindolylmethane (DIM) in human breast cancer cells. Biochem Pharmacol 63: 1085-1097.

253. Sanz C, Benito A, Inohara N, Ekhterae D, Nunez G, et al. (2000) Specific and rapid induction of the proapoptotic protein Hrk after growth factor withdrawal in hematopoietic progenitor cells. Blood 95: 2742-2747.

254. Platt KL, Dienes HP, Tommasone M, Luch A (2004) Tumor formation in the neonatal mouse bioassay indicates that the potent carcinogen dibenzo[def,p]chrysene (dibenzo[a,l]pyrene) is activated in vivo via its trans-11,12-dihydrodiol. Chem Biol Interact 148: 27-36.

255. Anderson LM, Jones AB, Riggs CW, Ohshima M (1985) Fetal mouse susceptibility to transplacental lung and liver carcinogenesis by 3-methylcholanthrene: positive correlation with responsiveness to inducers of aromatic hydrocarbon metabolism. Carcinogenesis 6: 1389-1393.

256. Miller MS, Leone-Kabler S, Rollins LA, Wessner LL, Fan M, et al. (1998) Molecular pathogenesis of transplacentally induced mouse lung tumors. Exp Lung Res 24: 557-577.

257. Swinney RM, Beuten J, Collier AB, 3rd, Chen TT, Winick NJ, et al. (2011) Polymorphisms in CYP1A1 and ethnic-specific susceptibility to acute lymphoblastic leukemia in children. Cancer Epidemiol Biomarkers Prev 20: 1537-1542.

258. Vijayakrishnan J, Houlston RS (2010) Candidate gene association studies and risk of childhood acute lymphoblastic leukemia: a systematic review and meta-analysis. Haematologica 95: 1405-1414.

259. Bosetti C, Filomeno M, Riso P, Polesel J, Levi F, et al. (2012) Cruciferous vegetables and cancer risk in a network of case-control studies. Ann Oncol [Epub ahead of print].

260. Richman EL, Carroll PR, Chan JM (2012) Vegetable and fruit intake after diagnosis and risk of prostate cancer progression. Int J Cancer 131: 201-210.

261. Davis CD, Zeng H, Finley JW (2002) Selenium-enriched broccoli decreases intestinal tumorigenesis in multiple intestinal neoplasia mice. J Nutr 132: 307-309.

262. Keum YS, Khor TO, Lin W, Shen G, Kwon KH, et al. (2009) Pharmacokinetics and pharmacodynamics of broccoli sprouts on the suppression of prostate cancer in transgenic adenocarcinoma of mouse prostate (TRAMP) mice: implication of induction of Nrf2, HO-1 and apoptosis and the suppression of Akt-dependent kinase pathway. Pharm Res 26: 2324-2331.

263. Weng JR, Tsai CH, Kulp SK, Chen CS (2008) Indole-3-carbinol as a chemopreventive and anti-cancer agent. Cancer Lett 262: 153-163.

264. Ho E, Clarke JD, Dashwood RH (2009) Dietary sulforaphane, a histone deacetylase inhibitor for cancer prevention. J Nutr 139: 2393-2396.

265. Aronchik I, Bjeldanes LF, Firestone GL (2010) Direct inhibition of elastase activity by indole-3-carbinol triggers a CD40-TRAF regulatory cascade that disrupts NF-kappaB transcriptional activity in human breast cancer cells. Cancer Res 70: 4961-4971.

266. Skupinska K, Misiewicz-Krzeminska I, Stypulkowski R, Lubelska K, Kasprzycka-Guttman T (2009) Sulforaphane and its analogues inhibit CYP1A1 and CYP1A2 activity induced by benzo[a]pyrene. J Biochem Mol Toxicol 23: 18-28.

267. Skupinska K, Misiewicz-Krzeminska I, Lubelska K, Kasprzycka-Guttman T (2009) The effect of isothiocyanates on CYP1A1 and CYP1A2 activities induced by polycyclic aromatic hydrocarbons in Mcf7 cells. Toxicol In Vitro 23: 763-771.

268. Kalpana Deepa Priya D, Gayathri R, Sakthisekaran D (2011) Role of sulforaphane in the anti-initiating mechanism of lung carcinogenesis in vivo by modulating the metabolic activation and detoxification of benzo(a)pyrene. Biomed Pharmacother 65: 9-16.

269. Priya DK, Gayathri R, Gunassekaran GR, Sakthisekaran D (2011) Protective role of sulforaphane against oxidative stress mediated mitochondrial dysfunction induced by benzo(a)pyrene in female Swiss albino mice. Pulm Pharmacol Ther 24: 110-117.

270. Priya DK, Gayathri R, Gunassekaran G, Murugan S, Sakthisekaran D (2011) Chemopreventive role of sulforaphane by upholding the GSH redox cycle in pre- and post-initiation phases of experimental lung carcinogenesis. Asian Pac J Cancer Prev 12: 103-110.

271. Hanlon N, Coldham N, Gielbert A, Kuhnert N, Sauer MJ, et al. (2008) Absolute bioavailability and dose-dependent pharmacokinetic behaviour of dietary doses of the chemopreventive isothiocyanate sulforaphane in rat. Br J Nutr 99: 559-564.

272. Calkins K, Devaskar SU (2011) Fetal origins of adult disease. Curr Probl Pediatr Adolesc Health Care 41: 158-176.

273. Kassie F, Anderson LB, Scherber R, Yu N, Lahti D, et al. (2007) Indole-3-carbinol inhibits 4-(methylnitrosamino)-1-(3-pyridyl)-1-butanone plus benzo(a)pyrene-induced lung tumorigenesis in A/J mice and modulates carcinogen-induced alterations in protein levels. Cancer Res 67: 6502-6511.

274. Zhang Y, Kensler TW, Cho CG, Posner GH, Talalay P (1994) Anticarcinogenic activities of sulforaphane and structurally related synthetic norbornyl isothiocyanates. Proc Natl Acad Sci (USA) 91: 3147-3150.

275. Steinkellner H, Rabot S, Freywald C, Nobis E, Scharf G, et al. (2001) Effects of cruciferous vegetables and their constituents on drug metabolizing enzymes involved in the bioactivation of DNA-reactive dietary carcinogens. Mutat Res 480-481: 285-297.

276. Park JY, Bjeldanes LF (1992) Organ-selective induction of cytochrome P-450-dependent activities by indole-3-carbinol-derived products: influence on covalent binding of benzo[a]pyrene to hepatic and pulmonary DNA in the rat. Chem Biol Interact 83: 235-247.

277. Shi Z, Dragin N, Galvez-Peralta M, Jorge-Nebert LF, Miller ML, et al. (2010) Organ-specific roles of CYP1A1 during detoxication of dietary benzo[a]pyrene. Mol Pharmacol 78: 46-57.

278. Fang C, Zhang QY (2010) The role of small-intestinal P450 enzymes in protection against systemic exposure of orally administered benzo[a]pyrene. J Pharmacol Exp Ther 334: 156-163.

279. Luch A, Platt KL, Seidel A (1998) Synthesis of fjord region tetraols and their use in hepatic biotransformation studies of dihydrodiols of benzo[c]chrysene, benzo[g]chrysene and dibenzo[a,l]pyrene. Carcinogenesis 19: 639-648.

280. Buters JT, Mahadevan B, Quintanilla-Martinez L, Gonzalez FJ, Greim H, et al. (2002) Cytochrome P450 1B1 determines susceptibility to dibenzo[a,l]pyrene-induced tumor formation. Chem Res Toxicol 15: 1127-1135.

281. Uno S, Dalton TP, Derkenne S, Curran CP, Miller ML, et al. (2004) Oral exposure to benzo[a]pyrene in the mouse: detoxication by inducible cytochrome P450 is more important than metabolic activation. Mol Pharmacol 65: 1225-1237.

282. Pappa G, Bartsch H, Gerhauser C (2007) Biphasic modulation of cell proliferation by sulforaphane at physiologically relevant exposure times in a human colon cancer cell line. Mol Nutr Food Res 51: 977-984.

283. Nakamura BN, Mohar I, Lawson GW, Cortes MM, Hoang YD, et al. (2012) Increased sensitivity to testicular toxicity of transplacental benzo[a]pyrene exposure in male glutamate cysteine ligase modifier subunit knockout (Gclm-/-) mice. Toxicol Sci 126: 227-241.

284. Perera FP, Rauh V, Whyatt RM, Tang D, Tsai WY, et al. (2005) A summary of recent findings on birth outcomes and developmental effects of prenatal ETS, PAH, and pesticide exposures. Neurotoxicology 26: 573-587.

285. Oganesian A, Hendricks JD, Pereira CB, Orner GA, Bailey GS, et al. (1999) Potency of dietary indole-3-carbinol as a promoter of aflatoxin B1-initiated hepatocarcinogenesis: results from a 9000 animal tumor study. Carcinogenesis 20: 453-458.

286. Lubet RA, Heckman BM, De Flora SL, Steele VE, Crowell JA, et al. (2011) Effects of 5,6-benzoflavone, indole-3-carbinol (I3C) and diindolylmethane (DIM) on chemically-induced mammary carcinogenesis: is DIM a substitute for I3C? Oncol Rep 26: 731-736.

287. Cho HJ, Park SY, Kim EJ, Kim JK, Park JH (2011) 3,3'-Diindolylmethane inhibits prostate cancer development in the transgenic adenocarcinoma mouse prostate model. Mol Carcinog 50: 100-112.

288. Wu TY, Saw CL, Khor TO, Pung D, Boyanapalli SS, et al. (2011) In vivo pharmacodynamics of indole-3-carbinol in the inhibition of prostate cancer in transgenic adenocarcinoma of mouse prostate (TRAMP) mice: Involvement of Nrf2 and cell cycle/apoptosis signaling pathways. Mol Carcinog [Epub ahead of print].

289. Gao N, Cheng S, Budhraja A, Liu EH, Chen J, et al. (2012) 3,3'-Diindolylmethane exhibits antileukemic activity in vitro and in vivo through a Akt-dependent process. PLoS One 7: e31783.

290. Pappa G, Strathmann J, Lowinger M, Bartsch H, Gerhauser C (2007) Quantitative combination effects between sulforaphane and 3,3'-diindolylmethane on proliferation of human colon cancer cells in vitro. Carcinogenesis 28: 1471-1477.

291. Noyan-Ashraf MH, Wu L, Wang R, Juurlink BH (2006) Dietary approaches to positively influence fetal determinants of adult health. FASEB J 20: 371-373.

292. Larsen-Su SA, Williams DE (2001) Transplacental exposure to indole-3-carbinol induces sex-specific expression of CYP1A1 and CYP1B1 in the liver of Fischer 344 neonatal rats. Toxicol Sci 64: 162-168.

293. Yoxall V, Kentish P, Coldham N, Kuhnert N, Sauer MJ, et al. (2005) Modulation of hepatic cytochromes P450 and phase II enzymes by dietary doses of sulforaphane in rats: Implications for its chemopreventive activity. Int J Cancer 117: 356-362.

294. Faulk C, Dolinoy DC (2011) Timing is everything: the when and how of environmentally induced changes in the epigenome of animals. Epigenetics 6: 791-797.

295. Margueron R, Reinberg D (2010) Chromatin structure and the inheritance of epigenetic information. Nat Rev Genet 11: 285-296.

296. Uribe-Lewis S, Woodfine K, Stojic L, Murrell A (2011) Molecular mechanisms of genomic imprinting and clinical implications for cancer. Expert Rev Mol Med 13: e2.

297. Swaney WT (2011) Genomic imprinting and mammalian reproduction. Horm Behav 59: 369-374.

298. Nakabayashi K, Trujillo AM, Tayama C, Camprubi C, Yoshida W, et al. (2011) Methylation screening of reciprocal genome-wide UPDs identifies novel human-specific imprinted genes. Hum Mol Genet 20: 3188-3197.

299. Koukoura O, Sifakis S, Soufla G, Zaravinos A, Apostolidou S, et al. (2011) Loss of imprinting and aberrant methylation of IGF2 in placentas from pregnancies complicated with fetal growth restriction. Int J Mol Med 28: 481-487.

300. Murphy SK, Adigun A, Huang Z, Overcash F, Wang F, et al. (2012) Gender-specific methylation differences in relation to prenatal exposure to cigarette smoke. Gene 494: 36-43.

301. Zeisel SH (2009) Epigenetic mechanisms for nutrition determinants of later health outcomes. Am J Clin Nutr 89: 1488S-1493S.

302. Shorey LE, Hagman AM, Williams DE, Ho E, Dashwood RH, et al. (2012) 3,3'-diindolylmethane induces G(1) arrest and apoptosis in human acute T-cell lymphoblastic leukemia cells. PLoS One 7: e34975.

303. Roman-Gomez J, Jimenez-Velasco A, Barrios M, Prosper F, Heiniger A, et al. (2007) Poor prognosis in acute lymphoblastic leukemia may relate to promoter hypermethylation of cancer-related genes. Leuk Lymphoma 48: 1269-1282.

304. Linhart HG, Lin H, Yamada Y, Moran E, Steine EJ, et al. (2007) Dnmt3b promotes tumorigenesis in vivo by gene-specific de novo methylation and transcriptional silencing. Genes Dev 21: 3110-3122.

305. Stumpel DJ, Schotte D, Lange-Turenhout EA, Schneider P, Seslija L, et al. (2011) Hypermethylation of specific microRNA genes in MLL-rearranged infant acute lymphoblastic leukemia: major matters at a micro scale. Leukemia 25: 429-439.

306. Kuang SQ, Ling X, Sanchez-Gonzalez B, Yang H, Andreeff M, et al. (2007) Differential tumor suppressor properties and transforming growth factor-beta responsiveness of p57KIP2 in leukemia cells with aberrant p57KIP2 promoter DNA methylation. Oncogene 26: 1439-1448.

307. Dunwell T, Hesson L, Rauch TA, Wang L, Clark RE, et al. (2010) A genome-wide screen identifies frequently methylated genes in haematological and epithelial cancers. Mol Cancer 9: e44.

308. Taylor KH, Pena-Hernandez KE, Davis JW, Arthur GL, Duff DJ, et al. (2007) Large-scale CpG methylation analysis identifies novel candidate genes and reveals methylation hotspots in acute lymphoblastic leukemia. Cancer Res 67: 2617-2625.

309. Yu S, Kong AN (2007) Targeting carcinogen metabolism by dietary cancer preventive compounds. Curr Cancer Drug Targets 7: 416-424.

310. Aggarwal BB, Shishodia S (2006) Molecular targets of dietary agents for prevention and therapy of cancer. Biochem Pharmacol 71: 1397-1421.

311. Parasramka MA, Ho E, Williams DE, Dashwood RH (2012) MicroRNAs, diet, and cancer: new mechanistic insights on the epigenetic actions of phytochemicals. Mol Carcinog 51: 213-230.

312. Ho E, Beaver LM, Williams DE, Dashwood RH (2011) Dietary factors and epigenetic regulation for prostate cancer prevention. Adv Nutr 2: 497-510.

313. Chinni SR, Sarkar FH (2002) Akt inactivation is a key event in indole-3-carbinol-induced apoptosis in PC-3 cells. Clin Cancer Res 8: 1228-1236.

314. Telang NT, Katdare M, Bradlow HL, Osborne MP, Fishman J (1997) Inhibition of proliferation and modulation of estradiol metabolism: novel mechanisms for breast cancer prevention by the phytochemical indole-3-carbinol. Proc Soc Exp Biol Med 216: 246-252.

315. Rahman KM, Aranha O, Sarkar FH (2003) Indole-3-carbinol (I3C) induces apoptosis in tumorigenic but not in nontumorigenic breast epithelial cells. Nutr Cancer 45: 101-112.

316. Chen DZ, Qi M, Auborn KJ, Carter TH (2001) Indole-3-carbinol and diindolylmethane induce apoptosis of human cervical cancer cells and in murine HPV16-transgenic preneoplastic cervical epithelium. J Nutr 131: 3294-3302.

317. Jin Y (2011) 3,3'-Diindolylmethane inhibits breast cancer cell growth via miR-21-mediated Cdc25A degradation. Mol Cell Biochem 358: 345-354.

318. Liang P, Song F, Ghosh S, Morien E, Qin M, et al. (2011) Genome-wide survey reveals dynamic widespread tissue-specific changes in DNA methylation during development. BMC Genomics 12: e231.

319. Saeed AI, Bhagabati NK, Braisted JC, Liang W, Sharov V, et al. (2006) TM4 microarray software suite. Methods Enzymol 411: 134-193.

320. Khan AA, Janke A, Shimokawa T, Zhang H (2011) Phylogenetic analysis of kindlins suggests subfunctionalization of an ancestral unduplicated kindlin into three paralogs in vertebrates. Evol Bioinform Online 7: 7-19.

321. Ekstrom EJ, Sherwood V, Andersson T (2011) Methylation and loss of Secreted Frizzled-Related Protein 3 enhances melanoma cell migration and invasion. PLoS One 6: e18674.

322. Iwanari M, Nakajima M, Kizu R, Hayakawa K, Yokoi T (2002) Induction of CYP1A1, CYP1A2, and CYP1B1 mRNAs by nitropolycyclic aromatic hydrocarbons in various human tissue-derived cells: chemical-, cytochrome P450 isoform-, and cell-specific differences. Arch Toxicol 76: 287-298.

323. Chen YH, Dai HJ, Chang HP (2003) Suppression of inducible nitric oxide production by indole and isothiocyanate derivatives from Brassica plants in stimulated macrophages. Planta Med 69: 696-700.

324. Yu W, Hegarty JP, Berg A, Chen X, West G, et al. (2011) NKX2-3 transcriptional regulation of endothelin-1 and VEGF signaling in human intestinal microvascular endothelial cells. PLoS ONE 6: e20454.

325. Dejeux E, El abdalaoui H, Gut IG, Tost J (2009) Identification and quantification of differentially methylated loci by the pyrosequencing technology. Methods Mol Biol 507: 189-205.

326. Raj K, Mufti GJ (2006) Azacytidine (Vidaza(R)) in the treatment of myelodysplastic syndromes. Ther Clin Risk Manag 2: 377-388.

327. Hesson LB, Dunwell TL, Cooper WN, Catchpoole D, Brini AT, et al. (2009) The novel RASSF6 and RASSF10 candidate tumour suppressor genes are frequently epigenetically inactivated in childhood leukaemias. Mol Cancer 8: e42.

328. Starkova J, Zamostna B, Mejstrikova E, Krejci R, Drabkin HA, et al. (2010) HOX gene expression in phenotypic and genotypic subgroups and low HOXA gene expression as an adverse prognostic factor in pediatric ALL. Pediatr Blood Cancer 55: 1072-1082.

329. Matsushita C, Yang Y, Takeuchi S, Matsushita M, Van Dongen JJ, et al. (2004) Aberrant methylation in promoter-associated CpG islands of multiple genes in relapsed childhood acute lymphoblastic leukemia. Oncol Rep 12: 97-99.

330. Jin Y, Zou X, Feng X (2010) 3,3'-Diindolylmethane negatively regulates Cdc25A and induces a G2/M arrest by modulation of microRNA 21 in human breast cancer cells. Anticancer Drugs 21: 814-822.

331. Ruifrok AC, Johnston DA (2001) Quantification of histochemical staining by color deconvolution. Anal Quant Cytol Histol 23: 291-299.

APPENDICES

A1 Modulation of DNA methylation by dietary indoles in a model of T-Cell lymphoblastic leukemia

Lyndsey E. Shorey[1,2], Pushpinder Kaur[1,2], E. Andrés Houseman[3,4], Emily Ho[2,3,5], Roderick H. Dashwood[1,2], and David E. Williams[1,2]

[1]Department of Environmental and Molecular Toxicology, [2]Linus Pauling Institute, [3]School of Biological and Population Health Sciences, [4]Department of Biostatistics, [5]Department of Nutrition and Exercise Sciences, Oregon State University, Corvallis, OR 97330, USA.

Formatted for submission to *Nutrition and Cancer*

A1.1 Abstract

Acute lymphoblastic leukemia/lymphoma (ALL) is the most common malignancy among children and cases of T-cell origin are less responsive to conventional therapy than their B-cell counterparts. Cruciferous vegetables have been demonstrated to be chemoprotective in a number of cancer cell types due to their high content of indoles and isothiocyanates. Previously, we demonstrated that indole-3-carbinol (I3C) is an effective transplacental chemopreventive agent in a dibenzo[*def,p*]chrysene (DBC)-induced model of murine T-cell lymphoblastic lymphoma. We further confirmed that treatment of human T-ALL cell lines with I3C and 3,3'-diindolylmethane (DIM), the primary product of I3C condensation, reduces cell proliferation, viability, and expression of cell-cycle proteins. Aberrant DNA methylation is a recognized event in the development of cancer and pharmacological demethylation of promoter associated CpG islands to restore expression of epigenetically silenced genes is of therapeutic interest.

To this end, we utilized genome-wide DNA methylation analysis to identify potential epigenetic therapeutic targets of I3C and DIM in a model of T-ALL. By differential methylation region (DMR) analysis with stringent Bonferroni correction for multiple testing, 1,699 DMR probes were identified which mapped to 298 unique transcripts. The differential degree of hypomethylation by I3C compared with DIM is consistent with previous findings that DIM is a more potent therapeutic in this model [302]. I3C (60 μM) significantly reduced methylation in 53% of DMRs yet increased methylation in the remaining 173 gene-mapped DMRs. DIM treatment in the consumer available supplement formulation known as BioResponse-DIM (B-DIM; 5 μM) or in the pure crystalline form (C-DIM; 5μM or 15 μM) reduced methylation in over 500 probes and more than 200 genes. Functional annotation of differentially hypomethylated genes revealed that homeobox genes and transcription factors were most commonly represented with negative regulators of apoptosis and Wnt/Frizzled families also among the top gene clusters. Our results support demethylation of these

critical cancer-survival pathways by dietary indoles derived from cruciferous vegetables as a potential chemopreventative mechanism.

A1.2 Introduction

Acute lymphoblastic leukemia (ALL) is a heterogeneous disease and results from the proliferation of arrested lymphoid precursor cells at various stages of differentiation [37]. In addition to genetic anomalies, including chromosomal translocations, inversions, fusions and duplications, epigenetic alterations with aberrant gene expression also contribute to deregulated growth and disease progression. In particular DNA methylation at CpG dinucleotides, regulated in part by DNA methyltransferase (DNMT) activity, and in association with chromatin conformational changes mediated by histone modifying enzymes, often leads to transcriptional silencing [303]. Unscheduled expression of *DNMT3* family members promotes cellular transformation through a mechanism involving *de novo* methylation of specific tumor suppressor genes [304]. Interestingly, methylation of miRNAs promoters plays a pivotal role in ALL, which might also result in gene silencing [305].

Recent work indicates that regional hypermethylation of certain genes as well as genome wide hypomethylation, features of carcinogenesis, leads to genomic instability and inactivation of tumor suppressor genes (TSGs), and is associated with poor prognosis and disease relapse in ALL [155]. Several studies have tried to identify methylation hotspots implicated in the pathogenesis or prognosis of ALL [156-158,306,307]. For example, Taylor et al., identified 262 aberrantly methylated CpG sites related to the promoter region of genes involved in transcription, cell growth, nucleotide binding, transport, apoptosis and cell signaling [308]. Furthermore, a methylator phenotype in T-ALL has been proposed as a clinically relevant prognostic biomarker, whereby methylation of multiple genes may be a predictive in determining disease outcome [155,303].

Unlike genetic mutations, epigenetic lesions are potentially reversible and therefore may be good therapeutic targets. A growing body of evidence suggests that

phytochemicals in the diet exert multiple cancer protective properties including modulation of carcinogen metabolism, induction of cell-cycle arrest and alteration of histone deacetylase and DNMT activities [309-312]. Cruciferous vegetables (i.e. broccoli, cabbage, Brussels sprouts) contain many bioactive components, including indole-3-carbinol (I3C) and its major acid condensation product 3,3'-diindolylmethane (DIM), that exhibit both chemopreventative and chemotherapeutic properties[72,121]. Epidemiological evidence suggests that modification of the diet to increase consumption of cruciferous vegetables is sufficient to reduce cancer risk [70]. Furthermore, maternal consumption of vegetables was inversely associated with risk of childhood ALL in a population-based study [226]. Numerous *in vitro* studies have demonstrated that I3C suppresses proliferation and induces apoptosis in dose and time dependent manner in cancer cells [313-315]. Like I3C, DIM also inhibits invasion, angiogenesis and induces apoptosis by regulating signaling pathways involving AKT, NF-κB, β-catenin and caspase associated pathways [240,316].

Previously, we determined that dietary indoles derived from cruciferous vegetables are chemotherapeutic in human T-ALL cell lines at various stages of differentiation *in vitro* and in a xenograft model [302]. Furthermore, maternal consumption of I3C was chemopreventative in a chemically induced murine transplacental model of T-ALL [32]. Although preclinical findings on the potential therapeutic benefits of I3C and DIM have drawn a great deal of attention in recent years, I3C and DIM have not been previously characterized as inhibitors of DNA methylation. However, DIM is capable of selectively degrading class I HDAC proteins in human colon cancer cells through a proteasome-dependent mechanism and increasing miR-21 expression [119,317]. Collectively these findings support the hypothesis that I3C/DIM may elicit chemotherapeutic effects in a population of T-ALL cells through reversal of epigenetic lesions including aberrant DNA methylation. To this end, we performed an unbiased genome-wide screening approach to determine changes in DNA methylation patterns in a model of T-ALL upon treatment with dietary indoles.

A1.3 Materials and methods

Cell line and culture conditions. The human T-cell lymphoblastic leukemia cell line (CCRF-CEM, herein referred to as CEM) was purchased from American Type Culture Collection (Manassas, VA) and maintained in phenol red-free RPMI-1640 medium (Sigma-Aldrich) containing 10% (v/v) charcoal-stripped, heat-inactivated fetal bovine serum (FBS; Atlas Biologicals, Fort Collins, CO) in a humidified incubator at 37°C with 5% CO_2. Crystalline DIM (C-DIM) and I3C were purchased from Sigma-Aldrich Co. (St. Louis, MO) and BioResponse-DIM (B-DIM) was kindly provided by BioResponse, LCC (Boulder, CO), which was certified to contain 30% DIM (wt/wt) by Eurofins-Alpha Laboratories (Petaluma, CA). Experimental concentrations reported in this study were adjusted accordingly. Phytochemicals were prepared as concentrated stock solutions in DMSO, which were stored protected from light at -80°C. For each replicate experiment, cryopreserved cells were thawed into fresh media and cultured according to ATCC recommendations. Concentrations chosen for methylation analysis did not significantly alter cell viability or proliferation based on previously established dose-response curves for CEM [302]. Cells were seeded 24 hr prior to treatment and on the day of treatment, dilutions of DIM and I3C were prepared so that all experimental treatments contained 0.1% DMSO (v/v), including a vehicle control. After 24 hr of treatment cells were collected by centrifugation, rinsed in PBS, and stored at -80°C until further analysis.

Methylated DNA immunoprecipitation (MeDIP). Chemicals and reagents for MeDIP were purchased from the vendors recommended by Nimblegen in their detailed protocol. Genomic DNA was isolated from CEM cells using the Qiagen DNeasy kit with optional RNAse on column digestion, according to manufacturer protocols. High quality genomic DNA was digested overnight with Mse I (T/TAA) to produce fragments from 200 - 1,000 bp (assessed by gel electrophoresis) while keeping CpG islands intact. Fragmented DNA was heat denatured and immunoprecipitated (IP) overnight with monoclonal antibody against 5-methyl

cytidine, captured on protein A agarose beads, washed to remove non-specific material, purified and amplified according to Nimblegen sample preparation instructions and as previously described [318]. Input DNA refers to digested genomic DNA taken through immunoprecipitation steps without 5-methyl cytidine antibody.

Raw data processing and peak identification with Nimblescan software. Hybridization, scanning of arrays, and initial data processing was conducted at the Center for Genome Research and Biocomputing (CGRB) core service facility at Oregon State University according to NimbleGen protocols, as described in detail at http://www.nimblegen.com. In brief, IP and input DNA are labeled with Cy5 and Cy3 dye coupled 9mer primers, respectively, by Klenow fragment-catalyzed primer extension, co-hybridized overnight, washed and scanned. Raw intensity data is extracted from array images for both Cy5 and Cy3 channels using the Nimblescan software package into channel specific "pair files". This software further computes the scaled $\log_2$ –ratio for each probe (using the bi-weight mean for the $\log_2$ –ratio of all probe values, centered around zero) of IP to input DNA. Thus positive ratios represent enrichment of methylation at the genomic position of the probe. A sliding window one-sided Kolmogorov-Smirnov test (750bp window), placed around the scaled $\log_2$ –ratio for each consecutive probe, returns what is called the *P*-score ($-\log_{10}$ *p*-value), and determines whether the probes are drawn from a significantly more positive distribution of intensity $\log_2$ -ratios than those in the rest of the array. Lastly, a methylation peak is defined as a genomic region with at least 2 consecutive probes with a *P*-score ≥ 2.

Assessment of MeDIP data quality and consistency. To evaluate data consistency, the $\log_2$ -ratio of experimental replicates within a treatment were plotted against one another using scatterplots as shown in Supplemental Figure S-A1.1. The Pearson correlation coefficient (r) was generated from the linear fit of the scatterplot data. Furthermore, boxplots of pre- and post- processed $\log_2$ratio values were compared across arrays to verify normalization in R (http://www.r-project.org/). In two of 15 originally processed arrays there was an obvious discrepancy in the

hybridization efficiency, as evidenced by the raw image intensity and the scatterplot analyses. These arrays were subsequently replaced and the new arrays showed marked improvement in hybridization and consistency with the original 13 arrays passing quality checks, thus the 2 original poorly performing arrays were not included in analysis (Supplemental Figure S-A1.1). The Pearson correlation coefficient between replicates ranged from r = 0.56 to 0.83 with an average of 0.71, showing good consistency between replicates, considering the expected variability of performing three separate cell culture experiments in addition to any technical variability.

Identification of methylated regions by manual data filtering. An initial screen was conducted to identify conserved and unique methylated genes among samples. The peaks generated with NimbleScan are of variable size as they are defined as at least 2 consecutive probes with a *P*-score of ≥ 2, and peaks within 500 bp of one-another are merged. Thus, it is not possible to compare specific peaks between samples without breaking the peaks into smaller consistent units. We later conducted DMR ANOVA-based analysis with Bonferroni multiple testing correction for *p*-value adjustment at the probe-level as a separate analysis method with decreased false positives (see below). For the initial screen, filtering was done to remove peaks with a *P*-score of less than 2.5, and to remove duplicate gene names, in order to obtain a list of unique genes within each sample having methylation enrichment. A Venn diagram tool for bioinformatics "Venny" (http://bioinfogp.cnb.csic.es/tools/venny/index.html) was then used to compare filtered sample lists of genes. Within each treatment, unique genes were identified having methylation enrichment in one or more CpG islands in 3/3 replicates. Conserved gene lists among replicates were further compared across treatments. Methylation enrichment in all control samples, but not in all samples of a particular treatment, was considered a potential treatment de-methylating effect and vice-versa as outlined in Figure A1.1.

Identification of differentially methylated regions (DMRs) between control and phytochemical treated samples. A bioinformatics script specifically designed for

differential methylation analysis was created for use in R (http://www.r-project.org/) by NimbleGen. Raw intensity data was extracted from array images for both Cy5 and Cy3 channels using the NimbleScan software package into channel specific "pair files" and imported into the R statistical programming environment using a custom Nimblegen R-script. Quantile normalization of signal intensities across the arrays was performed on a per channel basis before calculation and bi-weight scaling within a sample of the $\log_2$ -ratio for each probe. Differential methylation analysis within R utilized a sliding window ANOVA, where the ratios of probes within a window were tested for significance between groups. Multiple testing *p*-value correction was performed using the stringent Bonferroni method to generate a list of differentially methylated regions (DMRs), meeting a *p*-value cutoff of 0.01. Within the list of differentially methylated probes, column filters were applied to the regression coefficients in order to summarize the number of positively and negatively differentially methylated probes for each specific treatment (Table A1.3).

Hierarchical clustering of DMRs. The DMR analysis within R generates fitted $\log_2$ -ratios for each array, the regression coefficients for each treatment versus control, and an overall F-test *p*-value or score at each probe, based on the sliding window ANOVA. Thus, we can visually compare either the fitted log -ratios of all arrays or the regression coefficients (log intensity treatment – log intensity control) using hierarchical clustering. The freely available MultiExperiment Viewer software (MeV), part of the TM4 Microarray Software Suite, was used to cluster first the fitted $\log_2$ -ratios and subsequently the regression coefficients using the default Pearson correlation metric [319]. Within each transcript having multiple significantly altered probes, average values were calculated for easy visualization (Figure A1.3).

Functional analysis of methylation enrichment. DMRs were mapped to the nearest primary transcript using NimbleScan software and column filters were applied to the regression coefficients in order to generate lists of positively and negatively differentially methylated transcripts for each specific treatment. Lists of transcripts having differential methylation following indole treatment, based on statistical

analysis, were then uploaded to the Database for Annotation, Visualization and Integrated Discovery (DAVID) (http://david.abcc.ncifcrf.gov/) to identify enrichment of functionally related gene lists. The default categories within this tool were selected for functional enrichment analysis: OMIM_DISEASE, COG_ONTOLOGY, SP_PIR_KEYWORDS, UP_SEQ_FEATURE, GOTERM_BP_FAT, GOTERM_MF_FAT, GOTERM_CC_FAT, BBID, BIOCARTA, KEGG_PATHWAY, INTERPRO, PIR_SUPERFAMILY, and SMART. Clusters with an Enrichment Score greater than or equal to 1.3 were considered significant, meaning that the geometric mean of *p*-values by Fisher's Exact test for all genes within the cluster was less than or equal to 0.05.

RNA isolation and real time PCR (RTPCR). Total cellular RNA was extracted from treated and untreated CCRF-CEM cells using the RNeasy Mini Kit (Qiagen, Valencia, CA), according to the manufacturer's protocol. Reference RNA, obtained from $CD3^+$ T-lymphocytes pooled from a number of normal adults was purchased from Miltenyi Biotec (Germany). Total RNA (2 µg) was used for cDNA synthesis using Superscript III First Strand Synthesis kit (Invitrogen, Grand Island, NY). Untreated and 5'-aza-2'-deoxycytidine (5'-AZA-dC) treated CEM cells were similarly extracted and reverse transcribed. Due to the limited amount of treated cells from the same experiments as used for the arrays, the TrueLabeling-AMP™ Linear RNA Amplification Kit was applied to generate ample sample for RTPCR validation of multiple genes (SABiosciences, Valencia, CA). Identification and selection of 10 candidate genes was based on DAVID analysis showing enrichment of particular pathways, literature review for known hypermethylated genes in T-ALL, and highly significant results by DMR analysis. The expression of the selected genes was evaluated by iQ5 Multicolor Real Time PCR Detection System (BioRad, Hercules, CA) in duplicate with the RT2 SYBR Green Fluor PCR Master mix (Qiagen), with primers and PCR conditions given in Table A1.1. Glyceraldehyde-3-phosphate dehydrogenase (*GAPDH*) gene expression was used as an internal control. Relative gene expression was calculated using the $\Delta\Delta C_t$ method [235] with the housekeeping

gene *GAPDH* selected for normalization. Transcripts were considered undetectable if C_t >35 and the number 35 was used in performing $\Delta\Delta C_t$ calculations.

Table A1.1 Primer sequences and conditions for re-expression analysis by RTPCR.

Gene name	Forward primer (5' – 3')	Reverse primer (5' – 3')	OAT[a]	Reference
FERMT3	GAGACCCACCTG CAGCCCCCAG	AAACACCCGCAG CTCCCATGAC	60	[320]
DUSP4	GTCAACGTGCGC TGTAACAC	GAACAGAATTCT GGGTACTCGG	56	[307]
MAP2K3	CTACATGGCCCCT GAGAGGAT	TCCAGACGTCGG ACTTGACA	60	RTprimerDB
WT1	GCTGTCCCACTTA CAGATGCA	TCAAAGCGCCAG CTGGAGTTT	60	[321]
BMP4	TGAGCCTTTCCAG CAAGTTT	CTTCCCCGTCTCA GGTATCA	56	Primer 3
FRZB	AAACTGTAGAGG GGCAAGCA	GGCAGCCAGAGC TGGTATAG	52	Primer 3
CYP1B1	AACGTCATGAGT GCCGTGTGT	GGCCGGTACGTT CTCCAAATC	58	[322]
DAXX	TCTCCTTGGACCC CACAAATG	TCAGGCCCTGGCT TGTTGATG	56	[323]
NKX2-3	CCACCCCTTTCTC AGTCAAA	CTGCGGCTAGTG AGTTCAAA	60	[324]
HSD17B7	GCTGACCCAGGG TGATAAGA	CTTGCACTGCGA GATGATGT	54	Primer 3
GAPDH	GAAGGTGAAGGT CGGAGTC	GAAGATGGTGAT GGGATTTC	60	RTPrimerDB

[a] Optimal annealing temperature

DNA extraction and bisulfite conversion. Isolation of cell genomic DNA was performed using DNeasy Blood and Tissue kit (Qiagen) with optional on column RNase digestion, according to the manufacturer's recommendations. DNA concentration was determined by measuring the intensity of absorbance of DNA solution with Picogreen dsDNA Quantitation Kit (Molecular Probes, USA), an ultrasensitive fluorescence based method for measuring double stranded DNA quantity. Bisulfite modification of genomic DNA for methylation analysis was carried

out with EZ DNA methylation Gold KitTM protocol (Zymo Research, CA). Bisulfite DNA was stored in -20°C until use.

Table A1.2 Primer sequences and conditions used for pyrosequencing.

Gene name		Sequence (5' – 3')	# CpGs	OAT[a]	(bp)
BMP4	forward	AGGGATTTTATATAGTGAAATGATA GAG	10	52	153
	reverse	AAAAAAATATCACCCAATCTAAC			
	sequencing	TTTATATAGTGAAATGATAGAGG			
HSD17B7	forward	ATTGGAGGGATTAGTTTAG	13	52	140
	reverse	CACACTTCCAAACAATAAA			
	sequencing	GGAGGGATTAGTTTAGA			
FERMT3	forward	ATGGAGGGGATGAAGATAGTTT	10	52	160
	reverse	TAATCTACTCCACAATCTTCAAA			
	sequencing	GGGGATGAAGATAGTTTT			
DUSP4	forward	GGGAAAAGTTTTTTAGGAGGTA	12	56	190
	reverse	CTCCCCCTAAATTTAACTATTAT			
	sequencing	TGTAGTAGGAGTTGGGGAGA			
WT1	forward	AGTTTGGATTAGGATAAGTTAAGTT	9	52	169
	reverse	ATAAACACATACACCTCCAATA			
	sequencing	AAGTTTTTTTTTATTTTTAGAAT			

[a] Optimal annealing temperature

DNA methylation analysis by pyrosequencing**.** Pyrosequencing is a fast, simple, quantitative, robust and high-throughput approach which treats each CpG site as a C/T polymorphism and estimates the proportion of methylation in methylated and unmethylated alleles [325]. PCR and sequencing primers were designed using Pyrosequencing Assay Design Software for 5 genes based on CpG island sequences from the UCSC genome browser (hg18 build), and were validated using bisulfite modified DNA from untreated CEM cells (Table A1.2). Pyrosequencing was conducted at the Protein And Nucleic acid (PAN) facility at Stanford University,

California, USA with the Qiagen Pyromark Q24 instrument and PyroMark PCR Kit (Qiagen).

A1.4 Results

Initial screening for methylated regions within CCRF-CEM genome

The platform we employed was the 3 x 720K CpG Island Plus RefSeq Promoter Array for the human genome which profiles 30,848 transcripts, 22,532 promoters, and 27,532 CpG Islands using 50-75bp probes tiled across the promoter regions (range from 2440 bp upstream to 610 bp downstream). We were interested to compare genomic methylation peaks within and across treatments using the mapped peaks files (described above) generated with NimbleScan, in order to identify conserved methylated regions across all samples, and those conserved within control samples but altered by treatment with dietary agents as an initial screen. Methylation enrichment is defined as a significantly more positive distribution of intensity log-ratios than those in the rest of the array using a one-sided Kolmogorov-Smirnov (KS) test and 750 bp sliding window. Furthermore a methylation peak is defined as at least 2 adjacent probes with methylation enrichment ($p<0.01$). Methylation enrichment in a particular gene was conservatively defined if one or more peaks were identified in all three replicates. The initial filter and screen approach identified only 20 transcripts that were consistently identified by peak analysis across all samples but 4411 transcripts that had conserved methylation enrichment in any treatment (~14% of transcripts represented on array). In control treated samples 3,410 transcripts were enriched for methylation, and 49 - 61% of these transcripts were similarly methylated across treated samples by Venn analysis (Table A1.3, Figure A1.1).

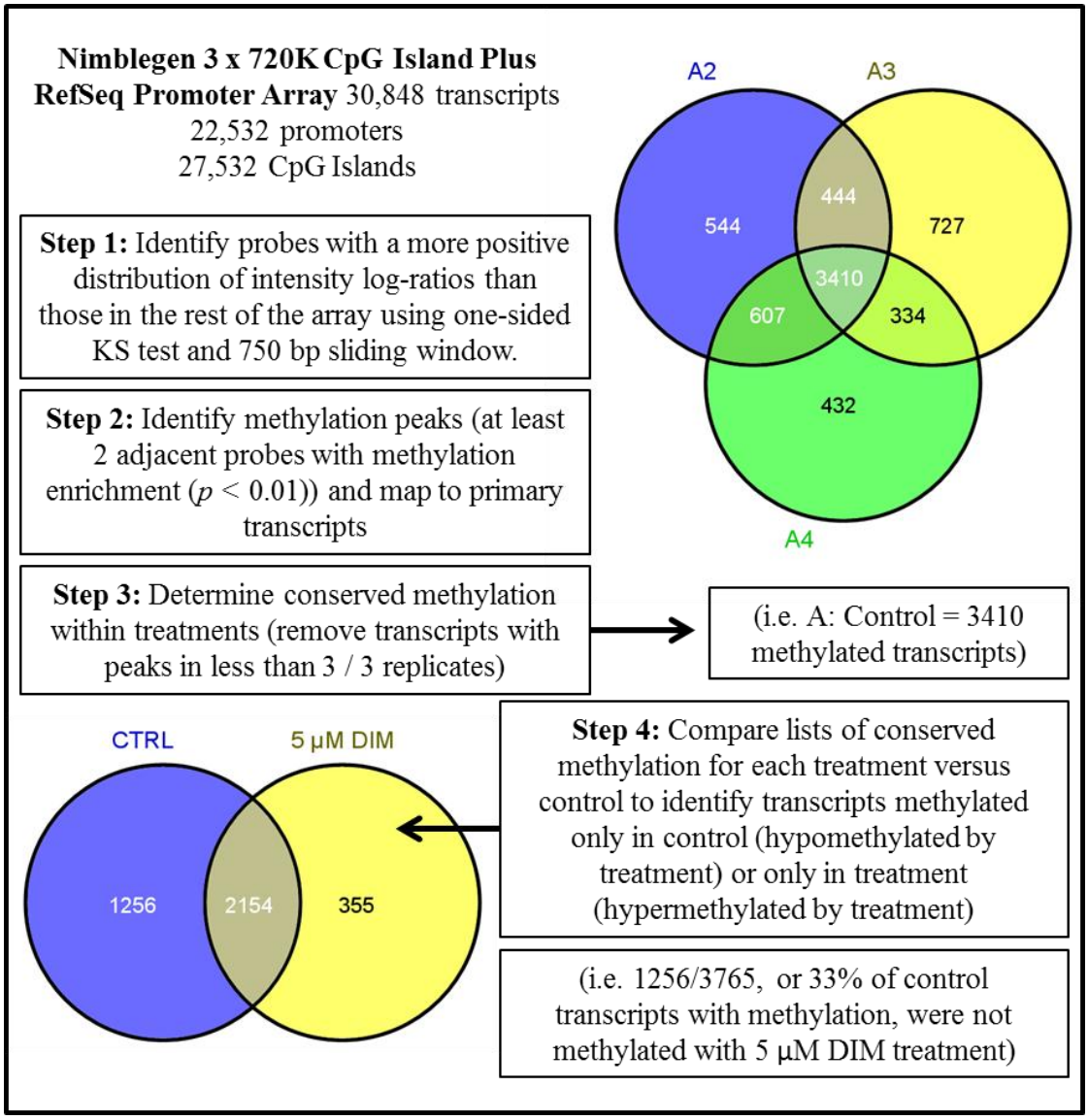

Figure A1.1 Platform statistics and schematic for Venn diagram analysis used to determine differentially methylated transcripts based on peak data.

After removing conserved transcripts with methylation enrichment in all samples from our analysis, a pattern of hypomethylation was evident for pure crystalline DIM (C-DIM) and the bioavailable DIM formula (B-DIM). Out of the differentially methylated transcripts 78% and 76% were hypomethylated (C-DIM and

B-DIM respectively) at only a 5 μM concentration, while treatment with 15 μM C-DIM increased the level of hypomethylation to 87%. A total of 755 transcripts (2.44% of the total array) were hypomethylated by all DIM treatments (Table A1.3). Conversely, I3C treatment (60 μM) slightly elevated the number of transcripts with methylation enrichment compared with control (Table A1.3).

Table A1.3 Summary statistics for differential methylation with indole treatment.

vs CTRL (Bonferroni DMR)		**60 μM I3C**	**5 μM B-DIM**	**5 μM C-DIM**	**15 μM C-DIM**
hypo	transcripts	172 (58%)	210 (70%)	240 (81%)	249 (84%)
hyper	transcripts	126 (42%)	88 (30%)	58 (19%)	49 (16%)
vs CTRL (Venn analysis)		**60 μM I3C**	**5 μM B-DIM**	**5 μM C-DIM**	**15 μM C-DIM**
hypo	transcripts	710 (41%)	1140 (76%)	1258 (78%)	1632 (87%)
hyper	transcripts	1030 (59%)	365 (24%)	354 (22%)	242 (13%)

Genome-wide identification of differentially methylated regions (DMRs)

To determine whether changes in DNA methylation observed by manual Venn diagram analysis were statistically significant, a sliding window ANOVA within R was utilized. Differential methylation analysis with strict Bonferroni correction for multiple testing identified 982 unique probes with significantly different methylation relative to control. Many (76%) probes within the enriched data set mapped to primary transcripts, 298 of which were unique (Supplemental Table S-A1.1). The enriched data set revealed a strikingly similar pattern of differential methylation in DIM or I3C treated samples compared to results generated by Venn diagram analysis, although with much fewer total genes as expected based on the stringency of Bonferroni MTC (Table A1.3).

Of the DMRs identified, the majority were hypomethylated by all three DIM treatments versus control (5 μM B-DIM - 70%; 5 μM C-DIM - 81%; and 15 μM C-DIM - 84% of transcripts) and the lists of genes hypomethylated by the three DIM treatments were remarkably similar (Figure A1.2, Supplemental Table S-A1.1). As

suggested by initial Venn analysis, nearly an equivalent number of probes or transcripts were hypermethylated as hypomethylated in samples treated with I3C relative to control. I3C and DIM treatments produced more similar lists of differentially hypomethylated transcripts than divergent, however, among 298 transcripts, only seven were commonly hypermethylated in all of the treatments, namely *RHBDL1, NCRNA00085, SEPT9, TP53TG3B, P4HA2, MYLPF*, and *C1orf9*.

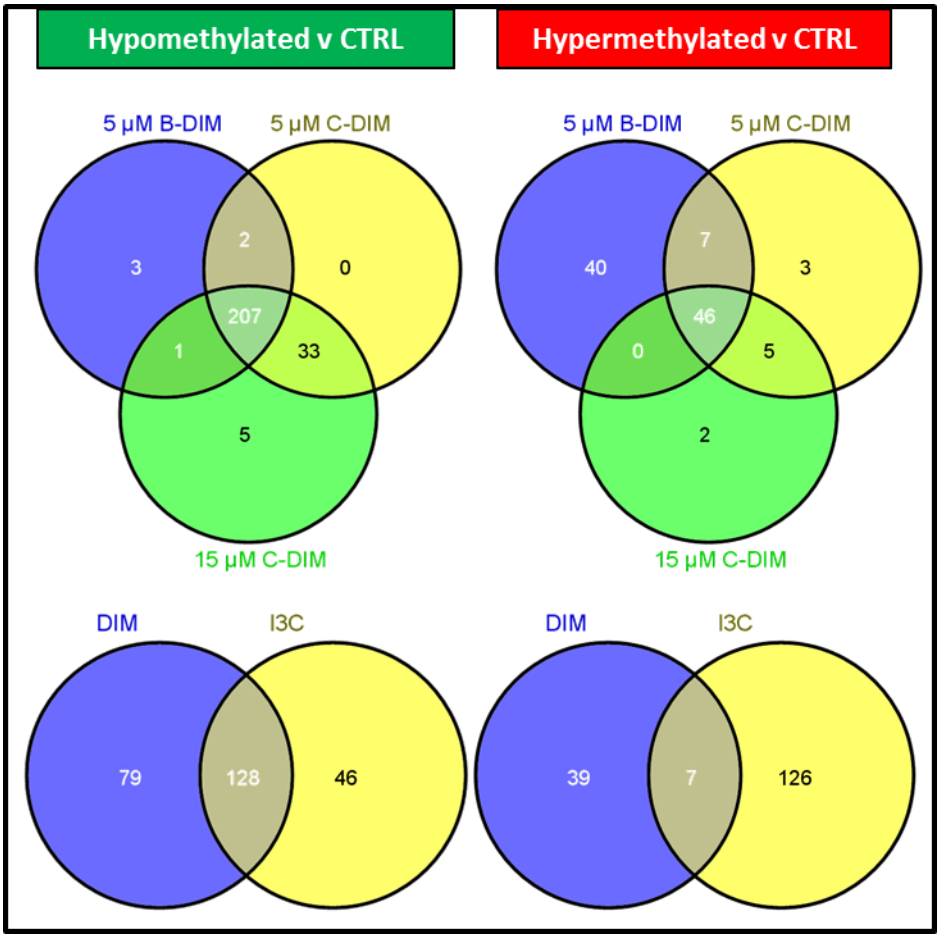

Figure A1.2 Comparison of gene lists generated by DMR analysis.
Probes identified by DMR analysis with Bonferroni MTC and were mapped to primary transcripts and sorted according to regression coefficients (fold change from control); therefore some genes were identified as having both hypo- and hyper-methylated probes.

The 298 genes identified by DMR analysis were subjected to hierarchical clustering based on relative intensity (representative of methylation) in response to dietary indoles, of which I3C treatment was the most divergent (Figure A1.3). The differential intensity in these heat maps suggests that although the DIM treatments appeared to alter many of the same transcripts (Figure A1.2), the magnitude of change varied across concentrations and formulas of DIM used.

Functional categories of DMRs

We next established the functional profile of genes, using the DAVID software, on the basis of gene ontology descriptions, in hypo- and hypermethylated gene sets. The functional clusters and enrichment scores for each treatment and pattern of methylation relative to control are shown in Table A1.4. As expected based on the profiles of differential methylation changes between I3C and DIM treatments, the functional categories identified by DAVID analysis were more similar in the three DIM treatments compared to I3C. Commonly hypomethylated categories among DIM treatments included those related to transcriptional regulation (i.e. homeobox, nucleus, DNA-binding), development (i.e. embryonic morphogenesis, skeletal system morphogenesis, cartilage development, muscle development, cell fate commitment, anterior/posterior patterning), apoptosis, or carcinogenesis (i.e. colorectal cancer, basal cell carcinoma, Wnt/Frizzled signaling, melanogenesis). Surprisingly, many of these categories were similarly identified as hypermethylated by I3C treatment at 60μM.

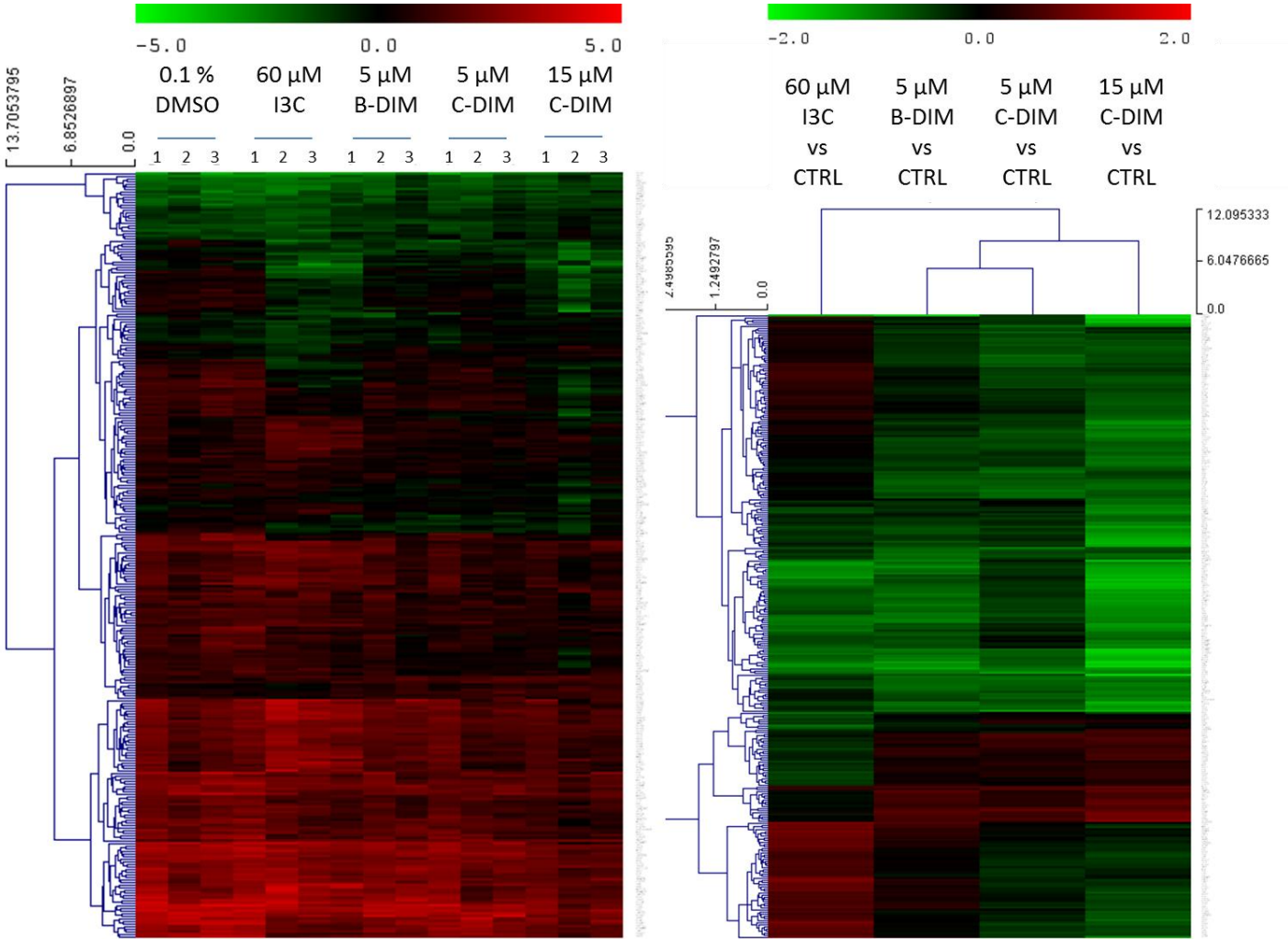

Figure A1.3 Hierarchical clustering of average log-ratios across arrays (left) and of regression coefficients (treatment intensity minus control) (right).

Table A1.4 Functional clustering of DMRs

Hypomethylated VS Ctrl			
60 μM I3C	5 μM B-DIM	5 μM C-DIM	15 μM C-DIM
none significant	**E-score: 2.22** development homeobox transcription regulation nucleus DNA-binding **E-score: 1.79** embryonic organ morphogenesis skeletal system morphogenesis cartilage development **E-score: 1.72** cell fate commitment negative regulation of apoptosis regulation of apoptosis regulation of neuron apoptosis **E-score: 1.42** embryonic organ morphogenesis regionalization anterior/posterior pattern formation **E-score: 1.38** muscle organ development	**E-score: 2.59** homeobox DNA-binding transcription regulation nucleus **E-score: 2.25** negative regulation of apoptosis regulation of apoptosis **E-score: 1.78** colorectal cancer domain:FZ basal cell carcinoma Lys-Thr-X-X-X-Trp motif short sequence motif:PDZ-binding Wnt signaling pathway pathways in cancer GPCR, family 2-like melanogenesis Frizzled protein **E-score: 1.68** skeletal system development skeletal system morphogenesis chordate embryonic development	**E-score: 2.56** homeobox DNA-binding transcription regulation nucleus **E-score: 2.22** negative regulation of apoptosis regulation of apoptosis **E-score: 1.81** colorectal cancer domain:FZ basal cell carcinoma Lys-Thr-X-X-X-Trp motif short sequence motif:PDZ-binding Wnt signaling pathway pathways in cancer GPCR, family 2-like melanogenesis Frizzled protein **E-score: 1.67** skeletal system development skeletal system morphogenesis chordate embryonic development

Table A1.4 Functional clustering of DMRs (continued)

Hypomethylated VS Ctrl			
60 μM I3C	5 μM B-DIM	5 μM C-DIM	15 μM C-DIM
	muscle tissue development striated muscle tissue development	embryonic skeletal system development **E-score: 1.57** skeletal system morphogenesis **E-score: 1.39** muscle organ development muscle tissue development striated muscle tissue development **E-score: 1.37** positive regulation of cell migration regulation of locomotion **E-score: 1.33** colorectal cancer glioma MAPK signaling pathway melanoma prostate cancer **E-score: 1.30** intrinsic to plasma membrane glycoprotein	embryonic skeletal system development **E-score: 1.56** skeletal system morphogenesis **E-score: 1.38** muscle organ development muscle tissue development striated muscle tissue development **E-score: 1.36** positive regulation of cell migration regulation of locomotion **E-score: 1.32** regulation of oxido-reductase activity membrane organization

Table A1.4 Functional clustering of DMRs (continued)

Hypermethylated VS Ctrl			
60 μM I3C	5 μM B-DIM	5 μM C-DIM	15 μM C-DIM
E-score: 2.17 glycoprotein membrane cell membrane transmembrane receptor **E-score: 1.77** negative regulation of apoptosis regulation of apoptosis **E-score: 1.73** glycoprotein signal peptide **E-score: 1.68** Frizzled protein short sequence motif:PDZ-binding colorectal cancer basal cell carcinoma melanogenesis pathways in cancer wnt signaling pathway GPCR, family 2-like	**E-score: 1.59** glycoprotein membrane transmembrane disulfide bond	**E-score: 1.34** cognition olfaction sensory perception cell membrane GPCR, rhodopsin-like superfamily g-protein coupled receptor disulfide bond glycosylation site:N-linked (GlcNAc...) transmembrane region rhodopsin-like G protein-coupled receptors transducer glycoprotein sensory transduction plasma membrane	**E-score: 1.63** cell membrane cognition olfaction sensory perception GPCR, rhodopsin-like superfamily g-protein coupled receptor disulfide bond glycosylation site:N-linked (GlcNAc...) transmembrane region rhodopsin-like G protein-coupled receptors Transducer Glycoprotein sensory transduction Receptor **E-score: 1.34** Tetratricopeptide repeat

Re-expression of DMR target genes

As aberrant DNA methylation is often associated with unscheduled gene silencing, we next selected a subset of genes to analyze for transcriptional expression. We choose 10 candidate genes for validation based on DMR results and literature review (Table A1.1), most of which appeared to be hypomethylated by I3C and DIM treatment by Nimblegen microarray analysis (Supplemental Figure S-A1.2). We used 5'-aza-2'-deoxycytidine (5'-AZA-dC; 5μM) treated cells as a positive control for re-expression experiments and T-Cell ($CD3^+$) RNA as a normal control. In the "normal" (healthy) pool of T-Cell RNA, expression of *DUSP4*, *MAP2K3*, *BMP4*, and *WT1* (44% of tested genes) was significantly higher than in the untreated CEM T-ALL population, in support of the observed hypermethylation among these targets in our array analysis (Table A1.5). Only *FERMT3* and *BMP4* transcripts were significantly increased upon treatment with 5'-AZA-dC (Table A1.5, Figure A1.4-top). Furthermore, the following indole-hypomethylated genes (*MAP2K3*, *DUSP4*, *DAXX*, *NKX2-3*, *WT1*, *HSD17B7*, and *FRZB*) also exhibited significantly higher expression in at least one of the treatment groups, which suggests that these dietary phytochemicals can stimulate the re-expression of genes with possible therapeutic importance in leukemogenesis (Figure A1.4-bottom).

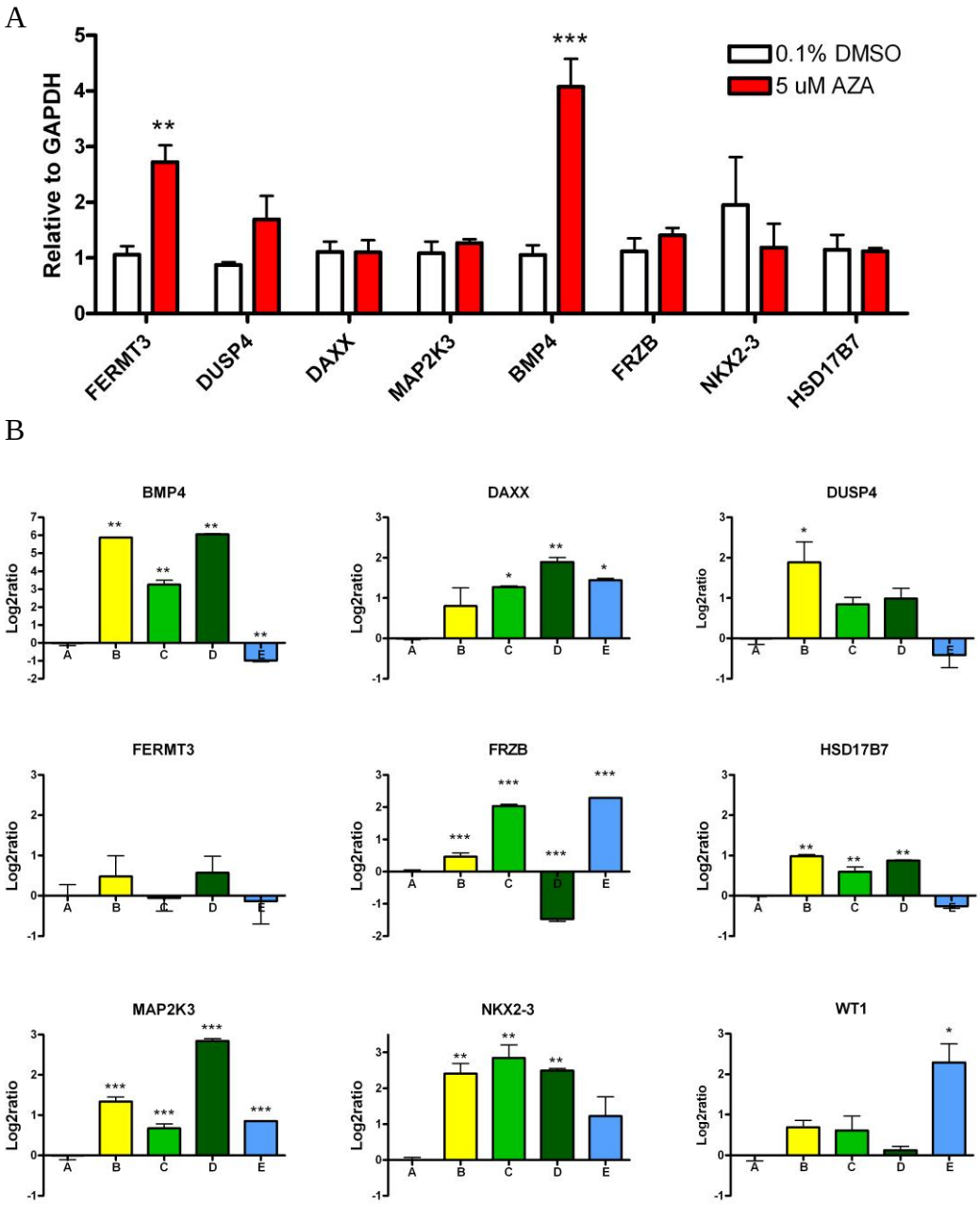

Figure A1.4 Re-expression of hypermethylated genes in T-ALL following treatment with (A) 5'-AZA-dC, (B) I3C or DIM for 24 hr.

Relative expression was determined using RTPCR and the Pfaffl method. Log_2 transformed fold-change from control is shown (A - control; B - 60 μM I3C; C - 5 μM B-DIM; D - 5 μM C-DIM; E - 15 μM C-DIM) with significance denoted by $*p < 0.05$, $**p < 0.01$, $***p < 0.001$ versus control with Dunnett's post hoc test.

Table A1.5 Summary of RTPCR results in a healthy T-cell population versus untreated and treated CEM cells.

Gene symbol	Gene name	untreated CEM expression (ave.Ct)	healthy T-cell expression (ave.Ct)	5-AZA versus control (CEM)		I3C/DIM versus control (CEM)		pairwise comparisons [c]			
				induction	pairwise comparisons [a]	induction	overall p-value [b]	A vs B	A vs C	A vs D	A vs E
FERMT3	fermitin family member 3	Yes (25)	Yes (22)	Yes	p< 0.01	No					
DUSP4	dual specificity phosphatase 4	No (>35)[d]	Yes (22)	Yes	(n.s.)	Yes	*p = 0.0188*	*p < 0.05*			
MAP2K3	mitogen-activated protein kinase kinase 3	No (>35)	Yes (27)	No		Yes	*p < 0.0001*	*p < 0.01*	*p < 0.01*	*p < 0.01*	*p < 0.01*
WT1	Wilms tumor 1	No (>35)	Yes (33)	not tested		Yes	*p = 0.0119*				*p < 0.01*
BMP4	bone morphogenetic protein 4	Yes (33)	Yes (25)	Yes	p<0.001	Yes	*p < 0.0001*	*p < 0.01*	*p < 0.01*	*p < 0.01*	*p < 0.01*
FRZB	frizzled-related protein	No (>35)	Yes (34)	No		Yes	*p < 0.0001*	*p < 0.05*	*p < 0.01*	*p < 0.01*	*p < 0.01*
CYP1B1	cytochrome P450, family 1, subfamily B, polypeptide 1	No (>35)	Yes (33)	not tested		not tested	*n/a*	n/a			
DAXX	death-domain associated protein	Yes (25)	Yes (27)	No		Yes	*p = 0.0093*		*p < 0.05*	*p < 0.01*	*p < 0.05*
NKX2-3	NK2 homeobox 3	Yes (28)	No (37)	No		Yes	*p = 0.0067*		*p < 0.05*	*p < 0.01*	*p < 0.01*
HSD17B7	hydroxysteroid (17-beta) dehydrogenase 7	Yes (22)	Yes (29)	No		Yes	*p < 0.0001*		*p < 0.01*	*p < 0.01*	*p < 0.01*
GAPDH	glyceraldehyde-3-phosphate dehydrogenase	Yes (15)	Yes (18)	No		No					

[a] Gene symbols in bold were further assessed by pyrosequencing.

[b] Samples not meeting threshold at or after 35 cycles (Ct) were considered not detectable

[c] A - control; B - 60 μM I3C; C - 5 μM B-DIM; D - 5 μM C-DIM; E - 15 μM C-DIM

[d] The $\log_2$ fold change versus control was assessed by ANOVA to generate the overall *p* -value. Pairwise *p* -values were generated using Dunnett's MTC, comparing each treatment versus control

Validation of DMR target genes methylation by pyrosequencing

A subset of genes showing differential expression in normal versus neoplastic T-cells (CEM), or in untreated versus 5'-AZA-dC treated neoplastic cells, were further assessed by pyrosequencing. Genomic DNA from untreated CEM cells was bisulfite modified and analyzed over 9-13 CpG sites, depending on the gene (Table A1.2). *WT1* had the highest average methylation of the five genes tested (79%) compared with *BMP4* (66%), *DUSP4* (48%), *FERMT3* (2.5%), and *HSD17B7 (1.2%)* as shown in Supplemental Figure S-A1.3. We are currently in the process of determining any treatment related methylation changes at the selected CpG sites.

A1.5 Discussion

Hypermethylation of specific CpG sites and genome wide hypomethylation is associated with genomic instability and inactivation of tumor suppressor genes (TSGs), and also with poor prognosis and disease relapse in ALL [155]. For example, genome-wide DNA methylation analysis of 12 childhood leukemia cell lines and 64 primary childhood ALL samples identified 30 genes that were methylated ≥25% in childhood ALL, amongst which 9 genes differentiate by methylation frequency in B and T-cell ALL cases [307]. Using the Nimblegen 3 x 720K CpG Island Plus RefSeq Promoter Array, we identified methylation enrichment in 4411 transcripts (~14% of array transcripts) across all samples by conserved peak analysis (Figure A1.1).

Azacitidine or 5-azacytidine (5-AZA or AZA), a DNA methylation inhibitor and analog of 5'-AZA-dC, is used clinically for myelodysplastic syndromes in order to increase time to leukemic transformation and thus functions in part as a chemopreventative agent [326]. We propose that phytochemicals derived from cruciferous vegetables, namely I3C and DIM, with known anticancer effects may also act through epigenetic mechanisms, and altered DNA methylation by these phytochemicals has not, to date, been reported on. Differential methylation analysis following treatment of the acute T-cell lymphoblastic leukemia cell line (CEM) with

sub-cytostatic/cytotoxic concentrations of these dietary compounds revealed marked hypomethylation of multiple genes (Table A1.3, Figures A1.2 and A1.3).

Our analysis confirmed methylation enrichment within genes that have previously been studied in clinical samples or model cell lines of T-ALL, including *TERT, WNT2B, CYP1B1*, *HLX1*, *DLX4*, *RASSF3, WT1* and *DUSP4*) [160,307,327-329]. Additionally, this approach allowed us to identify novel genes with altered methylation by I3C and/or DIM as potential therapeutic targets of T-ALL, including those involved in apoptosis (i.e. *DAXX*, *TRAF7, BCL210*), Jak-STAT signaling pathway (i.e. *TYK2*), transcriptional regulation (i.e. *ALX*, *MSX1*), and metastasis (i.e. *KISS1*). Functional analysis of hypo- and hypermethylated gene lists using the DAVID tool revealed that homeobox genes, transcription factors, negative regulators of apoptosis and cancer-related pathways were significantly de-methylated with DIM treatment (Table A1.4), in support of reversible methylation by dietary agents as a potential alternative or adjuvant to standard therapy.

We previously reported that higher concentrations of I3C than DIM were necessary to reduce the growth and survival of CEM and other T-ALL cell lines, suggesting that DIM formation *in vivo* may be necessary for these effects [302]. In agreement with these results, I3C treatment resulted in a divergent pattern of differential methylation relative to three DIM treatment regimes. I3C is known to self-oligomerizes to form additional products that may contribute to these divergent effects [81]. Efforts to validate the DMR results included both re-expression analysis and pyrosequencing. We confirmed by pyrosequencing a high degree of CpG methylation for *BMP4* and *WT1* (Supplemental Figure S-A1.3).

Methylation at CpG sites proximal to the promoter of genes is often associated with inactive transcription and potentially reversible by inhibition of methylation, however this is not always the case (i.e. in the presence of a mutation or deletion). Therefore we were surprised to see a high number (67%) of the selected genes for validation with increased expression in CEM cells following treatment with dietary indoles. Expression for three of these genes was not detectable by RTPCR in

untreated CEM cells but was restored after treatment with I3C and/or DIM. Moreover, multiple genes showed higher expression in RNA from a healthy T-cell population or in CEM following treatment with 5-AZA, suggesting that these genes may be important to leukemogenesis (Figure A1.4).

DIM has previously been reported to alter Class I HDAC expression in human colon cancer and microRNA 21 in human breast cancer cells [119,330]. We report for the first time that I3C/DIM treatment also modulates DNA methylation, in a model of T-cell lymphoblastic leukemia. Furthermore, we identified a number of biological pathways to be hypermethylated in untreated cells that have been reported on previously in T-ALL. For example, integrated gene expression and DNA methylation analysis in clinical ALL samples identified overlapping and novel therapeutic targets with enrichment in the WNT and MAPK signaling pathways [156]. Hypomethylation of established and novel genes, by DIM in particular, supports our previous study showing reduced proliferation and increased apoptosis in a number of T-ALL lines, and suggests an epigenetic mechanism is involved in this chemoprotective effect.

Acknowledgements: This project was primarily funded by the National Cancer Institute (grant number P01 CA90890) and was made possible, in part, by contributions from the Center for Genome Research and Biocomputing and the Linus Pauling Institute at Oregon State University, and the Protein and Nucleic Acid facility at Stanford University. The authors wish to thank Ana Hsu, Carmen Wong, and Laura Beaver, for their technical expertise and experimental suggestions.

A2 Supplemental materials

A2.1 Supplemental methods

TUNEL analysis *in vitro*. The *In Situ* Cell Death Detection kit with Fluorocein (Roche Applied Science, Indianapolis, IN) was used to label DNA strand breaks and Guava Express Plus software (Millipore, Billerica, MA) was used to sort and quantify the amount of TdT incorporation. Briefly, cells were fixed in 1% paraformaldehyde (PFA) containing Triton X-100 on ice for 45 min. Cells were pelleted, rinsed, resuspended in ice cold 70% EtOH and stored at -20°C at least overnight to permeabilize prior to suspension in the TdT label/TdT enzyme mix for 1 hr at 37°C in the dark. Labeled cells were then rinsed with PBS, re-fixed in 4% PFA on ice for 20 min, resuspended in PBS and stored in the dark for up to one week at 4°C. Treatment of cells with 500 U DNase I produced a major population of high intensity TdT-fluorescein labeling and was used as a positive control for this assay, whereas a sample incubated with TdT label/no enzyme served as the negative control to gate background fluorescence. The percentage of TdT-fluorescein labeled cells was determined using the standard formula for the apoptotic index (AI), which was calculated as follows: AI = (number of TUNEL-positive cells/total number of cells) x 100.

These fixed and labeled samples were also visualized by fluorescence microscopy on a Zeiss Axiovert 200 fluorescent microscope. Stained samples were pelleted and resuspended in ProlongGold antifade reagent with DAPI (Invitrogen, Carlsbad, CA) and mounted between glass coverslips. Exposure settings were standardized using control samples before taking consecutive 20x magnification images of a single field with FITC and DAPI filters. These images were re-colored by filter channel and globally adjusted for brightness and contrast (when necessary) prior to merging into a single image file (ImageJ, National Institutes of Health).

CEM cell xenograft study. The xenograft experiment using human CEM cells was split into five cohorts in order to ensure consistent and adequate quantity and viability (>95%) of cells for injections. Each cohort consisted of four control mice and two mice for each treatment group. Mice within a cohort were randomized into six cages and fed control diet or diets containing 500 ppm I3C, 2000 ppm I3C or 100 ppm DIM (350 ppm BR-DIM) for one week prior to inoculation with CEM cells. All diets were provided to mice *ad libitum*; fresh food was provided daily, and diet consumption was monitored daily on a per cage basis. Two days prior to inoculation, hair along the back of each mouse was removed with electric

clippers to improve injection site visibility and measurement. Freshly collected CEM cells in a 1:1 (v/v) solution of medium/Matrigel were injected subcutaneously (*s.c.*) at two sites along the back of each mouse (anterior and posterior, 10^7 cells/site). Experimental diets continued for four weeks during xenograft growth. Starting on day 7 after inoculation, animal weights and nodule dimensions were assessed every third day with digital scale and digital calipers, respectively. Xenograft volumes were calculated using the equation for an ellipsoid ($L \times W^2 \times \pi/6$). During the first cohort of the experiment, we observed that anterior xenografts were difficult to palpate and were inconsistent compared to the same animal posterior site and within a given treatment group. The method of scruff restraint during *s.c.* injection likely resulted in inconsistent cell inoculations at the anterior position; thus, the anterior site was excluded from analyses for xenograft volume. Subsequent cohorts were similarly treated, though, to provide for consistency of experiment design. Four weeks following engraftment, mice were euthanized by CO_2 asphyxiation and necropsied. Blood was collected from the hepatic vein prior to excision of CEM cell xenografts and select tissues. The solid xenografts were weighed and divided into four quadrants of approximately equal volume and size, one of which was fixed in 10% neutral buffered formalin and processed for immunohistochemistry. The remaining xenograft fractions and tissues were immediately frozen in liquid nitrogen and stored at -80°C for future analysis.

TUNEL analysis of human CEM cell xenografts. Serial sections of xenografts were stained using the *In Situ* Cell Death Detection kit, POD (Roche) with the following modifications: 20 μg/ml Proteinase K for 15 min at 37°C and dilution of the POD converter solution 1:1 with buffer containing 1% BSA for 30 min at 37°C. Nova Red (Vector Laboratories; Burlingame, CA) was used as the chromagen, in place of DAB, and slides were counterstained with hematoxylin (Dako, Denmark). Multiple non-overlapping fields were imaged at 40x magnification for each section. At least 10 images per section, from a minimum of three sections per group, were analyzed with ImageJ software (≥30 images per treatment group), using the color deconvolution method of Ruifrok and Johnston [331]. Briefly, an initial image was used to determine the color vectors for the two stains, TUNEL positive (red), and TUNEL negative (blue). These values were added to the Color-Deconvolution algorithm that was then run on each subsequent image to separate the colors into discrete images. The blue (negative) monochrome image was processed according to the MBF-ImageJ Manual for Particle Analysis, a multi-step process that results in the distinction

of cellular boundaries to allow automatic counting by the software. Manual counting was used for determination of TUNEL-positive cells on all images (to eliminate false positive detection) and on a subset of blue monochrome images to validate the automatic counting process. The apoptotic-index (AI) was calculated as follows: AI = (manual count TUNEL positive/auto count negative) x 100.

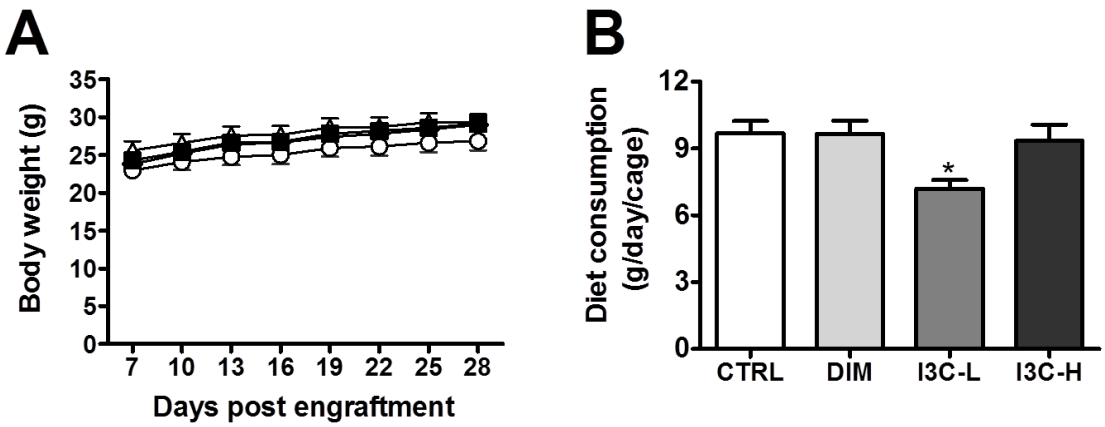

Supplemental Figure S-3.1 Weight gain and daily diet consumption.
Male NOD.CB17-*Prkdc*^{scid}/SzJ mice were fed diets containing 100 ppm DIM (350 BR-DIM, ◆), 500 ppm I3C (△, I3C-L), 2000 ppm I3C (○, I3C-H) or control diet (■) throughout the xenograft study. (A) Following engraftment with CEM cells, animals were weighed every third day to monitor the rate of weight gain. A significant effect of experimental diet was not observed on weight gain, as determined by a two-way repeated-measures ANOVA (source of variation and *p*-value: diet treatment, $p = 0.543$; time, $p < 0.0001$; interaction, $p = 0.053$; subjects matching, $p < 0.001$). (B) Average food intake was assessed daily on a per cage basis (two subjects per cage). *, $p < 0.05$ as determined by one-way ANOVA with Dunnett's post-hoc multiple comparisons test compared to control (CTRL) diet.

Supplemental Table S-3.1 DIM-induced changes in expression of genes associated with apoptosis pathway in human CEM cells.

			Length of treatment †			
			4 hrs		24 hrs	
Unigene	**Symbol** *	**Description**	**Log_2 R**	***p*-value**	**Log_2 R**	***p*-value**
TNF ligand family						
Hs.592244	***CD40LG***	CD40 ligand	**0.75**	**0.019**	**0.62**	**0.043**
Hs.2007	*FASLG*	Fas ligand (TNF superfamily, member 6)	0.56	0.153	0.37	0.612
Hs.36	*LTA*	Lymphotoxin alpha (TNF superfamily, member 1)	nd ‡	nd	0.14	0.258
Hs.241570	***TNF***	Tumor necrosis factor (TNF superfamily, member 2)	**-0.63**	**0.016**	-0.39	0.026
Hs.478275	*TNFSF10*	Tumor necrosis factor (ligand) superfamily, member 10	0.38	0.123	0.23	0.421
Hs.501497	*CD70*	CD70 molecule	0.00	0.981	-0.04	0.852
Hs.654445	***TNFSF8***	Tumor necrosis factor (ligand) superfamily, member 8	**0.90**	**0.026**	0.34	0.009
TNF Receptor & Death Domain Family						
Hs.472860	*CD40*	CD40 molecule, TNF receptor superfamily member 5	**0.70**	0.521	**-1.12**	0.255
Hs.244139	*FAS*	Fas (TNF receptor superfamily, member 6)	0.21	0.160	0.00	0.993
Hs.1116	*LTBR*	Lymphotoxin beta receptor (TNFR superfamily, member 3)	0.25	0.811	**-0.70**	0.542
Hs.279594	***TNFRSF1A***	Tumor necrosis factor receptor superfamily, member 1A	**1.22**	**0.002**	-0.46	0.331
Hs.654459	*TNFRSF9*	Tumor necrosis factor receptor superfamily, member 9	**0.70**	0.475	**-1.22**	0.068
Hs.591834	*TNFRSF10A*	Tumor necrosis factor receptor superfamily, member 10a	-0.11	0.822	-0.11	0.866
Hs.521456	*TNFRSF10B*	Tumor necrosis factor receptor superfamily, member 10b	0.41	0.067	0.50	0.072
Hs.81791	*TNFRSF11B*	Tumor necrosis factor receptor superfamily, member 11b	**-1.02**	0.253	**-1.56**	0.136
Hs.443577	*TNFRSF21*	Tumor necrosis factor receptor superfamily, member 21	0.06	0.384	-0.31	0.149
Hs.462529	***TNFRSF25***	Tumor necrosis factor receptor superfamily, member 25	nd	nd	**-1.15**	**0.015**
Hs.355307	*CD27*	CD27 molecule	0.15	0.142	0.01	0.904
Hs.380277	*DAPK1*	Death-associated protein kinase 1	-0.08	0.671	-0.21	0.162
Hs.86131	*FADD*	Fas (TNFRSF6)-associated via death domain	0.12	0.603	-0.48	0.057
Hs.460996	*TRADD*	TNFRSF1A-associated via death domain	0.00	1.000	0.10	0.492
Bcl-2 family						
Hs.370254	*BAD*	BCL2-associated agonist of cell death	0.36	0.083	**-0.66**	0.283
Hs.377484	*BAG1*	BCL2-associated athanogene	-0.46	0.024	-0.25	0.084
Hs.523309	*BAG3*	BCL2-associated athanogene 3	0.07	0.559	0.01	0.907
Hs.194726	*BAG4*	BCL2-associated athanogene 4	0.03	0.830	-0.42	0.130
Hs.485139	*BAK1*	BCL2-antagonist/killer 1	0.11	0.615	-0.30	0.068
Hs.624291	*BAX*	BCL2-associated X protein	0.21	0.168	0.16	0.536
Hs.150749	*BCL2*	B-cell CLL/lymphoma 2	0.28	0.074	-0.15	0.433

			Length of treatment †			
			4 hrs		24 hrs	
Unigene	**Symbol** *	**Description**	**Log_2 R**	***p*-value**	**Log_2 R**	***p*-value**
Hs.227817	*BCL2A1*	BCL2-related protein A1	-0.19	0.379	0.32	0.539
Hs.516966	*BCL2L1*	BCL2-like 1	**0.61**	0.081	-0.31	0.606
Hs.283672	***BCL2L10***	BCL2-like 10 (apoptosis facilitator)	**1.05**	0.459	**0.63**	**0.023**
Hs.469658	*BCL2L11*	BCL2-like 11 (apoptosis facilitator)	-0.51	0.113	-0.04	0.799
Hs.410026	*BCL2L2*	BCL2-like 2	0.24	0.134	-0.01	0.945
Hs.486542	*BCLAF1*	BCL2-associated transcription factor 1	-0.36	0.016	-0.41	0.080
Hs.591054	*BID*	BH3 interacting domain death agonist	-0.31	0.073	-0.21	0.153
Hs.475055	*BIK*	BCL2-interacting killer (apoptosis-inducing)	-0.11	0.656	**-0.71**	0.066
Hs.145726	*BNIP1*	BCL2/adenovirus E1B 19kDa interacting protein 1	0.19	0.311	**-0.70**	0.058
Hs.646490	*BNIP2*	BCL2/adenovirus E1B 19kDa interacting protein 2	0.21	0.211	0.00	0.977
Hs.144873	*BNIP3*	BCL2/adenovirus E1B 19kDa interacting protein 3	-0.38	0.054	-0.58	0.004
Hs.131226	*BNIP3L*	BCL2/adenovirus E1B 19kDa interacting protein 3-like	-0.10	0.645	-0.18	0.081
Hs.87247	*HRK*	Harakiri, BCL2 interacting protein (contains only BH3 domain)	**0.88**	**0.014**	**1.35**	**0.004**
Hs.632486	*MCL1*	Myeloid cell leukemia sequence 1 (BCL2-related)	-0.38	0.077	-0.20	0.077
Caspase family & death effectors						
Hs.2490	*CASP1*	Caspase 1, apoptosis-related cysteine peptidase (interleukin 1, beta, convertase)	-0.07	0.576	0.25	0.117
Hs.5353	*CASP10*	Caspase 10, apoptosis-related cysteine peptidase	0.51	0.018	0.23	0.067
Hs.466057	*CASP14*	Caspase 14, apoptosis-related cysteine peptidase	**-0.82**	0.294	**-0.65**	0.529
Hs.368982	*CASP2*	Caspase 2, apoptosis-related cysteine peptidase	0.00	0.981	-0.48	0.000
Hs.141125	*CASP3*	Caspase 3, apoptosis-related cysteine peptidase	0.14	0.687	-0.33	0.010
Hs.138378	*CASP4*	Caspase 4, apoptosis-related cysteine peptidase	0.45	0.275	0.15	0.239
Hs.213327	*CASP5*	Caspase 5, apoptosis-related cysteine peptidase	**0.84**	0.556	**-0.96**	0.361
Hs.654616	*CASP6*	Caspase 6, apoptosis-related cysteine peptidase	-0.04	0.770	-0.04	0.673
Hs.9216	*CASP7*	Caspase 7, apoptosis-related cysteine peptidase	0.01	0.918	-0.23	0.083
Hs.599762	*CASP8*	Caspase 8, apoptosis-related cysteine peptidase	0.40	0.215	0.18	0.668
Hs.329502	*CASP9*	Caspase 9, apoptosis-related cysteine peptidase	0.23	0.060	0.30	0.409
Hs.390736	*CFLAR*	CASP8 and FADD-like apoptosis regulator	0.20	0.369	0.04	0.779
IAP family						
Hs.710305	*NAIP*	NLR family, apoptosis inhibitory protein	0.12	0.382	0.06	0.424
Hs.696238	*BIRC2*	Baculoviral IAP repeat-containing 2	0.41	0.029	0.16	0.168
Hs.127799	*BIRC3*	Baculoviral IAP repeat-containing 3	0.48	0.016	0.04	0.743
Hs.150107	*BIRC6*	Baculoviral IAP repeat-containing 6	-0.28	0.053	-0.14	0.292
Hs.348263	*BIRC8*	Baculoviral IAP repeat-containing 8	**-0.82**	0.294	**-1.01**	0.325
Hs.356076	*XIAP*	X-linked inhibitor of apoptosis	0.28	0.171	-0.16	0.210

			Length of treatment †			
			4 hrs		24 hrs	
Unigene	**Symbol** *	**Description**	**Log_2 R**	***p*-value**	**Log_2 R**	***p*-value**
TRAF family						
Hs.522506	*TRAF2*	TNF receptor-associated factor 2	**1.14**	0.166	**-1.90**	0.054
Hs.510528	*TRAF3*	TNF receptor-associated factor 3	**1.17**	0.011	**-1.42**	0.112
Hs.8375	*TRAF4*	TNF receptor-associated factor 4	nd	nd	**-1.51**	**0.017**
CARD family						
Hs.552567	*APAF1*	Apoptotic peptidase activating factor 1	0.25	0.140	-0.46	0.068
Hs.193516	*BCL10*	B-cell CLL/lymphoma 10	-0.06	0.817	0.23	0.390
Hs.405153	*NOD1*	Nucleotide-binding oligomerization domain containing 1	0.08	0.360	-0.19	0.035
Hs.200242	*CARD6*	Caspase recruitment domain family, member 6	0.28	0.344	**0.69**	0.134
Hs.446146	*CARD8*	Caspase recruitment domain family, member 8	nd	nd	0.33	0.287
Hs.38533	*CRADD*	CASP2 and RIPK1 domain containing adaptor with death domain	0.08	0.740	-0.07	0.541
Hs.513667	*NOL3*	Nucleolar protein 3 (apoptosis repressor with CARD domain)	0.18	0.423	0.55	0.078
Hs.499094	*PYCARD*	PYD and CARD domain containing	-0.01	0.910	0.01	0.869
Hs.103755	*RIPK2*	Receptor-interacting serine-threonine kinase 2	**0.66**	0.105	0.16	0.116
CIDE domain family						
Hs.249129	*CIDEA*	Cell death-inducing DFFA-like effector a	-0.16	0.822	**-1.91**	0.257
Hs.642693	*CIDEB*	Cell death-inducing DFFA-like effector b	-0.03	0.829	**-1.01**	0.093
Hs.484782	*DFFA*	DNA fragmentation factor, 45kDa, alpha polypeptide	-0.06	0.744	-0.32	0.206
p53 and DNA damage response						
Hs.431048	*ABL1*	C-abl oncogene 1, receptor tyrosine kinase	0.36	0.000	0.08	0.720
Hs.525622	*AKT1*	V-akt murine thymoma viral oncogene homolog 1	0.00	0.992	**-0.79**	0.095
Hs.80409	*GADD45A*	Growth arrest and DNA-damage-inducible, alpha	0.40	0.191	0.37	0.091
Hs.654481	*TP53*	Tumor protein p53	0.18	0.452	-0.16	0.448
Hs.523968	*TP53BP2*	Tumor protein p53 binding protein, 2	0.01	0.905	-0.23	0.176
Hs.697294	*TP73*	Tumor protein p73	0.06	0.938	-0.39	0.157
Anti-apoptosis						
Hs.550061	*BRAF*	V-raf murine sarcoma viral oncogene homolog B1	0.34	0.009	-0.15	0.161
Hs.435556	*BFAR*	Bifunctional apoptosis regulator	0.00	0.989	0.03	0.744
Hs.643120	*IGF1R*	Insulin-like growth factor 1 receptor	-0.28	0.248	0.01	0.921

Note: Genes are categorized according to functional groupings as outlined by the Human Apoptosis RT² Profiler™ PCR Array gene table; some genes belong to more than one category.

* Gene symbols in bold meet criteria for fold-change threshold and statistical significance.

† Log_2 fold-change (R) values are shown in bold if level of change is >1.5-fold (Log_2 R<-0.58 or >0.58) compared to vehicle (0.1% DMSO) control. *P*-values are compared to vehicle treatment as determined by a Student's *t*-test assuming equal variances. Genes highlighted in blue passed both fold-change and statistics criteria for at least one time-point.

‡ nd, not detected by RT^2 PCR profiler array at this time point (C_t >35).

Supplemental Table S-4.1 Histological observations from early mortality animals (10 weeks of age or less).

ID	4F8M1	6G11M1	4F8M4	3G4M1	2E4M1	2F4M1	2E4M2	3G5F1	6E10F1	4F8M5
TREATMENT	10 % broccoli sprout	400 ppm SFN	10 % broccoli sprout	400 ppm SFN	10% Brussels sprout	10 % broccoli sprout	10% Brussels sprout	400 ppm SFN	10% Brussels sprout	10 % broccoli sprout
GENDER	M	M	M	M	M	M	M	F	F	M
AGE (weeks)	4.7	4.9	5.0	5.0	6.3	6.3	6.7	9.0	9.7	10.0
THYMUS	ongoing involusion	involuted	na (trachea)	na	atrophy	lymphoma	nsf	na	nsf (involuting)	lymphoma
LIVER	nsf	nsf	nsf	na	nsf	moderate lipidosis fine to large vacuolar	heaptic hemangioma; rest nsf	hypertrophy; minimal fatty	diffuse mild vacuolar change	minimal lymphoma
SPLEEN	na	Hyperplasia/EMH (lymphoma?)	nsf	na	nsf		severe EMH	nsf	suspect lymphoma	? Recut=lymphoma
REPRODUCTIVE	A: massive hemorrhage and necrosis (torsion? Infarct?); B: mild hemorrhage, inactive tubules	inactive; tubular atrophy	Bilateral mild hemorrhage, inactive tubules	na	bialteral massive testicular hemorrhage mf tubular necrosis; dilated sex gland	atrophy and dilation; few tubules filled with sperm and large cells; dilation sex gland	rare tubular atrophy; hyperplasia sex gland epithelium	na	?	ectatic gland; testes some tubules with sperm but reduced/absent precursors
LUNG	nsf	nsf	nsf	bacterial colonies multifocal; multifocal hyperplasia; suspect granuloma (mineral or bacteria?)	nsf	diffuse mod atelectasis; pleural lymphoma; mf early hyperplasia	nsf	nsf	massive acute hemorrhage; nsf	atelectasis, congestion; mild lymphoma

Supplemental Table S-4.1 Histological observations from early mortality animals (10 weeks of age or less) (continued).

ID	4F8M1	6G11M1	4F8M4	3G4M1	2E4M1	2F4M1	2E4M2	3G5F1	6E10F1	4F8M5
HEART	multifocal severe mineralization	subendocardial hemorrhage	mild multifocal mineralization; rare myofiber degeneration	numerous bacterial colonies; rare mineralization	minimal acute mf hemorrhage	lymphoma (epicardial lymphocytes)	nsf	nsf	acute myocardial necrosis; mild mineralization	minimal lymphoma
KIDNEY	nsf	nsf	nsf	unilateral bacterial colonies large	nsf	minimal lymphoma; nsf	nsf	nsf	nsf	minimal lymphoma
SI	nsf	nsf	nsf	nsf	nsf	nsf	nsf (rotten)	nsf	nsf	nsf, pancreas nsf
STOMACH	massive submucosal hemorrhage esp glandular	nsf	nsf (no non-glandular)	nsf (no glandular)	mild hyperplasia margo	nsf (glandular only)	nsf (glandular only)	nsf (full)	nsf (non-glandular only)	nsf
ADRENAL	na	nsf	na	nsf (cortex only)	na	na	na	nsf	na	na
OTHER		pancreas nsf			salivargy gland nsf				pancreas nsf	
Dx	?? hemorrhage, cardiac mineralization	?? unclear	?? hemorrhage, cardiac mineralization	sepsis -origin undetermined	testicular hemorrhage and necrosis	thymic lymphoma	hepatic hemangioma; suspect anemia	?? congestion	acute myocardial necrosis; mild mineralization	thymic lymphoma

Key: nsf = no significant finding; EMH = extramedullary hematopoiesis; mf = multifocal

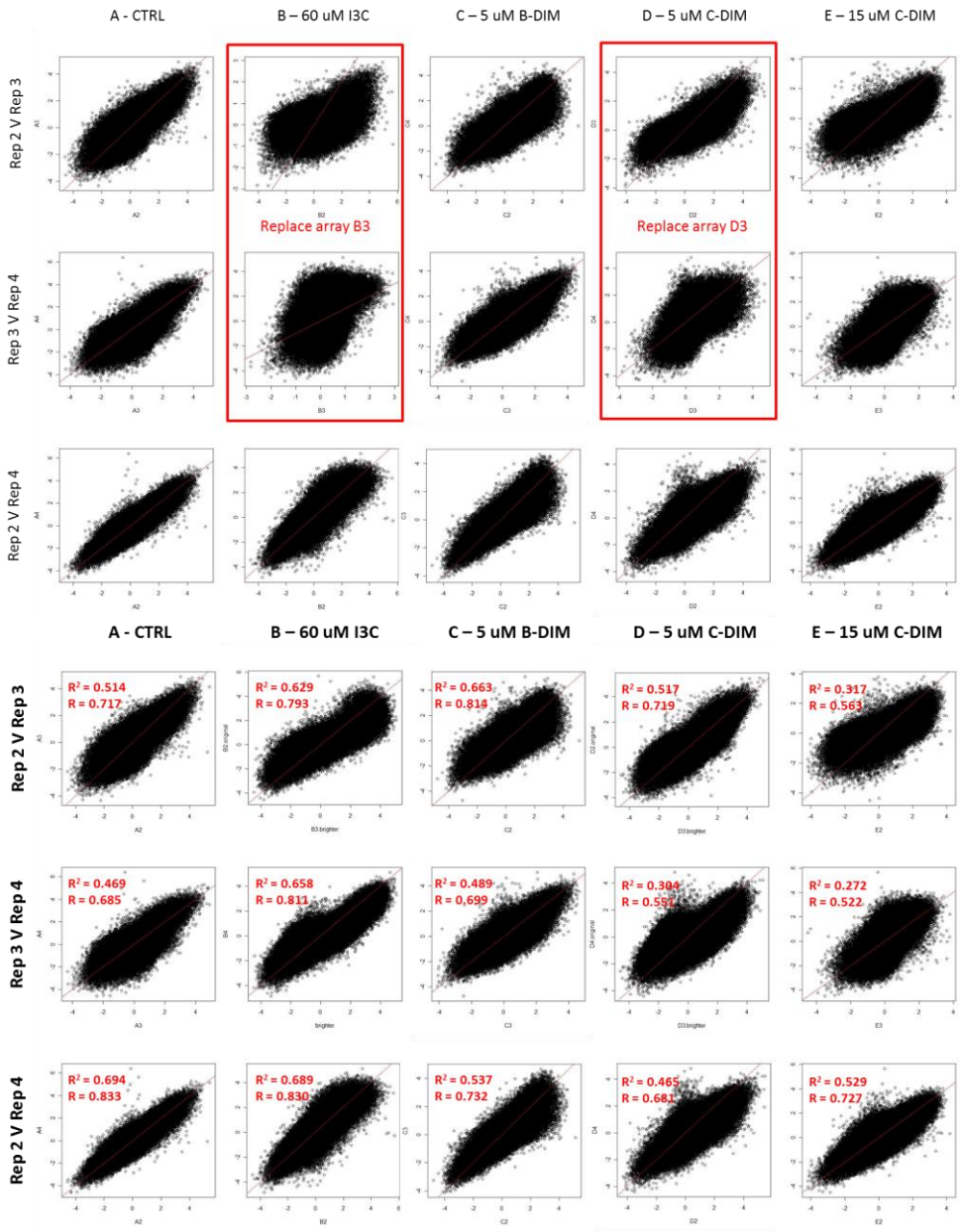

Supplemental Figure S-A1.1 Scatterplots and regression coefficients comparing replicate arrays within a treatment.

(Top) The initially hybridized arrays showed poor correlation with the two other replicates within that treatment (B3 and D3). These arrays were replaced and hybridized with the same labeled samples and the replacement arrays showed improved correlation (Bottom). Thus the replacement arrays were used in downstream analysis.

Supplemental Table S-A1.1 Transcripts identified by DMR analysis with Bonferroni MTC and magnitude of change in intensity from control treatment.

Gene symbol	Gene description	60 µM I3C		5 µM B-DIM		5 µM C-DIM		15 µM C-DIM	
		min	max	min	max	min	max	min	max
A2LD1	AIG2-like domain 1	0.09	0.09	-0.74	-0.74	-0.72	-0.72	-0.74	-0.74
ABCB7	ATP-binding cassette, sub-family B (MDR/TAP), member 7	-0.53	-0.47	-0.92	-0.87	-0.62	-0.49	-0.87	-0.81
ADARB2	adenosine deaminase, RNA-specific, B2	0.31	0.35	-0.08	-0.03	-0.33	-0.20	-0.82	-0.63
ADD2	adducin 2 (beta)	0.57	0.57	0.21	0.21	-0.11	-0.11	-0.57	-0.57
ALDH3B1	aldehyde dehydrogenase 3 family, member B1	0.75	0.75	0.21	0.21	-0.22	-0.22	-0.46	-0.46
ALDH4A1	aldehyde dehydrogenase 4 family, member A1	0.58	0.65	-0.25	-0.07	-0.21	-0.12	-0.70	-0.55
ALOX12B	arachidonate 12-lipoxygenase, 12R type	-0.41	-0.39	-0.12	-0.04	0.18	0.22	0.09	0.18
ALPP	alkaline phosphatase, placental	0.19	0.29	-0.32	-0.25	-0.43	-0.34	-0.59	-0.50
ALPPL2	alkaline phosphatase, placental-like 2	0.01	0.26	-0.44	-0.22	-0.63	-0.38	-0.82	-0.44
ALX1	ALX homeobox 1	-0.34	-0.34	-0.87	-0.87	-0.86	-0.86	-0.99	-0.99
ALX3	ALX homeobox 3	-0.05	-0.03	-0.63	-0.51	-0.86	-0.73	-0.69	-0.64
APCDD1	adenomatosis polyposis coli down-regulated 1	0.02	0.02	-0.36	-0.36	-0.45	-0.45	-0.90	-0.90
APOA4	apolipoprotein A-IV	0.06	0.06	-0.24	-0.24	-0.50	-0.50	-0.58	-0.58
APOBEC3D	apolipoprotein B mRNA editing enzyme, catalytic polypeptide-like 3D	-0.14	-0.14	-0.44	-0.41	-0.40	-0.39	-0.93	-0.89
ARHGAP22	Rho GTPase activating protein 22	-0.10	-0.10	-0.52	-0.52	-0.36	-0.36	-0.94	-0.94
ARX	aristaless related homeobox	-0.31	-0.26	-0.83	-0.66	-0.81	-0.72	**-1.23**	**-1.04**
ASB12	ankyrin repeat and SOCS box-containing 12	-0.24	-0.10	0.21	0.36	0.47	0.62	0.42	0.53
ATP11A	ATPase, class VI, type 11A	-0.09	0.06	-0.35	-0.30	-0.49	-0.32	**-1.20**	-0.98
ATP2B3	ATPase, Ca++ transporting, plasma membrane 3	0.50	0.50	-0.04	-0.04	-0.15	-0.15	-0.43	-0.43
ATP5G2	ATP synthase, H+ transporting, mitochondrial Fo complex, subunit C2 (subunit 9)	**-1.13**	**-1.13**	-0.52	-0.52	-0.31	-0.31	**-1.42**	**-1.42**
ATP8B5P	ATPase, class I, type 8B, member 5, pseudogene	-0.56	-0.54	-0.62	-0.62	-0.26	-0.23	-0.96	-0.94
BAIAP2	BAI1-associated protein 2	0.54	0.56	0.24	0.34	-0.31	-0.26	-0.51	-0.45
BANP	BTG3 associated nuclear protein	0.01	0.01	-0.52	-0.52	-0.41	-0.41	**-1.16**	**-1.16**
BCL2L10	BCL2-like 10 (apoptosis facilitator)	-0.21	-0.21	-0.40	-0.40	-0.66	-0.66	-0.66	-0.66
BEND3	BEN domain containing 3	0.61	0.85	0.05	0.20	-0.40	-0.21	-0.50	-0.31
BNC1	basonuclin 1	-0.20	-0.04	-0.71	-0.49	-0.94	-0.77	-0.53	-0.43
BRD1	bromodomain containing 1	-0.37	-0.17	-0.79	-0.79	-0.95	-0.82	-0.96	-0.84
BRD9	bromodomain containing 9	0.14	0.27	-0.36	-0.30	-0.48	-0.33	-0.95	-0.87
C10orf92	chromosome 10 open reading frame 92	0.43	0.51	-0.19	-0.07	-0.49	-0.41	**-1.83**	**-1.57**
C12orf57	chromosome 12 open reading frame 57	-0.92	-0.72	-0.98	-0.92	-0.83	-0.77	**-1.75**	**-1.43**
C14orf23	chromosome 14 open reading frame 23	0.78	0.89	0.05	0.09	-0.27	-0.26	-0.12	-0.08
C16orf42	chromosome 16 open reading frame 42	-0.57	-0.48	-0.71	-0.62	-0.05	0.03	**-1.09**	-0.89
C18orf1	chromosome 18 open reading frame 1	-0.32	-0.32	-0.14	-0.14	-0.43	-0.43	-0.97	-0.97

Gene symbol	Gene description	60 µM I3C		5 µM B-DIM		5 µM C-DIM		15 µM C-DIM	
		min	max	min	max	min	max	min	max
C19orf70	chromosome 19 open reading frame 70	-0.70	-0.62	-0.61	-0.52	-0.25	-0.15	**-1.15**	**-1.07**
C1orf9	chromosome 1 open reading frame 9	0.02	0.31	0.71	0.75	0.50	0.53	0.84	0.89
C20orf114	chromosome 20 open reading frame 114	-0.83	-0.69	-0.70	-0.63	-0.35	-0.29	**-1.24**	**-1.16**
C21orf129	chromosome 21 open reading frame 129	-0.91	-0.91	**-1.02**	**-1.02**	-0.15	-0.15	**-1.46**	**-1.46**
C22orf34	chromosome 22 open reading frame 34	0.17	0.27	-0.41	-0.40	-0.68	-0.61	-0.65	-0.63
C2CD4A	C2 calcium-dependent domain containing 4A	-0.04	-0.01	-0.78	-0.77	-0.73	-0.70	-0.78	-0.70
C2orf16	chromosome 2 open reading frame 16	-0.86	-0.48	-0.89	-0.61	-0.58	-0.43	**-1.35**	**-1.11**
C5orf55	chromosome 5 open reading frame 55	-0.53	-0.45	-0.84	-0.74	-0.82	-0.72	**-1.06**	-0.90
C9orf129	chromosome 9 open reading frame 129	0.48	0.55	-0.11	0.03	-0.66	-0.51	-0.68	-0.59
C9orf64	chromosome 9 open reading frame 64	0.92	0.92	0.35	0.35	-0.07	-0.07	-0.14	-0.14
CA5BP	carbonic anhydrase VB pseudogene	-0.96	-0.77	-0.64	-0.48	-0.35	-0.22	**-1.60**	**-1.37**
CACNA1H	calcium channel, voltage-dependent, T type, alpha 1H subunit	0.23	0.26	-0.37	-0.31	-0.58	-0.46	-0.52	-0.47
CACNG7	calcium channel, voltage-dependent, gamma subunit 7	-0.95	-0.95	-0.90	-0.90	-0.44	-0.44	**-1.02**	**-1.02**
CALB1	calbindin 1, 28kDa	0.20	0.21	-0.27	-0.24	-0.50	-0.44	**-1.05**	**-1.05**
CALCR	calcitonin receptor	0.52	0.58	-0.20	-0.11	-0.53	-0.49	-0.52	-0.43
CCDC39	coiled-coil domain containing 39	-0.81	-0.71	**-1.06**	-0.91	-0.62	-0.59	**-1.44**	**-1.23**
CCND2	cyclin D2	-0.53	-0.53	-0.26	-0.26	-0.33	-0.33	-0.96	-0.96
CDC7	cell division cycle 7 homolog (S. cerevisiae)	-0.68	-0.40	0.16	0.26	0.24	0.36	0.29	0.47
CHID1	chitinase domain containing 1	-0.60	-0.60	-0.82	-0.82	-0.47	-0.47	**-1.12**	**-1.12**
CKAP2	cytoskeleton associated protein 2	-0.04	-0.04	0.54	0.54	0.58	0.58	0.57	0.57
CLCNKB	chloride channel Kb	-0.30	-0.26	-0.41	-0.39	-0.52	-0.42	-0.79	-0.76
CLDN4	claudin 4	0.21	0.21	-0.29	-0.29	-0.58	-0.58	-0.59	-0.59
CLEC18A	C-type lectin domain family 18, member A	0.14	0.14	-0.09	-0.09	-0.21	-0.21	-0.64	-0.64
CLIC5	chloride intracellular channel 5	-0.06	0.00	-0.81	-0.71	-0.94	-0.90	-0.75	-0.63
CLPTM1L	CLPTM1-like	-0.99	-0.87	**-1.33**	**-1.22**	-0.79	-0.63	**-1.75**	**-1.63**
COL4A5	collagen, type IV, alpha 5	-0.99	-0.92	**-1.01**	**-1.00**	-0.40	-0.37	**-1.07**	**-1.01**
CRIPAK	cysteine-rich PAK1 inhibitor	0.38	0.38	-0.13	-0.13	-0.38	-0.38	-0.39	-0.39
CROCCP2	ciliary rootlet coiled-coil, rootletin pseudogene 2	0.78	0.81	0.28	0.35	0.17	0.18	-0.13	-0.07
CSPG4	chondroitin sulfate proteoglycan 4	0.38	0.38	-0.11	-0.11	-0.41	-0.41	-0.63	-0.63
CTDP1	CTD (carboxy-terminal domain, RNA polymerase II, polypeptide A) phosphatase, subunit 1	0.21	0.21	-0.35	-0.35	-0.73	-0.73	-0.93	-0.93
CTH	cystathionase (cystathionine gamma-lyase)	-1.00	-0.85	-0.62	-0.55	-0.30	-0.23	**-1.28**	**-1.19**
DAB2IP	DAB2 interacting protein	-0.70	-0.63	-0.97	-0.90	-0.32	-0.31	**-1.23**	**-1.13**
DBH	dopamine beta-hydroxylase (dopamine beta-monooxygenase)	-0.58	-0.58	-0.81	-0.81	-0.40	-0.40	**-1.20**	**-1.20**
DCD	dermcidin	-0.10	-0.08	0.48	0.50	0.33	0.33	0.74	0.77

Gene symbol	Gene description	60 µM I3C		5 µM B-DIM		5 µM C-DIM		15 µM C-DIM	
		min	max	min	max	min	max	min	max
DCHS2	dachsous 2 (Drosophila)	0.52	0.52	0.11	0.11	-0.21	-0.21	-0.52	-0.52
DDX60	DEAD (Asp-Glu-Ala-Asp) box polypeptide 60	-0.02	-0.02	0.56	0.56	0.43	0.43	0.88	0.88
DEGS2	degenerative spermatocyte homolog 2, lipid desaturase (Drosophila)	-0.82	-0.82	-0.89	-0.89	-0.64	-0.64	**-1.08**	**-1.08**
DIP2C	DIP2 disco-interacting protein 2 homolog C (Drosophila)	-0.37	0.11	-0.33	-0.12	-0.50	-0.31	**-1.57**	-1.00
DLX1	distal-less homeobox 1	-0.08	-0.05	-0.70	-0.61	-0.88	-0.61	-0.96	-0.74
DNAJC5	DnaJ (Hsp40) homolog, subfamily C, member 5	0.31	0.31	-0.29	-0.29	-0.23	-0.23	-0.47	-0.47
DOT1L	DOT1-like, histone H3 methyltransferase (S. cerevisiae)	-0.26	-0.19	-0.45	-0.34	-0.35	-0.17	**-1.10**	-0.96
DUSP28	dual specificity phosphatase 28	0.21	0.23	-0.32	-0.26	-0.58	-0.55	-0.20	-0.14
EGFR	epidermal growth factor receptor	0.51	0.51	0.02	0.02	-0.27	-0.27	-0.38	-0.38
ELANE	elastase, neutrophil expressed	-0.51	-0.42	-0.89	-0.81	-0.79	-0.69	**-1.01**	-0.98
ENO2	enolase 2 (gamma, neuronal)	-0.28	-0.28	0.15	0.15	0.33	0.33	0.35	0.35
ERICH1	glutamate-rich 1	-0.53	-0.48	0.15	0.17	0.05	0.05	0.33	0.39
EXOC2	exocyst complex component 2	**-1.03**	**-1.03**	**-1.11**	**-1.11**	-0.50	-0.50	**-1.25**	**-1.25**
EXTL2	exostoses (multiple)-like 2	-0.28	-0.12	0.56	0.64	0.46	0.58	0.92	0.95
FAM120A	family with sequence similarity 120A	0.19	0.21	-0.17	-0.17	-0.60	-0.56	-0.89	-0.81
FAM120B	family with sequence similarity 120B	-0.87	-0.74	-0.74	-0.68	-0.38	-0.32	**-1.51**	**-1.44**
FAM123C	family with sequence similarity 123C	-0.37	-0.37	-0.84	-0.84	-0.61	-0.61	-0.76	-0.76
FAM163B	family with sequence similarity 163, member B	-0.68	-0.59	-0.85	-0.77	-0.38	-0.33	**-1.32**	**-1.31**
FBXL6	F-box and leucine-rich repeat protein 6	-0.02	0.10	-0.61	-0.45	-0.68	-0.56	-0.79	-0.62
FBXO25	F-box protein 25	-0.50	-0.44	0.17	0.20	0.21	0.27	0.13	0.24
FERMT3	fermitin family member 3	-0.73	-0.57	**-1.04**	-0.80	-0.78	-0.67	**-1.54**	**-1.34**
FOXK1	forkhead box K1	0.65	0.65	0.10	0.10	-0.24	-0.24	-0.31	-0.31
FRMD1	FERM domain containing 1	-0.75	-0.69	-0.74	-0.70	-0.50	-0.47	**-1.23**	**-1.13**
FSTL3	follistatin-like 3 (secreted glycoprotein)	0.62	0.62	0.27	0.27	-0.22	-0.22	-0.53	-0.53
FZD1	frizzled homolog 1 (Drosophila)	0.14	0.59	-0.28	-0.12	-0.66	-0.40	-0.78	-0.51
FZD10	frizzled homolog 10 (Drosophila)	0.60	0.62	0.03	0.08	-0.37	-0.37	-0.41	-0.35
FZD2	frizzled homolog 2 (Drosophila)	0.68	0.77	0.27	0.30	-0.38	-0.31	-0.30	-0.30
GALNS	galactosamine (N-acetyl)-6-sulfate sulfatase	0.77	0.77	0.26	0.26	0.06	0.06	-0.26	-0.26
GALNT13	UDP-N-acetyl-alpha-D-galactosamine:polypeptide N-acetylgalactosaminyltransferase 13 (GalNAc-T13)	0.54	0.58	0.06	0.07	-0.35	-0.35	-0.43	-0.41
GALNT9	UDP-N-acetyl-alpha-D-galactosamine:polypeptide N-acetylgalactosaminyltransferase 9 (GalNAc-T9)	0.15	0.25	-0.24	-0.22	-0.37	-0.30	-0.66	-0.60
GAS2L2	growth arrest-specific 2 like 2	-0.39	-0.36	-0.35	-0.27	-0.12	0.04	-0.85	-0.81
GAS6	growth arrest-specific 6	-0.46	-0.01	-0.55	-0.05	-0.37	-0.20	-0.88	-0.68

Gene symbol	Gene description	60 µM I3C		5 µM B-DIM		5 µM C-DIM		15 µM C-DIM	
		min	max	min	max	min	max	min	max
GATA1	GATA binding protein 1 (globin transcription factor 1)	-0.86	-0.78	-0.36	-0.30	-0.02	0.07	-0.57	-0.46
GDNF	glial cell derived neurotrophic factor	0.69	0.69	-0.04	-0.04	-0.19	-0.19	-0.33	-0.33
GGT1	gamma-glutamyltransferase 1	-0.61	-0.61	-0.80	-0.80	-0.52	-0.52	**-1.06**	**-1.06**
GMPPB	GDP-mannose pyrophosphorylase B	-0.18	-0.17	-0.35	-0.34	-0.79	-0.73	-0.64	-0.63
GNA12	guanine nucleotide binding protein (G protein) alpha 12	0.18	0.25	-0.46	-0.35	-0.63	-0.48	**-1.07**	-0.87
GPATCH3	G patch domain containing 3	-0.60	-0.60	-0.74	-0.74	-0.98	-0.98	-0.59	-0.59
GPIHBP1	glycosylphosphatidylinositol anchored high density lipoprotein binding protein 1	0.58	0.58	0.03	0.03	-0.34	-0.34	-0.35	-0.35
GPR132	G protein-coupled receptor 132	0.62	0.62	0.28	0.28	-0.12	-0.12	-0.45	-0.45
GREB1	growth regulation by estrogen in breast cancer 1	0.72	0.74	-0.03	0.10	-0.45	-0.29	-0.55	-0.39
GRIN2B	glutamate receptor, ionotropic, N-methyl D-aspartate 2B	-0.49	-0.49	-0.80	-0.80	-0.74	-0.74	-0.79	-0.79
HCCS	holocytochrome c synthase	-0.29	-0.19	0.20	0.35	0.29	0.46	0.36	0.69
HIST1H2AH	histone cluster 1, H2ah	-0.11	-0.01	-0.60	-0.57	-0.63	-0.56	-0.94	-0.85
HLX	H2.0-like homeobox	-0.31	-0.31	-0.84	-0.84	-0.62	-0.62	-0.56	-0.56
HMX3	H6 family homeobox 3	-0.19	-0.18	-0.82	-0.82	-0.71	-0.67	-0.91	-0.90
HRNR	hornerin	-0.54	-0.50	-0.78	-0.76	-0.48	-0.46	**-1.10**	**-1.03**
HSD17B7	hydroxysteroid (17-beta) dehydrogenase 7	-0.87	-0.64	-0.96	-0.81	-0.75	-0.61	**-1.68**	**-1.54**
HSD17B7P2	hydroxysteroid (17-beta) dehydrogenase 7 pseudogene 2	-0.92	-0.85	-0.81	-0.77	-0.80	-0.70	**-1.55**	**-1.54**
HSPA1A	heat shock 70kDa protein 1A	0.84	0.84	0.46	0.46	0.00	0.00	-0.31	-0.31
HSPA1B	heat shock 70kDa protein 1B	0.25	**1.05**	-0.25	0.44	-0.28	0.08	-0.84	-0.18
HTR2A	5-hydroxytryptamine (serotonin) receptor 2A	-0.56	-0.47	-0.09	-0.01	0.10	0.11	-0.10	0.03
IL17RE	interleukin 17 receptor E	-0.85	-0.80	-0.67	-0.60	-0.23	-0.22	**-1.16**	**-1.07**
IP6K2	inositol hexakisphosphate kinase 2	-0.47	-0.22	0.34	0.40	0.15	0.41	0.42	0.55
IRX4	iroquois homeobox 4	0.44	0.44	0.07	0.07	-0.24	-0.24	-0.50	-0.50
ITGB4	integrin, beta 4	-0.51	-0.43	-0.66	-0.61	-0.33	-0.30	**-1.09**	**-1.09**
JAG2	jagged 2	0.49	0.53	0.13	0.22	-0.18	-0.13	-0.66	-0.64
JAKMIP3	Janus kinase and microtubule interacting protein 3	0.41	0.48	-0.15	-0.03	-0.18	-0.14	-0.72	-0.55
KBTBD6	kelch repeat and BTB (POZ) domain containing 6	-0.57	-0.39	-0.73	-0.52	-0.62	-0.44	**-1.90**	**-1.48**
KEL	Kell blood group, metallo-endopeptidase	-0.57	-0.25	0.05	0.20	0.31	0.54	0.22	0.63
KIAA1683	KIAA1683	0.51	0.51	0.20	0.20	-0.12	-0.12	-0.45	-0.45
KISS1	KiSS-1 metastasis-suppressor	-0.83	-0.59	-0.74	-0.53	-0.46	-0.36	-0.92	-0.82
KLHDC4	kelch domain containing 4	0.39	0.39	-0.13	-0.13	-0.33	-0.33	-0.65	-0.65
KRT6B	keratin 6B	-0.41	-0.30	-0.47	-0.40	-0.37	-0.28	**-1.26**	**-1.19**
KRT6C	keratin 6C	-0.51	-0.24	-0.74	-0.61	-0.42	-0.35	**-1.47**	**-1.34**
LBX1	ladybird homeobox 1	0.04	0.10	-0.56	-0.45	-0.68	-0.55	-0.78	-0.66

Gene symbol	Gene description	60 µM I3C		5 µM B-DIM		5 µM C-DIM		15 µM C-DIM	
		min	max	min	max	min	max	min	max
LDHAL6B	lactate dehydrogenase A-like 6B	-0.04	-0.01	-0.63	-0.57	-0.51	-0.50	-0.86	-0.84
LHX8	LIM homeobox 8	0.21	0.21	-0.32	-0.32	-0.68	-0.68	-0.58	-0.58
LOC200726	hCG1657980	0.75	0.75	0.24	0.24	-0.20	-0.20	-0.31	-0.31
LOC254559	hypothetical LOC254559	0.50	0.62	0.03	0.10	-0.31	-0.28	-0.68	-0.60
LOC255167	hypothetical LOC255167	0.11	0.11	-0.40	-0.40	-0.53	-0.53	-0.35	-0.35
LOC283404	hypothetical LOC283404	-0.44	-0.38	-0.19	-0.04	-0.03	0.09	0.42	0.54
LOC401463	hypothetical LOC401463	0.05	0.09	-0.54	-0.51	-0.32	-0.29	-0.73	-0.65
LOC90834	hypothetical protein BC001742	-0.22	-0.14	-0.73	-0.70	-0.56	-0.46	**-1.03**	**-1.00**
LRPAP1	low density lipoprotein receptor-related protein associated protein 1	0.42	0.52	-0.05	-0.02	-0.54	-0.47	-0.69	-0.63
LRRC52	leucine rich repeat containing 52	-0.32	-0.32	0.24	0.24	0.53	0.53	0.63	0.63
MAB21L2	mab-21-like 2 (C. elegans)	0.39	0.49	-0.41	-0.27	-0.90	-0.72	**-1.12**	-0.90
MAD1L1	MAD1 mitotic arrest deficient-like 1 (yeast)	-1.00	0.87	**-1.38**	0.40	-0.94	0.01	**-2.04**	-0.17
MAGEB10	melanoma antigen family B, 10	-0.33	-0.25	-0.84	-0.76	-0.52	-0.49	-0.55	-0.51
MAGED2	melanoma antigen family D, 2	-0.34	-0.18	0.36	0.52	0.22	0.28	0.51	0.57
MAGI3	membrane associated guanylate kinase, WW and PDZ domain containing 3	-0.09	-0.09	0.55	0.55	0.27	0.27	0.69	0.69
MANF	mesencephalic astrocyte-derived neurotrophic factor	-0.51	-0.51	-0.55	-0.55	-0.03	-0.03	-0.84	-0.84
MCF2L	MCF.2 cell line derived transforming sequence-like	-0.02	0.22	-0.50	-0.28	-0.46	-0.27	**-1.75**	**-1.30**
MDP1	magnesium-dependent phosphatase 1	-0.91	-0.91	-0.55	-0.55	-0.37	-0.37	**-1.39**	**-1.39**
METTL3	methyltransferase like 3	-0.84	-0.75	**-1.01**	-0.91	-0.70	-0.62	**-1.49**	**-1.38**
MKI67IP	MKI67 (FHA domain) interacting nucleolar phosphoprotein	-0.13	-0.09	-0.64	-0.55	-0.81	-0.70	**-1.02**	-0.88
MLC1	megalencephalic leukoencephalopathy with subcortical cysts 1	0.01	0.01	-0.01	-0.01	-0.24	-0.24	-0.85	-0.85
MMP9	matrix metallopeptidase 9 (gelatinase B, 92kDa gelatinase, 92kDa type IV collagenase)	0.81	0.87	0.46	0.51	-0.10	-0.02	-0.47	-0.44
MRPL32	mitochondrial ribosomal protein L32	**-1.25**	**-1.23**	-0.69	-0.68	-0.18	-0.17	**-1.42**	**-1.29**
MRPL33	mitochondrial ribosomal protein L33	-0.52	-0.52	-0.56	-0.56	-0.55	-0.55	**-1.27**	**-1.27**
MSC	musculin	-0.25	0.07	-0.65	-0.42	-0.75	-0.65	-0.99	-0.79
MST1P2	macrophage stimulating 1 (hepatocyte growth factor-like) pseudogene 2	0.04	0.16	-0.50	-0.34	-0.79	-0.67	-0.71	-0.48
MSX1	msh homeobox 1	0.49	0.49	-0.42	-0.42	-0.66	-0.66	-0.42	-0.42
MUC21	mucin 21, cell surface associated	-0.38	-0.38	0.15	0.15	0.24	0.24	0.31	0.31
MYLPF	myosin light chain, phosphorylatable, fast skeletal muscle	0.39	0.41	0.54	0.54	0.60	0.60	0.76	0.83
NCRNA00085	non-protein coding RNA 85	0.94	0.94	0.64	0.64	0.09	0.09	0.06	0.06
NCRNA00245	non-protein coding RNA 245	0.08	0.21	-0.37	-0.37	-0.65	-0.51	-0.75	-0.60
NDUFA4L2	NADH dehydrogenase (ubiquinone) 1 alpha subcomplex, 4-like 2	-0.89	-0.52	-0.96	-0.69	-0.40	-0.25	**-1.34**	**-1.11**

Gene symbol	Gene description	60 µM I3C		5 µM B-DIM		5 µM C-DIM		15 µM C-DIM	
		min	max	min	max	min	max	min	max
NEUROD1	neurogenic differentiation 1	-0.20	-0.20	-0.41	-0.41	-0.03	-0.03	-0.80	-0.80
NFKBIE	nuclear factor of kappa light polypeptide gene enhancer in B-cells inhibitor, epsilon	-0.42	-0.40	0.29	0.31	0.20	0.20	0.30	0.31
NR2E1	nuclear receptor subfamily 2, group E, member 1	0.31	0.34	-0.14	-0.13	-0.51	-0.49	-0.67	-0.59
NXF2	nuclear RNA export factor 2	**-1.24**	**-1.18**	-0.85	-0.71	-0.43	-0.28	**-1.09**	-0.93
OBSL1	obscurin-like 1	-0.41	0.44	-0.35	0.16	-0.28	-0.21	**-1.01**	-0.47
OLFM1	olfactomedin 1	-0.64	-0.64	-0.85	-0.85	-0.68	-0.68	-0.90	-0.90
OLIG3	oligodendrocyte transcription factor 3	0.01	0.03	-0.76	-0.71	-0.72	-0.68	-0.89	-0.82
OPN1LW	opsin 1 (cone pigments), long-wave-sensitive	0.04	0.04	-0.52	-0.52	-0.42	-0.42	-0.83	-0.83
OPRK1	opioid receptor, kappa 1	0.00	0.13	-0.74	-0.40	-0.72	-0.57	-0.47	-0.35
OPRL1	opiate receptor-like 1	0.92	1.00	0.04	0.13	-0.43	-0.29	-0.67	-0.49
OR2B11	olfactory receptor, family 2, subfamily B, member 11	-0.64	-0.64	-0.70	-0.70	-0.32	-0.32	-0.86	-0.86
OR2T29	olfactory receptor, family 2, subfamily T, member 29	-0.47	-0.39	0.09	0.15	0.21	0.27	0.39	0.45
OR4E2	olfactory receptor, family 4, subfamily E, member 2	-0.10	-0.10	0.32	0.35	0.56	0.65	0.46	0.51
OR51E1	olfactory receptor, family 51, subfamily E, member 1	-0.58	-0.58	0.01	0.01	0.08	0.08	0.05	0.05
OR5AR1	olfactory receptor, family 5, subfamily AR, member 1	-0.58	-0.35	0.31	0.41	0.24	0.31	0.42	0.59
OR6V1	olfactory receptor, family 6, subfamily V, member 1	-0.42	-0.39	0.14	0.15	0.09	0.13	0.21	0.24
OR8S1	olfactory receptor, family 8, subfamily S, member 1	-0.52	-0.41	-0.14	-0.09	0.32	0.36	0.24	0.32
OXA1L	oxidase (cytochrome c) assembly 1-like	**-1.03**	**-1.03**	-0.86	-0.86	-0.37	-0.37	**-1.29**	**-1.29**
P4HA2	prolyl 4-hydroxylase, alpha polypeptide II	0.43	0.43	0.34	0.34	0.65	0.65	0.63	0.63
PANX1	pannexin 1	-0.05	-0.01	0.47	0.53	0.53	0.60	0.80	0.96
PAQR9	progestin and adipoQ receptor family member IX	0.84	0.84	0.38	0.38	-0.04	-0.04	-0.16	-0.16
PAX9	paired box 9	0.62	0.69	0.25	0.43	-0.44	-0.32	-0.63	-0.52
PCBP3	poly(rC) binding protein 3	0.25	0.94	-0.47	0.15	-0.71	-0.34	-0.61	-0.47
PCDH17	protocadherin 17	0.17	0.30	-0.55	-0.45	-0.79	-0.70	-0.29	-0.28
PCDHGB6	protocadherin gamma subfamily B, 6	0.42	0.42	-0.14	-0.14	-0.49	-0.49	-0.35	-0.35
PCSK2	proprotein convertase subtilisin/kexin type 2	0.14	0.29	-0.47	-0.37	-0.82	-0.66	-0.63	-0.53
PDE3A	phosphodiesterase 3A, cGMP-inhibited	-0.02	0.36	-0.44	-0.29	-0.42	-0.28	-0.88	-0.47
PDGFRB	platelet-derived growth factor receptor, beta polypeptide	**-1.08**	**-1.06**	-0.82	-0.79	-0.38	-0.37	**-1.32**	**-1.27**
PDYN	prodynorphin	-0.37	-0.31	0.22	0.32	0.16	0.19	0.31	0.50
PLA2R1	phospholipase A2 receptor 1, 180kDa	-0.27	-0.27	-0.04	-0.04	-0.21	-0.21	0.54	0.54
POFUT2	protein O-fucosyltransferase 2	0.67	0.75	-0.09	-0.03	-0.34	-0.32	-0.52	-0.50
POTEB	POTE ankyrin domain family, member B	0.47	0.61	-0.14	0.13	-0.39	-0.12	-0.81	-0.45
POTEC	POTE ankyrin domain family, member C	0.26	0.35	-0.22	-0.10	-0.41	-0.29	-0.71	-0.61

Gene symbol	Gene description	60 µM I3C		5 µM B-DIM		5 µM C-DIM		15 µM C-DIM	
		min	max	min	max	min	max	min	max
POTED	POTE ankyrin domain family, member D	0.27	0.41	-0.09	0.08	-0.35	-0.28	-0.78	-0.69
POTEG	POTE ankyrin domain family, member G	-0.13	-0.07	-0.60	-0.51	-0.83	-0.73	**-1.15**	-0.95
PPME1	protein phosphatase methylesterase 1	**-1.22**	**-1.06**	**-1.19**	**-1.06**	-0.69	-0.61	**-1.71**	**-1.49**
PPP1R12C	protein phosphatase 1, regulatory (inhibitor) subunit 12C	-0.45	-0.45	-0.37	-0.37	-0.32	-0.32	**-1.27**	**-1.27**
PRIMA1	proline rich membrane anchor 1	0.46	0.54	-0.24	-0.17	-0.56	-0.43	-0.51	-0.45
PRKCG	protein kinase C, gamma	-0.40	-0.40	-0.28	-0.28	0.32	0.32	0.12	0.12
PRPF6	PRP6 pre-mRNA processing factor 6 homolog (S. cerevisiae)	-0.22	-0.09	-0.55	-0.48	-0.46	-0.45	**-1.50**	**-1.34**
PRR21	proline rich 21	0.28	0.28	-0.02	-0.02	-0.14	-0.14	-0.63	-0.63
PRR5-ARHGAP8	PRR5-ARHGAP8 readthrough	-0.22	-0.18	-0.47	-0.40	-0.58	-0.52	**-1.02**	-0.97
PRSS30P	protease, serine, 30 homolog (mouse), pseudogene	0.24	0.24	-0.10	-0.10	-0.15	-0.15	-0.65	-0.65
PTCD2	pentatricopeptide repeat domain 2	**-1.01**	-0.95	-0.68	-0.64	-0.40	-0.37	**-1.52**	**-1.52**
PTPRN2	protein tyrosine phosphatase, receptor type, N polypeptide 2	0.78	0.82	-0.08	-0.04	-0.56	-0.43	-0.71	-0.58
QRFP	pyroglutamylated RFamide peptide	0.61	0.61	-0.02	-0.02	-0.36	-0.36	-0.20	-0.20
RAB11FIP3	RAB11 family interacting protein 3 (class II)	0.20	0.27	-0.13	0.00	-0.51	-0.37	**-1.34**	**-1.14**
RASA3	RAS p21 protein activator 3	-0.38	-0.32	-0.64	-0.58	-0.43	-0.39	**-1.08**	**-1.00**
RBM12	RNA binding motif protein 12	-0.89	-0.87	-0.28	-0.25	-0.24	-0.19	-0.08	-0.08
RBMXL3	RNA binding motif protein, X-linked-like 3	0.88	**1.14**	0.19	0.51	-0.32	-0.17	-0.45	-0.36
RBP3	retinol binding protein 3, interstitial	-0.19	-0.10	-0.65	-0.62	-0.79	-0.74	-0.92	-0.74
RFNG	RFNG O-fucosylpeptide 3-beta-N-acetylglucosaminyltransferase	0.66	0.73	-0.11	0.05	-0.37	-0.34	-0.60	-0.49
RGPD1	RANBP2-like and GRIP domain containing 1	-0.13	-0.13	0.48	0.48	0.36	0.36	0.57	0.57
RHBDL1	rhomboid, veinlet-like 1 (Drosophila)	0.78	0.88	0.29	0.38	-0.28	0.01	-0.09	0.03
RHOXF2	Rhox homeobox family, member 2	0.79	0.79	0.18	0.18	-0.12	-0.12	-0.17	-0.17
RNF17	ring finger protein 17	0.15	0.19	-0.52	-0.46	-0.52	-0.48	-0.73	-0.65
RNF25	ring finger protein 25	-0.81	-0.56	-0.88	-0.75	-0.52	-0.44	**-1.30**	**-1.11**
ROR2	receptor tyrosine kinase-like orphan receptor 2	0.00	0.00	-0.21	-0.21	-0.62	-0.62	**-1.04**	**-1.04**
RPH3AL	rabphilin 3A-like (without C2 domains)	-0.74	-0.65	**-1.04**	-0.92	-0.51	-0.42	**-1.25**	**-1.10**
RPL37	ribosomal protein L37	-0.52	-0.52	-0.53	-0.53	-0.10	-0.10	-0.71	-0.71
RXRG	retinoid X receptor, gamma	-0.48	-0.48	-0.93	-0.93	-0.57	-0.57	**-1.07**	**-1.07**
SCAMP3	secretory carrier membrane protein 3	-0.54	-0.51	-0.49	-0.33	-0.41	-0.36	**-1.05**	-0.98
SCARB1	scavenger receptor class B, member 1	0.64	0.68	-0.12	0.12	-0.32	-0.05	-0.93	-0.64
SCARNA22	small Cajal body-specific RNA 22	-0.43	-0.42	-0.85	-0.78	-0.40	-0.39	-0.76	-0.69
SDC2	syndecan 2	0.52	0.52	0.07	0.07	-0.38	-0.38	-0.21	-0.21
SELENBP1	selenium binding protein 1	-0.74	-0.70	-0.21	-0.11	-0.11	-0.08	-0.03	0.04
SEPT9	septin 9	0.51	0.51	0.43	0.48	0.46	0.50	0.23	0.36
SETBP1	SET binding protein 1	-0.47	-0.47	0.16	0.16	0.06	0.06	0.25	0.25

Gene symbol	Gene description	60 µM I3C		5 µM B-DIM		5 µM C-DIM		15 µM C-DIM	
		min	max	min	max	min	max	min	max
SFMBT1	Scm-like with four mbt domains 1	0.87	0.87	0.25	0.25	-0.28	-0.28	-0.35	-0.35
SGEF	Src homology 3 domain-containing guanine nucleotide exchange factor	-0.09	-0.09	-0.36	-0.36	-0.38	-0.38	-0.80	-0.80
SH3BGRL2	SH3 domain binding glutamic acid-rich protein like 2	**-1.20**	**-1.20**	-0.94	-0.94	-0.38	-0.38	**-1.15**	**-1.15**
SH3BP4	SH3-domain binding protein 4	0.14	0.19	-0.45	-0.41	-0.89	-0.81	-0.58	-0.45
SHC3	SHC (Src homology 2 domain containing) transforming protein 3	-0.03	-0.02	-0.67	-0.64	-0.73	-0.67	-0.52	-0.49
SIX6	SIX homeobox 6	0.52	0.52	-0.12	-0.11	-0.38	-0.28	-0.26	-0.21
SLC22A2	solute carrier family 22 (organic cation transporter), member 2	0.09	0.09	-0.34	-0.34	-0.58	-0.58	-0.63	-0.63
SLC25A48	solute carrier family 25, member 48	0.24	0.24	-0.34	-0.34	-0.66	-0.66	-0.44	-0.44
SLC32A1	solute carrier family 32 (GABA vesicular transporter), member 1	-0.24	-0.24	0.37	0.37	0.11	0.11	0.60	0.60
SLC46A1	solute carrier family 46 (folate transporter), member 1	0.35	0.42	-0.20	-0.15	-0.51	-0.45	-0.58	-0.48
SLC6A18	solute carrier family 6, member 18	-0.45	-0.45	-0.90	-0.90	-0.71	-0.71	**-1.31**	**-1.31**
SMOC2	SPARC related modular calcium binding 2	0.49	0.49	0.08	0.08	-0.19	-0.19	-0.34	-0.34
SNORD115-1	small nucleolar RNA, C/D box 115-1	-0.34	-0.34	-0.42	-0.42	-0.32	-0.32	-0.79	-0.79
SNX2	sorting nexin 2	-0.04	-0.04	0.45	0.45	0.31	0.31	0.79	0.79
SNX29	sorting nexin 29	**-1.27**	**-1.03**	**-1.20**	**-1.09**	-0.88	-0.70	**-1.73**	**-1.60**
SNX32	sorting nexin 32	-0.54	-0.42	0.07	0.11	0.27	0.32	0.34	0.41
SOX9	SRY (sex determining region Y)-box 9	0.04	0.04	-0.62	-0.62	-0.56	-0.56	-0.55	-0.55
SPACA5	sperm acrosome associated 5	-0.29	-0.13	0.18	0.24	0.17	0.34	0.43	0.50
SSTR1	somatostatin receptor 1	0.57	0.57	-0.17	-0.17	-0.35	-0.35	-0.12	-0.12
SSU72	SSU72 RNA polymerase II CTD phosphatase homolog (S. cerevisiae)	0.80	0.80	0.27	0.27	-0.24	-0.24	-0.51	-0.51
SUPT7L	suppressor of Ty 7 (S. cerevisiae)-like	-0.88	-0.88	-0.99	-0.99	-0.50	-0.50	-0.95	-0.95
SYT6	synaptotagmin VI	0.03	0.19	-0.41	-0.29	-0.69	-0.51	-0.64	-0.49
TBC1D22A	TBC1 domain family, member 22A	0.44	0.44	-0.32	-0.32	-0.71	-0.71	-0.57	-0.57
TBCD	tubulin folding cofactor D	0.38	0.38	-0.25	-0.25	-0.58	-0.58	-0.59	-0.59
TERT	telomerase reverse transcriptase	-0.17	0.05	-0.37	-0.27	-0.11	-0.04	**-1.08**	-0.98
TFAP2A	transcription factor AP-2 alpha (activating enhancer binding protein 2 alpha)	0.02	0.05	-0.46	-0.45	-0.59	-0.53	-0.79	-0.78
TFF3	trefoil factor 3 (intestinal)	-0.11	-0.11	-0.52	-0.52	-0.34	-0.34	-0.84	-0.84
THAP4	THAP domain containing 4	0.40	0.44	-0.32	-0.29	-0.42	-0.37	-0.70	-0.67
TIMM8B	translocase of inner mitochondrial membrane 8 homolog B (yeast)	-0.62	-0.62	-0.29	-0.29	-0.17	-0.17	**-1.13**	**-1.13**
TMEM111	transmembrane protein 111	-0.37	-0.33	0.32	0.36	0.39	0.42	0.52	0.57
TMEM132C	transmembrane protein 132C	-0.32	-0.31	-0.64	-0.61	-0.52	-0.47	**-1.19**	**-1.18**
TMEM171	transmembrane protein 171	0.14	0.23	-0.52	-0.37	-0.86	-0.68	-0.65	-0.47
TMEM204	transmembrane protein 204	0.30	0.34	-0.36	-0.31	-0.43	-0.43	-0.76	-0.74

Gene symbol	Gene description	60 µM I3C		5 µM B-DIM		5 µM C-DIM		15 µM C-DIM	
		min	max	min	max	min	max	min	max
TMEM52	transmembrane protein 52	0.70	0.70	0.31	0.31	0.01	0.01	-0.27	-0.27
TMEM9	transmembrane protein 9	-0.38	-0.20	0.18	0.27	0.42	0.48	0.30	0.40
TOMM70A	translocase of outer mitochondrial membrane 70 homolog A (S. cerevisiae)	-0.12	-0.09	0.65	0.75	0.24	0.30	0.69	0.83
TP53	tumor protein p53	**-1.10**	**-1.09**	-0.97	-0.90	-0.41	-0.41	**-1.41**	**-1.29**
TP53TG3B	TP53 target 3B	-0.09	0.04	0.57	0.65	0.23	0.33	0.48	0.58
TRAF7	TNF receptor-associated factor 7	-0.28	-0.19	-0.73	-0.62	-0.80	-0.69	**-1.27**	**-1.21**
TRAIP	TRAF interacting protein	-0.75	-0.61	-0.83	-0.73	-0.49	-0.43	**-1.50**	**-1.41**
TRIP13	thyroid hormone receptor interactor 13	0.44	0.44	0.16	0.16	0.08	0.08	-0.42	-0.42
TRPC3	transient receptor potential cation channel, subfamily C, member 3	0.64	0.65	-0.07	-0.05	-0.42	-0.37	-0.51	-0.48
TSNARE1	t-SNARE domain containing 1	**-1.41**	**-1.27**	**-1.71**	**-1.48**	-0.50	-0.38	**-1.72**	**-1.50**
TUB	tubby homolog (mouse)	0.24	0.37	-0.23	-0.17	-0.51	-0.43	-0.85	-0.74
TYK2	tyrosine kinase 2	-0.94	-0.94	-0.98	-0.98	-0.95	-0.95	**-1.07**	**-1.07**
USP2	ubiquitin specific peptidase 2	-0.01	-0.01	-0.48	-0.48	-0.84	-0.84	-0.62	-0.62
VPS18	vacuolar protein sorting 18 homolog (S. cerevisiae)	-0.42	-0.28	-0.52	-0.39	-0.36	-0.26	**-1.03**	-0.96
VSX1	visual system homeobox 1	-0.87	-0.87	**-1.29**	**-1.29**	-0.92	-0.92	**-1.22**	**-1.22**
WNT2B	wingless-type MMTV integration site family, member 2B	-0.96	-0.94	-0.44	-0.38	-0.16	-0.08	**-1.08**	**-1.01**
YBX1	Y box binding protein 1	-0.06	-0.06	0.61	0.61	0.77	0.77	0.71	0.71
YTHDC2	YTH domain containing 2	-0.27	-0.19	0.01	0.19	0.18	0.25	0.54	0.61
ZC3H15	zinc finger CCCH-type containing 15	-0.09	-0.06	0.51	0.57	0.31	0.33	0.46	0.59
ZCCHC11	zinc finger, CCHC domain containing 11	-0.18	-0.06	0.30	0.45	0.22	0.33	0.66	0.69
ZDHHC11	zinc finger, DHHC-type containing 11	-0.57	-0.10	-0.58	-0.13	-0.34	-0.07	**-1.70**	-0.90
ZFYVE20	zinc finger, FYVE domain containing 20	-0.39	-0.39	0.33	0.33	0.01	0.01	0.30	0.30
ZNF192	zinc finger protein 192	-0.77	-0.77	-0.58	-0.58	-0.07	-0.07	-0.97	-0.97
ZNF214	zinc finger protein 214	0.03	0.15	-0.75	-0.58	-0.92	-0.70	-0.76	-0.51
ZNF394	zinc finger protein 394	-0.27	-0.24	-0.59	-0.52	-0.40	-0.29	**-1.40**	**-1.14**
ZNF540	zinc finger protein 540	-0.85	-0.74	**-1.05**	-0.89	**-1.30**	**-1.21**	**-1.09**	-0.95
ZNF566	zinc finger protein 566	-0.49	-0.21	-0.88	-0.75	**-1.28**	**-1.11**	**-1.48**	**-1.26**
ZNF595	zinc finger protein 595	-0.04	-0.04	0.51	0.51	0.48	0.48	**1.06**	**1.06**
ZNF785	zinc finger protein 785	0.83	0.83	0.27	0.27	-0.13	-0.13	-0.34	-0.34
ZNF787	zinc finger protein 787	0.85	0.90	0.12	0.27	-0.53	-0.44	**-1.11**	**-1.02**

Minimum "min" and maximum "max" represent the range of coefficients for transcripts having more than one probe identified as significant by DMR analysis with Bonferroni MTC. Coefficients are highlighted in green if they are negative, or hypomethylated, relative to control treatment and in red if they are positive, or hypermethylated. Coefficients are in bold if the fold-change from control is greater than or equal to 2 (i.e. $Log_2 < -1$ or > 1).

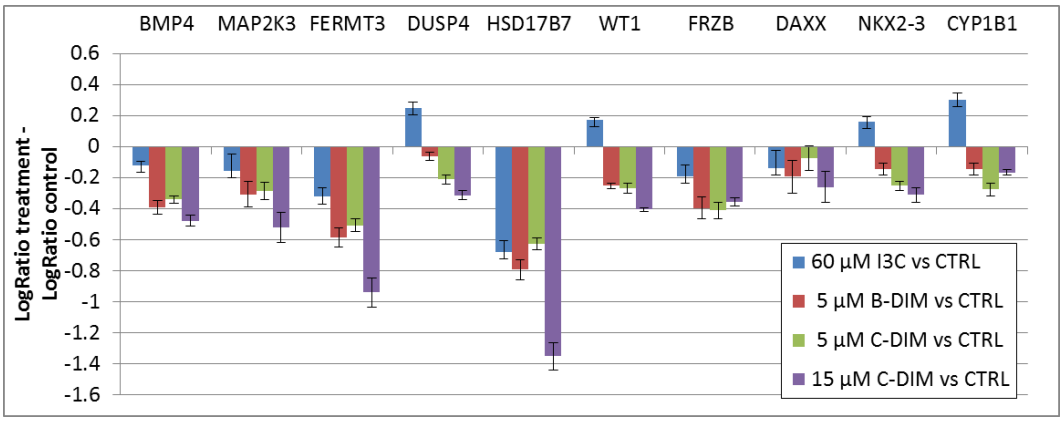

Supplemental Figure S-A1.2 Methylation relative to control for validation set of genes.

From the Nimblegen arrays the log-ratio (intensity) at each probe represents level of methylation. The average intensity of a probe for the control samples was subtracted from the average intensity across a treatment to determine fold change. Mean ± SEM fold change for all probes mapping to a particular gene of interest is plotted.

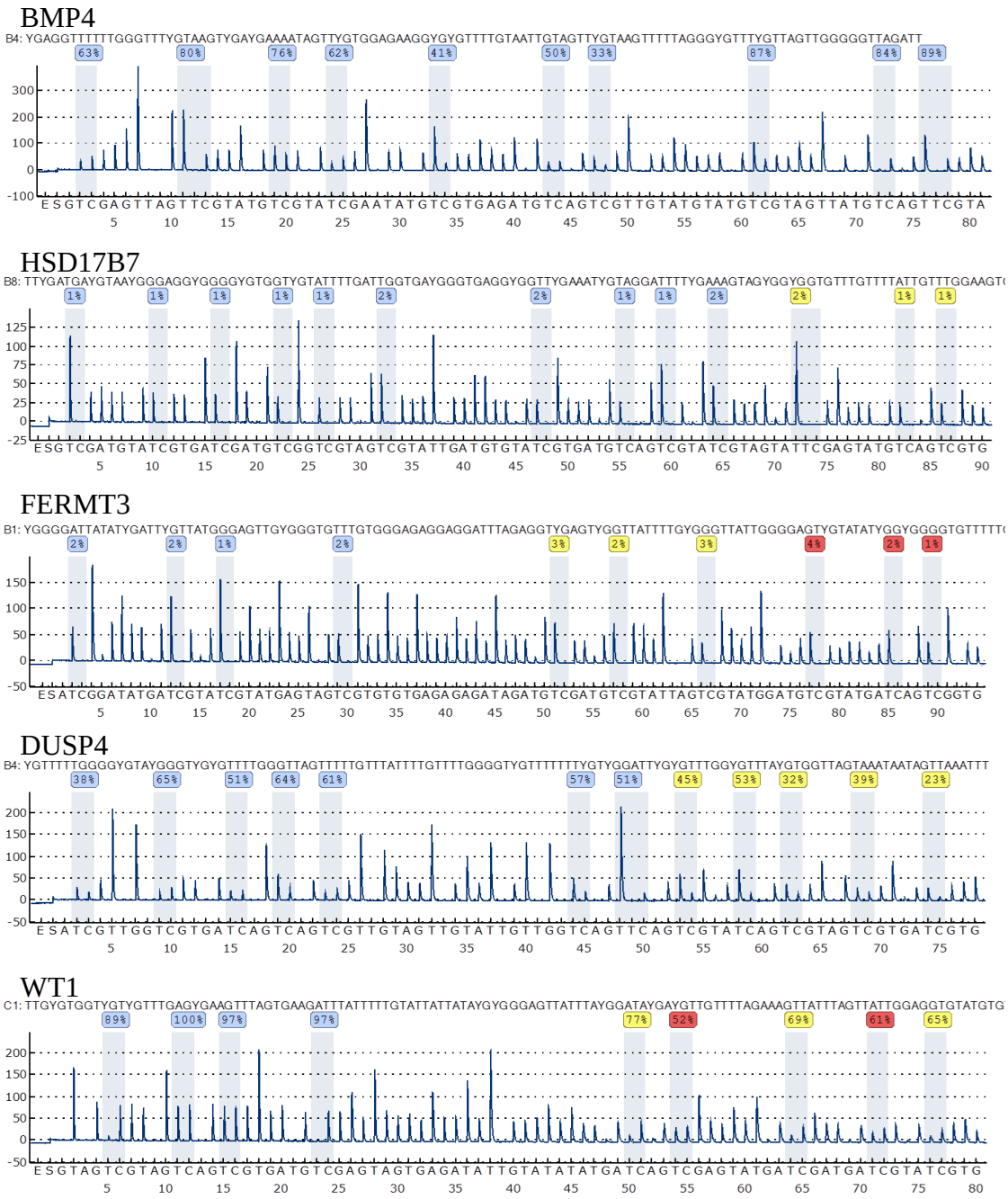

Supplemental Figure S-A1.3 Pyrograms for untreated CEM modified DNA for 5 genes selected for DMR validation.

Bisulfite modified DNA from untreated CEM cells was amplified and sumbitted for pyrosequencing to the Protein and Nucleic Acid facility at Stanford University.